Discovery and Delivery of Bioactive Natural Products

Yongle Du

Dissertation submitted to the faculty of Virginia Polytechnic Institute and State University in partial fulfillment of the requirements for the degree of

Doctor of Philosophy

In

Chemistry

David G. I. Kingston, chair

Richard D. Gandour

Paul R. Carlier

Webster L. Santos

May 2nd, 2018

Blacksburg, Virginia

Keywords: Natural Products, Antiplasmodial, Antiproliferative, Sesquiterpenoid, Neolignan, Diterpenoid, Coumarin, Butanolide

Copyright 2018, Yongle Du

Discovery and Delivery of Bioactive Natural Products

Yongle Du

Abstract

As a part of search for bioactive natural products from the plants in collaboration with the Natural Products Discovery Institute (NPDI), ten plant extracts were investigated for their antiplasmodial activity against *Plasmodium falciparum* Dd2 strain. Twenty-eight compounds (**2.1**–**2.4**, **3.1**–**3.5**, **4.1**–**4.6**, **5.1**, and **8.1**–**8.6**) were isolated, and twelve of them (**2.1**–**2.4**, **3.1**–**3.5**, **4.1**, **4.2**, and **5.1**) were new compounds. The structures of all these compounds were determined by analysis of their mass spectrometric, 1D and 2D NMR, and ECD spectrum. Among these natural products, there were three compounds with good antiplasmodial activity, trichospirolide A **2.1** with an IC_{50} value of 1.5 μM, malleastrumolide A **5.1** with an IC_{50} value of 2.7 μM, and (+)-lariciresinol **8.6** with an IC_{50} value of 3.7 μM.

In addition to the studies of drug delivery of bioactive natural product, doxorubicin (**9.1**), a novel thiolated doxorubicin analog were designed (**9.3**) and synthesized. Its analogs and PEG stabilizing ligands were then conjugated to gold nanoparticles and the resulting Au-Dox constructs were evaluated by TEM. The release of native drug can be achieved by the action of reducing agents, and that reductive drug release gave the cleanest drug release.

Discovery and Delivery of Bioactive Natural Products

Yongle Du

General Abstract

Natural products from plants have been used as medicines for a very long history, with the best known example of antimalarial drugs. There were two famous antimalarial natural products used as medicines. The first one is an alkaloid, quinine which was isolated from cinchona bark in 1817. Its analog chloroquine was discovered in 1934 and was very effective. But in 1950's the *Plasmodium* parasite developed resistance and chloroquine resistant *plasmodia* were widely spread all over the world. Today, the major antimalarial drug is a sesquiterpenoid, artemisinin which was isolated from artemisia in 1972. Unfortunately, the first report on drug resistance to artemisinin derivative have appeared in 2010. In the future, artemisinin may be useless. So we need to discover new antimalarial natural products. This dissertation focuses on the isolation and structural elucidation of fourteen new natural products with potential antimalarial activities from ten plant extracts.

Acknowledgement

Firstly, I would like to thank my advisor, Dr. David G. I. Kingston, for his exceptional mentorship. Through his mentorship, I learned how to learn and how to do the research. He also taught me the knowledge of natural product chemistry in his class CHEM6504. Thanks Dr. Kingston for your support and encouragement. I would also like to thank my committee, Dr. Richard Gandour, Dr. Paul Carlier, and Dr. Webster Santos. Dr. Gandour taught me the knowledge of computational chemistry in his lessons CHEM5506, and his punctiliousness for chemical research. Dr. Carlier taught me the knowledge of organic chemistry in his lessons CHEM5505 and medicinal chemistry in his lessons CHEM6564. Dr. Santos taught me the knowledge of chemical biology in his lessons CHEM6564. Thanks Dr. Gandour, Dr. Carlier and Dr. Santos for your help. I would also like to thank Dr. Felicia Etzkorn for teaching me the knowledge of molecular structure determination in her lessons CHEM5524.

I would also like to thank my mentor Dr. Yumin Dai, who taught me a lot of knowledge and techniques in the field of isolation and structural elucidation of natural products; he also helped me a lot as my great friend. I would also like to thank my other group members, Dr. Rolly Fuentes, Dr. Abdul Latif, Dr. Namki Cho, Dr. Yixi Liu, Dr. Alexander Eaton, Dr. Qingxi Su, Dr. Christopher Presley, Long Xia, and Ming Wang. I would like to thank Dr. Maria Belen Cassera and her group members for performing the antiplasmodial bioassay. I would also like to thank my friend, Dr. Xi Geng, who always discussed chemical research with me and taught me a lot.

I would like to thank my parents and my uncle for their support and encouragement. At last, I would like to thank my wife for her support, encouragement and love.

Table of Contents

Abstract ii

General Abstract iii

Acknowledgement iv

Table of Contents v

List of Abbreviations viii

List of Tables ix

List of Schemes xi

List of Figures xii

Chapter 1: Introduction 1

1.1 Introduction to natural products 1

1.2 Introduction to bioactivities of natural products 3

1.3 Methods of isolation 5

1.4 Methods of structural elucidation 8

1.5 References 10

Chapter 2: Antiplasmodial Sesquiterpenoid Lactones from *Trichospira verticillata* 13

2.1 Introduction 14

2.2 Results and Discussion 14

2.3 Experimental Section 30

2.4 References 35

Chapter 3: Antiplasmodial Diterpenoids and a Benzotropolone from *Petradoria pumila* 41

3.1 Introduction 41

3.2 Results and Discussion 42

3.3 Experimental Section 56

3.4 References 60

Chapter 4: An Antiplasmodial Coumarin and Norneolignan from *Aniba citrifolia* 64

4.1 Introduction 64

4.2 Results and Discussion 65
4.3 Experimental Section 75
4.4 References 80
Chapter 5: An Antiplasmodial Butanolide from *Malleastrum sp.* 83
5.1 Introduction 83
5.2 Results and Discussion 84
5.3 Experimental Section 89
5.4 References 92
Chapter 6: An Antiplasmodial Neolignan and Alkaloid from *Magnolia grandiflora* L.. 95
6.1 Introduction 95
6.2 Results and Discussion 96
6.3 Experimental Section 103
6.4 References 106
Chapter 7: Structure Reassignment of New Bicyclic Tetrahydro-α-pyrones 110
7.1 Introduction 110
7.2 Structure reassignment of Cryptorigidifoliol K from *Cryptocarya rigidifolia* 111
7.3 References 113
Chapter 8: Isolation of Known Bioactive Compounds 115
8.1 Introduction 115
8.2 Two known glucosides from *Trichocladus grandiflorus* 115
8.3 A known lignan and three known canthinone alkaloids from *Leitneria floridana* 117
8.4 Investigations of other antimalarial extracts 120
8.5 References 121
Chapter 9: Synthesis and Evaluation of Doxorubicin-Loaded Gold Nanoparticles for Tumor-Targeted Drug Delivery 123
9.1 Introduction 123
9.2 Results and Discussion 127

9.3 Experimental Section 134
9.4 References 141
Chapter 10: Conclusions 146
10.1 Summary of the structure elucidations 146
10.2 Summary of bioactivity of isolated natural products 146
10.3 Discussion of lost bioactivity 147
10.4 Future work 148
Appendix (1D and 2D NMR Spectra) 149

List of Abbreviations

ACT	Artemisinin-based Combination Therapy
COSY	Correlation Spectroscopy
DCM	Dichloromethane
DLS	Dynamic Light Scattering
DMF	Dimethylformamide
DMSO	Dimethyl Sulfoxide
DNP	Dictionary of Natural Prodaucts
ECD	Electronic Circular Dichroism
ELSD	Evaporative Light Scattering Detector
EtOAc	Ethyl Acetate
GSH	Glutathione
HEK	Human Embryonic Kidney
HMBC	Heteronuclear Multiple Bond Correlation
HPLC	High Performance Liquid Chromatography
HRESIMS	High Resolution Electrospray Ionization Mass Spectroscopy
HSQC	Heteronuclear Single Quantum Correlation
ICBG	International Cooperative Biodiversity Groups
ICPMS	Inductively Coupled Plasma Mass Spectrometry
MeCN	Acetonitrile
MeOH	Methanol
NIH	National Institutes of Health
NMR	Nuclear Magnetic Rosanance
NOESY	Nuclear Overhauser Effect Spectroscopy
NP	Nanoparticles
NPDI	Natural Products Discovery Institute
PEG	Polyethylene glycol
SPE	Solid Phase Extraction
TEM	Transmission Electron Microscopy
THF	Tetrahydrofuran
TLC	Thin Layer Chromatography

List of Tables

Table 2-1. NMR Spectroscopic Data for Compounds **2.1** in $CDCl_3$ 16

Table 2-2. Calculated Internuclear Distances and NOESY Signal Strength for **2.1** 18

Table 2-3. NMR Spectroscopic Data for Compounds **2.2** in $CDCl_3$ 20

Table 2-4. Calculated Internuclear Distances and NOESY Signal Strength for **2.2** 22

Table 2-5. Calculated Dihedral Angles and *J*-values for **2.2** 22

Table 2-6. NMR Spectroscopic Data for Compounds **2.3** in $CDCl_3$ 23

Table 2-7. Calculated Internuclear Distances and NOESY Signal Strength for **2.3** 25

Table 2-8. Calculated Dihedral Angle and *J*-value for **2.3** 25

Table 2-9. NMR Spectroscopic Data for Compound **2.4** in $CDCl_3$ (500 MHz) 26

Table 2-10. Calculated Internuclear Distances and NOESY Signal Strength for **2.4** 28

Table 2-11. Bioactivities of Compounds **2.1**–**2.4** 29

Table 3-1. NMR Spectroscopic Data for Compound **3.1** in $CDCl_3$ (500 MHz) 45

Table 3-2. The coupling constants and chemical shifts of relevant protons and carbons of compounds **S1**–**S2** 46

Table 3-3. NMR Spectroscopic Data for Compounds **3.2** in $CDCl_3$ (500 MHz) 48

Table 3-4. The coupling constants and chemical shifts of relevant protons and carbons of compounds **S3**–**S10** 50

Table 3-5. NMR Spectroscopic Data for Compounds **3.3** in $CDCl_3$ (500 MHz) 51

Table 3-6. NMR Spectroscopic Data for Compound **3.4** in $CDCl_3$ (500 MHz) 53

Table 3-7. NMR Spectroscopic Data for Compound **3.5** in $CDCl_3$ (500 MHz) 54

Table 3-8. NMR Spectroscopic Data for Compounds **3.6**–**3.7** in $CDCl_3$ (500 MHz) 55

Table 3-9. Biological Activity of compounds **3.1**–**3.7** 56

Table 4-1. NMR Spectroscopic Data for Compounds **4.1** in $CDCl_3$ (500 MHz) 67

Table 4-2. NMR Spectroscopic Data for Compounds **4.2** in $CDCl_3$ (500 MHz) 69

Table 4-3. NMR Spectroscopic Data for Compounds **4.3**–**4.4** in $CDCl_3$ (500 MHz) 71

Table 4-4. NMR Spectroscopic Data for Compounds **4.5**–**4.6** in $CDCl_3$ (500 MHz) 72

Table 4-5. NMR Spectroscopic Data for Compounds **4.7**–**4.8** in $CDCl_3$ (500 MHz).....73

Table 4-6. Biological Activity of compounds **4.1**–**4.8**.....74

Table 5-1. NMR Spectroscopic Data for Compound **5.1** in $CDCl_3$ (500 MHz).....86

Table 5-2. Bioactivities of malleastrumolide A **5.1** 88

Table 6-1. NMR Spectroscopic Data for Compounds **6.1** in $CDCl_3$ (500 MHz).....98

Table 6-2. NMR Spectroscopic Data for Compounds **6.2** in $CDCl_3$ (500 MHz).....100

Table 6-3. NMR Spectroscopic Data for Compounds **6.3**–**6.4** in $CDCl_3$ (500 MHz).....101

Table 6-4. NMR Spectroscopic Data for Compounds **6.5**–**6.6** in $CDCl_3$ (500 MHz).....102

Table 6-5. NMR Spectroscopic Data for Compounds **6.7**–**6.8** in $CDCl_3$ (500 MHz).....102

Table 7-1. NMR Spectroscopic Data for Compounds **7.2** in $CDCl_3$ (500 MHz).....112

Table 8-1. NMR Spectroscopic Data for Compounds **8.1** and **8.2** in Acetone-d_6 (500 MHz).....117

Table 8-2. NMR Spectroscopic Data for Compounds **8.3**–**8.5** in $CDCl_3$ (500 MHz).....119

Table 8-3. NMR Spectroscopic Data for Compounds **8.6** in CDCl3 (500 MHz).....119

Table 9-1. Standard curve for concentration of doxorubicin and area of absorption at 478 nm .131

List of Schemes

Scheme 9-1. Synthesis of doxorubicin derivative **9.3** 129

List of Figures

Figure 1-1. Reduction of resazurin **1.10** to resorufin **1.11** and even further reduction to hydroresorufin **1.12** 5

Figure 2-1. HMBC and NOESY correlations for trichospirolide A **2.1** 17

Figure 2-2. Comparison of experimental and calculated ECD and UV spectra of trichospirolide A (**2.1**) 19

Figure 2-3. HMBC and NOESY correlations for trichospirolide A **2.2** 21

Figure 2-4. Comparison of experimental and calculated ECD and UV spectra of trichospirolide B (**2.2**). 21

Figure 2-5. HMBC and NOESY correlations for trichospirolide C **2.3** 24

Figure 2-6. Comparison of experimental and calculated ECD and UV spectra of trichospirolide C (**2.3**) 24

Figure 2-7. HMBC and NOESY correlations for trichospirolide D **2.4** 27

Figure 2-8. Comparison of experimental and calculated ECD and UV spectra of trichospirolide D (**2.4**) 27

Figure 3-1. HMBC and NOESY correlations for petradoriolide A **3.1** 45

Figure 3-2. The ECD spectrum of petradoriolide A **3.1** 47

Figure 3-3. HMBC and NOESY correlations for petradoriolide B **3.2**. 48

Figure 3-4. he structures of similar compounds (**S3**– **S10**) 49

Figure 3-5. The ECD spectrum of petradoriolide B **3.2** 50

Figure 3-6. HMBC and NOESY correlations for petradoriolide C **3.3** 51

Figure 3-7. HMBC and NOESY correlations for petradoriolide C **3.4** 52

Figure 6-1. Key HMBC and COSY correlations of compound **6.1**. 99

Figure 6-2. Key HMBC correlations of compound **6.2**. 101

Figure 6-1. Key HMBC and COSY correlations of compound **6.1**. 99

Figure 7-1. Selected HMBC and COSY correlations of cryptorigidifoliol K **7.2**. 113

Figure 9-1. Proposed mechanism of doxorubicin release from gold-bound analog **9.3** by

glutathione (GSH). 129

Figure 9-2. TEM images of naked AuNPs. 130

Figure 9-3. Image analysis of >400 AuNP, 5 nm bins fit to a LogNormal distribution. 130

Figure 9-4. The HPLC of doxorubicin. 131

Figure 9-5. The HPLC of doxorubicin analog **9.3**. 131

Figure 9-6. Standard curve for concentration of doxorubicin 132

Figure 9-7. The HPLC of release of doxorubicin from **Au-9.3-1**. 133

Figure 9-8. The HPLC of release of doxorubicin from **Au-9.3-2**. 133

Figure 9-9. The HPLC of release of doxorubicin from **Au-9.3-3**. 134

Figure 9-10. The HPLC of release of doxorubicin from **Au-9.3-4.** 134

Chapter 1: Introduction

1.1 Introduction to natural products

1.1.1 The definition of natural products

Natural products are small molecules that are produced by a biological source.[1] They are divided into primary metabolites and secondary metabolites. Research on primary metabolites, which include carbohydrates, proteins, fats and nucleic acids, is the realm of biochemistry, while research on secondary metabolites, such as alkaloids, terpenes, lignans, neolignans, flavonoids and macrolides, is called natural products chemistry. The natural products described in this dissertation are all secondary metabolites.

1.1.2 The sources of natural products

A major source of natural products is plants, which have been used as medicines for thousands of years.[2] Many important natural products, like morphine **1.1**, paclitaxel **1.2**, quinine **1.3** and artemisin **1.4**, were isolated from the plants. The important analgesic morphine **1.1** is a constituent of the resin of *Papaver somniferum* L. (opium poppy), and was first isolated in 1803. *P. somniferum* is probably native to the Eastern Mediterranean, and its resin was used as a medicine by Sumerians and ancient Greeks thousands of years ago.[2] Paclitaxel **1.2** was isolated from the bark of *Taxus brevifolia* (Pacific Yew) in 1971;[3] it is now a major anticancer drug. The Pacific Yew is a conifer native to the Pacific Northwest of North America. Quinine **1.3** was first isolated from *Cinchona* bark in 1817.[4] *Cinchona* species are native to the tropical Andean forests of western South America, and its bark has been used for treating fevers and malaria by the Peruvians for many centuries. Artemisin **1.4** was isolated from *Artemisia annua, L.* in 1972.[5] This plant is native to temperate Asia and was used in

traditional Chinese medicine for treatment of chills and fever. It is now the most effective available antimalarial agent in current use.

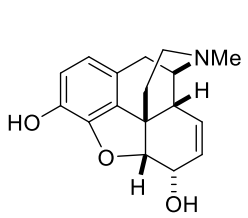

1.1

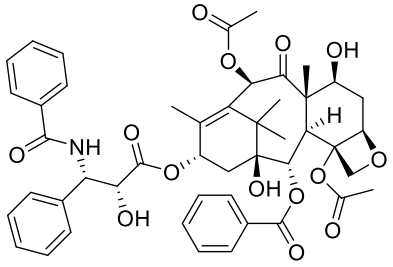

1.2

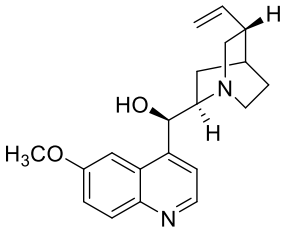

1.3

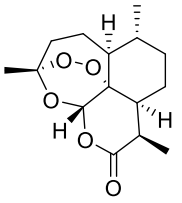

1.4

Another source of natural products is fungi. For example, penicillin G **1.5** and the anticancer agent doxorubicin **1.6** were both isolated from fungi. Penicillin G **1.5** was isolated from *Penicillium notatum*, and was the first truly effective antibiotic.[6-7] Doxorubicin **1.6** was isolated from *Streptomyces peucetius* subspecies caesius, which was obtained by mutagenic treatment of *S. pencetius*.[8]

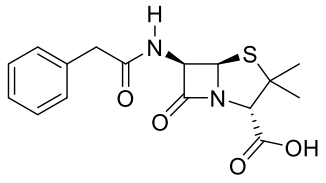

1.5

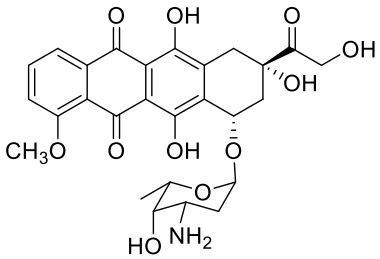

1.6

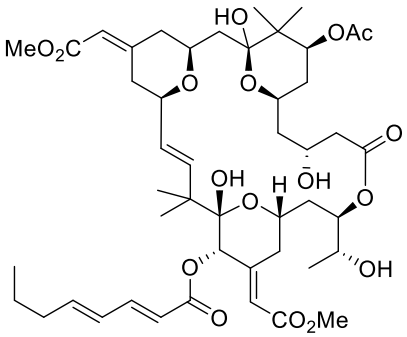

1.7

There are also some natural products from marine organisms, such as algae, sponges, ascidians, tunicates and bryozoans. For example, the potent cytotoxic agent bryostatin 1 **1.7** was isolated from the bryozoan *Bugula neritina* in 1982.[9]

1.1.3 The structures of natural products

The structures of natural products are varied, since they are derived from complex and diverse pathways in organisms. For example, terpenes are derived from the mevalonate

pathway, polyketides, long chain fatty acids, macrolides, and anthraquinones are derived from the acetate pathway, flavonoids are derived from mixed shikimate and acetate pathways, and lignans, neolignans and coumarins are derived from the shikimate pathway. Alkaloids are derived from amino acids in combination with acetate or shikimate pathways, while yet other natural products are produced by combinations of three different biosynthetic pathways.

1.2 Introduction to bioactivities of natural products

The diversity of natural products' structures lead to a diversity of natural products' bioactivities. And some natural products with the best bioactivities are used as drugs, as noted in section **1.1.2**. This dissertation is about the isolation of antiplasmodial natural products from plants.

1.2.1 Antiplasmodial natural products

Malaria is a serious and widespread disease, and is estimated to have caused 429,000 deaths in 2016.[10] Quinine **1.3** was the first effective antimalarial drug. In the 1930's, chloroquine **1.8**, which is also very effective in the treatment of malaria, was discovered as an analog of quinine **1.3**. But by the 1960's, the *Plasmodium* parasite developed resistance to chloroquine, and today resistant plasmodia strains are widely spread all over the world. The major antimalarial drug used today is artemisin **1.4**, which is usually used as part of an artemisinin-based combination therapy (ACT).[11] However, the malaria parasite *P. falciparum* has developed significant resistance to artemisinin in mainland Southeast Asia, although a 6-day course of treatment, as opposed to the normal 3-day course, is still effective in most cases.[12] There is thus a continuing need for the discovery of new and effective antimalarial drugs.

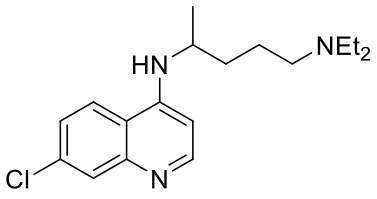

1.8

1.2.2 Antiplasmodial bioassay

The discovery of new antiplasmodial natural products uses the method of bioguided isolation and identification of the bioactive compounds in a complex mixture of natural plant products. The antiplasmodial bioassay necessary for this work was performed by Dr. Maria B. Cassera and her laboratory. The assay uses the *Plasmodium falciparum* Dd2 chloroquine-resistant strain for evaluation of the antiplasmodial activities of different fractions and isolated compounds. In this assay, the first step is to add blood, parasites and several concentrations of each sample into selected wells of a 96-well plate. The same is done with the positive control (artemisinin **1.4**). The negative control is dimethyl sulfoxide (DMSO). After 72 hours of incubation, the fluorescent tag SYBR Green I **1.9** is added to bind to the DNA of parasites. SYBR Green I **1.9** has low initial fluorescence and strong fluorescence after binding to DNA. Since the host erythrocytes lack DNA, the resulting fluorescence is determined by the amount of SYBR Green I **1.9** complexed with parasite DNA. Different intensities of fluorescence mean different quantities of DNA and thus different percentages of inhibition. The stronger the fluorescence, the lower the inhibition. The IC_{50} values (the concentration of compound or extract needed to inhibit the growth of the parasite by 50%) are then calculated from dose-response curves.[13]

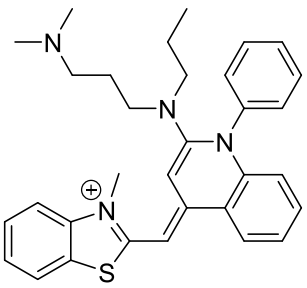

1.9

1.2.3 Antiproliferative bioassay

The antiproliferative bioassay was performed in the Kingston laboratory. This assay can be used to test a compound's antiplasmodial selectivity by evaluating its cytotoxicity using the A2780 human ovarian cancer cell line. The A2780 cells are adherent cells, so they are added first into a 96–well plate. After 4 hours for the cells to attach to the well, several concentrations of each sample are added with paclitaxel **1.2** as a positive control and DMSO as a negative control. After 48 hours incubation, the medium is treated with the fluorescent tag Alamar Blue **1.10**, which is reduced to a fluorescent species by uninhibited cells (Figure **1-1**). Then fluorescence is observed after 3–4 hours, and a dose–response curve allows calculation of IC_{50} values.[14]

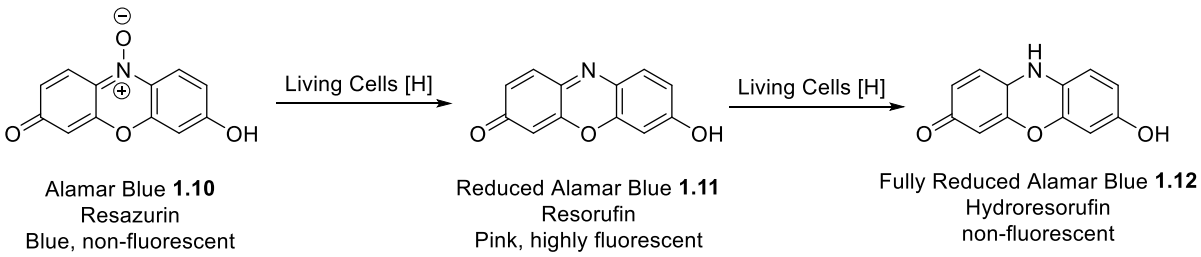

Figure 1-1. Reduction of resazurin **1.10** to resorufin **1.11** and even further reduction to hydroresorufin **1.12**

1.3 Methods of isolation

1.3.1 Bioguided isolation

Bioguided isolation focuses on the isolation of the bioactive compounds. After initial screening of the crude plant extracts, the active ones are chosen for fractionation. After liquid–liquid partition and open column separation, active fractions are selected for isolation of pure active compounds by high performance liquid chromatography (HPLC). Typically, the fractions which are obtained with an IC_{50} value of < 10 μg/mL after liquid-liquid partition and those obtained after separation on a open column or by HPLC with an IC_{50} value of < 5 μg/mL are thought to be worthy for isolation.[4]

1.3.2 Sources of plant extracts

The plant extracts were initially collected by the Merck company, and were then donated to the Natural Products Discovery Institute (NPDI). A second source of extracts was the ICBG (International Cooperative Biodiversity Group) library, prepared from plants collected in Madagascar. In this dissertation, Chapter 5 is about the isolation of compounds from an extract from the ICBG library. Other extracts mentioned in this dissertation were all from the NPDI library, which includes more than 22,000 plant extracts.

1.3.3 Liquid–liquid partition

Liquid–liquid partition is typically the first step for the separation of ethanolic extracts. Liquid–liquid partition allowed separation of the extract into a hexanes fraction of non-polar compounds, a dichloromethane fraction with mid-polar compounds and a water/methanol fraction with polar compounds. The colors of the hexanes, dichloromethane and water/methanol fractions were green, yellow and reddish brown in all the extracts investigated. In some case, the NPDI supplied a prefractionated dichloromethane extract, and initial liquid-liquid partition was not necessary.

1.3.4 Thin layer chromatography

Thin layer chromatography (TLC) is a very useful method to figure out the best solvent systems for open column chromatography, solid phase extractions and HPLC. It also could be used for separation of small fractions. The standard solvent systems for TLC of the hexane, dichloromethane, and water/methanol fractions are respectively hexane:acetone 9:1 for the hexane fraction, hexane:acetone 7:3 for the dichloromethane fraction, and dichloromethane: methanol 20:1 for the aqueous methanol fraction. Then according to the distributions of spots on the TLC plate, the contents of the different solvents could be changed to find the best solvent system for each fraction. The best solvent system for developing TLC plates is one that separates the spots as far as possible on the TLC plate, but the best solvent system for transfer to an open column is one that moves most of the spots on the bottom half of the TLC plate, with the best R_f values being between 0.3 and 0.5.

1.3.5 Open column liquid chromatography

Liquid chromatography is a common method for separation of plant constituents after liquid–liquid partition. Depending on the nature of the fraction, the stationary phase can be normal phase (silica gel) or reverse phase (C_{18}), which are used for separation of compounds with different polarities, or size exclusion (Sephadex LH-20) which is used for separation of compounds with different polarities and molecular weights, or a polyaromatic adsorbent resin (Diaion HP-20) which can be used for separation of glucosides and similar compounds, such as saponins. For example, Sephadex LH-20 is normally used for separation of complex hexanes and DCM fractions, while Diaion HP-20 is used for separation of water/methanol fractions, because these fractions usually contain glucosides.

1.3.6 Solid phase extraction

Solid phase extraction (SPE) uses a short prepacked column to separate a fraction into several simpler subfractions. In addition, SPE removes most compounds that bind strongly to the column, and thus increases the lifespan of expensive HPLC columns.

1.3.7 High performance liquid chromatography

HPLC is a universal method for isolation of compounds due to its wide selections of mobile phase and stationary phase. Few compounds cannot be separated by HPLC. The normal detectors for HPLC are UV-visible detectors and evaporative light scattering detectors (ELSD). The UV-visible detector is useful with compounds which contain chromophores. The ELSD is a universal detector which vaporizes the mobile phase and measures light scattered by particles of a nonvolatile analyte. The solvent system for reverse phase (C-18 or phenyl-hexyl) HPLC is always a mixture of acetonitrile and water or methanol and water. The solvent system for normal phase (silica gel or Diol) HPLC is always a mixture of hexanes and *i*-propanol or dichloromethane and acetonitrile.

1.4 Methods of structural elucidation

After isolation of pure natural products, the next step is structural elucidation. The first step is to calculate the molecular composition of a new compound using high resolution mass spectrometry. This is followed by determination of the atom connectivity, using various Nuclear magnetic resonance spectroscopy (NMR) methods, and finally the relative and absolute configurations need to be established.

1.4.1 High resolution electrospray mass spectrometry

High resolution electrospray ionization mass spectrometry (HRESIMS) is used to determine the compound's formula. The sample is ionized in an electric field to produce several ions. Then the ions are analyzed by using their mass-to-charge ratios to calculate their exact mass. The compounds always show protonated molecular ions and sodium adduct ions in the $ESI^{+}MS$. From the MS data, the molecular composition and the degree of unsaturation can be calculated.

1.4.2 Nuclear magnetic resonance spectroscopy

NMR is the primary method to determine the structures of natural products. ^{1}H and ^{13}C NMR are used to detect protons and carbons in different chemical and magnetic environments, since they show different chemical shifts in the NMR spectrum. Heteronuclear Single Quantum Correlation (HSQC) identifies which protons are directly attached to which carbons in the molecule. It also can distinguish methyl, methylene and methine groups. Heteronuclear Multiple Bond Correlation (HMBC) detects protons separated from carbon nuclei by two or three chemical bonds, and it is helpful in connecting substructures to assemble a complete planar structure. Nuclear Overhauser Effect Spectroscopy (NOESY) detects pairs of protons which are less than 4 Å apart in space. The configurations of double bonds and the relative configurations between two chiral centers can often be confirmed through NOESY.

1.4.3 Electronic circular dichroism

Electronic circular dichroism (ECD) is used to confirm the absolute configuration when a molecule contains one or more chiral chromophores, because the molar extinction coefficients of chiral chromophores for left circularly polarized light and right circularly

polarized light are different. This change in the ECD spectrum is known as the Cotton effect. Different absolute configurations show different Cotton effects.

1.4.4 Dereplication

Dereplication is the process of quickly identifying known compounds so as to focus efforts on new and novel compounds. Isolated natural products are examined by HRESIMS and ^{1}H NMR spectroscopy, and then the Dictionary of Natural Prodaucts (DNP) or Scifinder databases are searched to confirm them as new or known.[15] This process allows work to be concentrated on new bioactive compounds.

1.5 References

1. Anonymous All Natural. *Nat. Chem. Biol.* **2007,** *3* (7), 351.

2. Dias, D. A.; Urban, S.; Roessner, U. A Historical Overview of Natural Products in Drug Discovery. *Metabolites* **2012,** *2,* 303–336.

3. Wani, M. C.; Taylor, H. L.; Wall, M. E.; Coggon, P.; McPhail, A. T. Plant Antitumor Agents. 6. Isolation and Structure of Taxol, a Novel Antileukemic and Antitumor Agent from *Taxus brevifolia*. *J. Am. Chem. Soc.* **1971,** *93* (9), 2325–2327.

4. Batista, R.; Silva, A. D.; de Oliveira, A. B. Plant-Derived Antimalarial Agents: New Leads and Efficient Phytomedicines. Part II. Non-Alkaloidal Natural Products. *Molecules* **2009,** *14* (8), 3037–3072.

5. Balint, G. A. Artemisinin and its Derivatives - An Important New Class of Antimalarial Agents. *Pharmacol. Ther.* **2001,** *90* (2–3), 261–265.

6. Schnitzer, R. J.; Camagni, L. J.; Buck, M. Resistance of Small Colony Variants (G Forms) of a Staphylococcus towards the Bacteriostatic Activity of Penicillin. *Proc. Soc. Exp. Biol.*

Med. **1943,** *53* (1), 75–78.

7. Van Den Broek, P. J. Activity of Antibiotics against Microorgnisms Ingested by Mononuclear Phagocytes. *Eur. J. Clin. Microbiol. Infect. Dis.* **1991,** *10* (2), 114–118.

8. Arcamone, F.; Cassinel.G; Fantini, G.; Grein, A.; Orezzi, P.; Pol, C.; Spalla, C. Adriamycin, 14-Hydroxydaunomycin, a New Antitumor Antibiotic from *S. peucetius* var. *caesius*. *Biotechnol. Bioeng.* **1969,** *11* (6), 1101–1110.

9. Pettit, G. R.; Herald, C. L.; Doubek, D. L.; Herald, D. L.; Arnold, E.; Clardy, J. Anti-Neoplastic Agents. 86. Isolation and Structure of Bryoststin-1. *J. Am. Chem. Soc.* **1982,** *104* (24), 6846–6848.

10. Anonymous., *World Malaria Report 2017*. World Health Organization: Geneva, 2017; p 186.

11. Eastman, R. T.; Fidock, D. A. Artemisinin-Based Combination Therapies: a Vital Tool in Efforts to Eliminate Malaria. *Nature* **2009,** *7*, 864–874.

12. Ashley , E. A.; Dhorda , M.; Fairhurst , R. M.; Amaratunga , C.; Lim , P.; Suon , S.; Sreng , S.; Anderson , J. M.; Mao , S.; Sam , B.; Sopha , C.; Chuor , C. M.; Nguon , C.; Sovannaroth , S.; Pukrittayakamee , S.; Jittamala , P.; Chotivanich , K.; Chutasmit , K.; Suchatsoonthorn , C.; Runcharoen , R.; Hien , T. T.; Thuy-Nhien , N. T.; Thanh , N. V.; Phu , N. H.; Htut , Y.; Han , K.-T.; Aye , K. H.; Mokuolu , O. A.; Olaosebikan , R. R.; Folaranmi , O. O.; Mayxay , M.; Khanthavong , M.; Hongvanthong , B.; Newton , P. N.; Onyamboko , M. A.; Fanello , C. I.; Tshefu , A. K.; Mishra , N.; Valecha , N.; Phyo , A. P.; Nosten , F.; Yi , P.; Tripura , R.; Borrmann , S.; Bashraheil , M.; Peshu , J.; Faiz , M. A.; Ghose , A.; Hossain , M. A.; Samad , R.; Rahman , M. R.; Hasan , M. M.; Islam , A.; Miotto , O.; Amato , R.;

MacInnis , B.; Stalker , J.; Kwiatkowski , D. P.; Bozdech , Z.; Jeeyapant , A.; Cheah , P. Y.; Sakulthaew , T.; Chalk , J.; Intharabut , B.; Silamut , K.; Lee , S. J.; Vihokhern , B.; Kunasol , C.; Imwong , M.; Tarning , J.; Taylor , W. J.; Yeung , S.; Woodrow , C. J.; Flegg , J. A.; Das , D.; Smith , J.; Venkatesan , M.; Plowe , C. V.; Stepniewska , K.; Guerin , P. J.; Dondorp , A. M.; Day , N. P.; White , N. J. Spread of Artemisinin Resistance in *Plasmodium falciparum* Malaria. *New Engl. J. Med.* **2014,** *371* (5), 411–423.

13. Smilkstein, M.; Sriwilaijaroen, N.; Kelly, J. X.; Wilairat, P.; Riscoe, M. Simple and Inexpensive Fluorescence-based Technique for High-throughput Antimalarial Drug Screening. *Antimicrob. Agents Chemother.* **2004,** *48* (5), 1803–1806.

14. Cao, S.; Brodie, P. J.; Miller, J. S.; Randrianaivo, R.; Ratovoson, F.; Birkinshaw, C.; Andriantsiferana, R.; Rasamison, V. E.; Kingston, D. G. I. Antiproliferative Xanthones of *Terminalia calcicola* from the Madagascar Rain Forest. *J. Nat. Prod.* **2007,** *70* (4), 679–681.

15. Pauli, G. F.; Chen, S. N.; Lankin, D. C.; Bisson, J.; Case, R. J.; Chadwick, L. R.; Godecke, T.; Inui, T.; Krunic, A.; Jaki, B. U.; McAlpine, J. B.; Mo, S. Y.; Napolitano, J. G.; Orjala, J.; Lehtivarjo, J.; Korhonen, S. P.; Niemitz, M. Essential Parameters for Structural Analysis and Dereplication by ^{1}H NMR Spectroscopy. *J. Nat. Prod.* **2014,** *77* (6), 1473–1487.

Chapter 2: Antiplasmodial Sesquiterpenoid Lactones from *Trichospira verticillata*

This chapter is a slightly expanded version of a published article.[1] (Du, Y.; Pearce, K. C.; Dai, Y.; Krai, P.; Dalal, S.; Cassera, M. B.; Goetz, M.; Crawford, T. D.; Kingston, D. G. I. Antiplasmodial Sesquiterpenoid Lactones from *Trichospira verticillata*: Structure Elucidation by Spectroscopic Methods and Comparison of Experimental and Calculated ECD Data. *J. Nat. Prod.* **2017,** 80, 1639−1647.) Author contributions of the articles are described as follows in the order of the names listed. The author of this dissertation (Mr. Yongle Du) conducted the isolation and structural elucidation part of the isolated compounds, performed the A2780 bioassay on the isolated compound **2.4**, and drafted the manuscript. Mr. Kirk C. Pearce calculated the ECD and UV spectra, internuclear distances, dihedral angles and specific rotations of the isolated compounds under the direction of Dr. T. Daniel Crawford. Dr. Yumin Dai was a mentor for this work, and provided some important hints for the isolation and structural elucidation of the compounds, and he also proofread the manuscript before submission. Dr. Priscilla Krai and Dr. Seema Dalal carried out the antiplasmodial bioassay and the cytotoxicity bioassay against the normal cell line HEK293 (human embryonic kidney) under the direction of Maria B. Cassera. Dr. Michael Goetz from the Natural Products Discovery Institute (NPDI) provided the plant extract from the NPDI repository. Dr. David G. I. Kingston was a mentor for this work and the corresponding author for the published article. He also edited the final manuscript.

2.1 Introduction

2.1.1 Abstract

A dichloromethane extract of *Trichospira verticillata* (Asteraceae) from the Natural Products Discovery Institute was discovered to have good antiplasmodial activity (IC_{50} ~ 5 μg/mL). After purification by liquid-liquid partition and C_{18} reverse phase HPLC, four new germacranolide-type sesquiterpenoid lactones named trichospirolides A–D **(2.1**–**2.4)** were isolated. The structures of the new compounds were elucidated by analysis of their 1D and 2D NMR and MS data. The relative and absolute configurations were assigned based on a comparison of calculated and experimental ECD and UV spectra, specific rotations, internuclear distances, and coupling constants for all possible diastereomers for each compound. Among these four compounds, the conjugated dienone **2.1** displayed the most potent antiplasmodial activity, with an IC_{50} value of 1.5 μM.

2.1.2 Investigations of the genus *Trichospira*

Trichospira verticillata is the only species in the genus *Trichospira*, and is found in wetlands and pine savannas in the Atlantic regions of tropical South America and Cuba.[2] The phytochemistry of *T. verticillata* has not previously been investigated, and it was thus selected for bioassay-guided fractionation to isolate its antiplasmodial components.

2.2 Results and Discussion

2.2.1 Isolation of active compounds

A dichloromethane extract of the whole plant of *T. verticillata* was subjected to liquid-liquid partition to afford active hexanes and methanol fractions, with IC_{50} values against the drug-resistant Dd2 strain of *Plasmodium falciparum* of about 3 and 7 μg/mL,

respectively. The hexanes fraction was directly separated by C_{18} reverse-phase HPLC to yield four novel germacranolide-type sesquiterpenoid lactones which were named trichospirolides A–D (**2.1**–**2.4)**.

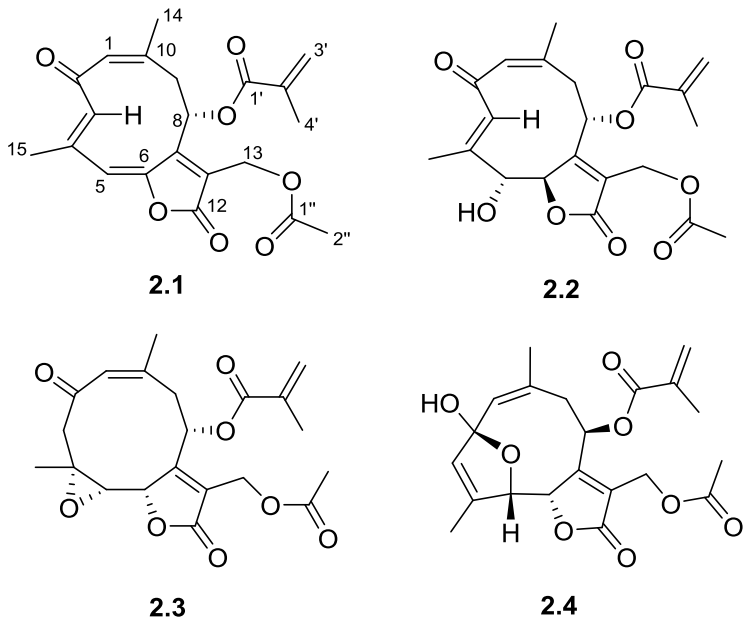

2.2.2 Structure elucidation of isolated compounds

Trichospirolide A (**2.1**) was isolated as a yellow powder. Its positive ion HRESIMS data revealed a peak for a protonated molecular ion at *m/z* 387.1441 and for a sodium adduct ion at *m/z* 409.1273, both corresponding to a molecular formula of $C_{21}H_{22}O_{7.}$ Its IR spectrum exhibited bands at 1773, 1749, 1723, and 1639 cm^{-1}, indicating the presence of three conjugated carbonyl groups, including two conjugated esters or lactones. Its UV spectrum, with absorptions at 298 and 252 nm, was consistent with dienone conjugation. The presence of an acetyl group was suggested by the ^{1}H NMR signal at δ_H 2.08 (H-2") and the ^{13}C NMR signals at δ_C 170.4 (C-1") and 20.9 (C-2"), and further confirmed by ^{2}J-HMBC cross-peaks between H-2" and C-1". Similarly, the ^{1}H NMR signals at δ_H 6.18 (H-3'a), 5.72 (H-3'b) and 1.96 (H-4') and the ^{13}C NMR signals at δ_C 165.9 (C-1'), 135.3 (C-2'), 127.5 (C-3') and 20.9

(C-4') indicated the presence of a methacryloyloxy group. The presence of this side group was also corroborated by ^{3}J-HMBC cross-peak between H-3'a and C-1', H-3'b and C-4', H-4' and C-1', and ^{2}J-HMBC correlation between H-3'b and C-2' (Table **2-1**).

Table 2-1. NMR Spectroscopic Data for Compound **2.1** in $CDCl_3$ (500 MHz)

Position.	δ_H, *J* in Hz	δ_C, type
1	6.12 s	131.9, CH
2		192.0, C
3a	6.57 s	135.1, CH
3b		
4		137.7, C
5	6.62 dd 1.0, 1.0	119.5, CH
6		147.9, C
7		153.5, C
8	5.95 d 8.0	73.0, CH
9a	3.48 d 16.0	40.5, CH_2
9b	2.86 dd 16.0, 8.0	
10		155.6, C
11		126.6, C
12		167.7, C
13a	5.01 d 12.5	55.6, CH_2
13b	4.91 d 12.5	
14	2.12 d 1.0	30.1, CH_3
15	2.08 dd 1.0, 1.0	17.3, CH_3
1'		165.9, C
2'		135.1, C
3'a	6.18 quint 1.0	127.5, CH_2
3'b	5.72 quint 1.0	
4'	1.96 dd 1.0, 1.0	20.9, CH_3
1"		170.4, C
2"	2.08 s	20.9, CH_3

The remaining fifteen carbons could be assigned to a germacranolide-type sesquiterpenoid skeleton by analysis of the 2D NMR spectroscopic data, including HSQC, and HMBC data.[3, 4] In particular, the presence of the 10 membered germacranolide ring was established by the HMBC cross-peaks between H-1 and C-3, H-3 and C-5, H-9 and C-1, H-5

and C-7, and H-8 and C-10. The C-14 and C-15 methyl carbons were assigned to C-10 and C-4, respectively, by observation of HMBC cross-peaks between H-1 and C-14, and H-3 and C-15. Moreover, HMBC cross-peaks between H-13 and C-7, as well as H-13 and the C-12 ester carbonyl carbon (δ_C 167.7), suggested the presence of an *α,β*-unsaturated lactone moiety located at C-6 (δ_C 147.9) and C-7. The acetoxy and methacryloyloxy substituents were determined to be attached to C-13 and C-8, respectively, based on the HMBC cross-peaks between H-13 and C-1'', and H-8 and C-1' (Figure **2-1**). The carbon–carbon double bonds in the 10 membered ring were assigned as 1(10)*Z* and 3*E* on the basis of a strong NOESY correlation between H-1 and H_3-14 and the absence of a strong correlation between H-3 and H_3-15. Strong correlations were also observed between H-3 and H-8 and between H-3 and H-9a (Figure **2-1**).

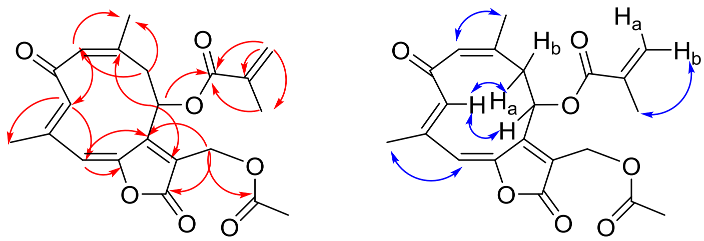

Figure 2-1. HMBC (red) and NOESY (blue) correlations for trichospirolide A **2.1**

The absolute configuration of trichospirolide A **2.1** was confirmed by a direct comparison of experimental and calculated ECD and UV spectra and specific rotations for all possible stereoisomers. Although the calculated and experimental data did not always agree completely, the differences between the data for the assigned structures and those with different configurations were large enough to give confidence in the correctness of the assigned structures.

In the case of trichospirolide A (**2.1**) the positive *π–π** Cotton effect at 248 nm ($\Delta\varepsilon_{237}$ = +19.2) could not be used to assign the absolute configuration of its single stereocenter

directly, since the simple rules proposed by Uchida and Kuriyame for the circular dichroism of α,β-unsaturated-γ-lactones[5] are not applicable in cases where there is an allylic oxygen substituent. Calculations of its ECD and UV spectra and optical rotations were carried out for the *S* enantiomer of trichospirolide A (**2.1**). The weighted average distances between hydrogens for the lowest energy conformers (Boltzmann population > 2 %) of the *S* enantiomer were calculated for comparison with the observed NOESY correlations, and the ECD and UV spectra and specific rotation were calculated from additional data.

Table 2-2. Calculated Internuclear Distances and NOESY Signal Strength for **2.1**

Proton Pair	Weighted average distance (Å)	NOESY intensity
H5-H15	3.19	medium
H3-H9a	1.94	strong
H3-H8	2.65	strong
H1-H14	3.01	medium
H8-H15	3.85	medium

The results of these calculations are shown in Figure **2-2** and Table **2-2**. The calculated and experimental ECD spectra for trichospirolide A (**2.1**) agree reasonably well, although the calculated maxima and minima are shifted to longer wavelengths as compared with the experimental data; this may be a result of the extended conjugation in trichospirolide A (**2.1**). The calculated internuclear distances also agree well with the observed NOESY signal strengths, giving added assurance to the correctness of the calculated conformations (Table **2-2**). In a final comparison, the experimental and calculated specific rotations of trichospirolide A **2.1** (–360º and –1,141º respectively) agreed with each other in sign, although not in magnitude. The reason for this can be understood from the UV spectra shown in Figure **2-2**, which show significantly longer wavelength absorptions than observed for compounds **2.2**–**2.4**. The calculated absorption around 367 nm lies close enough to the polarized light

wavelength of 589 nm such that the computed rotation is overestimated. This phenomenon has been described previously.[6] Based on these data the structure of trichospirolide A (**2.1**) was assigned as 1(10)*Z*,3*E*,5*E*,7(12)*Z*-(8*S*)-13-acetoxy-8-methacryloyloxy-2-oxogermacra-1,3,5,7-tetraen-6,12-olide.

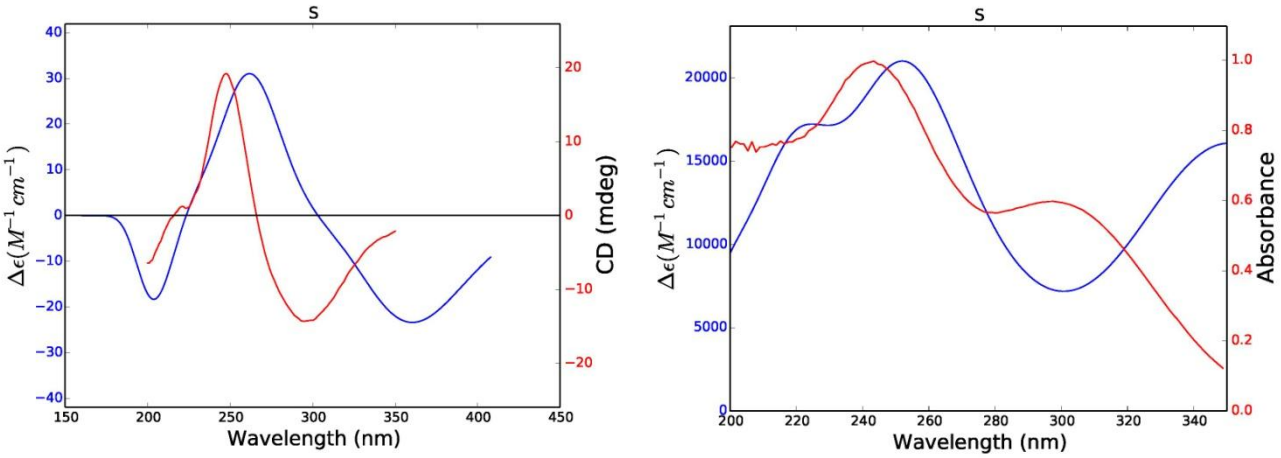

Figure 2-2. Comparison of experimental (red) and calculated (blue) ECD (left) and UV (right) spectra of trichospirolide A (**2.1**).

Trichospirolide B (**2.2**) was isolated as a yellow powder. Its positive ion HRESIMS revealed a peak for a protonated molecular ion at *m/z* 405.1561 and for a sodium adduct ion at *m/z* 427.1389, both corresponding to a molecular formula of $C_{21}H_{24}O_8$. Its IR spectrum exhibited an additional absorption at 3430 cm^{-1} as compared with the spectrum of trichospirolide A (**2.1**), indicating the presence of a hydroxy group, and this coupled with the difference of 18 Daltons between the molecular weights of trichospirolide A (**2.1**) and trichospirolide B (**2.2**) suggested that trichospirolide B (**2.2**) might be a hydration product of trichospirolide A (**2.1**). The UV spectrum of trichospirolide B (**2.2**) had its longest wavelength absorption at 247 nm, consistent with an enone function. Hydration of the C-5 double bond in trichospirolide A (**2.1**) was confirmed by the shielding of the chemical shifts

of C-5 and C-6 from δ_C 119.5 (CH) and 147.9 (C) in **2.1** to δ_C 80.6 (CH) and 86.3 (CH), respectively, in trichospirolide B (**2.2**). The ^{1}H and ^{13}C NMR data of trichospirolide B (**2.2**) (Table **2-3**) were similar to those of trichospirolide A (**2.1**) except as noted above, and were fully consistent with its structural assignment as a hydrate of trichospirolide A (**2.1**) with the hydroxy group at C-5. This assignment was confirmed by the HMBC cross-peaks shown in Figure **2-3**.

Table 2-3. NMR Spectroscopic Data for Compound **2.2** in $CDCl_3$ (500 MHz)

Position.	δ_H, *J* in Hz	δ_C, type
1	6.08 s	131.6, CH
2		194.0, C
3a	6.28 s	131.8, CH
3b		
4		138.7, C
5	4.19 d 8.8	80.6, CH
6	5.43 d 8.8	86.3, CH
7		163.2, C
8	4.98 d 8.0	73.1, CH
9a	3.37 dd 8.0, 15.2	38.9, CH_2
9b	2.76 d 15.2	
10		155.5, C
11		126.9, C
12		170.4, C
13a	4.87 d 12.4	55.4, CH_2
13b	4.82 d 12.4	
14	2.08 s	28.5, CH_3
15	1.94 d 1.0	13.5, CH_3
1'		166.6, C
2'		135.0, C
3'a	6.14 quint 1.0	127.7, CH_2
3'b	5.70 quint 1.0	
4'	1.93 dd 1.0, 1.0	18.2, CH_3
1"		170.5, C
2"	2.06 s	20.9, CH_3

The carbon–carbon double bonds in the 10 membered ring were assigned as 1(10)*Z* and 3*E* on the basis of NOESY crosspeaks between H-1 and H_3-14, and H-3 and H-5, and the absence of a strong crosspeak between H-3 and H_3-15 (Figure **2-3**). The vicinal coupling constant $^3J_{5,6}$ of 8.8 Hz was consistent with a H5-C5-C6-H6 dihedral angle in the 5º–25º or the 130º–150º range by Karplus equation.[7]

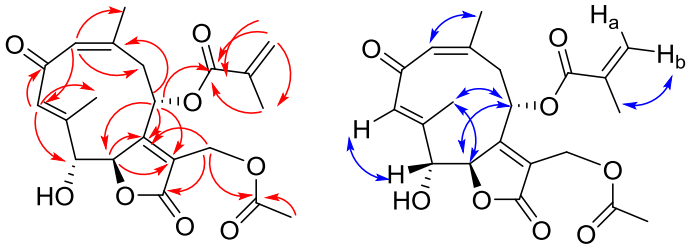

Figure 2-3. HMBC (red) and NOESY (blue) correlations for trichospirolide B **2.2**

The relative and absolute configurations of trichospirolide B (**2.2**) were established by comparison of experimental and calculated ECD and UV spectra. Calculations for trichospirolide B (**2.2**) were carried out for its *RRR*, *RSR*, *SRR*, and *SSR* diasatereomers. The calculated ECD and UV spectra for the *RRS* diastereomer of trichospirolide B (**2.2**) gave the best agreement with the experimental data (Figure **2-4**) and with one exception the calculated internuclear distances also agree well with the observed NOESY signal strengths (Table **2-4**).

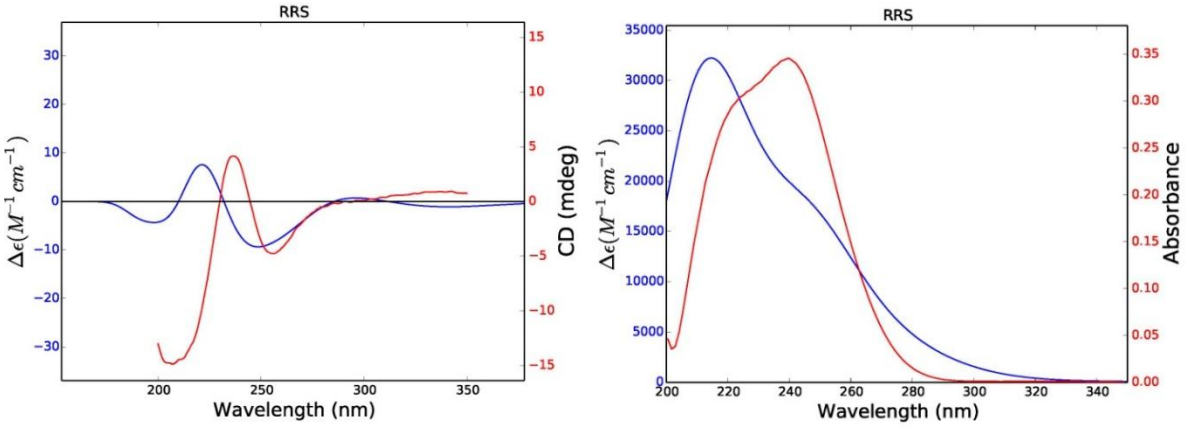

Figure 2-4. Comparison of experimental (red) and calculated (blue) ECD (left) and UV (right) spectra of trichospirolide B (**2.2**)

Table 2-4. Calculated Internuclear Distances and NOESY Signal Strength for **2.2**

Proton Pair	Weighted average distance (Å)	NOESY intensity
H3-H9a	2.16	strong
H3-H9b	3.86	medium
H3-H5	3.71	strong
H3-H8	3.26	v. weak
H1-H14	3.02	medium
H3'b-H4'	3.15	medium
H6-H15	4.72	medium
H6-H8	3.35	medium
H8-H15	3.01	strong
H5-H15	2.93	weak

The coupling constants for three key dihedral angles of the *RRS* enantiomer were also in agreement with this configuration (Table **2-5**), while the experimental and calculated specific rotations of this diastereomer (–140º and –221º respectively) agreed with each other in sign and reasonably well in magnitude. Based on these data, trichospirolide B (**2.2**) is assigned the structure 1(10)*Z*,3*E*,7(11)*Z*-(5*R*,6*R*,8*S*)-13-acetoxy-5-hydroxy-8-methacryloyloxy-2-oxo-germacra-1(10),3,7(11)-trien-6,12-olide.

Table 2-5. Calculated Dihedral Angles and *J*-values for **2.2**

Dihedral	Weighted average dihedral angle	Observed *J* value
H5-C5-C6-H6	–164.3º	8.8
H8-C8-C9-H9a	–88.6º	0
H8-C8-C9-H9b	156.9º	8.0

Trichospirolide C (**2.3**) had the molecular formula $C_{21}H_{24}O_8$ as determined by HRESIMS. Inspection of ^{1}H and ^{13}C NMR spectroscopic data of trichospirolide C **2.3** in comparison with those of trichospirolide B **2.2** (Table **2-6**) indicated that trichospirolide C (**2.3**) was also a germacranolide-type sesquiterpenoid lactone, with a similar structure to trichospirolide B (**2.2**). However, the C-3 and C-4 signals were shifted from δ_C 131.8 (CH) and 138.7 (C) in Trichospirolide B (**2.2**) to δ_C 52.9 (CH_2) and 56.9 (C) ppm in trichospirolide

C (**2.3**), indicating that the alkene group of trichospirolide B (**2.2**) was not present in trichospirolide C (**2.3**). The absence of an OH stretching frequency in the IR spectrum of trichospirolide C (**2.3**), together with the ^{13}C chemical shift of C-4, indicated the presence of an epoxide unit involving C-4 and C-5.[8] The vicinal coupling constant $^{3}J_{5,6}$ of 8.3 Hz was consistent with a H5-C5-C6-H6 dihedral angle in the 5º–25º or the 130º–150º range.[7] The HMBC and NOESY cross-peaks of trichospirolide C **2.3** (Figure **2-5**) supported the structural assignment; in particular the 1(10) *Z* double bond configuration was assigned on the basis of the H-1/H_3-14 NOESY cross-peak.

Table 2-6. NMR Spectroscopic Data for Compound **2.3** in $CDCl_3$ (500 MHz)

Position.	δ_H, *J* in Hz	δ_C, type
1	6.07 p 1.0	130.6, CH
2		201.0, C
3a	2.93 d 11.4	52.9, CH_2
3b	2.41 dd 11.4, 1.0	
4		56.9, C
5	2.86 d 9.3	60.4, CH
6	4.94 d 9.3	81.0, CH
7		162.6, C
8	5.10 t 6.7	67.8, CH
9a	3.18 dd 14.8, 6.7	36.3, CH_2
9b	2.70 dd 14.8, 6.7	
10		143.0, C
11		126.4, C
12		171.0, C
13a	4.87 s	55.2, CH_2
13b	4.87 s	
14	1.86 d 1.0	25.7, CH_3
15	1.70 s	19.6, CH_3
1'		166.4, C
2'		135.0, C
3'a	6.15 quint 1.0	127.8, CH_2
3'b	5.70 quint 1.0	
4'	1.93 dd 1.0,1.0	20.9, CH_3
1"		170.3, C
2"	2.06 s	20.9, CH_3

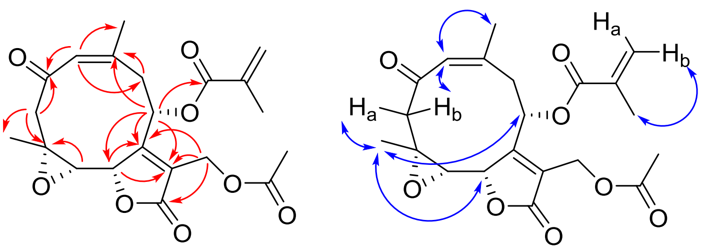

Figure 2-5. HMBC (red) and NOESY (blue) correlations for trichospirolide C **2.3**

Using the same procedure as above, the distance and energy data of the lowest energy conformations (Boltzmann population > 2%) of the *RRRR*, *RRSR*, *RSRR*, *RSSR*, *SRRR*, *SRSR*, *SSRR*, and *SSSR* diastereomers of trichospirolide C (**2.3**) were used to calculate weighted average internuclear distances and ECD and UV spectra; the resulting data were only consistent with the *RSSS* diastereomer of trichospirolide C (**2.3**). The experimental and calculated ECD and UV spectra for this diastereomer are shown in Figure **2-6**, and the calculated key internuclear distances and NOESY data are shown in Table **2-7**.

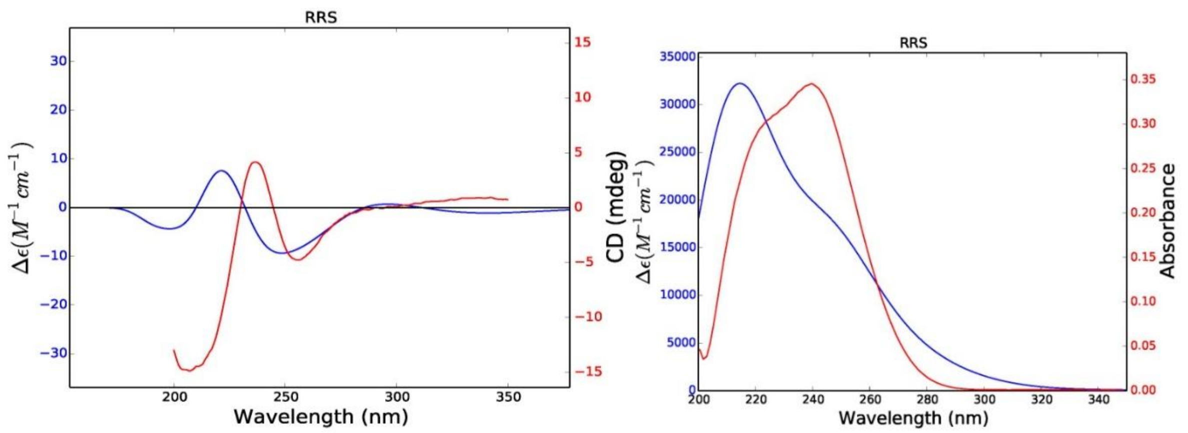

Figure 2-6. Comparison of experimental (red) and calculated (blue) ECD (left) and UV (right) spectra of trichospirolide C (**2.3**)

The calculated internuclear distances agree reasonably well with the observed NOESY correlations, although two correlations were observed with greater intensity than would have been expected from the calculated distances. The $^{3}J_{5,6}$ value of 9.3 Hz supports the assigned structure, which has a calculated dihedral angle of –24.6º (Table **2-8**). The experimental and calculated specific rotations of trichospirolide C **2.3** (–55.2º and –58.0º respectively) agreed

with each other in sign and in magnitude. Trichospirolide C **2.3** was thus assigned as 1(10)*Z*,7(11)*Z*-(4*R*,5*S*,6*S*,8*S*)-13-acetoxy-4,5-epoxy-8-methacryloyloxy-2-oxogermacra-1,7-dien-6,12-olide. It is structurally related to glaucolide E, whose structure was confirmed by X-ray crystallography.[9] It differs from glaucolide E by the configurations of the 1(10) double bond and the 4,5-epoxide, and by having a carbonyl group at C-2 instead of the acetoxy group of glaucolide E.

Table 2-7. Calculated Internuclear Distances and NOESY Signal Strength for **2.3**

Proton Pair	Weighted average distance (Å)	NOESY Intensity
H1-H14	3.03	medium
H1-H3a	3.65	medium
H1-H3b	3.81	medium
H8-H15	4.65	strong
H6-H15	4.44	strong
H3a-H15	3.16	strong
H3b-H5	3.81	strong

Table 2-8. Calculated Dihedral Angle and *J*-value for **2.3**

Dihedral	Weighted average dihedral angle	Observed *J* value
H5-C5-C6-H6	–24.6º	9.3

.

Trichospirolide D (**2.4**) was also isolated as a yellow powder. Its HRESIMS data showed peaks for protonated and sodium adduct molecular ions corresponding to the molecular formula $C_{21}H_{24}O_8$. Comparison of ^{1}H and ^{13}C NMR spectroscopic data of trichospirolide D (**2.4**) with those of trichospirolide B (**2.2**) (Table **2-9**) indicated that both compounds had the same skeleton, as well as acetoxy and methacryloyloxy groups. However, the carbon signal for C-2 of trichospirolide D (**2.4**) was shifted from 194.0 ppm in trichospirolide B (**2.2**) to 108.7 ppm in trichospirolide D (**2.4**), accompanied by a shielding of the ^{1}H NMR signals for

H-1, H-3 and H-5, suggesting the conversion of a carbonyl group to a hemiacetal group.[10] HMBC cross-peaks (Figure **2-7**) confirmed the formation of a five-membered ring, with the oxygen of the hemiacetal unit connecting C-5 and C-2 (Figure **2-7**). The NOESY correlations of trichospirolide D **2.4** (Figure **2-7**) indicated that both the 1(10) and 3 double bonds were *Z* configured, based on the H-1/H_3-14 and H-3/H_3-15 NOESY cross-peaks. The H5-C5-C6-H6 dihedral angle was estimated to be approximately 35º–55º or 115º–135º based on the observed $^3J_{5,6}$ value of 4.5 Hz. Trichospirolide D (**2.4**) proved to be moderately unstable, and samples decomposed on storage at –23 ºC.

Table 2-9. NMR Spectroscopic Data for Compound **2.4** in $CDCl_3$ (500 MHz)

Position.	δ_H, *J* in Hz	δ_C, type
1	5.71 s	129.1, CH
2		108.7, C
3	5.53 dq 1.0, 2.0	127.8, CH
4		142.0, C
5	5.32 ddd 5.5, 2.0,1.0	84.0, CH
6	5.55 d 5.5	82.3, CH
7		171.3, C
8	5.51 t 3.3	73.3, CH
9a	3.12 ddd 15.6, 3.4,1.5	35.5, CH_2
9b	2.35 dd 15.6, 3.4	
10		142.0, C
11		123.4, C
12		167.3, C
13a	4.82 d 12.4	55.7, CH_2
13b	4.75 d 12.4	
14	1.89 d 1.6	26.3, CH_3
15	1.80 dd 2.0, 1.0	13.1, CH_3
1'		166.3, C
2'		135.4, C
3'a	6.17 quint 1.0	127.0, CH_2
3'b	5.68 quint 1.0	
4'	1.96 dd 1.0, 1.0	18.3, CH_3
1"		170.4, C
2"	2.05 s	20.9, CH_3

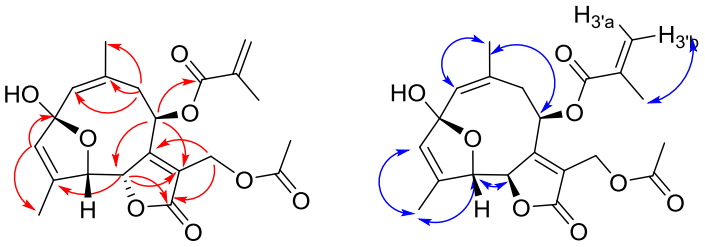

Figure 2-7. HMBC (red) and NOESY (blue) correlations for trichospirolide D **2.4**

The ECD and UV spectra and optical rotation of trichospirolide D (**2.4**) were calculated for its *RRRR, RRSR, RSRR, RSSR, SRRR, SRSR, SSRR, SSSR* diasteromers. In the event only the *SSSR* diasteromers gave data consistent with the experimental data (Figure **2-8**). Calculation of the weighted averages of key internuclear distances and comparison with NOESY data (Table **2-10**) also supported this assignment, as did the $^{3}J_{5,6}$ value of 5.5 Hz through the calculated H5-C5-C6-H6 dihedral angle of 54.3º. The experimental and calculated specific rotations of trichospirolide D **2.4** (–232.2º and –280.4º respectively) also agreed with each other in sign and magnitude. Based on these data, the structure of trichospirolide D **2.4** was assigned as 1(10)*Z*,3*Z*,7(11)*Z*-(2*S*,5*S*,6*S*,8*R*)-13-acetoxy-2,5-epoxy-2-hydroxy-8-*O*-methacryloyloxygermacra-1(10),3,7(11)-trien-6,12-olide, based on the good agreement of the spectroscopic data for this structure with the calculated data.

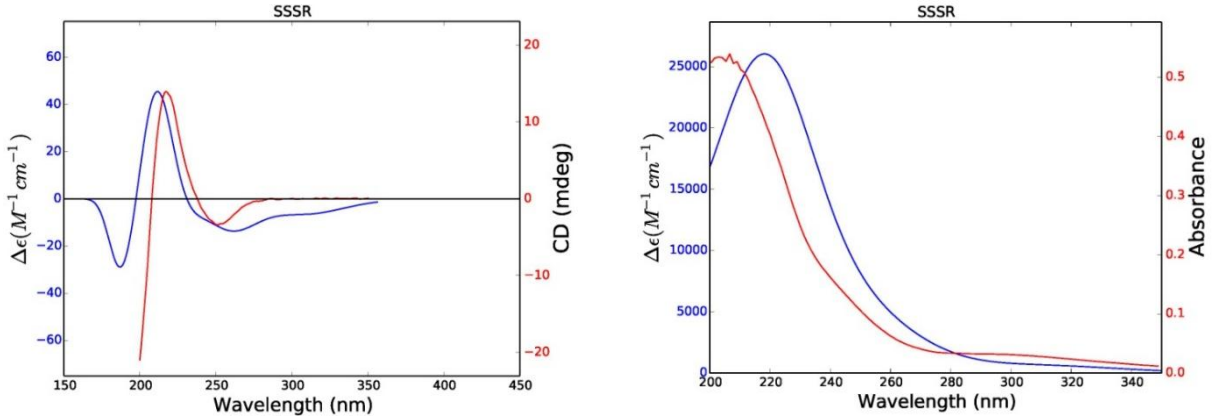

Figure 2-8. Comparison of experimental (red) and calculated (blue) ECD (left) and UV (right) spectra of trichospirolide D (**2.4**).

Table 2-10. Calculated Internuclear Distances and NOESY Signal Strength for **2.4**

Proton Pair	Weighted average distance (Å)	NOESY Intensity
H1-H14	3.03	medium
H3'b-H4'	3.15	medium
H3-H15	3.32	medium
H3-H9a	4.99	medium
H5-H15	3.35	medium

It is interesting to note that trichospirolide A–D **2.1**–**2.4** belong to two different stereochemical families, with **2.1**–**2.3** and **2.4** having the (8*S*) and (8*R*) configurations, respectively. In many cases a particular plant produces only one stereochemical series, as appears to be the case for instance with similar sesquiterpenoid lactones from *Eupatorium kiirunense*.[10] On the other hand, the existence of enantiomeric natural products is well documented,[11] and in particular both the *R* and *S* enantiomers of germacrene D are produced by Goldenrod (*Solidago canadensis*),[12] The production of both (8*R*) and (8*S*) isomers by *T. verticillata* is thus not an unprecedented event.

2.2.3 Bioactivities of isolated compounds

All the isolated compounds were tested for antiplasmodial activity against the Dd2 strain of *Plasmodium falciparum* and for toxicity to HEK293 cells. Trichospirolide A (**2.1**) showed moderate antiplasmodial activity, with an IC_{50} value of 1.5 μM, but it also showed similar toxicity to HEK293 cells and significant antiproliferative activity to A2780 ovarian cancer cells. Trichospirolides B–D (**2.2**–**2.4**) showed weak antiplasmodial activities, with IC_{50} values of 37.0, 12.1, and 44.3 μM, respectively, and correspondingly weak toxicity to HEK293 cells (Table **2-11**).

Table 2-11. Bioactivities of Compounds **2.1** – **2.4**

	2.1	**2.2**	**2.3**	**2.4**	Artemisinin	Paclitaxel
Dd2 (μM)	1.49 ± 0.29	37.05 ± 3.22	12.10 ± 0.45	44.33 ± 3.64	0.007	NT
HEK293 (μM)	3.5 ± 0.3	56.0 ± 7.8	23.8 ± 2.5	58.8 ± 1.6	NT	NT
A2780 (μM)	0.210 ± 0.003	NT	NT	NT	NT	0.028 ± 0.002

Sesquiterpenoid lactones are a series of well-known compounds, which have been reported to have various bioactivities, including antiplasmodial, antiproliferative, and antifungal activities.[13-15] Several bioactive germacranolide-type sesquiterpenoid lactones have been isolated recently, most often from the Asteraceae family.[16, 17] Previous structure-activity relationship studies indicated that the α,β-unsaturated γ-lactone unit, which could target cysteine residues in proteins by acting as a Michael acceptor, is important for the bioactivity of germacranolides.[18] This α,β-unsaturated γ-lactone unit is present in all four trichospirolides A–D, but their activities are varied due to modifications in the 10-membered ring. Trichospirolide A (**2.1**, *P. falciparum* IC_{50} 1.49 μM) was 25-fold more potent than trichospirolide B (**2.2**), and showed the highest antiplasmodial activity among the four compounds. Trichospirolide D (**2.4**), with an IC_{50} value of 44 μM, displayed the least antiplasmodial activity, and this may be due to the formation of a hemiacetal accompanied by the loss of an α,β-unsaturated carbonyl unit, since the presence of this system in germacranolides has been reported to be essential for bioactivity, regardless of the presence of a α,β-unsaturated γ-lactone moiety.[19] Moreover, the presence of the 4,5-epoxy group may be responsible for the fact that trichospirolide C (**2.3**, IC_{50} 12.1 μM) displayed a 3-fold higher

potency to *P. falciparum* than that of trichospirolide B (**2.2**, IC_{50} 37.1 μM).[20]

In spite of the promising antiplasmodial activity of trichospirolide A (**2.1**), it is not likely to be an antimalarial drug candidate because of its toxicity to mammalian cells, in common with most other germacranolide-type sesquiterpenoid lactones. Its relatively potent antiproliferative activity to A2780 ovarian cancer cells, only 10-fold less potent than paclitaxel, might indicate it to be a potential anticancer lead acting as a Michael acceptor.

2.3 Experimental Section

2.3.1 General Experimental Procedures

Optical rotations were recorded on a JASCO P-2000 polarimeter. UV and IR spectroscopic data were measured on a Shimadzu UV-1201 spectrophotometer and a MIDAC M-series FTIR spectrophotometer, respectively. ECD spectra were obtained on a JASCO J-815 spectrometer. NMR spectra were recorded in $CDCl_3$ on Bruker Avance 500 or 600 spectrometers. The chemical shifts are given in δ (ppm), and coupling constants (J) are reported in Hz. Mass spectra were obtained on an Agilent 6220 LC-TOF-MS in the positive ion mode.

2.3.2 Plant Material.

Whole plant specimens of *Trichospira verticillata* L. (S.F. Blake) were collected by Alexander Rodriguez alongside the main road in La Lagartera, Los Chiles, Alajuela Province, Costa Rica under the auspices of the National Biodiversity Institute of Costa Rica (INBIO). A herbarium sample is on deposit at this Institute under the accession number AR03477.

2.3.3 Antiplasmodial Bioassays.

The effect of each fraction and pure compound on parasite growth of the *P. falciparum* Dd2 strain was measured in a 72 h growth assay in the presence of drug as described previously with minor modifications. Briefly, ring stage parasite cultures (200 μL per well, with 1% hematocrit and 1% parasitemia) were grown for 72 h in the presence of increasing concentrations of the drug in a 5.05% CO_2, 4.93% O_2, and 90.2% N_2 gas mixture at 37 °C. After 72 h in culture, parasite viability was determined by DNA quantitation using SYBR Green I (50 μL of SYBR Green I in lysis buffer at 0.4 μL of SYBR Green I/mL of lysis buffer). The half-maximum inhibitory concentration (IC_{50}) calculation was performed with GraFit software using nonlinear regression curve fitting. IC_{50} values are the average of three independent determinations with each determination in duplicate and are expressed ± SEM.[21]

2.3.4 In vitro Cytotoxicity Against HEK293 Cells.

Compounds were evaluated for their cytotoxicity against the HEK293 (Human Embryonic Kidney) normal cell line. Briefly, 10,000 HEK cells per well were plated in a clear bottom 96 well plate. After allowing the cells to adhere, the media was replaced with 100 μL of media containing varying amounts of the test compound and incubated for 24 hours. Later, 10 μL of resazurin sodium salt (Sigma) at 0.125 mg/mL was added to each well and incubated for 2 h. Cell viability was determined by measuring the fluorescence at 585 nm after excitation at 540 nm.

2.3.5 In vitro Antiproliferative Activity Against A2780 Cells.

The A2780 ovarian cancer cell line antiproliferative bioassay was performed at Virginia Tech as previously reported.[22, 23] The A2780 cell line is a drug-sensitive ovarian cancer cell line.[24] Paclitaxel was used as the positive control.

2.3.6 Extraction and Isolation.

The dried and powdered whole plant of *T. verticillata* (731 g) was exhaustively extracted with EtOH in two 24-hour percolation steps; successive partition of the concentrated extract with hexanes and DCM gave an active DCM extract (about 10 g). For purposes of fractionation and purification, 0.517 g of the DCM extract designated 39114-5H was shipped to Virginia Tech for bioassay-guided isolation. A 0.358 g sample of 39114-5H (IC_{50} ~ 5 μg/mL) was suspended in aqueous MeOH [MeOH:H_2O (9:1), 100 mL], and extracted with hexane (3 × 100 mL portions). The hexanes fraction was evaporated in vacuo to afford 85 mg of hexanes with IC_{50} 2.5 ~ 5 μg/mL. The remaining aqueous MeOH fraction was centrifuged to give a supernatant (270 mg) with an IC_{50} value of > 10 μg/mL.

The hexanes fraction was directly applied on C_{18} HPLC, and eluted by 40 to 80% MeCN in H_2O gradient in 60 min to yield compound **2.2** (6.3 mg), compound **2.4** (4.3 mg), compound **2.3** (5.2 mg) and compound **2.1** (4.7 mg), with retention times of 19.5, 26.5, 31.5 and 34.7 minutes, respectively.

2.3.7 Computational Details.

Conformational searches involving fluctuations of the side chains on each ring conformer were generated using the Open Babel software[25] in conjunction with the MMFF94 force field[26] and the Confab systematic rotor conformer generator.[27] An energy cutoff was employed such that all diverse side chain conformers with a relative energy < 10 kcal/mol were kept. Geometries were optimized at the DFT/B3LYP/6-31G* level of theory[28-31] within a MeOH solvent simulated using the polarizable continuum model (PCM).[32] Harmonic vibrational frequencies were also computed at the same level of theory to ensure that no imaginary values

were present, thus confirming that all of the structures were minima on their respective potential energy surfaces. Thermal Gibbs free energies were obtained using partition functions computed within the harmonic oscillator/rigid rotor approximations,[33, 34] permitting the calculation of room temperature equilibrium Boltzmann populations. Excitation energies, rotatory strengths, and oscillator strengths for each transition (in the velocity representation) were calculated for the first 40 electronic states at the TDDFT/B3LYP/aug-cc-pVDZ level of theory,[28, 30, 31, 35, 36] again including the PCM description of the MeOH solvent. All quantum chemical calculations were performed using the Gaussian 09 electronic structure package.[37] The ECD spectra were subsequently simulated by overlapping Gaussian functions for each transition according to[38]

$$\Delta\varepsilon(\tilde{\nu}) = \frac{1}{(2.296 \times 10^{-39})\sqrt{\pi}\,\sigma}\sum_{a}\tilde{\nu}_{0a}R_{0a}\exp\left[-\left\{\frac{(\tilde{\nu}-\tilde{\nu}_{0a})}{\sigma}\right\}^{2}\right]$$

Where σ is defined as half the bandwidth at 1/e peak height, and $\tilde{\nu}_{0a}$ and R_{0a} are the excitation energy (in wavenumbers) and rotatory strength for transition $0 \rightarrow a$, respectively. The σ value is an empirical parameter, and we chose a value of 0.40 eV in agreement with the resolution of the experimental ECD bandwidths. The UV spectra were simulated by overlapping Gaussian functions for each transition according to

$$\Delta\varepsilon(\tilde{\nu}) = \frac{(1.3062974 \times 10^{8})}{\sigma}\sum_{a} f_i \exp\left[-\left\{\frac{(\tilde{\nu}-\tilde{\nu}_{0a})}{\sigma}\right\}^{2}\right]$$

Where σ is defined as half the bandwidth at 1/e peak height, and $\tilde{\nu}_{0a}$ and f_i are the excitation energy (in wavenumbers) and oscillator strength for transition $0 \rightarrow a$, respectively. The σ value is an empirical parameter, and we chose a value of 0.40 eV in agreement with the resolution of the experimental UV bandwidths.

Individual proton distances were calculated and averaged (using the Boltzmann populations above) to permit comparison with experimental NOESY data. In the case of methyl hydrogens, simple averages of the three individual Boltzmann averaged distances are reported.

Relative thermal Gibbs free energies and associated room temperature equilibrium Boltzmann populations of all unique conformers as well as weighted average ECD and UV spectra and specific rotations for all possible stereoisomers are included in Supporting Information.

2.3.8 Compound Information

Trichospirolide A (**2.1**): yellow powder; $[\alpha]_D^{21}$ –360.3º (c 7.16×10^{-4} g/mL, MeOH); UV (c 0.030 mM, MeOH) λ_{max} (ε) 298 nm (9464) 252 nm (13939); IR υ_{max} 2930, 1773, 1749,1723, 1639, 1231, 1149, 1030 cm^{-1}; ECD (c 0.030 mM, MeOH) $\Delta\varepsilon_{295}$ −14.3, $\Delta\varepsilon_{248}$ +19.2; HRESIMS *m/z* 409.1273 $[M+Na]^+$ (calcd. for $C_{21}H_{22}NaO_7$, 409.1258) and 387.1441 $[M+H]^+$ (calcd. for $C_{21}H_{23}O_7$, 387.1438); ^1H NMR (500 MHz, $CDCl_3$) and ^{13}C NMR (125 MHz, $CDCl_3$), see Table **2-1**.

Trichospirolide B (**2.2**): yellow powder; $[\alpha]_D^{21}$ –140.1º (c 3.14×10^{-4} g/mL, MeOH); UV (c 0.034 mM, MeOH) λ_{max} (ε) 247 nm (7353); IR υ_{max} 3430, 2930, 1767, 1723, 1639, 1231, 1153 cm^{-1}; ECD (c 0.034 mM, MeOH) $\Delta\varepsilon_{255}$ –4.2, $\Delta\varepsilon_{237}$ +3.7, $\Delta\varepsilon_{207}$ –13.2; HRESIMS *m/z* 427.1389 $[M+Na]^+$ (calcd for $C_{21}H_{24}NaO_8$, 427.1363) and 405.1561 $[M+H]^+$ (calcd for $C_{21}H_{25}O_8$, 405.1544); ^1H NMR (500 MHz, $CDCl_3$) and ^{13}C NMR (125 MHz, $CDCl_3$), see Table **2-3**.

Trichospirolide C (**2.3**): yellow powder; $[\alpha]_D^{21}$ –55.2º (c 5.62×10^{-4} g/mL, MeOH); UV (c

0.030 mM, MeOH) λ_{max} (ε) 229 nm (13134); IR υ_{max} 2930, 1773, 1749, 1723, 1689, 1233, 1153 cm^{-1}; ECD (c 0.030 mM, MeOH) $\Delta\varepsilon_{224}$ +10.1; HRESIMS *m/z* 427.1367 $[M+Na]^+$ (calcd. for $C_{21}H_{24}NaO_8$, 427.1363) and 405.1540 $[M+H]^+$ (calcd. for $C_{21}H_{25}O_8$, 405.1544); ^1H NMR (500 MHz, $CDCl_3$) and ^{13}C NMR (125 MHz, $CDCl_3$), see Table **2-6**.

Trichospirolide D (**2.4**): yellow powder; $[\alpha]_D^{21}$ –232.3º (c 3.1×10^{-4} g/mL, MeOH); UV (c 0.030 mM, MeOH) λ_{max} (ε) 234 nm (4227); IR υ_{max} 3427, 2930, 1767, 1721, 1233, 1154, 1041 cm^{-1}; ECD (c 0.030 mM, MeOH) $\Delta\varepsilon_{251}$ –3.4, $\Delta\varepsilon_{217}$ +14.0; HRESIMS *m/z* 427.1360 $[M+Na]^+$ (calcd. for $C_{21}H_{24}NaO_8$, 427.1363) and 405.1554 $[M+H]^+$ (calcd. for $C_{21}H_{25}O_8$, 405.1544); ^1H NMR (500 MHz, $CDCl_3$) and ^{13}C NMR (125 MHz, $CDCl_3$), see Table **2-9**.

2.4 References

1. Du, Y. P., K. C.; Dai, Y.; Krai, P.; Dalal, S.; Cassera, M. B.; Goetz, M.; Crawfood, T. D.; Kingston, D. G. I. Antiplasmodial Sesquiterpenoid Lactones from *Trichospira verticillata:* Structure Elucidation by Spectroscopic Methods and Comparison of Experimental and Calculated ECD Data. *J. Nat. Prod.* **2017,** *80*, 1639–1647.

2. Blake, S. *Trichospira Verticillata* (L.) *Torreya* **1915,** *15*, 106

3. Shen, Y.-C. L., K.; Kuo, Y.; Khalil, A. Cytotoxic Sesquiterpene Lactones from *Eupatorium kiirunense*, a Coastal Plant of Taiwan. *J. Nat. Prod.* **2005,** *68*, 745–750.

4. Spring, O. Z., R.; Reeb, S.; Vogler, B.; Da Costa, F. Sesquiterpene Lactones and a Myoinositol from Glandular Trichomes of Viguiera quinqueremis (Heliantheae; Asteraceae). *Phytochemistry* **2001,** *57*, 267–272.

5. Uchida, I.; Kuriyama, K. The π–π Circular Dichroism of *a,β*-unsaturated *γ*-lactones. *Tetrahedron Lett.* **1974,** *15* (43), 3761–3764.

6. Crawford, T. D.; Stephens, P. J. A Comparison of Time-Dependent Density-Functional Theory and Coupled Cluster Theory for the Calculation of the Optical Rotations of Chiral Molecules. *J. Phys. Chem. A* **2008,** *112*, 1339–1345.

7. Karplus, M. Vicinal Proton Coupling in Nuclear Magnetic Resonance. *J. Am. Chem. Soc.* **1963,** *85*, 2870–2871.

8. Catalán, C.; del R. Cuenca, M.; Hernández, L.; Joseph-Nathan, P. *cis,cis*-Germacranolides and Melampolides from *Mikania thapsoides*. *J. Nat. Prod.* **2003,** *66* (7), 949–953.

9. Van Calsteren, M.-R.; Jankowski, C. K.; Reyes-Chilpa, R.; Jimenez-Estrada, M.; Campos, M. G.; Zarazua-Lozada, M. O.; Lesage, D. X-ray and High-resolution ^{1}H and ^{13}C NMR of Smooth Muscle Relaxant Sesquiterpene Lactones. *Can. J. Chem.* **2008,** *86*, 1077–1084.

10. Shen, Y.-C.; Lo, K.; Kuo, Y.; Khalil, A. Cytotoxic Sesquiterpene Lactones from *Eupatorium kiirunense*, a Coastal Plant of Taiwan. *J. Nat. Prod.* **2005,** *68* (5), 745–750.

11. Finefield, J. M.; Sherman, D. H.; Kreitman, M.; M., W. R. Enantiomeric Natural Products: Occurrence and Biogenesis. *Angew. Chem. Int. Ed.* **2012,** *51*, 4802–4836.

12. Prosser, I.; Altug, I. G.; Phillips, A. L.; Konig, W. A.; Bouwmeester, H. J.; Beale, M. H. Enantiospecific (+)- and (-)-germacrene D Synthases, Cloned from Goldenrod, Reveal a Functionally Active Variant of the Universal Isoprenoid-biosynthesis Aspartate-rich Motif. *Arch. Biochem. Biophys.* **2004,** *432* (2), 136–144.

13. Barrero, A. F.; Oltra, J. E.; Álvarez, M.; Raslan, D. S.; Saúde, D. A.; Akssira, M. New Sources and Antifungal Activity of Sesquiterpene Lactones. *Fitoterapia* **2000,** *71* (1), 60–64.

14. Chung, I.-M.; Moon, H.-I. Antiplasmodial Activities of Sesquiterpene Lactone from

Carpesium cernum. *J. Enzyme Inhib. Med. Chem.* **2009,** *24* (1), 131–135.

15. Li, X.-W.; Weng, L.; Gao, X.; Zhao, Y.; Pang, F.; Liu, J.-H.; Zhang, H.-F.; Hu, J.-F. Antiproliferative and Apoptotic Sesquiterpene Lactones from *Carpesium faberi*. *Bioorg. Med. Chem. Lett.* **2011,** *21* (1), 366–372.

16. Chea, A.; Hout, S.; Long, C.; Marcourt, L.; Faure, R.; Azas, N.; Elias, R. Antimalarial Activity of Sesquiterpene Lactones from *Vernonia cinerea*. *Chem. Pharm. Bull.* **2006,** *54* (10), 1437–1439.

17. Pillay, P.; Vleggaar, R.; Maharaj, V.; Smith, P.; Lategan, C. Isolation and Identification of Antiplasmodial Sesquiterpene Lactones from *Oncosiphon piluliferum*. *J. Ethnopharmacol.* **2007,** *112* (1), 71–76.

18. Chaturvedi, D. Sesquiterpene Lactones : Structural Diversity and Their Biological Activities. In *Opportunity, Challenge and Scope of Natural Products in Medicinal Chemistry*, 2011; p313.

19. François, G.; Passreiter, C.; Woerdenbag, H.; Van Looveren, M. Antiplasmodial Activities and Cytotoxic Effects of Aqueous Extracts and Sesquiterpene Lactones from *Neurolaena lobata*. *Planta. Med.* **1996,** *62* (02), 126–129.

20. Ortet, R.; Prado, S.; Mouray, E.; Thomas, O. Sesquiterpene Lactones from the Endemic Cape Verdean *Artemisia gorgonum*. *Phytochemistry* **2008,** *69* (17), 2961–2965.

21. Dai, Y.; Harinantenaina, L.; Bowman, J.; Da Fonseca, I. O.; Brodie, P.; Goetz, M.; Cassera, M.; Kingston, D. G. I. Isolation of Antiplasmodial Anthraquinones from *Kniphofia ensifolia*, and Synthesis and Structure–activity Relationships of Related Compounds. *Bioorg. Med. Chem.* **2014,** *22* (1), 269–276.

22. Cao, S.; Brodie, P. J.; Miller, J. S.; Randrianaivo, R.; Ratovoson, F.; Birkinshaw, C.; Andriantsiferana, R.; Rasamison, V. E.; Kingston, D. G. I. Antiproliferative Xanthones of *Terminalia calcicola* from the Madagascar Rain Forest. *J. Nat. Prod.* **2007,** *70,* 679−681.

23. Pan, E.; Harinantenaina, L.; Brodie, P. J.; Miller, J. S.; Callmander, M. W.; Rakotonandrasana, S.; Rakotobe, E.; Rasamison, V. E.; Kingston, D. G. I. Four Diphenylpropanes and a Cycloheptadibenzofuran from *Bussea sakalava* from the Madagascar Dry Forest. *J. Nat. Prod.* **2010,** *73* (11), 1792−1795.

24. Louie, K. G.; Behrens, B. C.; Kinsella, T. J.; Hamilton, T. C.; Grotzinger, K. R.; McKoy, W. M.; Winker, M. A.; Ozols, R. F. Radiation Survival Parameters of Antineoplastic Drug-sensitive and -resistant Human Ovarian Cancer Cell Lines and Their Modification by Buthionine Sulfoximine. *Cancer Res.* **1985,** *45,* 2110−2115.

25. O'Boyle, N. M.; Banck, M.; James, C. A.; Morley, C.; Vandermeersch, T.; Hutchison, G. R. Open Babel: An open chemical toolbox. *J. Cheminform.* **2011,** *3* (1), 33.

26. Halgren, T. A. Merck Molecular Force Field. I. Basis, Form, Scope, Parameterization, and Performance of MMFF94. *J. Comput. Chem.* **1996,** *17,* 490−519.

27. O'Boyle, N. M.; Vandermeersch, T.; Flynn, C. J.; Maguire, A. R.; Hutchison, G. R. Confab - Systematic Generation of Diverse Low-energy Conformers. *J. Cheminf.* **2011,** *3,* 8.

28. Becke, A. D. Density-functional Thermochemistry. III. The Role of Exact Exchange. *J. Chem. Phys.* **1993,** *98,* 5648−5652.

29. Ditchfield, R.; Hehre, W. J.; Pople, J. A. Self-Consistent Molecular-Orbital Methods. IX. An Extended Gaussian-Type Basis for Molecular-Orbital Studies of Organic Molecules. *J. Chem. Phys.* **1971,** *54* (2), 724−728.

30. Stephens, P. J.; Devlin, F. J.; Chabalowski, C. F.; Frisch, M. J. Calculation of Vibrational Absorption and Circular Dichroism Spectra Using Density Functional Theory. *J. Phys. Chem.* **1994,** *98* (45), 11623−11627.

31. Lee, C.; Wang, W.; Parr, R. G. Development of the Colle−Salvetti Correlation-energy Formula into a Functional of the Electron Density. *Phys. Rev. B* **1988,** *37*, 785−789.

32. Miertuš, S.; Scrocco, E.; Tomasi, J. Electrostatic Interaction of a Solute with a Continuum. A Direct Utilization of ab initio Molecular Potentials for the Prevision of Solvent Effects. *Chem. Phys.* **1981,** *55*, 117−129.

33. McQuarrie, D. A. *Statistical Mechanics*. Harper and Row: New York, 1975; p 356.

34. Hehre, W. J.; Radom, L.; Schleyer, P. v. R.; Popel, P. A. J. *Ab Initio Molecular Orbital Theory.* Wiley-Interscience: New York, 1986; p 548.

35. Casida, M. E.; Jamorski, C.; Bohr, F.; Guan, J.; Salahub, D. R., Optical Properties from Density-Functional Theory. In *Theoretical and Computational Modeling of NLO and Electronic Materials*, Karna, S. P.; Yeates, A. T. Eds. American Chemical Society: Washington DC, 1996; Vol. 628, p 145.

36. Kendall, R. A.; Dunning Jr, T. H.; Harrison, R. J. Electron Affinities of the First-row Atoms Revisited. Systematic Basis Sets and Wave Functions. *J. Chem. Phys.* **1992,** *96* (9), 6796−6806.

37. Frisch, M. J.; Trucks, G. W.; Schlegel, H. B.; Scuseria, G. E.; Robb, M. A.; Cheeseman, J. R.; Scalmani, G.; Barone, V.; Mennucci, B.; Petersson, G. A.; Nakatsuji, H.; Caricato, M.; Li, X.; Hratchian, H. P.; Izmaylov, A. F.; Bloino, J.; Zheng, G.; Sonnenberg, J. L.; Hada, M.; Ehara, M.; Toyota, K.; Fukuda, R.; Hasegawa, J.; Ishida, M.; Nakajima, T.; Honda, Y.; Kitao,

O.; Nakai, H.; Vreven, T.; Montgomery, J. J. A. *Gaussian 09 Revision E.1*, Gaussian Inc.: Wallingford CT, 2009.

38. Stephens, P. J.; Harada, N. ECD Cotton Effect Approximated by the Gaussian Curve and Other Methods. *Chirality* **2010,** *22*, 229–233.

Chapter 3: Antiplasmodial Diterpenoids and a Benzotropolone from *Petradoria pumila*

This chapter is a slightly expanded version of an unpublished article of *Journal of Natural Products*. (Du, Y.; Valenciano, A. L.; Goetz, M.; Cassera, M. B.; Kingston, D. G. I., Four New Diterpenoids and a New Benzotropolone from *Petradoria pumila*.) Author contributions of the articles are described as follows in the order of the names listed. The author of this dissertation (Mr. Yongle Du) conducted the isolation and structural elucidation part of the isolated compounds, performed the A2780 bioassay on the isolated compound**s**, and drafted the manuscript. Dr. Ana Lisa Valenciano carried out the antiplasmodial bioassays on the fractions and the isolated compounds under the direction of Dr. Maria B. Cassera. Dr. Michael Goetz from Natural Products Discovery Institute (NPDI) provided the plant extract from the NPDI repository. Dr. David G. I. Kingston was a mentor for this work and the corresponding author for the published article. He also edited the final manuscript.

3.1 Introduction

3.1.1 Abstract

An extract of *Petradoria pumila* from the Natural Products Discovery Institute was found to have moderate antiplasmodial activity, with an IC_{50} value between 5 and 10 μg/mL. The four new diterpenoids petradoriolides A–D (**3.1**–**3.4**), the new benzotropolone petradoriolone I (**3.5**) and the two known compounds **3.6**–**3.7** were isolated after bioassay-directed fractionation. The structures and stereochemistries of the new compounds

were determined by interpretation of NMR spectroscopy, mass spectrometry and ECD spectra. Among these compounds, petradoriolide C (**3.3**) displayed the most potent antiplasmodial activity, with an IC_{50} value of 7.25 μM.

3.1.2 Investigations of the genus *Malleastrum*

Petradoria pumila is the only species in the genus *Petradoria*; it is known by the common name rock goldenrod, and is native to the southwestern USA.[1] This plant was selected for study after its detanninized extract showed moderate antiplasmodial activity against the chloroquine-resistant Dd2 strain of *Plasmodium falciparum*. The Asteraceae family is a rich source of bioactive compounds, including antimalarial sesquiterpenes and diterpenes.[2-4] However, there are no reports on the chemistry or antiplasmodial activity of *P. pumila*, so this extract was selected for investigation.

3.2 Results and Discussion

3.2.1 Isolation of active compounds

A dichloromethane extract of the stems and roots of *Petradoria pumila* was subjected to C-18 SPE to afford active acetonitrile and methanol fractions, with IC_{50} values against the drug-resistant Dd2 strain of *Plasmodium falciparum* of about 3 and 5 μg/mL, respectively. The acetonitrile fraction was separated by chromatography on a silica gel open column to generate fourteen sub-fractions. The active sub-fractions were separated by C-18 reversed phase HPLC to yield the four new diterpenoids petradoriolide A–D (**3.1**–**3.4**), the new benzotropolone petradoriolone I (**3.5**) and the two known compounds **3.6** – **3.7**.

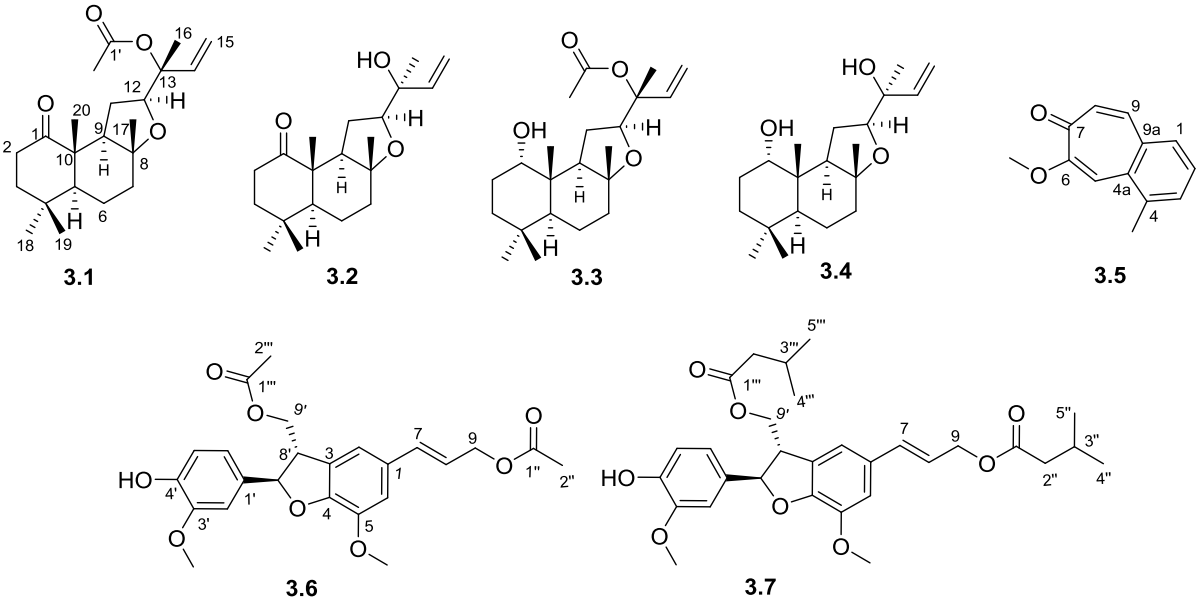

3.2.2 Structure elucidation of isolated compounds

Petradoriolide A (**3.1**) was isolated as a pale yellow powder. Its positive ion HRESIMS revealed a peak for a sodium adduct ion at *m/z* 385.2364, corresponding to a molecular formula of $C_{22}H_{34}O_4$. The ^{1}H NMR (Table **3-1**) and HSQC spectra displayed signals for six methyl groups (δ_H 1.58, H-16; 1.20, H-17; 1.03, H-18; 1.01, H-19; 1.14, H-20; 2.03, H-2'), five alkyl methylenes (δ_H 2.64 and 2.30, H-2; 1.82 and 1.65, H-3; 1.80 and 1.51, H-6; 1.96 and 1.40, H-7; 2.41 and 1.85, H-11), two alkyl methines (δ_H 1.44, H-5; 1.72, H-9), one oxygen-bearing methine (δ_H 3.88, H-12) and one terminal olefin (δ_H 6.05, dd, 17.6, 11.0, H-14; 5.21, dd, 11.0, 0.8 and 5.15, dd, 17.6, 0.8, H-15). The presence of an acetoxy group was confirmed by ^2J-HMBC correlations between H-2' and C-1' (δ_C 170.0). The remaining twenty carbons, two oxygens, and thirty-one protons comprised an 8,12-epoxylabdane (**3.1**)[5] or an 8,13- epoxylabdane (**3.1a**)[6] type diterpene skeleton.

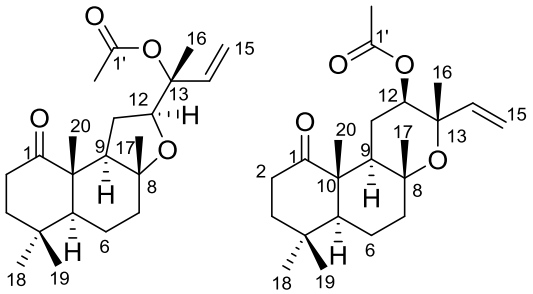

3.1 **3.1a**

Structures **3.1** and **3.1a** are both consistent with ^{2}J-HMBC correlations between H-5 and C-6 (δ_C 22.0), H-7 and C-6, H-9 and C-8 (δ_C 81.5), and by ^{3}J-HMBC correlations between H-2 and C-4 (δ_C 32.0), H-3 and C-5 (δ_C 53.9), H-7 and C-5, H-9 and C-5, H-9 and C-7 (δ_C 39.7), H-11 and C-8, H-11 and C-13 (δ_C 82.8), and H-15 and C-13. The positions of the five methyl groups in either skeleton were assigned by ^{3}J-HMBC correlations between H-14 and C-16 (δ_C 19.4), H-17 and C-7, H-17 and C-9 (δ_C 53.0), H-18 and C-3 (δ_C 39.0), H-18 and C-5, H-18 and C-19 (δ_C 31.4), H-19 and C-3, H-19 and C-5, H-19 and C-18 (δ_C 23.7), H-5 and C-20 (δ_C 15.2), and H-9 and C-20. The ketone group was assigned to the C-1 position, based on ^{3}J-HMBC correlations between H-20 and C-1 (δ_C 215.8) and H-3 and C-1. The acetoxy group was assigned to C-12 in **3.1a** or C-13 in **3.1** on the basis of ^{2}J-HMBC correlations between H-12 and C-11 (δ_C 26.3), and H-12 and C-13, and ^{3}J-HMBC correlations between H-12 and C-16. There were two possible structures pyran ring **3.1a** or furan ring **3.1** assumed only from HMBC (Figure **3-1**). The identification of **3.1** as the correct isomer was then made on the basis of the chemical shift of H-12 (3.88 ppm, dd, J = 10.1, 5.5 Hz), which is more shielded than the 4.2 ppm predicted for the esterified oxymethine of **3.1a**. In addition, the $J_{11,12}$ coupling constants of 10.1 and 5.5 Hz were consistent with the values of 9.5 and 5 Hz observed for the related compound 13-hydroxy-8α,12β-epoxylabd-14-ene,[7] and the ^{1}H NMR

shifts of H-11 (1.85 and 2.41 ppm) were consistent with the shifts of 1.89 and 2.81 ppm observed for these protons in the related compound scapairrin D.[8]

Table 3-1. NMR Spectroscopic Data for Compound **3.1** in $CDCl_3$ (500 MHz)

position	δ_H, *J* in Hz	δ_C, type
1		215.8, C
2a	2.30 ddd 15.3, 9.1, 4.9	35.0, CH_2
2b	2.64 ddd 15.3, 8.6, 4.8	
3a	1.82 m	39.0, CH_2
3b	1.65 m	
4		32.0, C
5	1.44 m	53.9, CH
6a	1.80 m	22.0, CH_2
6b	1.51 m	
7a	1.96 dt 12.1, 3.1	39.7, CH_2
7b	1.40 m	
8		81.5, C
9	1.72 m	53.0, CH
10		50.1, C
11a	2.41 dt 11.0, 5.5	26.3, CH_2
11b	1.85 m	
12	3.88 dd 10.1. 5.5	85.4, CH
13		82.8, C
14	6.05 dd 17.6, 11.0	140.1, CH
15a	5.21 dd 11.0, 0.8	114.4, CH_2
15b	5.15 dd 17.6, 0.8	
16	1.58 s	19.4, CH_3
17	1.20 s	25.3, CH_3
18	1.03 s	23.7, CH_3
19	1.01 s	31.4, CH_3
20	1.14 s	15.2, CH_3
1’		170.0, C
2’	2.03 s	22.1, CH_3

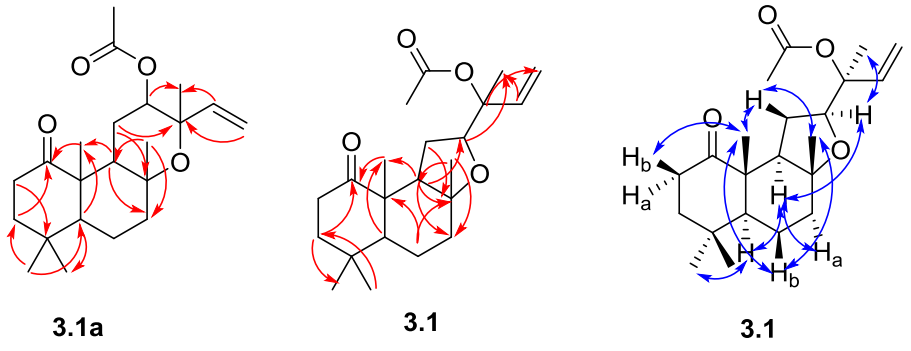

Figure 3-1. HMBC (red) and NOESY (blue) correlations for petradoriolide A **3.1**

The relative configuration of petradoriolide A (**3.1**) was assigned as *5S*,8R*,9R*,10S* 12S*,13R** based on NOESY correlation between H-2b and H-20, H-5 and H-9, H-7 and H-9, H_3-17 (δ_H 1.20) and H-6b (δ_H 1.51), H_3-20 (δ_H 1.14) and H-6b (δ_H 1.51), and between H-9 and H-12 (Figure **3-1**). The relative configurations of C-12 and C-13 were assigned tentatively by the NOESY correlation between H-12 and H_3-16, consistent with an internuclear distance of 2.4 Å in an energy-minimized structure, and this conclusion was confirmed by comparisons with the chemical shifts of the relevant carbons of the known compounds (8*R*,12*R*,13*S*)-13-acetoxy-8,12-epoxy-labd-14-ene and (8*R*,12*S*,13*R*)-13-acetoxy-8,12-epoxy-labd-14-ene.[5] The chemical shifts of C-12 and C-17 of the (12*S*,13*R*) isomer, at 85.3 and 25.1 ppm respectively, agreed well with the values for the corresponding carbons in **3.1**. The chemical shifts of C-12 and C-17 of the (12*R*,13*S*) isomer were 80.3 and 21.3 ppm respectively. Details of these comparisons are provided in Table **3-2**.

Table 3-2. The coupling constants and chemical shifts of relevant protons and carbons of compounds **S1** – **S2**

Position	**S1** (12*R*,13*S*)	**S2** (12*S*,13*R*)	Compound **3.1**
H-12	4.17 m	3.83 m	3.88 dd 10.1. 5.5
H-14	6.05 dd 17.5, 11.0	5.95 dd 17.5, 11.0	6.05 dd 17.6, 11.0
H-15a	5.21 d 17.5	5.14 d 17.5	5.21 dd 11.0, 0.8
H-15b	5.24 d 11.0	5.20 d 11.0	5.15 dd 17.6, 0.8
H-16	1.56	1.63	1.58 s
H-17	1.13	1.16	1.20 s
C-8	81.2	81.5	81.5
C-12	80.3	85.3	85.4
C-13	84.0	83.4	82.8
C-14	139.4	139.6	140.1
C-15	114.9	114.6	114.4
C-16	18.9	20.0	19.4
C-17	21.3	25.1	25.3

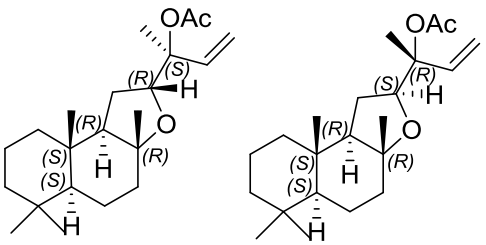

Its absolute configuration was determined by electronic circular dichroism. The negative $n-\pi^*$ Cotton effect at 304 nm (Figure **3-2**) indicated the absolute configuration of petradoriolide A (**3.1**) to be *5S,8R,9R,10S,12S,13R*.[9] The structure of petradoriolide A (**3.1**) was thus assigned as (5*S*,8*R*,9*R*,10*S*,12*S*,13*R*)-13-acetoxy-8,12-epoxy-1-oxolabd-14-ene.

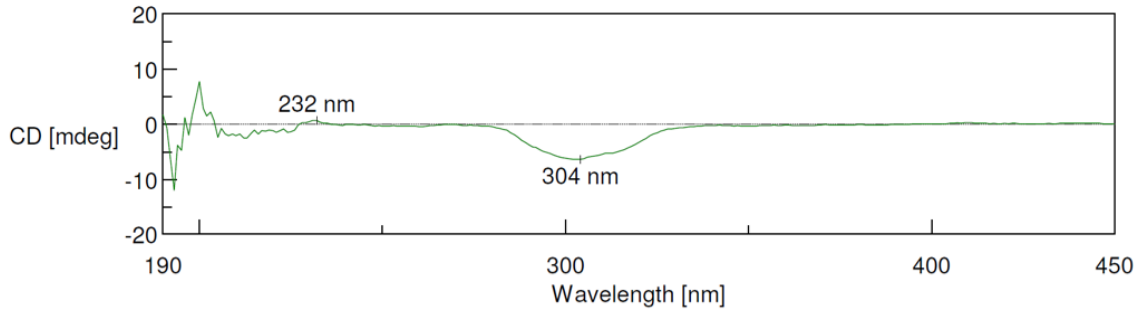

Figure 3-2. The ECD spectrum of petradoriolide A **3.1**

Petradoriolide B (**3.2**) was isolated as a pale yellow powder. Its positive ion HRESIMS revealed a peak for a sodium adduct ion at *m/z* 343.2225, corresponding to a molecular formula of $C_{20}H_{32}O_3$. The difference of 42 Da between the molecular weights of **3.1** and **3.2** suggested that **3.2** might be a deacetylated product of **3.1**. This was supported by the disappearances of the chemical shifts of the acetate group at δ_C 170.0 (C), 22.1 (CH_3) and δ_H 2.03 (CH_3), as shown in Table **3-3**. The assignment was confirmed by the HMBC correlations shown in Figure **3-3**.

Table 3-3. NMR Spectroscopic Data for Compounds **3.2** in $CDCl_3$ (500 MHz)

position	δ_H, *J* in Hz	δ_C, type
1		215.7, C
2a	2.29 ddd 15.4, 8.9, 4.9	35.1, CH_2
2b	2.67 ddd 15.4, 8.9, 4.9	
3a	1.82 m	39.2, CH_2
3b	1.65 ddd 13.9, 8.9, 4.9	
4		32.3, C
5	1.42 m	54.3, CH
6a	1.80 m	21.8, CH_2
6b	1.50 m	
7a	1.95 dt 12.1, 3.2	39.9, CH_2
7b	1.41 m	
8		81.2, C
9	1.76 m	53.4, CH
10		50.1, C
11a	2.40 ddd 11.0, 5.1, 5.1	25.9, CH_2
11b	1.88 ddd 13.4, 11.0, 10.2	
12	3.89 dd 10.2, 5.1	85.2, CH
13		73.1, C
14	5.98 dd 17.3, 10.7	145.0, CH
15a	5.30 dd 17.3, 1.3	112.8, CH_2
15b	5.11 dd 10.7, 1.3	
16	1.20 s	23.2, CH_3
17	1.21 s	25.6, CH_3
18	1.03 s	23.4, CH_3
19	1.00 s	32.2, CH_3
20	1.15 s	15.2, CH_3

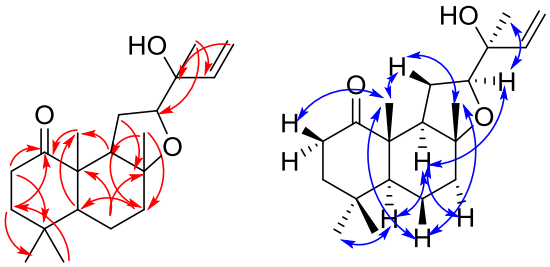

Figure 3-3. HMBC (red) and NOESY (blue) correlations for petradoriolide B **3.2**

The relative configuration of petradoriolide B (**3.2**) was assigned as *5S*,8R*,9R*,10S* 12S*,13S** by the observation of the same NOESY correlations as observed for compound **3.1** (shown in Figure **3-3**), and additionally, by comparisons between the chemical shifts of H-12, 16, and 17 and of C-12 – C-16 for **3.2** with those of related compounds **S3**–**S10** in the

literature (shown in Figure **3-4**). The compounds **S3**–**S10** all have 8,12-epoxy-13-dihydroxy-labd-14-ene skeletons, but have different configurations at C-12 and C-13. Comparison of ^{1}H NMR and ^{13}C NMR data for **3.2** with those of compounds **S3**–**S10**[7, 10-12] showed the best correlation with compound **S3**, the *5S*,8R*,9R*,10S*,12S*,13S** isomer (Table **3-4**), as explained below.

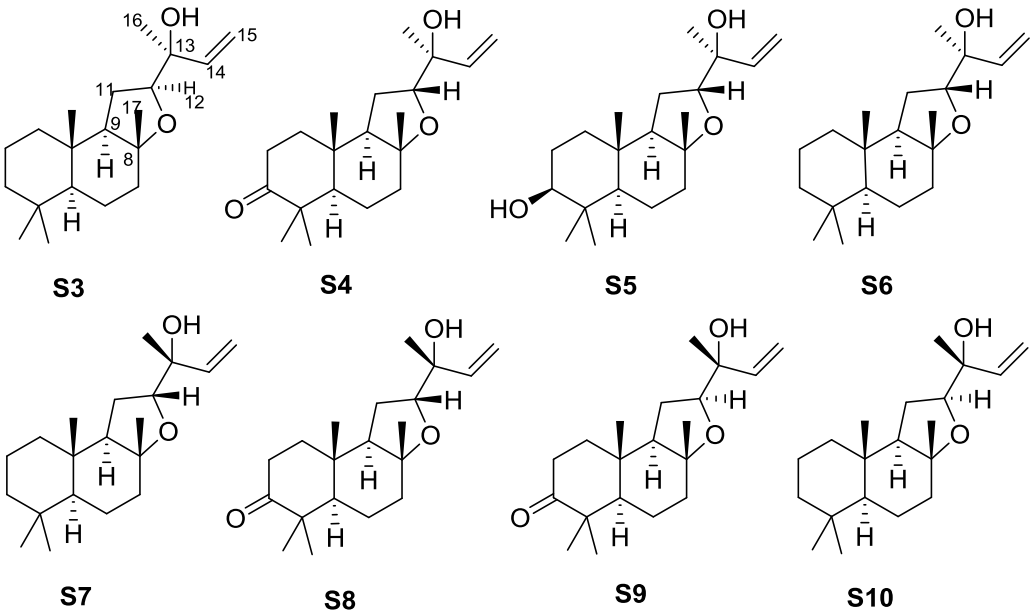

Figure 3-4. The structures of similar compounds (**S3–S10**)

Specifically, the trans-diaxial coupling constants of H-12 (~10 Hz) for compounds **S3**, **S9** and **S10** with *8R*,9R*,12S** configurations were a little larger than those of H-12 for compound **S4** to **S8** with *8R*,9R*,12R** configurations. The chemical shifts of C-12 and C-13 in *8R*,9R*,12S** compounds (**S3**, **S9** and **S10**) were around 85 and 73 ppm, while the chemical shifts of C-12 and C-13 in *8R*,9R*,12R** compounds (**S4** to **S8**) were around 81.5 and 74.5 ppm. The chemical shifts of C-14 and C-15 in *12S*,13S** compounds (**S3**, **S7** and **S8**) were around 143 ~ 144 and 112.5 ppm, while the chemical shifts of C-12 and C-13 in *12R*,13S** compounds (**S4**–**S6**, **S9**, and **S10**) were around 141 and 113.6 ppm. The chemical shifts of C-16 in *12R*,13S** compounds (**S4**–**S6**, **S9**, and **S10**) were around 25~26 ppm, while

the chemical shifts of C-16 in *12R*,13R** compounds (**S3**, **S7**, and **S8**) were around 23 ppm (Table **3-4**). In summary, the chemical shifts of the relevant protons and carbons of petradoriolide B (**3.2**) agrees best with those of compound **S3** with the *5S*,8R*,9R*,10S* 12S*,13S** relative configuration.

Table 3-4. The coupling constants and chemical shifts of relevant protons and carbons of compounds **L1** – **L8**

Position	**L1**[10, 12]	**L2**[11]	**L3**[11]	**L4**[10]	**L5**[7, 10, 12]	**L6**[11]	**L7**[11]	**L8**[7, 10]	**Cmpd 3.2**
H-12	3.83 dd 9.9, 5.4	3.88 dd 9.0, 3.6	3.89 dd 9.3, 3.4	3.91 dd 8.8, 3.9	3.92 t 6.4	3.94 dd 7.9, 4.7	3.79 dd 10.0, 5.4	3.78 dd 9.5, 5.5	3.89 dd 10.2, 5.1
H-16	1.17 s	1.21 s	1.23 s	1.26 s	1.20 s	1.21 s	1.30 s	1.29 s	1.20 s
H-17	1.17 s	1.12 s	1.11 s	1.13 s	1.12 s	1.16 s	1.19 s	1.15 s	1.21 s
C-12	85.2	81.3	81.5	81.7	81.6	81.4	85.2	85.4	85.2
C-13	73.1	74.3	74.5	74.6	74.5	74.4	73.3	73.3	73.1
C-14	144.2	140.9	141.1	141.2	143.1	142.8	140.9	141.0	145.0
C-15	112.5	113.6	113.6	113.6	112.9	113.0	113.6	113.4	112.8
C-16	23.2	24.6	24.9	24.9	23.4	23.6	25.9	25.9	23.2
C-17	25.3	20.8	21.3	21.4	21.2	20.7	24.9	25.5	25.3

The absolute configuration of petradoriolide B (**3.2**) was determined by electronic circular dichroism (Figure **3-5**) to be the same as that of petradoriolide A (**3.1**). Its structure was thus assigned as (5*S*,8*R*,9*R*,10*S*,12*S*,13*S*)-8,12-epoxy-13-hydroxy-1-oxolabd-14-ene.

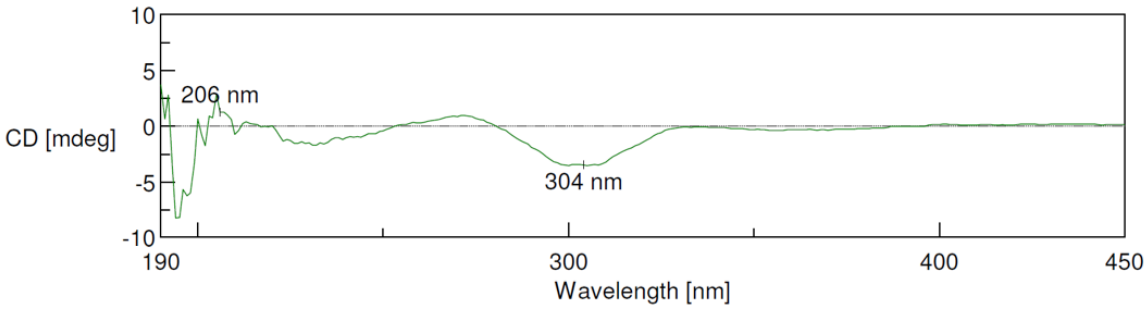

Figure 3-5. The ECD spectrum of petradoriolide B **3.2**

Petradoriolide C (**3.3**) was isolated as a pale yellow powder. Its positive ion HRESIMS revealed a peak for a sodium adduct ion at *m/z* 387.2504, corresponding to a molecular formula of $C_{22}H_{36}O_4$. The difference of 2 Da between the molecular weights of **3.1** and **3.3** suggested that **3.3** might be a dihydro product of **3.1**, and this was confirmed by the change of

chemical shift for C-1 from δ_C 215.8 (C) in **3.1** to δ_C 72.8 (CH) in **3.3**, as showed in Table **3-5**, and by the HMBC correlations shown in Figure **3-6**.

Table 3-5. NMR Spectroscopic Data for Compounds **3.3** in $CDCl_3$ (500 MHz)

position	δ_H, *J* in Hz	δ_C, type
1	3.50 m	72.8, CH
2a	1.47 m	26.2, CH_2
2b	2.11 m	
3a	1.63 m	35.6, CH_2
3b	1.20 m	
4		33.1, C
5	1.42 m	48.7, CH
6a	1.79 m	21.4, CH_2
6b	1.32 m	
7a	1.93 m	40.8, CH_2
7b	1.46 m	
8		81.7, C
9	2.02 m	53.2, CH
10		40.0, C
11a	1.74 m	24.5, CH_2
11b	1.69 m	
12	3.93 dd 9.8, 6.0	85.7, CH
13		83.3, C
14	6.05 dd 17.6, 11.1	140.4, CH
15a	5.20 dd 11.1, 1.0	114.6, CH_2
15b	5.15 dd 17.6, 1.0	
16	1.58 s	19.4, CH_3
17	1.18 s	25.5, CH_3
18	0.84 s	20.9, CH_3
19	0.91 s	33.4, CH_3
20	0.87 s	17.0, CH_3
1’		170.0, C
2’	2.03	22.4, CH_3

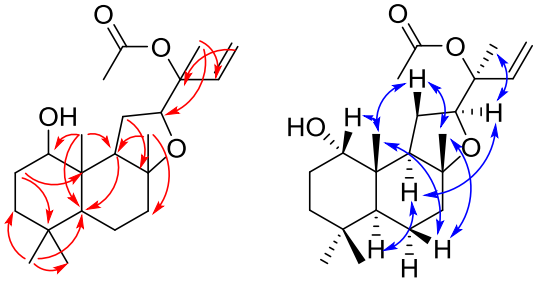

Figure 3-6. HMBC (red) and NOESY (blue) correlations for petradoriolide C **3.3**

The relative configuration of petradoriolide C (**3.3**) was assigned as *1S*,5S*,8R*,9R*,10S*,12S*,13R** based on the the NOESY correlations shown in Figure **3-6**, with the correlation between H-1 and H-20 establishing the configuration at C-1. The absolute configuration of compound **3.3** was assumed to be the same as those of compounds **3.1**. The structure of petradoriolide C (**3.3**) was thus assigned as (1*S*,5*S*,*8R*,9*R*,10*S*, 12*S*,13*R*)-13-acetoxy-8,12-epoxy-1-hydroxylabd-14-ene.

Petradoriolide D (**3.4**) was isolated as a pale yellow powder. Its positive ion HRESIMS revealed a peak for a sodium adduct ion at *m/z* 345.2421, corresponding to a molecular formula of $C_{20}H_{34}O_3$. The difference of 42 Da between the molecular weights of **3.3** and **3.4** suggested that **3.4** might be the deacetylated product of **3.3**. This was confirmed by the absence of the signals at δ_C 170.0 (C), 22.4 (CH_3) and δ_H 2.03 (CH_3), as showed in Table **3-6**, and by the HMBC cross-peaks shown in Figure **3-7**.

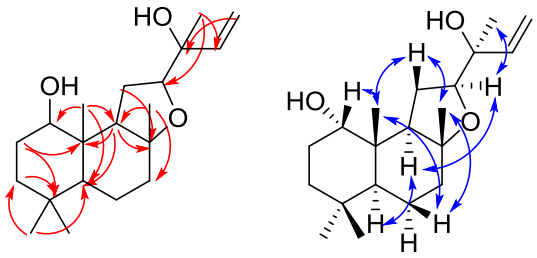

Figure 3-7. HMBC (red) and NOESY (blue) correlations for petradoriolide D **3.4**

The relative configuration of compound **3.4** was assigned as (1*S**,5*S**,8*R**,9*R**,10*S**,12*S**,13*S**) based on the NOESY correlations shown in Figure **3-7**, with the correlation between H-1 and H-20 establishing the configuration at C-1. The absolute configuration of **3.4** was also inferred from that of **3.2**. The structure of petradoriolide D (**3.4**) was thus assigned as (1*S*,5*S*,8*R*,9*R*,10*S*,12*S*,13*S*)-8,12-epoxy-1,13-dihydroxylabd-14-ene.

Table 3-6. NMR Spectroscopic Data for Compounds **3.4** in $CDCl_3$ (500 MHz)

position	δ_H, *J* in Hz	δ_C, type
1	3.52 m	72.4, CH
2a	1.51 m	26.0, CH_2
2b	2.11 m	
3a	1.59 m	35.4, CH_2
3b	1.20 m	
4		33.1, C
5	1.45 m	48.4, CH
6a	1.81 dd 13.7, 3.5	21.2, CH_2
6b	1.33 m	
7a	1.92 dt 12.0, 3.2	40.4, CH_2
7b	1.44 dt 12.0, 3.0	
8		81.6, C
9	2.06 dd13.0, 5.3	53.1, CH
10		40.1, C
11a	1.76 m	23.6, CH_2
11b	1.72 m	
12	3.91 dd 9.7, 5.9	85.1, CH
13		73.1, C
14	5.97 dd 17.3, 10.7	144.6, CH
15a	5.30 dd 17.3, 1.3	112.5, CH_2
15b	5.11 dd 10.7, 1.3	
16	1.19 s	23.2, CH_3
17	1.20 s	25.5, CH_3
18	0.84 s	21.0, CH_3
19	0.91 s	33.3, CH_3
20	0.86 s	16.8, CH_3

It is noteworthy that the configurations of the two acetates **3.1** and **3.3** at C-13 are the opposite of those of the corresponding alcohols. This raises the intriguing possibility that the acetates are biosynthesized by a process involving inversion of configuration, rather than by simple acetylation of a hydroxyl group.

Petradoriolone (**3.5**) was isolated as a yellowish oil. Its positive ion HRESIMS revealed a peak for a protonated molecular ion at *m/z* 201.0920 and for a sodium adduct ion at *m/z* 223.0743, both corresponding to a molecular formula of $C_{13}H_{12}O_2$. The ^{1}H NMR and HSQC spectra displayed signals for one methoxy group (δ_H 3.99), one methyl group (δ_H 2.70, H-9),

and six olefin methines (δ_H 7.59, H-1; 7.41, H2; 7.51, H-3; 7.30, H-5; 7.02, H-8; 7.62, H-9), as showed in Table **3-7**.

Table 3-7. NMR Spectroscopic Data for Compound **3.5** in $CDCl_3$ (500 MHz)

position	δ_H, *J* in Hz	δ_C, type	position	δ_H, *J* in Hz	δ_C, type
1	7.59 d 8.0	132.6, CH	7		181.7, C
2	7.41 dd 8.0, 7.5	127.7, CH	8	7.02 d 13.0	131.5, CH
3	7.51 d 7.5	132.9, CH	9	7.62 d 13.0	142.1, CH
4		137.5, C	9a		133.5, C
4a		132.5, C	6-OMe	3.99	55.8, CH_3
5	7.30 s	111.7, CH	4-Me	2.70	21.8, CH_3
6		157.0, C			

The benzocyclohepten-7-one skeleton was confirmed by ^3J-HMBC correlations between H-1 and C-9 (δ_C 142.1), H-1 and C-4a (δ_C 132.5), H-2 and C-4 (δ_C 137.5), H-2 and C-9a (δ_C 133.5), H-6 and C-7 (δ_C 181.7), H-6 and C-8 (δ_C 131.5), H-5 and C-4, H-5 and C-9a, H-5 and C-7, H-8 and C-6 (δ_C 157.0), H-8 and C-9a, H-9 and C-1 (δ_C 132.6), H-9 and C-4a, H-9 and C-7 and ^2J-HMBC correlations between H-5 and C-6.[13] The methyl and methoxyl groups were assigned to C-4 and C-6 respectively, as determined by ^3J-HMBC correlations between Me and C-3 (δ_C 132.9), Me and C-4a, OMe and C-6 (Figure **3-8**). The structure of petradoriolone I (**3.5**) was thus assigned as 6-methoxyl-4-methyl-benzotropolone.

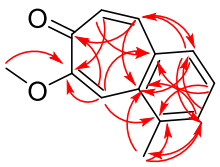

Figure 3-8. HMBC correlations of petradoriolone I (**3.5**)

Compounds **3.6** and **3.7** were known arylcoumaran neolignans,[14, 15] with later reassignments of the relative configurations of C-7' and C-8' of compound **3.6**[16] and the absolute configuration of compound **3.6** confirmed by CD data.[17] Compound **3.6** was thus identified as (7*E*)-(7'*R*,8'*S*)-4'-hydroxy-3',5-dimethoxy-4,7'-epoxy-8',3-neolig-7-en-9,9'-diyl

diacetate. Compound **3.7** was identified as (7*E*)-(7'*R*,8'*S*)-4'-hydroxy-3',5-dimethoxy-4,7'-epoxy-8',3-neolig-7-en-9,9'-diyl di-3-methylbutanoate by comparison of its spectroscopic data with those of **3.6** and with literature data, as showed in Table **3-8**.[18]

Table 3-8. NMR Spectroscopic Data for Compounds **3.6**–**3.7** in $CDCl_3$ (500 MHz)

	3.6		**3.7**	
position	δ_H, *J* in Hz	δ_C, type	δ_H, *J* in Hz	δ_C, type
1		129.7, C		130.6, C
2	6.88 s	109.8, CH	6.90	110.7, CH
3		126.9, C		127.9, C
4		147.3, C		148.1, C
5		143.6, C		144.4, C
6	6.89 s	114.8, CH	6.91	115.5, CH
7	6.60 d 15.8	134.3, CH	6.59 d 16	134.0, CH
8	6.16 dt 15.8, 6.6	120.8, CH	6.15 dt 16, 6.6	121.4, CH
9	4.71 dd 6.6, 1.0	64.7, CH_2	4.72 dd 6.6, 1.3	64.9, CH_2
5-OMe	3.87 s	55.4, CH_3	3.90 s	56. , CH_3
1'		131.3, C		132.2, C
2'	6.89 s	107.8, CH	6.92	108.5
3'		147.5, C		146.7, C
4'		144.5, C		145.0, C
5'	6.88 s	113.6, CH	6.91	114.3, CH
6'	6.88 s	118.8, CH	6.91	119.5, CH
7'	5.47 d 7.0	88.4, CH	5.47 d 7.3	88.9, CH
8'	3.78 m	49.7, CH	3.77 q 6.8	50.5, CH
9'a	4.44 dd 11.2, 5.5	64.8, CH_2	4.42 dd 11.1, 5.4	64.8, CH_2
9'b	4.30 dd 11.2, 7.5		4.33 dd 11.1, 7.3	
3'-OMe	3.91 s	55.6, CH_3	3.86 s	56.0, CH_3
4'-OH	5.62		5.63	
1"		170.1, C		173.1, C
2"	2.10 s	20.3, CH_3	2.24 m	43.5, CH_2
3"			2.13 m	25.5
4"			0.97 d 6.6	22.5, CH_3
5"			0.97 d 6.6	22.5, CH_3
1"'		170.0, C		172.9, C
2"'	2.03	20.1, CH_3	2.14 m	43.3, CH_2
3"'			2.03 m	25.5, CH
4"'			0.90 d 6.9	22.4, CH_3
5"'			0.90 d 6.9	22.4, CH_3

3.2.3 Bioactivities of isolated compounds

All isolated compounds were tested for antiplasmodial activity against the Dd2 strain of *P. falciparum*. Petradoriolide C (**3.3**) displayed moderate antiplasmodial activity, with an IC_{50} value of 7.25 μM. The new diterpenes petradoriolide A–D (**3.1**–**3.4**) and petradoriolone I (**3.5**) were also tested for antiproliferative activity against the A2780 ovarian cancer cells. None of them displayed significant activity, all having IC_{50} values higher than 20 μM, as showed in Table **3-9**.

Table 3-9. Biological Activity of compounds **3.1**–**3.7**

Compound	*P. falciparum* Dd2 IC_{50} (μM)	A2780 IC_{50} (μM)
1	NA	> 50
2	> 20	> 50
3	7.25 ± 0.63	> 50
4	> 20	> 50
5	> 20	> 50
6	NA	NT
7	> 20	NT
Artemisinin	0.0085 ± 0.3	NT
Paclitaxel	NT	0.013 ± 0.001

3.3 Experimental Section

3.3.1 General Experimental Procedures

Optical rotations were recorded on a JASCO P-2000 polarimeter. UV and IR spectroscopic data were measured on a Shimadzu UV-1201 spectrophotometer and a MIDAC M-series FTIR spectrophotometer, respectively. ECD spectra were obtained on a JASCO J-815 circular dichroism spectrometer. NMR spectra were recorded in $CDCl_3$ on Bruker Avance 500 or 600 spectrometers. The chemical shifts are given in δ (ppm), and coupling

constants (*J*) are reported in Hz. Mass spectra were obtained on an Agilent 6220 LC-TOF-MS in the positive ion mode.

3.3.2 Plant Material.

Stem and root material of a small shrub identified as *Petradoria pumila* (Nutt.) Greene was collected on May 26, 2001. The plant material was collected and identified by Daniel Atha with Michael Windham and Molly Windham. The plant material was collected 50 meters south of Utah Highway 121 at mile marker 28, about 12 miles west of Vernal, Uinta County, Utah, at an altitude of 1,687 m (5,535 ft). A voucher specimen is deposited at the New York Botanical Number under barcode 01269145.

3.3.3 Antiplasmodial Bioassays.

The effect of each fraction and pure compound on parasite growth of the *P. falciparum* Dd2 strain was measured in a 72 h growth assay in the presence of drug as described previously.[4] Briefly, ring stage parasite cultures (100 μL per well, with 1 % hematocrit and 1 % parasitemia) were then grown for 72 h in the presence of increasing concentrations of the drug in a 5% CO_2, 5% O_2, and 90% N_2 gas mixture at 37 °C. After 72 h in culture, parasite viability was determined by DNA quantitation using SYBR Green I. The half-maximum inhibitory concentration (IC_{50}) calculation was performed with GraphPad Prism using nonlinear regression curve fitting. The IC_{50} values are the average of three independent determinations with each determination in duplicate and are expressed ± SEM.

3.3.4 In vitro Antiproliferative Activity Against A2780 Cells.

The A2780 ovarian cancer cell line antiproliferative bioassay was performed at Virginia Tech as previously reported.[19, 20] The A2780 cell line is a drug-sensitive ovarian cancer cell

line.[21] Paclitaxel was used as the positive control.

3.3.5 Extraction and Isolation.

The dried and powdered collection of stems and roots of *Petradoria pumila* was exhaustively extracted with ethanol in two 24-hour percolation steps followed by partition into hexanes, methylene chloride and aqueous sub-fractions. For purposes of fractionation and purification, the methylene chloride fraction designated 112461-09G was shipped to Virginia Tech for bioassay-guided isolation. A 340 mg portion of this extract was detanninized by dissolving it in MeOH and filtering it through a 12 x 3.5 cm polyamide column. The filtrate was evaporated and subjected to a 12 x 3.5 cm C-18 SPE column with elution with MeCN (150 mL) followed by MeOH (150 mL) to afford MeCN and MeOH fractions with IC_{50} values of 3 and 5 μg/mL. The MeCN fraction was separated by chromatography on an open silica gel column with $CHCl_3$:MeOH 9:1 to generate fourteen subfractions (**C3-1.1**–**C3-1.14**). Fraction **C3-1.2** (12.0 mg) with an IC_{50} value of 8 μg/mL was purified by HPLC on a C-18 column using MeOH:H_2O from 70:30 to 100:0 in 30 mins to yield compound **3.7** (0.6 mg) with a retention time of 24.2 min. Fraction **C3-1.4** (6.0 mg) with an IC_{50} value of 5 μg/mL was separated by HPLC on a C-18 column using MeOH and H_2O gradient from 70% MeOH to 100% MeOH in 30 mins to yield compound **3.6** (0.7 mg) and compound **3.1** (1.1 mg) with retention times of 11.2, and 21.5 min. Fraction **C3-1.7** (8.0 mg) with an IC_{50} value of 3 μg/mL was separated by HPLC on a C-18 column using a MeOH:H_2O gradient from 50% MeOH to 100% MeOH in 40 mins to yield compound **3.5** (2.0 mg) and compound **3.2** (1.0 mg) with retention times of 19.1 and 32.0 min. Fraction

C3-1.9 (14.3 mg) with an IC_{50} value of 5 μg/mL was purified by HPLC on a C-18 column using MeOH:H_2O from 60:40 to 100:0 in 30 mins and then MeOH alone for 10 min to yield compound **3.3** (1.1 mg) with a retention time of 31.2 min. Fraction **C3-1.11** (7.2 mg) with an IC_{50} value of 2.5 μg/mL was purified by HPLC on a C-18 column using MeO:H_2O from 60:40 to 100:0 in 30 mins to yield compound **3.4** (0.6 mg) with a retention time of 28.3 min. The active MeOH fraction was also fractionated by C-18 HPLC but failed to yield any pure compounds.

3.3.6 Compound Information

Petradoriolide A (**3.1**): yellow powder; $[\alpha]_D^{21}$ +16.9º (c 6.5×10^{-4} g/mL, MeOH); UV (c 0.248 mM, MeOH) λ_{max} (ε) 220 nm (6167), 295 nm (4926); ECD (c 0.248 mM, MeOH) $\Delta\varepsilon_{304}$ – 0.8; HRESIMS *m/z* 385.2364 $[M+Na]^+$ (calcd. for $C_{22}H_{34}NaO_4$, 385.2349); ^{1}H NMR (500 MHz, $CDCl_3$) and ^{13}C NMR (125 MHz, $CDCl_3$), see Table **3-1**.

Petradoriolide B (**3.2**): yellow powder; $[\alpha]_D^{21}$ +24.1º (c 2.9×10^{-4} g/mL, MeOH); UV (c 0.604 mM, MeOH) λ_{max} (ε) 206 nm (2528), 279 nm (415); ECD (c 0.604 mM, MeOH) $\Delta\varepsilon_{298}$ – 0.17; HRESIMS *m/z* 343.2225 $[M+Na]^+$ (calcd. for $C_{20}H_{32}NaO_3$, 343.2244); ^{1}H NMR (500 MHz, $CDCl_3$) and ^{13}C NMR (125 MHz, $CDCl_3$), see Table **3-3**.

Petradoriolide C (**3.3**): yellow powder; $[\alpha]_D^{21}$ +12.1º (c 1.65×10^{-4} g/mL, MeOH); HRESIMS *m/z* 387.2504 $[M+Na]^+$ (calcd. for $C_{22}H_{36}NaO_4$, 387.2506); ^{1}H NMR (500 MHz, $CDCl_3$) and ^{13}C NMR (125 MHz, $CDCl_3$), see Table **3-5**.

Petradoriolide D (**3.4**): yellow powder; $[\alpha]_D^{21}$ +34.0º (c 2.35×10^{-4} g/mL, MeOH); HRESIMS *m/z* 345.2421 $[M+Na]^+$ (calcd. for $C_{20}H_{34}NaO_3$, 345.2400); ^{1}H NMR (500 MHz, $CDCl_3$) and ^{13}C NMR (125 MHz, $CDCl_3$), see Table **3-6**.

Petradoriolone I (**3.5**): yellow oil; HRESIMS *m/z* 223.0743 $[M+Na]^+$ (calcd. for $C_{13}H_{12}NaO_2$, 223.0730) and 201.0920 $[M+H]^+$ (calcd. for $C_{13}H_{13}O_2$, 201.0910); ^1H NMR (500 MHz, $CDCl_3$) and ^{13}C NMR (125 MHz, $CDCl_3$), see Table **3-7**.

(7E)-(7'R,8'S)-4'-hydroxy-3',5-dimethoxy-4,7'-epoxy-8',3-neolig-7-en-9,9'-diyl diacetate (**3.6**): yellow oil; $[\alpha]_D^{21}$ −62.1° (c 1.45×10^{-4} g/mL, MeOH); HRESIMS *m/z* 465.1537 $[M+Na]^+$ (calcd. for $C_{24}H_{26}NaO_8$, 465.1520); ^1H NMR (500 MHz, $CDCl_3$) and ^{13}C NMR (125 MHz, $CDCl_3$), see Table **3-8**.

(7E)-(7'R,8'S)-4'-hydroxy-3',5-dimethoxy-4,7'-epoxy-8',3-neolig-7-en-9,9'-diyl di-3-methylbutanoate. (**3.7**): yellow oil; $[\alpha]_D^{21}$ −63.2° (c 0.95×10^{-4} g/mL, MeOH); HRESIMS *m/z* 549.2485 $[M+Na]^+$ (calcd. for $C_{30}H_{38}NaO_8$, 549.2459); ^1H NMR (500 MHz, $CDCl_3$) and ^{13}C NMR (125 MHz, $CDCl_3$), see Table **3-8**.

3.4 References

1. Anderson, L. C. Studies on *Petradoria* (Compositae): Anatomy, Cytology, Taxonomy. *Trans. Kansas Acad. Sci.* **1963,** *66*, 632–684.

2. Liu, Y.; Rakotondraibe, L. H.; Brodie, P. J.; Wiley, J. D.; Cassera, M. B.; Goetz, M.; Kingston, D. G. I. Antiproliferative and Antimalarial Sesquiterpene Lactones from *Piptocoma antillana* from Puerto Rico. *Nat. Prod. Comm.* **2014,** *9* (10), 1403–1406.

3. Su, Q.; Dalal, S.; Goetz, M.; Cassera, M. B.; Kingston, D. G. I. New Antiplasmodial Diterpenes from *Gutierrezia sarothrae*. *Nat. Prod. Comm.* **2016,** *11* (6), 719–721.

4. Du, Y.; Pearce, K. C.; Dai, Y.; Krai, P.; Dalal, S.; Cassera, M. B.; Goetz, M.; Crawford, T. D.; Kingston, D. G. I. Antiplasmodial Sesquiterpenoid Lactones from *Trichospira verticillata*: Structure Elucidation by Spectroscopic Methods and Comparison of Experimental and

Calculated ECD Data. *J. Nat. Prod.* **2017,** *80* (5), 1639−1647.

5. Wahlberg, I.; Nordfors, K.; Nishida, T.; Enzell, C. R.; Berg, J. E. Oxidative Transformations of the Side Chains in the (12*E*)-Abienol and (12*Z*)-Abienol. *Acta Chem. Scand., Ser. B* **1983,** *37* (3), 209−218.

6. Garcia-Granados, A.; Fernandez, A.; Gutierrez, M. C.; Martinez, A.; Quiros, R.; Rivas, F.; Arias, J. M. Biotransformation of Ent-13-epi-Manoyl Oxides Difunctionalized at C-3 and C-12 by Filamentous Fungi. *Phytochemistry* **2004,** *65* (1), 107−115.

7. Zdero, C.; Bohlmann, F.; King, R. M. Diterpenes and Norditerpenes from the Aristeguetia Group. *Phytochemistry* **1991,** *30* (9), 2991−3000.

8. Zhang, J.; Li, Y.; Zhu, R.; Li, L.; Wang, Y.; Zhou, J.; Qiao, Y.; Zhang, Z.; Lou, H. Scapairrins A-Q, Labdane-Type Diterpenoids from the Chinese Liverwort *Scapania irrigua* and Their Cytotoxic Activity. *J. Nat. Prod.* **2015,** *78* (8), 2087−2094.

9. Murphy, W. S. Octant Rule - its Place in Organic Stereochemistry. *J. Chem. Ed.* **1975,** *52* (12), 774−776.

10. Barrero, A. F.; Sanchez, J. F.; Alvarezmanzaneda, E. J.; Altarejos, J.; Munoz, M.; Haidour, A. Synthesis of nor-Ambreinolide from (+)-cis-Abienol. *Tetrahedron* **1994,** *50* (22), 6653−6662.

11. Shen, Y.-C. Preparation of ambrox from labdanes of *Dysoxylum hongkongense*, and the preparation of new diterpenoids from *Dysoxylum hongkongense*. US 9,260,404 BI, 2016: Feb 16.

12. Wahlberg, I.; Nordfors, K.; Nishida, T.; Enzell, C. R.; Berg, J. E. Oxidative Transformations of the Side Chains in the (12E)-Abienol and (12Z)-Abienol *Acta Chem.*

Scand., Ser. B **1983,** *37* (3), 209–218.

13. Albrecht, S.; Al-Lakkis-Wehbe, M.; Orsini, A.; Defoin, A.; Pale, P.; Salomon, E.; Tarnus, C.; Weibel, J. M. Amino-benzosuberone: A Novel Warhead for Selective Inhibition of Human Aminopeptidase-N/CD13. *Bioorg. Med. Chem.* **2011,** *19* (4), 1434–1449.

14. Bohlmann, F.; Jakupovic, J.; Schuster, A.; King, R. M.; Robinson, H. Naturally-occurring Terpene Derivatives. 380. Guaianolides and Homoditerpenes from *Lasiolaena morii*. *Phytochemistry* **1982,** *21* (1), 161–165.

15. Bohlmann, F.; Jakupovic, J.; Warning, U.; Grenz, M.; Chauthi, T. V.; King, R. M.; Robinson, H. Sesquiterpenes with New Carbon Skeletons, Furoeremophilanes, Secoeremophilanes and Other Constituents from Argentinean *Senecio* species. *Bull. Soc. Chim. Belges* **1986,** *95* (9-10), 707–736.

16. Li, S. M.; Iliefski, T.; Lundquist, K.; Wallis, A. F. A. Reassignment of Relative Stereochemistry at C-7 and C-8 in Arylcoumaran Neolignans. *Phytochemistry* **1997,** *46* (5), 929–934.

17. Kim, K. H.; Ha, S. K.; Kim, S. Y.; Youn, H. J.; Lee, K. R. Constituents of *Limonia acidissima* Inhibit LPS-induced Nitric Oxide Production in BV-2 Microglia. *J. Enz. Inhib. Med. Chem.* **2010,** *25* (6), 887–892.

18. Jakupovic, J.; Eid, F.; Bohlmann, F.; El-Dahm, S. Malabaricane Derivatives from *Pyrethrum santolinozdes*. *Phytochemistry* **1987,** *26*, 1536–1538.

19. Cao, S.; Brodie, P. J.; Miller, J. S.; Randrianaivo, R.; Ratovoson, F.; Birkinshaw, C.; Andriantsiferana, R.; Rasamison, V. E.; Kingston, D. G. I. Antiproliferative Xanthones of *Terminalia calcicola* from the Madagascar Rain Forest. *J. Nat. Prod.* **2007,** *70* (4), 679–681.

20. Pan, E. D.; Harinantenaina, L.; Brodie, P. J.; Miller, J. S.; Callmander, M. W.; Rakotonandrasana, S.; Rakotobe, E.; Rasamison, V. E.; Kingston, D. G. I. Four Diphenylpropanes and a Cycloheptadibenzofuran from *Bussea sakalava* from the Madagascar Dry Forest. *J. Nat. Prod.* **2010,** *73* (11), 1792−1795.

21. Louie, K. G.; Behrens, B. C.; Kinsella, T. J.; Hamilton, T. C.; Grotzinger, K. R.; McKoy, W. M.; Winker, M. A.; Ozols, R. F. Radiation Survival Parameters of Antineoplastic Drug-sensitive and Drug-resistant Human Ovarian-cancer cell-lines and their Modification by Buthionine Sulfoximine. *Cancer Res.* **1985,** *45* (5), 2110−2115.

Chapter 4: An Antiplasmodial Coumarin and Norneolignan from *Aniba citrifolia*

This chapter is a slightly expanded version of an article that is in preparation for submission of Chemistry and Biodiversity. (Du, Y.; Dai, Y.; Dalal, S.; Cassera, M. B.; Clement, J.; Goetz, M.; Kingston, D. G. I., The Antiplasmodial Coumarin Anibomarin A and the Norneolignan Anibignan A from *Aniba citrifolia* submitted to Chemistry and Biodiversity.) Author contributions to the article are described as follows in the order of the names listed. The author of this dissertation (Mr. Yongle Du) isolated and determined the structures of isolated compounds, performed the A2780 bioassay on the isolated compounds, and drafted the manuscript. Dr. Yumin Dai was a mentor for this work, and provided some important hints for the isolation and structural elucidation of the compounds, and also proofread the manuscript before submission. Dr. Seema Dalal carried out the antiplasmodial bioassays on the fractions and the isolated compounds under the direction of Maria B. Cassera. Dr. Jason Clement and Dr. Michael Goetz from the Natural Products Discovery Institute (NPDI) provided the plant extract from the NPDI repository. Dr. David G. I. Kingston was a mentor for this work and the corresponding author for the published article. He also edited the final manuscript.

4.1 Introduction

4.1.1 Abstract

In our continuing search for novel natural products with antiplasmodial activity, an

extract of *Aniba citrifolia* was found to have good activity, with an IC_{50} value less than 1.25 μg/mL. After bioassay-directed isolation, the new coumarin anibomarin A (**4.1**), the new norneolignan anibignan A (**4.2**), and the six known neolignans **4.3**–**4.8** were obtained. Their structures were determined based on analyses of 1- and 2-D NMR spectroscopic and mass spectrometric data, and the absolute configuration of anibignan A (**4.2**) was assigned from its ECD spectrum. Anibomarin A (**4.2**) displayed weak antiplasmodial activity, with an IC_{50} value of 18.2 μM.

4.1.2 Investigations of the genus *Aniba*

An extract of *Aniba citrifolia* was found to have good antiplasmodial activity against the chloroquine-resistant Dd2 strain of *P. falciparum*, with an IC_{50} value less than 1.25 μg/mL. The genus *Aniba*, which includes at least forty-eight species, is a neotropical flowering plant genus widely distributed in the Caribbean and Central and South America.[1] Members of the genus are good sources of flavonoids, alkaloids, and neolignans[2] with a broad range of bioactivities, including antimicrobial[3] and anticancer activities.[2-5] However, except for one report on the antimalarial activity of synthetic aniba A-type dimers,[6] there have been no reports of antiplasmodial or antimalarial compounds from members of the genus, and this extract was thus selected for investigation of its antiplasmodial constituents.

4.2 Results and Discussion

4.2.1 Isolation of active compounds

An extract of the whole plant of *Aniba citrifolia* was subjected to liquid–liquid partition to afford hexanes, dichloromethane and methanol/water fractions. All three fractions displayed antiplasmodial activity against the drug-resistant Dd2 strain of *Plasmodium*

falciparum, with IC_{50} values of < 1.25, <<< 1.25 and < 1.25 μg/mL, respectively. The new coumarin anibomarin A (**4.1**) and the new norneolignan anibignan A (**4.2**), along with the six known neolignans **4.3**–**4.8** were obtained by bioassay-guided isolation from the hexanes and dichloromethane fractions. The major bioactive components from the aqueous methanol fraction were most likely tannins, since this fraction lost activity after passage through a polyamide column.

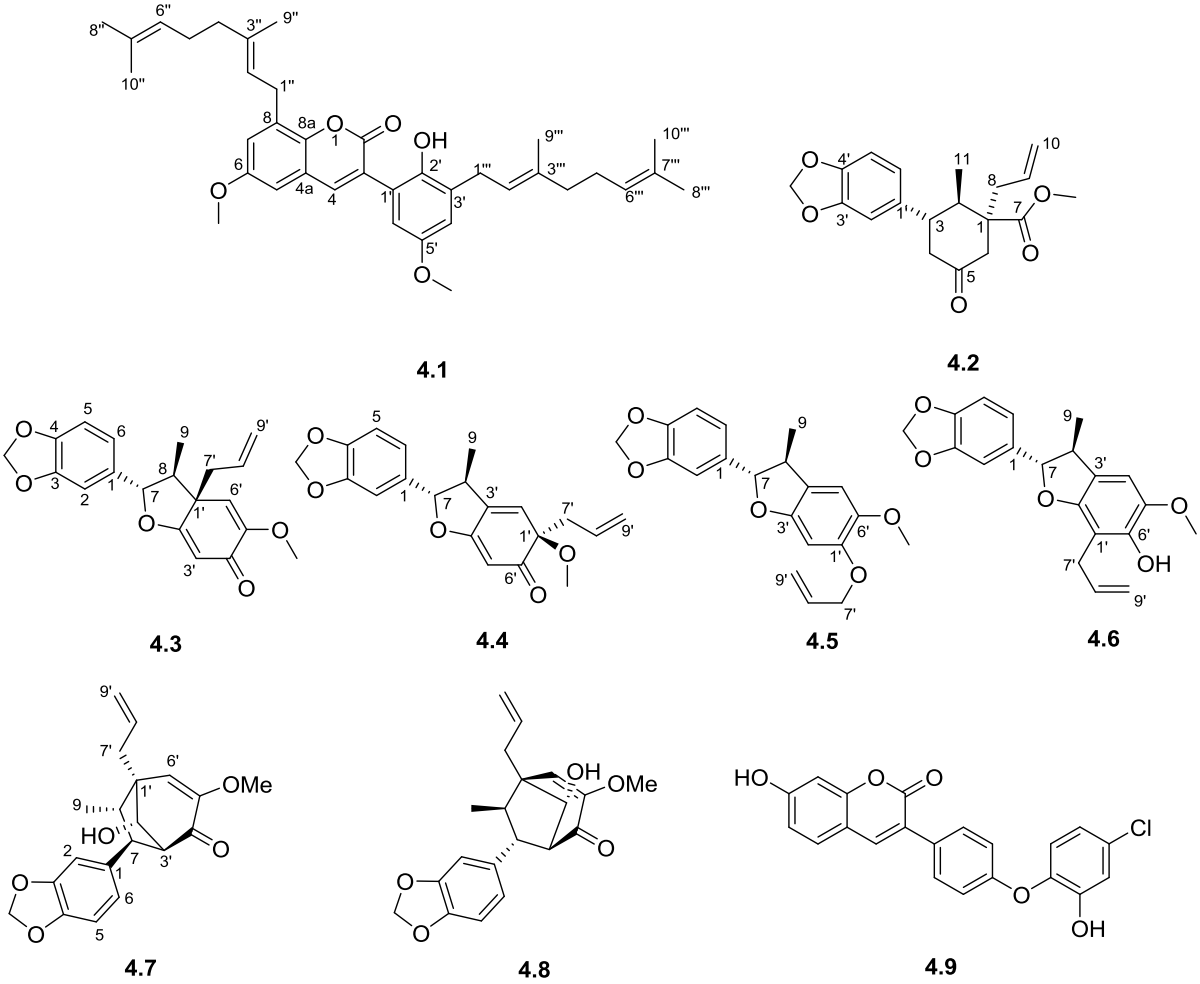

4.2.2 Structure elucidation of isolated compounds

Anibomarin A (**4.1**) was isolated as a yellow oil. Its positive ion HRESIMS revealed a peak for a protonated molecular ion at *m/z* 571.3412 and for a sodium adduct ion at *m/z* 593.3229, both corresponding to the molecular formula of $C_{37}H_{46}O_5$ for **4.1**. Its UV spectrum,

with absorptions at 208 nm, 288 nm and 355 nm, suggested that it was a 3-arylcoumarin derivative.[7] Its ^{1}H NMR (shown in Table **4-1**) and HSQC spectra displayed signals for two methoxy groups (δ_H 3.79 and 3.86), six vinyl methyl groups (δ_H 1.75, H-9" (3H); 1.74, H-9"' (3H); 1.68, H-8" and H-8"' (6H); 1.60, H-10" and H-10"' (6H)), six methylene protons (δ_H 3.61, H-1" (1H); 3.45, H-1"' (1H); 2.12, H-5" and H-5"' (2H); 2.07, H-4" and H-4"' (2H)), five aromatic methines (δ_H 7.87, H-4; 7.05, H-7; 6.84, H-4'; 6.83, H-5; 6.67, H-6'), four vinyl methines (5.36, H-2"'; 5.35, H-2"; 5.11, H-6"'; 5.10, H-6") and a hydroxyl group (δ_H 7.15).

Table 4-1. NMR Spectroscopic Data for Compounds **4.1** in $CDCl_3$ (500 MHz)

position	δ_H, *J* in Hz	δ_C, type	position	δ_H, *J* in Hz	δ_C, type
2		163.1, C	2"	5.35 m	120.3, CH
3		127.7, C	3"		138.5, C
4	7.87 s	144.3, CH	4"	2.07 m	39.9, CH_2
4a		119.8, C	5"	2.12 m	26.9, CH_2
5	6.83 d 3.0	107.1, CH	6"	5.10 m	124.2, CH
6		156.5, C	7"		131.7, C
7	7.05 d 3.0	120.7, CH	8"	1.68 s	25.8, CH_3
8		131.5, C	9"	1.75 s	16.3, CH_3
8a		146.1, C	10"	1.60 s	17.9, CH_3
1'		124.1, C	1"'	3.45 d 7.3	29.2, CH_2
2'		146.9, C	2"'	5.36 m	122.1, CH
3'		133.1, C	3"'		137.2, C
4'	6.84 d 3.0	116.9, CH	4"'	2.07 m	39.9, CH_2
5'		153.8, C	5"'	2.12 m	26.7, CH_2
6'	6.67 d 3.0	113.1, C	6"'	5.11 m	124.4, CH
6-OMe	3.86 s	55.9, CH_3	7"'		131.8, C
5'-OMe	3.79 s	55.9, CH_3	8"'	1.68 s	25.8, CH_3
2'-OH	7.15 s		9"'	1.74 s	16.4, CH_3
1"	3.61 d 7.3	27.6, CH_2	10"'	1.60 s	17.9, CH_3

The presence of a 3-phenyl coumarin skeleton was indicated by ^{3}*J*-HMBC correlations between H-6' and C-3 (δ_C 127.7) and H-4 and C-1' (δ_C 124.1), and supported by the correlations between H-4' and C-2' (δ_C 146.9), H-4' and C-6' (δ_C 113.1), H-6' and C-2' (δ_C 146.9), H-4 and C-2 (δ_C 163.1), H-4 and C-8a (δ_C 146.1), H-4 and C-5 (δ_C 107.1), H-5 and C-8a (δ_C 146.1), H-7 and C-5 (δ_C 107.1), H-7 and C-8a (δ_C 146.1).[8] The hydroxyl group was

assigned to C-2' (δ_C 146.9) based on the observed ^3J-HMBC correlations between OH and C-1' (δ_C 124.1) and OH and C-3' (δ_C 133.1). The two methoxy groups were assigned to C-6 (δ_C 156.5) and C-5' (δ_C 153.8) based on the ^3J-HMBC correlations between OCH_3 (δ_H 3.85) and C-6, and OCH_3 (δ_H 3.79) and C-5'. The remaining twenty carbons and thirty-four protons composed two myrcene-type monoterpene side chains, as confirmed by ^3J-HMBC correlations between H-1" and C-3", H-2" and C-9", H-2" and C-4", H-9" and C-4", H-4" and C-6", H-5" and C-3", H-5" and C-7", H-6" and C-8", H-6" and C-10", H-10" and C-8"; H-1'" and C-3'", H-2'" and C-9'", H-2'" and C-4'", H-9'" and C-4'", H-4'" and C-6'", H-5'" and C-3'", H-5'" and C-7'", H-6'" and C-8'", H-6'" and C-10'", H-10'" and C-8'". These two identical side chains were linked to C-8 and C-3', indicated by ^3J-HMBC correlations between H-1" and C-7, H-1" and C-8a, H-1" and C-2', H-1" and C-4' (Figure **4-1**).

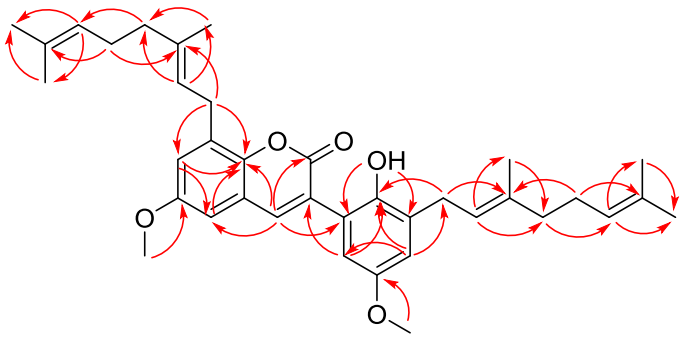

Figure 4-1. HMBC correlations for anibomarin A (**4.1**)

The configurations of the C-2" and C-2'" carbon-carbon double bonds were assigned as *E* based on the NOESY crosspeaks between H-1" and H-9", H-2" and H-5", H-1'" and H-9'", H-2'" and H-4'", as shown in Figure **4-2**. In conclusion, anibomarin A **4.1** was assigned as 8-((2"*E*)-3",7"-dimethylocta-2",6"-dien-1"-yl)-6-methoxy-3-(3'-((2'"*E*)-3'",7'"-dimethylocta-2'" ,6'"-dien-1'"-yl-2'-hydroxyl-5'-methoxyl)phenylcoumarin.

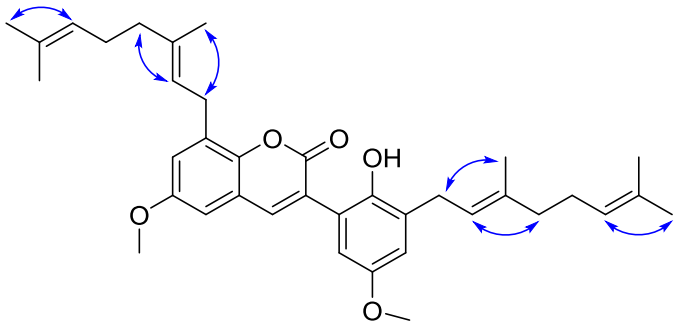

Figure 4-2. NOESY correlations for anibomarin A (**4.1**)

Anibignan A (**4.2)** was also isolated as yellow oil. Its positive ion HRESIMS revealed a peak for a protonated molecular ion at *m/z* 331.1543 and for a sodium adduct ion at *m/z* 353.1372, both corresponding to a molecular formula of $C_{19}H_{22}O_5$. The ^{1}H NMR (shown in Table **4-2**) and HSQC spectra displayed signals for one methoxy group (δ_H 3.67), one methyl group (δ_H 0.87, H-11), one methylenedioxy group (δ_H 5.95), one olefinic methylene group (δ_H 5.18, 5.12 H-10), three alkyl methylene groups (δ_H 2.81, 2.32, H-4; 2.65, 2.49, H-6; 2.38, 2.19, H-8), one olefinic methine (δ_H 5.71, H-9), two alkyl methines (δ_H 3.03, H-3; 2.28, H-2) and three aromatic protons of an ABX spin system (δ_H 6.73 d, *J*=1.7 Hz, H-2'; 6.76 d, *J*=7.9 Hz, H-5'; 6.69 dd, *J*=7.9, 1.7 Hz, H-6').

Table 4-2. NMR Spectroscopic Data for Compounds **4.2** in $CDCl_3$ (500 MHz)

position	δ_H, *J* in Hz	δ_C, type	position	δ_H, *J* in Hz	δ_C, type
1		53.0, C	10a	5.18 dd 10.2, 1.3	120.0, CH_2
2	2.28 dq 11.7, 7.0	46.1, CH	10b	5.12 dd 17.0, 1.3	
3	3.03 td 11.7, 7.7	47.1, CH	11	0.87 d 7.0	13.0, CH_3
4a	2.81 dd 18.5, 7.7	39.1, CH_2	1'		136.8, C
4b	2.32 dd 18.5, 11.7		2'	6.73 d 1.7	107.4, CH
5		220.0, C	3'		148.1, C
6a	2.65 d 16.0	47.3, CH_2	4'		146.5, C
6b	2.49 d 16.0		5'	6.76 d 7.9	108.4, CH
7		172.4, C	6'	6.69 dd 7.9, 1.7	121.1, CH
8a	2.38 ddt 13.5, 6.5 1.3	43.0, CH_2	OCH_2O	5.95 s	101.1, CH_2
8b	2.19 dd, 13.5, 8.5		OMe	3.67 s	52.1, CH_3
9	5.71 dddd, 17, 10.2, 8.5, 6.5	133.0, CH			

The methylenedioxy group was attached to the benzene ring with the ABX spin system, indicated by ^{3}J-HMBC correlations between OCH_2O (δ_H 5.95) and C-3' (δ_C 148.1), OCH_2O (δ_H 5.95) and C-4' (δ_C 146.5), H-2' and C-4', H-5' and C-3', H-6' and C-4'. The presence of a methyl ester was confirmed by ^{3}J-HMBC correlations between OCH_3 (δ_H 3.67) and C-7 (δ_C 172.4). The presence of an allyl group was indicated by signals for H-8 (δ_H 2.38 ddt, 13.5, 6.5, 1.3; 2.38 dd, 13.5, 8.5), H-9 (δ_H 5.71 dddd, 17.0, 10.2, 8.5, 6.2) and H-10 (δ_H 5.18 dd, 10.2, 1.3; 5.12 dd, 17.0, 1.3), and was confirmed by a ^{3}J-HMBC correlation between H-10 and C-8 (δ_C 43.0). The presence of a 4-methylcyclohexanone unit was indicated by signals for the remaining seven carbons and nine protons: H_2-4 (δ_H 2.81 dd, 18.5, 7.7; 2.32 dd, 18.5, 11.7), H_2-6 (δ_H 2.65 d, 16.0; 2.49 d, 16.0), H-3 (δ_H 3.03 dt, 11.7, 7.7), H-2 (δ_H 2.28 dq, 11.7, 7.0), and H_3-11 (δ_H 0.87 d, 7.0). This partial structure was confirmed by ^{2}J-HMBC correlations between H-4 and C-5 (δ_C 220.0), H-6 and C-5 and ^{3}J-HMBC correlations between H-4 and C-2 (δ_C 46.1), H-6 and C-2, H-3 and C-11 (δ_C 13.0), H-11 and C-1 (δ_C 53.0). The benzene ring was attached to C-3 based on the observed ^{3}J-HMBC correlations between H-3 and C-2' (δ_C 107.4), H-3 and C-6' (δ_C 121.1), H-2 and C-1' (δ_C 136.8). The methyl ester and allyl groups were linked at C-1, indicated by the ^{3}J-HMBC correlations between H-6 and C-7 (δ_C 172.4), H-2 and C-8 (δ_C 43.0), and H-6 and C-8 (Figure **4-3**).

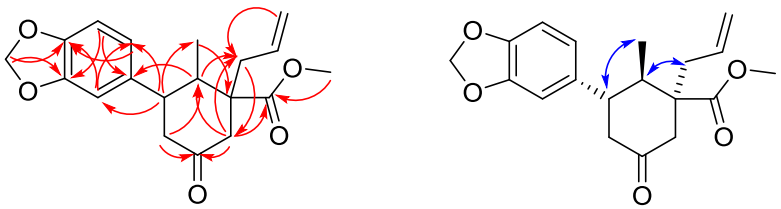

Figure 4-3. HMBC (red) and NOESY (blue) correlations for anibignan A (**4.2**)

The relative configurations of carbons C-1, C-2 and C-3 were assigned as 1*S**,2*R**,3*S**

based on NOESY crosspeaks between H-8 and H-2, H-3 and H-11, as shown in Figure **4-3**. The absolute configuration of **4.2** was determined by its electronic circular dichroism spectrum. C-3 was assigned as *S* based on the positive n–π* Cotton effect at 298 nm.[9] The structure of anibignan A (**4.2**) was thus assigned as methyl (1*S*,2*R*,3*S*)-1-allyl-3-(benzo[d][1,3]dioxol-5-yl)-2-methyl-5-oxocyclohexane-1-carboxylate.

Compounds **4.3**–**4.4** were identified as (+)-burchellin **4.3**,[10] (7*S*,8*S*,1'*R*)-$\Delta^{8'}$-1'-methoxy-3,4-methylenedioxy-1',6'-dihydro-6'-oxo-7-*O*-4',8,3'-neolignan **4.4**, as reported in Tables **4-3**.

Table 4-3. NMR Spectroscopic Data for Compounds **4.3**–**4.4** in $CDCl_3$ (500 MHz)

	4.3		**4.4**	
position	δ_H, *J* in Hz	δ_C, type	δ_H, *J* in Hz	δ_C, type
1		131.6, C		131.4, C
2	6.76 dd 1.0, 0.6	106.9, CH	6.83 m	106.4, CH
3		148.5, C		148.1, C
4		148.4, C		148.3, C
5	6.81 dd 7.8, 0.6	108.3, CH	6.84 m	107.5, CH
6	6.78 dd 7.8, 1.0	120.9, CH	6.83 m	120.3, CH
7	5.16 d 9.9	91.6, CH	5.03 d 7.9	93.9, CH
8	2.27 dq 9.9, 6.9	49.6, CH	3.02 dqd 7.9, 6.7, 2.5	42.7, CH
9	1.15 d 6.9	8.0, CH_3	1.34 d 6.7	16.3, CH_3
OCH_2O	5.98 s	101.5, CH_2	6.00 s	101.1, CH_2
1'		51.4, C		81.4, C
2'		181.4, C	6.19 d 2.5	134.4, CH
3'	5.80 s	102.1, CH		140.0, C
4'		182.5, C		172.2, C
5'		153.6, C	5.68 s	99.2, CH
6'	5.41 s	109.9, CH		199.8, C
7'a	2.54 dd 13.5, 7.0	36.8, CH_2	2.53 dd 13.3, 7.5	45.5, CH_2
7'b	2.33 dd 13.5, 7.6		2.47 dd 13.3, 7.5	
8'	5.54 dddd 17.0, 10.1, 7.6, 7.0	131.2, CH	5.69 m	131.1, CH
9'a	5.08 dd 10.1, 1.7	120.3, CH_2	5.07 m	119.0, CH_2
9'b	5.00 dd 17.0, 1.7		5.05 m	
OMe	3.68 s	55.1, CH_3	3.17 s	54.0, CH_3

Compounds **4.5**–**4.6** were identified as (7*S*,8*S*)-$\Delta^{8'}$-6'-methoxy-3,4-methylenedioxy-7-*O*-3',8,4',1'-*O*-7'-neolignan **4.5**,[11] *trans*-2,3-dihydro-7-allyl-6-hydroxy-5-methoxy-3-methyl-2-(3,4-methylenedioxyphenyl)benzofuran **4.6**,[11-13] as reported in Tables **4-4**.

Table 4-4. NMR Spectroscopic Data for Compounds **4.5**–**4.6** in $CDCl_3$ (500 MHz)

	4.5		**4.6**	
position	δ_H, *J* in Hz	δ_C, type	δ_H, *J* in Hz	δ_C, type
1		134.6, C		135.5, C
2	6.91 d 1.7	105.4, CH	6.90 d 1.7	106.0, CH
3		147.2, C		147.8, C
4		147.6, C		147.7, C
5	6.80 d 7.9	108.1, CH	6.79 d 7.9	108.0, CH
6	6.87 dd 7.9, 1.9	119.9, CH	6.85 dd 7.9, 1.7	119.5, CH
7	5.03 d 8.7	93.0, CH	5.02 d 8.5	91.9, CH
8	3.36 dq 8.7 6.8	45.5, CH	3.30 ddd 8.5, 6.8, 1.0	46.3, CH
9	1.36 d 6.8	18.1, CH_3	1.36 d 6.8	18.7, CH_3
OCH_2O	5.96 s	100.8, CH_2	5.95 s	100.8, CH_2
1'		148.9, C		109.1, C
2'	6.50 s	97.0, CH		152.0, C
3'		152.0, C		120.7, C
4'		122.2, C	6.55 d 1.0	104.6, CH
5'	6.70 s	108.8, CH		141.2, C
6'		143.7, C		143.9, C
7'	4.58 dt 5.4, 1.5	69.9, CH_2	3.42 dt 5.8, 1.5	28.2, CH_2
8'	6.07 ddt 17.3, 10.7, 5.4	133.3, CH	6.03 ddt 17.1, 10.0, 5.8	135.4, CH
9'a	5.41 ddd 17.3, 1.5, 1.5	118.0, CH_2	5.08 ddt 17.1, 2.0, 1.5	115.3, CH_2
9'b	5.28 ddd 10.7, 1.5, 1.5		5.00 ddt 10.0, 2.0, 1.5	
OMe	3.84 s	57.1, CH_3	3.85 s	57.0, CH_3

Compounds **4.7**–**4.8** were identified as (7*S*,8*S*,1'*S*,2'*S*,3'*S*)-$\Delta^{5',8'}$-2'-hydroxy-5'-methoxy-3,4-methylenedioxy-4'-oxo-7,3',8,1'-neolignan **4.7**,[14] and (7*R*,8*R*,1'*S*,2'*R*,3'*S*)-$\Delta^{5',8'}$-2'-hydroxy-6'-methoxy-3,4-methylenedioxy-4'-oxo-7.3',8.1'-neolignan **4.8**,[14] as reported in Tables **4-5**.

Table 4-5. NMR Spectroscopic Data for Compounds **4.7**–**4.8** in $CDCl_3$ (500 MHz)

	4.7		**4.8**	
position	δ_H, *J* in Hz	δ_C, type	δ_H, *J* in Hz	δ_C, type
1		132.8, C		136.2, C
2	6.53 d 1.9	108.6, CH	7.09 d 1.8	109.4, CH
3		147.5, C		147.6, C
4		146.9, C		146.5, C
5	6.69 d 7.9	108.3, CH	6.72 d 8.0	108.0, CH
6	6.54 dd 7.9, 1.9	121.5, CH	6.78 dd 8.0, 1.8	122.2, CH
7	3.06 dd 6.6, 6.6	50.4, CH	2.48 dm 8.0	54.4, CH
8	2.42 qd 7.1, 6.6	46.7, CH	2.39 qd 6.9, 8.0	49.0, CH
9	1.22 d 7.1	17.8, CH_3	0.98 d 6.9	14.0, CH_3
OCH_2O	5.91 s	100.7, CH_2	5.95 s	100.9, CH_2
1'		49.2, C		55.0, C
2'	4.23 dd 4.6, 1.9	81.4, CH	4.05 s	79.8, CH
3'	3.30 dd 4.6, 6.6	62.8, CH	3.00 s	63.8, CH
4'		193.7, C		195.2, C
5'		152.2, C		151.8, C
6'	5.89 d 1.9	119.9, CH	5.67 s	120.8, CH
7'a	2.51 d 7.4	37.6, CH_2	2.53 m	37.4, CH_2
7'b	2.51 d 7.4		2.46 m	
8'	6.05 ddt 17.5, 10, 7.4	134.7, CH	5.89 ddm 17, 11.4	135.6, CH
9'a	5.32 dd 17.5, 1.5	119.7, CH_2	5.25 dd 17.0, 2.0	118.1, CH_2
9'b	5.28 dd 10, 1.5		5.16 dd 11.4, 2.0	
OMe	3.69 s	55.3, CH_3	3.69 s	55.8, CH_3

4.2.3 Bioactivities of isolated compounds

All isolated compounds were tested for antiplasmodial activity against the Dd2 strain of *Plasmodium falciparum*. Although the crude extract showed strong antiplasmodial activity, only anibomarin A (**4.1**) displayed antiplasmodial activity, with an IC_{50} value of 18.2 μM, as showed in Table **4-6**. However, this moderate antiplasmodial activity might possibly be improved by appropriate structural modifications, such as changing the length of the alkyl chain or introducing electron-withdrawing groups on the benzene ring, as was done for the

synthetic compound **4.9** which had submicromolar activity against *P. falciparum* enoyl-ACP-reductase and micromolar activity against the drug-resistant *P. falciparum* K1 Strain.[15]

Table 4-6. Biological Activity of compounds **4.1**–**4.8**.

Compound	*P. falciparum* Dd2 IC_{50} (μM)	A2780 IC_{50} (μM)
4.1	18.2 ± 0.4	NT
4.2	> 100	> 50
4.3	> 30	> 50
4.4	NA	> 50
4.5	~ 30	47 ± 5
4.6	~ 30	35 ± 3
4.7	> 100	> 50
4.8	NA	> 50
Artemisinin	0.0065 ± 0.0005	NT
Paclitaxel	NT	0.013 ± 0.001

The lack of antimalarial activity in the compounds isolated from an active extract was disappointing, and several experiments were carried out to determine the reason for loss of activity. One possibility considered was synergism, and this was tested for by mixing compounds **4.1**–**4.8** and testing the mixture. This "reconstituted extract" did not have improved activity, thus eliminating synergism as the cause of activity loss, at least in this case. A second possible explanation is that tannins in the extract gave false positive results in the bioassay. The crude active extract (IC_{50} <<< 1.25 μg/mL) was thus detanninized by passing it through a polyamide column and then retested, and the detanninized extract was less active than the crude extract, so tannins do appear to contribute to the observed bioactivity of crude extracts. Some antimalarial activity remained, however, with the detanninized fraction having an IC_{50} value of 1.25 μg/mL. After liquid-liquid partition of detanninized extract, the dichloromethane fraction showed very good antiplasmodial activity, with an IC_{50} value of

<<< 1.25 μg/mL. After separation on a Sephadex LH-20 open column, some antiplasmodial activity was lost, but some column fractions were still active. Attempts were made to separate these active fractions on silica gel, diol, and C-18 open columns or by HPLC. The active fraction separated by silica gel open column or by HPLC lost activity completely. The active fraction separated by diol open column or HPLC lost most of its bioactivity, and no active compounds could be isolated from the moderately active subfractions that were obtained. The active fraction separated by C-18 open column or HPLC also lost much of its activity, but two active subfractions were obtained. They appeared to consist of mixtures of lignans and long chain compounds, as judged by ^{1}H NMR analysis, and they could not be separated further on a C-18 column.

It thus appears that the loss of bioactivity is primarily due to a combination of false positive activity due to tannins and to the decomposition or irreversible absorption of compounds on silica gel or diol columns.

The new norneolignan anibignan A (**4.2)** and neolignans **4.3**–**4.8** were also tested for antiproliferative activity against the A2780 ovarian cancer cells. Although anibignan A has some structural similarities with the potent antiproliferative compound bifidenone,[16] neither it nor any of the other compounds showed any significant activity, with IC_{50} values more than 50 μM in most cases; the most active compound is compound **4.6** (IC_{50} 35 μM).

4.3 Experimental Section

4.3.1 General Experimental Procedures

Optical rotations were recorded on a JASCO P-2000 polarimeter. UV and IR spectroscopic data were measured on a Shimadzu UV-1201 spectrophotometer and a MIDAC

M-series FTIR spectrophotometer, respectively. ECD spectra were obtained on a JASCO J-815 circular dichroism spectrometer. NMR spectra were recorded in $CDCl_3$ on Bruker Avance 500 or 600 spectrometers. The chemical shifts are given in δ (ppm), and coupling constants (*J*) are reported in Hz. Mass spectra were obtained on an Agilent 6220 LC-TOF-MS in the positive ion mode.

4.3.2 Plant Material.

Bark, woody parts, and twigs of a tree identified as a member of the genus *Aniba* were collected on September 11, 1992 near Groete Creek, 27 km from Bartica, Essequibo Islands-West Demerara region, Guyana, at an altitude of 50 m (164 ft). The plant material was collected and identified by Suroojnauth Tiwari. A voucher specimen is deposited at the New York Botanical Number under barcode 01269145.

4.3.3 Antiplasmodial Bioassays.

The effect of each fraction and pure compound on parasite growth of the *P. falciparum* Dd2 strain was measured in a 72 h growth assay in the presence of drug as described previously with minor modifications. Briefly, ring stage parasite cultures (100 μL per well, with 1% hematocrit and 1% parasitemia) were then grown for 72 h in the presence of increasing concentrations of the drug in a 5% CO_2, 5% O_2, and 90% N_2 gas mixture at 37 °C. After 72 h in culture, parasite viability was determined by DNA quantitation using SYBR Green I. The half-maximum inhibitory concentration (IC_{50}) calculation was performed with GraphPad Prism software using nonlinear regression curve fitting. IC_{50} values are the average of three independent determinations with each determination in duplicate and are expressed ± SD and artemisinin was used as positive control.[17]

4.3.4 In vitro Antiproliferative Activity Against A2780 Cells.

The A2780 ovarian cancer cell line antiproliferative bioassay was performed at Virginia Tech as previously reported.[18, 19] The A2780 cell line is a drug-sensitive ovarian cancer cell line.[20] Paclitaxel was used as the positive control.

4.3.5 Extraction and Isolation.

The dried and powdered bark (915 g) was exhaustively extracted with methanol in two 24-hour percolation steps and the resulting solution was evaporated to yield 47.4 g of crude extract. For purposes of fractionation and purification, a 2.55 g portion of this methanol extract designated 40258-10A was shipped to Virginia Tech for bioassay-guided isolation. This extract (2.0 g) was dissolved in aqueous MeOH (MeOH-H_2O 9:1, 100 mL), and extracted with hexanes (100 mL) three times. Then the aqueous layer was diluted to 60% MeOH (v/v) with H_2O and extracted with DCM (150 mL) three times. The hexanes fraction (305.0 mg) had an IC_{50} value of < 1.25 μg/mL. The DCM fraction was left 1071.0 mg after evaporated in rotavapor with an IC_{50} value of <<< 1.25 μg/mL. The remaining aqueous MeOH fraction (600 mg) had an IC_{50} value of < 1.25 μg/mL.

The hexanes fraction was loaded on to the Sephadex LH-20 column to afford five fractions (**C4-1.1** – **C4-1.5**). Fraction **C4-1.2** (38.8 mg) with IC_{50} value of ~ 5 μg/mL was purified by HPLC on a C-18 column using acetonitrile:H_2O from 45:55 to 100:0 in 70 mins to yield four known neolignans **4.3** (0.7 mg), **4.4** (0.4 mg), **4.5** (1.0 mg) and **4.6** (0.9 mg), with retention times of 22.3, 26.5, 45.0 and 47.0 min. Fraction **C4-1.3** (40.0 mg) with IC_{50} value of ~ 1.25 μg/mL was separated by HPLC on a C-18 column using acetonitrile and H_2O gradient from 80% acetonitrile to 100% acetonitrile in 35 mins to yield a new coumarin

anibomarin A (**4.1**) (0.7 mg), with retention times of 12.5 min.

The DCM fraction was also separated by Sephadex LH-20 to afford five fractions (**C4-2.1**–**C4-2.5**). Fraction **C4-2.2** (157.3 mg) with IC_{50} value of 1.25 ~ 2.5 μg/mL was fractionated by diol open column with chloroform:MeOH 9:1 to generate ten subfractions (**C4-2.2.1**–**C4-2.2.10**) and the first fraction **C4-2.2.1** (18.4 mg) was further separated by HPLC on a C-18 column using acetonitrile and H_2O gradient from 90% acetonitrile to 100% acetonitrile in 20 mins and then acetonitrile alone for 15 min to yield a new norneolignan anibignan A **4.2** (1.2 mg) with retention times of 28.0 min.. Fraction **C4-2.3** (108.6 mg) was purified by HPLC on a C-18 column using acetonitrile:H_2O from 45:55 to 100:0 in 60 mins to yield two known neolignans **4.7** (0.6 mg) and **4.8** (0.4 mg), with retention times of 32.8 and 52.0 min.

4.3.6 Compound Information

Anibomarin A (**4.1**): yellow oil; UV (c 0.3507 mM, MeOH) λ_{max} (ε) 208 nm (36480), 288 nm (10655), 355 nm (6195); HRESIMS *m/z* 593.3229 $[M+Na]^+$ (calcd. for $C_{37}H_{46}NaO_5$, 593.3237) and 571.3412 $[M+H]^+$ (calcd. for $C_{37}H_{47}O_5$, 571.3418); ^{1}H-NMR (500 MHz, $CDCl_3$) and ^{13}C-NMR (125 MHz, $CDCl_3$), see Table **4-1**.

Anibignan A (**4.2)**: yellow oil; $[\alpha]_D^{21}$ +40.3º (c 4×10^{-4} g/mL, MeOH); UV (c 0.0249 mM, MeOH) λ_{max} (ε) 204 nm (26278), 233 nm (4683), 285 nm (3408); ECD (c 0.0249 mM, MeOH) $\Delta\varepsilon_{298} + 3.4$; HRESIMS *m/z* 353.1372 $[M+Na]^+$ (calcd. for $C_{19}H_{22}NaO_5$, 353.1359) and 331.1543 $[M+H]^+$ (calcd. for $C_{19}H_{23}O_5$, 331.1540); ^{1}H-NMR (500 MHz, $CDCl_3$) and ^{13}C-NMR (125 MHz, $CDCl_3$), see Table **4-2**.

(+)-Burchellin (**4.3**): yellow oil; $[\alpha]_D^{21}$ +47.6º (c 4×10^{-4} g/mL, MeOH); HRESIMS *m/z*

363.1131 $[M+Na]^+$ (calcd. for $C_{20}H_{20}NaO_5$, 363.1203) and 341.1319 $[M+H]^+$ (calcd. for $C_{20}H_{21}O_5$, 341.1384); ^{1}H-NMR (500 MHz, $CDCl_3$) and ^{13}C-NMR (125 MHz, $CDCl_3$), see Table **4-3**.

(7S,8S,1'R)-$\Delta^{8'}$-1'-Methoxy-3,4-methylenedioxy-1',6'-dihydro-6'-oxo-7-O-4',8.3'-neolignan (**4.4**): yellow oil; $[\alpha]_D^{21}$ +58.6º (c 4×10^{-4} g/mL, MeOH); HRESIMS *m/z* 363.1130 $[M+Na]^+$ (calcd. for $C_{20}H_{20}NaO_5$, 363.1203) and 341.1318 $[M+H]^+$ (calcd. for $C_{20}H_{21}O_5$, 341.1384); ^{1}H-NMR (500 MHz, $CDCl_3$) and ^{13}C-NMR (125 MHz, $CDCl_3$), see Table **4-3**.

(7S,8S)-$\Delta^{8'}$-6'-Methoxy-3,4-methylenedioxy-7-O-3',8.4',1'-O-7'-neolignan (**4.5**): yellow oil; $[\alpha]_D^{21}$ +14.4º (c 4×10^{-4} g/mL, MeOH); HRESIMS *m/z* 341.1366 $[M+H]^+$ (calcd. for $C_{20}H_{21}O_5$, 341.1384); ^{1}H-NMR (500 MHz, $CDCl_3$) and ^{13}C-NMR (125 MHz, $CDCl_3$), see Table **4-4**.

trans-2,3-Dihydro-7-allyl-6-hydroxy-5-methoxy-3-methyl-2-(3,4-methylenedioxyphenyl)-benzofuran (**4.6**): yellow oil; $[\alpha]_D^{21}$ +41.3º (c 4×10^{-4} g/mL, MeOH); HRESIMS *m/z* 341.1381 $[M+H]^+$ (calcd. for $C_{20}H_{21}O_5$, 341.1384); ^{1}H-NMR (500 MHz, $CDCl_3$) and ^{13}C-NMR (125 MHz, $CDCl_3$), see Table **4-4**.

(7S,8S,1'S,2'S,3'S)-$\Delta^{5',8'}$-2'-Hydroxy-5'-methoxy-3,4-methylenedioxy-4'-oxo-7.3',8.1'-neolignan (**4.7**): yellow oil; $[\alpha]_D^{21}$ +26.3º (c 4×10^{-4} g/mL, MeOH); HRESIMS *m/z* 365.1353 $[M+Na]^+$ (calcd. for $C_{20}H_{22}NaO_5$, 365.1359) and 343.1537 $[M+H]^+$ (calcd. for $C_{20}H_{23}O_5$, 343.1540); ^{1}H-NMR (500 MHz, $CDCl_3$) and ^{13}C-NMR (125 MHz, $CDCl_3$), see Table **4-5**.

(7R,8R,1'S,2'R,3'S)-$\Delta^{5',8'}$-2'-Hydroxy-6'-methoxy-3,4-methylenedioxy-4'-oxo-7.3',8.1'-neolignan (**4.8**): yellow oil; $[\alpha]_D^{21}$ –55.3º (c 4×10^{-4} g/mL, MeOH); HRESIMS *m/z* 365.1369 $[M+Na]^+$ (calcd. for $C_{20}H_{22}NaO_5$, 365.1359) and 343.1551 $[M+H]^+$ (calcd. for $C_{20}H_{23}O_5$,

343.1540); ^{1}H-NMR (500 MHz, $CDCl_3$) and ^{13}C-NMR (125 MHz, $CDCl_3$), see Table **4-5**.

4.4 References

1. Anonymous The Plant List. http://www.theplantlist.org/ (accessed 14th September, 2017).

2. Fernandes, J. B.; Gottlieb, O. R.; Xavier, L. M. The Chemistry of Brazilian Lauraceae. 48. Chemosystematic Implications of Flavonoids in *Aniba riparia*. *Biochem. Syst. Ecol.* **1978,** *6* (1), 55–58.

3. Klausmeyer, P.; Chmurny, G. N.; McCloud, T. G.; Tucker, K. D.; Shoemaker, R. H. A Novel Antimicrobial Indolizinium Alkaloid from *Aniba panurensis*. *J. Nat. Prod.* **2004,** *67* (10), 1732–1735.

4. Kupchan, S. M.; Stevens, K. L.; Rohlfing, E. A.; Sickles, B. R.; Sneden, A. T.; Miller, R. W.; Bryan, R. F. New Cytotoxic Neolignans from *Aniba megaphylla* Mez. *J. Org. Chem.* **1978,** *43* (4), 586–590.

5. Aiba, C. J.; Fernandes, J. B.; Gottlieb, O. R.; Soaresmaia, J. G. Chemistry of Brazilian Lauraceae. 30. Neolignans from an *Aniba* Species. *Phytochemistry* **1975,** *14* (7), 1597–1604.

6. McCracken, S. T.; Kaiser, M.; Boshoff, H. I.; Boyd, P. D.; Copp, B. R. Synthesis and Antimalarial and Antituberculosis Activities of a Series of Natural and Unnatural 4-Methoxy-6-styryl-pyran-2-ones, Dihydro Analogues and Photo-dimers. *Bioorg. Med. Chem.* **2012,** *20* (4), 1482–1493.

7. Kinoshita, T.; Saitoh, T.; Shibata, S. A New 3-Arylcoumarin from Licorice Root. *Chem. Pharm. Bull.* **1978,** *26* (1), 135–140.

8. Sashidhara, K. V.; Rao, K. B.; Singh, S.; Modukuri, R. K.; Teja, G. A.; Chandasana, H.;

Shukla, S.; Bhatta, R. S. Synthesis and Evaluation of New 3-Phenylcoumarin Derivatives as Potential Antidepressant Agents. *Bioorg. Med. Chem. Lett.* **2014,** *24* (20), 4876–4880.

9. Moffitt, W.; Woodward, R. B.; Moscowitz, A.; Klyne, W.; Djerassi, C. Structure and the Optical Rotatory Dispersion of Saturated Ketones. *J. Am. Chem. Soc.* **1961,** *83*, 4013–4018.

10. Duan, S.; Zhang, P.; Yu, P. Neolignans and Lignan from *Piper wallichii*. *Zhongguo Zhongyao Zazhi* **2010,** *35* (2), 180–182.

11. Yanez, X.; Dediaz, A. M. P.; Diaz, P. P. Neolignans from *Mezilaurus itauba*. *Phytochemistry* **1986,** *25* (8), 1953–1956.

12. Buchi, G.; Chu, P.-S. Synthesis of Two Benzofuran Neolignans. *J. Org. Chem.* **1978,** *43* (19), 3717–3719.

13. Khan, M. R.; Gray, A. I.; Waterman, P. G. Neolignans from Stem Bark of *Ocotea veraguensis*. *Phytochemistry* **1987,** *26* (4), 1155–1158.

14. De Carvalho, M. G.; Yoshida, M.; Gottlieb, O. R.; Gottlieb, H. E. The Chemistry of Brazilian Lauraceae. 86. Bicyclooctanoid, Carinatone and Megaphone Type Neolignans from *Ocotea porosa*. *Phytochemistry* **1988,** *27* (7), 2319–2323.

15. Belluti, F.; Perozzo, R.; Lauciello, L.; Colizzi, F.; Kostrewa, D.; Bisi, A.; Gobbi, S.; Rampa, A.; Bolognesi, M. L.; Recanatini, M.; Brun, R.; Scapozza, L.; Cavalli, A. Design, Synthesis, and Biological and Crystallographic Evaluation of Novel Inhibitors of *Plasmodium falciparum* Enoyl-ACP-reductase (PfFabl). *J. Med. Chem.* **2013,** *56* (19), 7516–7526.

16. Williams, R. B.; Martin, S. M.; Lawrence, J. A.; Norman, V. L.; O'Neil-Johnson, M.; Eldridge, G. R.; Starks, C. M. Isolation and Identification of the Novel Tubulin

Polymerization Inhibitor Bifidenone. *J. Nat. Prod.* **2017,** *80* (3), 616–624.

17. Du, Y.; Pearce, K. C.; Dai, Y.; Krai, P.; Dalal, S.; Cassera, M. B.; Goetz, M.; Crawford, T. D.; Kingston, D. G. I. Antiplasmodial Sesquiterpenoid Lactones from *Trichospira verticillata*: Structure Elucidation by Spectroscopic Methods and Comparison of Experimental and Calculated ECD Data. *J. Nat. Prod.* **2017,** *80* (5), 1639–1647.

18. Cao, S.; Brodie, P. J.; Miller, J. S.; Randrianaivo, R.; Ratovoson, F.; Birkinshaw, C.; Andriantsiferana, R.; Rasamison, V. E.; Kingston, D. G. I. Antiproliferative Xanthones of *Terminalia calcicola* from the Madagascar Rain Forest. *J. Nat. Prod.* **2007,** *70* (4), 679–681.

19. Pan, E. D.; Harinantenaina, L.; Brodie, P. J.; Miller, J. S.; Callmander, M. W.; Rakotonandrasana, S.; Rakotobe, E.; Rasamison, V. E.; Kingston, D. G. I. Four Diphenylpropanes and a Cycloheptadibenzofuran from *Bussea sakalava* from the Madagascar Dry Forest. *J. Nat. Prod.* **2010,** *73* (11), 1792–1795.

20. Louie, K. G.; Behrens, B. C.; Kinsella, T. J.; Hamilton, T. C.; Grotzinger, K. R.; McKoy, W. M.; Winker, M. A.; Ozols, R. F. Radiation Survival Parameters of Antineoplastic Drug-Sensitive and Drug-Resistant Human Ovarian-Cancer Cell-Lines and Their Modification by Buthionine Sulfoximine. *Cancer Res.* **1985,** *45* (5), 2110–2115.

Chapter 5: An Antiplasmodial Butanolide from *Malleastrum sp.*

This chapter is a slightly expanded version of a published article.[1] (Du, Y.; Abedi, A. K.; Valenciano, A. L.; Fernández-Murga, M. L.; Cassera, M.; Rasamison, V. E.; Applequist W. L.; Miller, J. S.; Kingston, D. G. I., Isolation of the New Antiplasmodial Butanolide Malleastrumolide A from a *Malleastrum sp*. (Meliaceae) from Madagascar. *Chemistry & Biodiversity* **2017**, *14*, e1700331 doi: 10.1002/cbdv.201700331.) Author contributions of the articles are described as follows in the order of the names listed. The author of this dissertation (Mr. Yongle Du) determined the structure of the bioactive compound, performed the A2780 bioassay on the isolated compound, and drafted the manuscript. Mr. Alexander Abedi isolated the active compound with guidance from the author. Dr. L. M. Randrianjanaka made the plant collection, and Dr. Vincent E. Rasamison made the extract from this collection. Ms. Ana Lisa Valenciano and Dr. Maria L. Fernández-Murga carried out the antiplasmodial bioassays on the fractions and the isolated compound under the direction of Dr. Maria B. Cassera. Dr. David G. I. Kingston was a mentor for this work and the corresponding author for the published article. He also edited the final manuscript.

5.1 Introduction

5.1.1 Abstract

An extract of a *Malleastrum* sp. (Meliaceae) collected in Madagascar by the Madagascar International Cooperative Biodiversity Group was found to have antimalarial activity, with an IC_{50} value between 2.5 and 5 μg/mL. After purification by liquid–liquid partition,

chromatography on a Diaion open column, C-18 SPE and C-18 reverse phase HPLC, the new butanolide malleastrumolide A (**5.1**) was isolated. The structure of malleastrumolide A (**5.1**) was determined by mass spectrometry and by NMR and ECD spectroscopy. The double bond position was determined by cross-metathesis and mass spectrometry. The compound has antiproliferative activity against the A2780 ovarian cancer cell line with an IC_{50} value of 17.44 μM and antiplasmodial activity against the drug-resistant Dd2 strain of *Plasmodium falciparum* with an IC_{50} value of 2.74 μM.

5.1.2 Investigations of the genus *Malleastrum*

The genus *Malleastrum* was collected as part of the Madagascar International Cooperative Biodiversity Group (ICBG) program. Previous work on antiproliferative compounds from Madagascar ICBG collections of this genus resulted in the discovery of new limonoids and diterpenes,[2, 3] but there have been no reports on antimalarial compounds isolated from this genus. It was thus selected for bioassay-guided fractionation to isolate its antiplasmodial components.

5.2 Results and Discussion

5.2.1 Isolation of active compounds

An extract of the wood of a tree of the *Malleastrum* genus (Meliaceae) was found to have moderate antiplasmodial activity against the Dd2 drug-resistant strain of *P. falciparum*, and was selected for isolation studies. Liquid-liquid partition between aqueous methanol and hexanes and then dichloromethane indicated that all fractions had some antiplasmodial activity, with IC_{50} values of about 7, 1.25 and 7 μg/mL for the hexanes, dichloromethane, and aqueous methanol fractions, respectively. The major aqueous methanol fraction was separated

by chromatography on a Diaion open column, by C-18 SPE, and by C-18 reverse phase HPLC to yield the new long-chain butanolide malleastrumolide A (**5.1**).

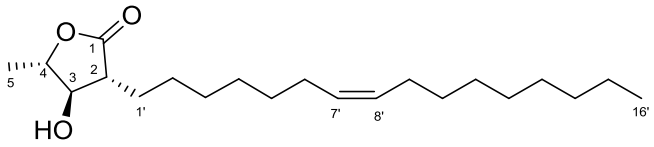

5.1

5.2.2 Structure elucidation of isolated compounds

Malleastrumolide A was isolated as a yellow powder. Its positive ion HRESIMS revealed a peak for a protonated molecular ion at *m/z* 339.2897 and for a sodiated molecular ion at *m/z* 361.2714, both corresponding to a molecular formula of $C_{21}H_{38}O_3$. Its IR spectrum exhibited bands at 3398 and 1761 cm^{-1}, indicating the presence of hydroxyl and ester carbonyl groups.[4] The presence of a hydroxylated lactone was suggested by ^{1}H NMR signals at δ_H 2.55 (td 8.1, 5.7, H-2), 3.84 (td 8.1, 5.7, H-3), and 4.20 (dq 6.4, 6.4) and by ^{13}C NMR signals at δ_C 175.8 (C-1), 48.6 (C-2), 79.1 (C-3) and 79.8 (C-4). The hydroxylactone partial structure was confirmed by ^{2}J-HMBC correlations between H-2 and C-3, H-3 and C-4, and ^{3}J-HMBC correlations between H-4 and C-1, H-4 and C-2 (Table **5-1** and Figure **5-1**).[4]

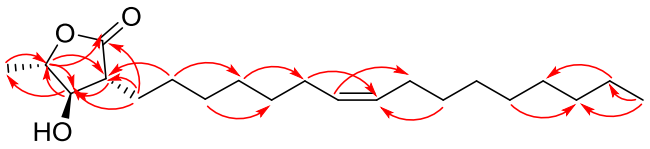

Figure 5-1. HMBC correlations for malleastrumolide A **5.1**

The methyl group was connected to C-4 as indicated by ^{2}J-HMBC correlations between H-5 and C-4, and ^{3}J-HMBC correlations between H-5 and C-3 (Fig. 5.1). The presence of an unsaturated C_{16} chain, with a terminal methyl group at δ_H 0.88 (t 6.9, H-16') and δ_C 14.1 (C-16'), was inferred from the ^{1}H NMR and ^{13}C NMR spectra. The olefinic protons appeared at δ_H 5.34 (m, 2 H) and δ_C 129.9 and 130.0 (2 C). The CH_2 groups of the side chain resonated

at δ_H 2.01 (m, 4 H), 1.86 (m, 1 H), 1.60 (m, 1 H), 1.48 (m, 1 H), 1.27-1.34 (m, 19 H) and at δ_C 22.6, 26.8-31.9 (13 C). The long side chain was attached to C-2, based on the ^2J-HMBC correlations between H-1' and C-2, and ^3J-HMBC correlations between H-1' and C-1, H-1' and C-3, H-2' and C-2 (Figure **5-1**).

Table 5-1. NMR spectroscopic Data for Compound **5.1** in $CDCl_3$ (500 MHz)

Position	δ_H, *J* in Hz	δ_C, type
1		175.8, C
2	2.55 td, 8.1, 5.7	48.6, CH
3	3.84 dd, 8.1, 6.4	79.1, CH
4	4.20 dq, 6.4, 6.4	79.8, CH
5	1.46 d, 6.4	18.2, CH_3
1'	1.82–1.91 m	28.4, CH_2
	1.55–1.64 m	
2'	1.47–1.54 m	26.8, CH_2
	1.29–1.35 m	
3'	1.24–1.29 m	29.4, CH_2
4'	1.24–1.29 m	29.4, CH_2
5'	1.31–1.35 m	29.5, CH_2
6'	1.98–2.05 m	27.2, CH_2
7'	5.30–5.39 m	129.9, CH
8'	5.30–5.39 m	130.0, CH
9'	1.98–2.05 m	27.2, CH_2
10'	1.31–1.35 m	29.5, CH_2
11'	1.31–1.35 m	29.5, CH_2
12'	1.24–1.29 m	29.4, CH_2
13'	1.24–1.29 m	29.4, CH_2
14'	1.24–1.29 m	31.9, CH_2
15'	1.24–1.29 m	22.6, CH_2
16'	0.88 t, 6.9	14.1, CH_3

The position the of double bond was determined by the cross-metathesis method.[5] Malleastrumolide A **5.1** was reacted with methyl acrylate and second-generation Hoveyda-Grubbs catalyst, and the crude product was analyzed by positive ion HRESIMS.

The major peak at *m/z* 307 corresponded to $C_{15}H_{24}O_5Na^+$, and peaks at *m/z* 285 and 591 corresponded to $C_{15}H_{24}O_5+H^+$ and to $(C_{15}H_{24}O_5)_2Na^+$, respectively. This analysis confirmed the position of the double bond as between C-7' and C-8' (Figure. **5-2**).

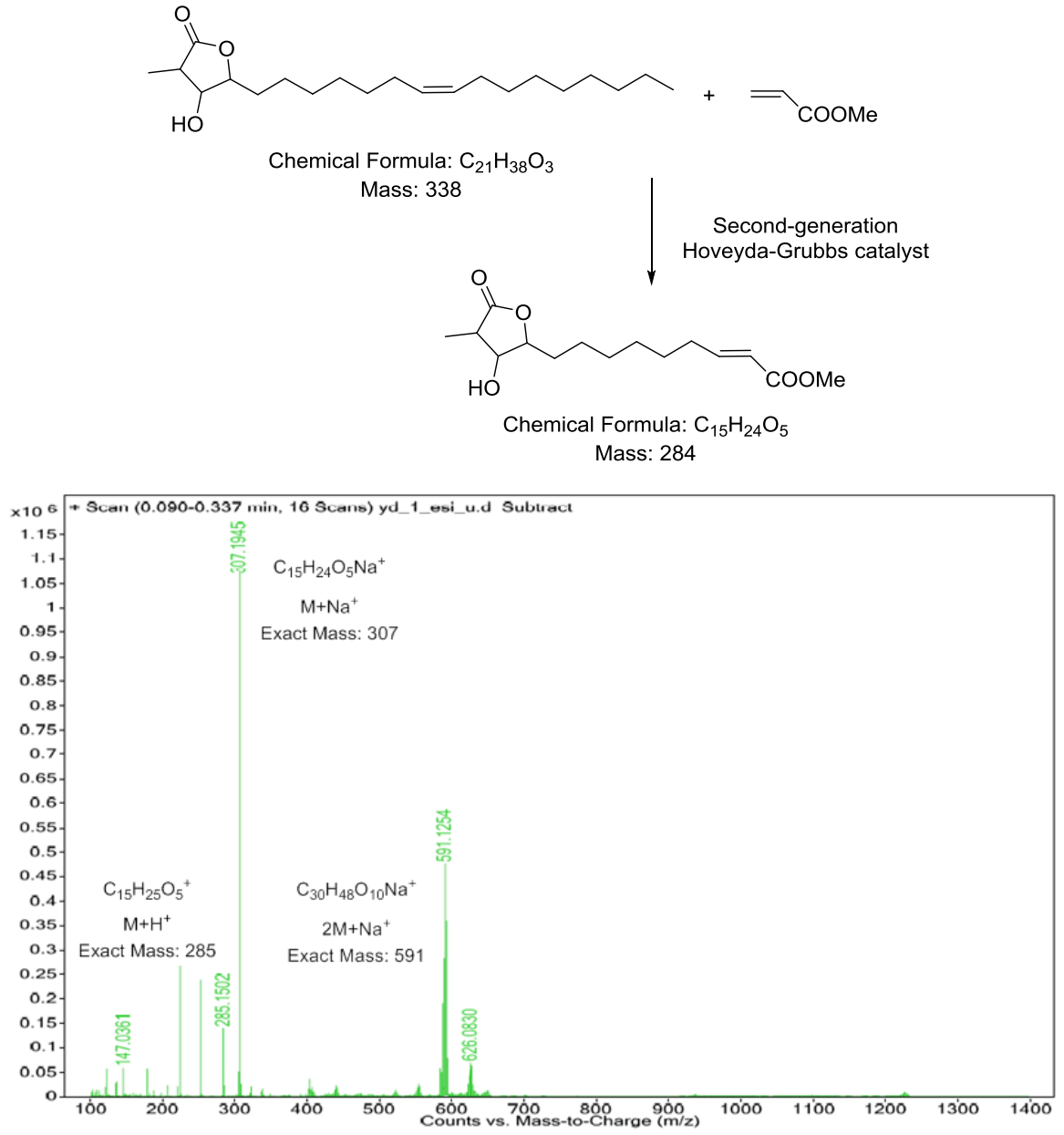

Figure 5-2. Cross-metathesis reaction of malleastrumolide A **5.1** and the mass spectrum of the crude product

The relative configuration of the double bond was assigned as *Z* based on the single ^{1}H NMR signal at δ_H 5.34 (m, H-7' and H-8') and ^{13}C NMR signals at δ_C 129.9 and 130.0 (C-7' and C-8').[6, 7] The relative configuration of the lactone was assigned as 2*R**, 3*R**, 4*S** by the

^{13}C NMR signals at δ_C 79.1 (C-3) and 79.8 (C-4),[8] and by the NOESY crosspeaks between H-1' and H-3, H-2 and H-4, and H-3 and H-5, as shown in Figure **5-3**.

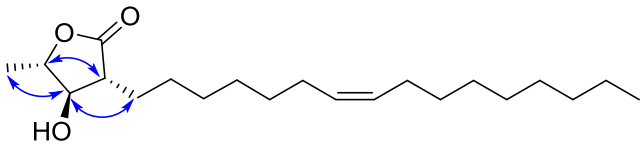

Figure 5-3. NOESY correlations for malleastrumolide A **5.1**

The absolute configuration of malleastrumolide A was assigned by its ECD spectrum (Figure **5-4**). The n→π* transition band at 216 nm showed a negative Cotton effect, defining the absolute configuration of C-2 as *R*.[9, 10] The structure and absolute stereochemistry of malleastrumolide A was thus assigned as (2*R*,3*R*,4*S*)-2-((*Z*)-hexadec-7-en-1-yl)-3-hydroxy -4-methylbutanolide.[4]

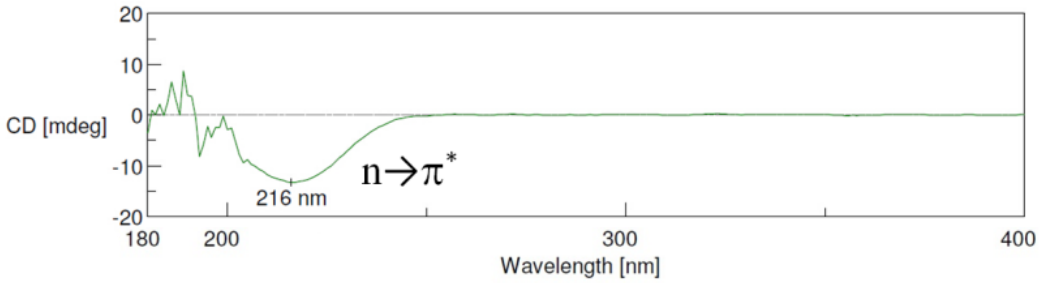

Figure 5-4. The ECD spectra of malleastrumolide A **5.1**

5.2.3 Bioactivities of isolated compounds

Malleastrumolide A was tested for antiplasmodial activity against the Dd2 strain of *P. falciparum* and for antiproliferative activity to A2780 ovarian cancer cells. It displayed moderate antiplasmodial activity (Table **5-2**), with an IC_{50} value of 2.74 μM, and weak antiproliferative activity, with an IC_{50} value of 17.44 μM.

Table 5-2. Bioactivities of malleastrumolide A **5.1**

	Malleastrumolide A	Artemisinin	Paclitaxel
P. falciparum Dd2 (μM)	2.74 ± 0.27	0.007 ± 0.002	NT
A2780 (μM)	17.44 ± 2.07	NT	0.028 ± 0.002

5.3 Experimental Section

5.3.1 General Experimental Procedures

Optical rotations were recorded on a JASCO P-2000 polarimeter. UV and IR spectroscopic data were measured on a Shimadzu UV-1201 spectrophotometer and a MIDAC M-series FTIR spectrophotometer, respectively. ECD spectra were obtained on a JASCO J-815 circular dichroism spectrometer. NMR spectra were recorded in $CDCl_3$ on Bruker Avance 500 or 600 spectrometers. The chemical shifts are given in δ (ppm), and coupling constants (*J*) are reported in Hz. Mass spectra were obtained on an Agilent 6220 LC-TOF-MS in the positive ion mode.

5.3.2 Plant Material.

Plant specimens of *Malleastrum* (Baill.) J.-F. Leroy were collected on July 16, 2000 in the Province of Toamasina in the Alaotra-Mangoro region in Zahamena National Park in secondary forest with *Lantana cam*ara, on a ridge at an elevation of 880 m at coordinates 17°28'28"S, 048°44'12"E. The plant was a tree 8 m tall with a diameter at breast height of 12 cm. The leaves had a tobacco-like smell, and the tree had a green calyx and its petals were yellow-orange on the outside, and white on the inside. Voucher specimens are deposited at the herbarium of the Missouri Botanical Garden Herbarium and were collected by L.M. Randrianjanaka, S. Rakotonandrasana, J. Randriamanarivo & L.P. Rakotosoa 564 (MO).

The genus *Malleastrum* (Baill.) J.-F. Leroy is endemic to Madagascar and comprises 20 currently accepted species. However, there appear to be at least 4 additional species new to science among recently collected specimens, and the plant material in this study is almost

certainly from one of those species that is new to science but still waiting to be named and described.

5.3.3 Antiplasmodial Bioassays.

The effect of each fraction and pure compound on parasite growth of the *P. falciparum* Dd2 strain was measured in a 72 h growth assay in the presence of drug as described previously with minor modifications. Briefly, ring stage parasite cultures (100 μL per well, with 1% hematocrit and 1% parasitemia) were then grown for 72 h in the presence of increasing concentrations of the drug in a 5% CO_2, 5% O_2, and 90% N_2 gas mixture at 37 °C. After 72 h in culture, parasite viability was determined by DNA quantitation using SYBR Green I. The half-maximum inhibitory concentration (IC_{50}) calculation was performed with GraphPad Prism software using nonlinear regression curve fitting. IC_{50} values are the average of three independent determinations with each determination in duplicate and are expressed ± SD and artemisinin was used as positive control.[11]

5.3.4 In vitro Antiproliferative Activity Against A2780 Cells.

The A2780 ovarian cancer cell line antiproliferative bioassay was performed at Virginia Tech as previously reported.[12, 13] The A2780 cell line is a drug-sensitive ovarian cancer cell line.[14] Paclitaxel was used as the positive control.

5.3.5 Extraction and Isolation.

Dried and powdered the wood of *Malleastrum sp.* (350 g) was exhaustively extracted with ethanol in two 24-hour percolation steps to yield 10.1 g of extract. For purposes of fractionation and purification, a portion of this extract (1.95 g) designated MG0433 was shipped to Virginia Tech for bioassay and chemical studies. A total of 1.3 g of this sample

(IC_{50} 2.5~5 μg/mL) was suspended in aqueous MeOH (MeOH-H_2O 9:1, 100 mL), and extracted with hexane (3 × 100 mL portions). The aqueous MeOH layer was diluted to 60% MeOH (v/v) with H_2O and extracted with DCM (3 × 100 mL portions). The hexane fraction was evaporated in vacuo to leave 180 mg of material with IC_{50} 5~10 μg/mL. The residue from the DCM fraction (20.7 mg) was the most active fraction with an IC_{50} value of < l.25 μg/mL. The remaining aqueous MeOH fraction was centrifuged to give a supernatant (800 mg) with an IC_{50} of 5~10 μg/mL.

The aqueous MeOH fraction was directly applied on Diaion open column to yield 40% aqueous MeOH fraction (280 mg) with no activity, 70% aqueous MeOH fraction (188 mg) with no activity, 100% MeOH fraction (115 mg) with an IC_{50} of ~10 μg/mL and 100% acetone fraction (47 mg) with an IC_{50} of < 1.25 μg/mL. The DCM fraction and acetone fraction were combined due to the the similarity of their TLC patterns. The combined fraction was directly applied on C_{18} HPLC, and eluted by 60% to 100% acetonitrile in water gradient in 30 min to yield malleastrumolide A **5.1** (7.0 mg), with retention time of 41.7 minutes.

5.3.6 Determination of Double-Bond Position

Malleastrumolide A **5.1** (0.5 mg) was dissolved in a 10:1 mixture of $CHCl_3$ and methyl acrylate (0.5 mL), and 50 mg (5–10 mol%) of second generation Hoveyda–Grubbs catalyst was added. The mixture was stirred at room temperature for 3 h, and a 10μL aliquot was injected into the Agilent TOF HRESI mass spectrometer to generate a positive ion HRESIMS (Figure. **5-2**)[5]

5.3.7 Compound Information

Malleastrumolide A (**5.1**). yellow powder; $[\alpha]_D^{21}$ –11.3º (c 4×10^{-4} g/mL, MeOH); UV (c

0.296 mM, MeOH) λ_{max} (ε) 203 nm (1464); IR υ_{max} 3398, 2927, 2858,1781, 1761, 1665, 1461 cm^{-1}; ECD (c 0.296 mM, MeOH) $\Delta\varepsilon_{216}$ −13.4; HRESIMS *m/z* 361.2714 $[M+Na]^+$ (calcd. for $C_{21}H_{38}NaO_3$, 361.2713) and 339.2897 $[M+H]^+$ (calcd. for $C_{21}H_{39}O_3$, 339.2894); ^{1}H-NMR (500 MHz, $CDCl_3$) and ^{13}C-NMR (125 MHz, $CDCl_3$), see Table **5-1**.

5.4 References

1. Du, Y. A., A. K.; Valenciano, A. L.; Fernández-Murga, M. L.; Cassera, M.; Rasamison, V. E.; Applequist W. L.; Miller, J. S.; Kingston, D. G. I. Isolation of the New Antiplasmodial Butanolide Malleastrumolide A from a *Malleastrum sp.* (Meliaceae) from Madagascar. *Chemistry & Biodiversity* **2017**. doi: 10.1002/cbdv.201700331.

2. Liu, Y.; Wiedle, C. H.; Brodie, P. J.; Callmander, M. W.; Rakotondrajaona, R.; Rakotobe, E.; Rasamison, V. E.; Kingston, D. G. I. Antiproliferative Diterpenes from a *Malleastrum* sp. from the Madagascar Dry Forest. *Nat. Prod. Commun.* **2015,** *10* (9), 1509–1512.

3. Murphy, B. T.; Brodie, P.; Slebodnick, C.; Miller, J. S.; Birkinshaw, C.; Randrianjanaka, L. M.; Andriantsiferana, R.; Rasamison, V. E.; TenDyke, K.; Suh, E. M.; Kingston, D. G. I. Antiproliferative Limonoids of a *Malleastrum* sp. from the Madagascar Rainforest. *J. Nat. Prod.* **2008,** *71* (3), 325–329.

4. Allouche, N.; Apel, C.; Martin, M. T.; Dumontet, V.; Gueritte, F.; Litaudon, M. Cytotoxic Sesquiterpenoids from Winteraceae of Caledonian Rainforest. *Phytochemistry* **2009,** *70* (4), 546–553.

5. Kwon, Y.; Lee, S.; Oh, D. C.; Kim, S. Simple Determination of Double-Bond Positions in Long-Chain Olefins by Cross-Metathesis. *Angew. Chem., Int. Ed.* **2011,** *50* (36), 8275–8278.

6. Pupo, M. T.; Vieira, P. C.; Fernandes, J. B.; da Silva, M. γ-Lactones from *Trichilia claussenii*. *Phytochemistry* **1998,** *48* (2), 307–310.

7. Yawer, M. A.; Ahmed, E.; Malik, A.; Ashraf, M.; Rasool, M. A.; Afza, N. New Lipoxygenase-inhibiting Constituents from *Calligonum polygonoides*. *Chem. Biodiversity* **2007,** *4* (7), 1578–1585.

8. Lorenzo, M.; Brito, I.; Cueto, M.; D'Croz, L.; Darias, J. C-13 NMR-based Empirical Rules to Determine the Configuration of Fatty Acid Butanolides. Novel γ-Dilactones from *Pterogorgia* spp. *Org,. Lett.* **2006,** *8* (22), 5001–5004.

9. Beecham, A. F. Circular Dichroism in Lactones. *Tetrahedron Lett.* **1968,** *19*, 2355-2360.

10. Polonski, T. Optical-Activity of Lactones and Lactams. 1. Conformational Dependence of the Circular-Dichroism of 1,3-Dioxolan-4-Ones. *Tetrahedron* **1983,** *39* (19), 3131–3137.

11. Du, Y.; Pearce, K. C.; Dai, Y.; Krai, P.; Dalal, S.; Cassera, M. B.; Goetz, M.; Crawford, T. D.; Kingston, D. G. I. Antiplasmodial Sesquiterpenoid Lactones from *Trichospira verticillata*: Structure Elucidation by Spectroscopic Methods and Comparison of Experimental and Calculated ECD Data. *J. Nat. Prod.* **2017,** *80* (5), 1639–1647.

12. Cao, S.; Brodie, P. J.; Miller, J. S.; Randrianaivo, R.; Ratovoson, F.; Birkinshaw, C.; Andriantsiferana, R.; Rasamison, V. E.; Kingston, D. G. I. Antiproliferative Xanthones of *Terminalia calcicola* from the Madagascar Rain Forest. *J. Nat. Prod.* **2007,** *70* (4), 679–681.

13. Pan, E. D.; Harinantenaina, L.; Brodie, P. J.; Miller, J. S.; Callmander, M. W.; Rakotonandrasana, S.; Rakotobe, E.; Rasamison, V. E.; Kingston, D. G. I. Four Diphenylpropanes and a Cycloheptadibenzofuran from *Bussea sakalava* from the Madagascar Dry Forest. *J. Nat. Prod.* **2010,** *73* (11), 1792–1795.

14. Louie, K. G.; Behrens, B. C.; Kinsella, T. J.; Hamilton, T. C.; Grotzinger, K. R.; McKoy, W. M.; Winker, M. A.; Ozols, R. F. Radiation Survival Parameters of Antineoplastic Drug-Sensitive and Drug-Resistant Human Ovarian-Cancer Cell-Lines and Their Modification by Buthionine Sulfoximine. *Cancer Res.* **1985,** *45* (5), 2110–2115.

Chapter 6: An Antiplasmodial Neolignan and an Alkaloid from *Magnolia grandiflora L.*

This chapter is a modified version of a published article.[1] (Latif, A.; Du, Y.; Dalal, S. R.; Fernández-Murga, M. L.; Merino, E. F.; Cassera, M. B.; Goetz, M.; Kingston, D. G. I., Bioactive Neolignans and Other Compounds from Magnolia grandiflora L.: Isolation and Antiplasmodial Activity. *Chem.Biodiversity* **2017**, 14, e1700209). Author contributions of the articles are described as follows in the order of the names listed. Dr. Abdul Latif isolated the compounds and determined the structures of the other compounds, the author of this dissertation (Mr. Yongle Du) determined the structure of compound **6.2**, Ms. Seema Dalal and Dr. Emilio Merino carried out the antiplasmodial bioassays under the direction of Dr. Maria Cassera, and Dr. Michael Goetz provided the crude extract. Dr. David G. I. Kingston was a mentor for this work and the corresponding author for the published article. He also edited the final manuscript.

6.1 Introduction

6.1.1 Abstract

Bioassay-guided fractionation of a methanol extract of *Magnolia grandiflora* against *Plasmodium falciparum* yielded two new (**6.1** and **6.2**) and six known (**6.3**–**6.8**) bioactive compounds. The structures of the new compounds were assigned by mass spectrometric and 1D and 2D NMR data. Known compounds were identified by comparison of ^{1}H NMR and MS data with literature data. The two known neolignans **6.3** and **6.4** showed moderate

antiplasmodial activity with IC_{50} values of 2.8 ± 0.1 and 3.4 ± 0.1 μM, respectively. Weak antiplasmodial activity was recorded for compounds **6.1**, **6.2**, **6.5**, **6.6**, **6.7** and **6.8**, with IC_{50} values of 38 ± 2, 23 ± 2, 16.5 ± 0.2, 86 ± 1, 44 ± 4 and 114 ± 9 μM, respectively.

6.1.2 Investigations of the genus *Magnolia*

Magnolia grandiflora is a well-investigated plant species, and is known to contain alkaloids,[2] flavonoids, phenolic compounds,[3] glycosides,[4, 5] sesquiterpene lactones,[6-8] and volatile compounds.[9] It has been reported in Traditional Chinese Medicine as a reliever of colds, headaches, and stomach ache.[2] It has not however been reported to contain any antimalarial compounds, and it was thus selected for investigation.

6.2 Results and Discussion

6.2.1 Isolation of active compounds

A methanol extract of *M. grandiflora* was subjected to liquid-liquid partitioning to eventually afford an ethyl acetate soluble fraction with an IC_{50} value of 10 μg/mL against the pyrimethamine, chloroquine, and mefloquine-resistant Dd2 strain of *Plasmodium falciparum*. Bioassay-guided isolation using solid phase extraction over C_{18} silica followed by C_{18} HPLC gave two new compounds (**6.1** and **6.2**) along with six known compounds (**6.3**–**6.8**).

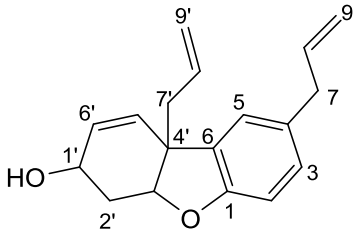

6.1

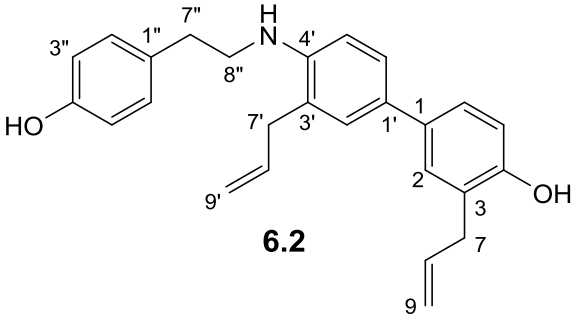

6.2

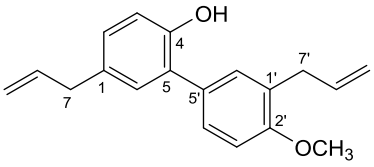

6.3

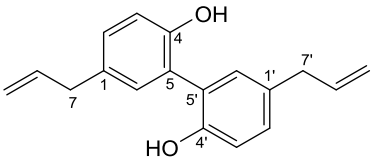

6.4

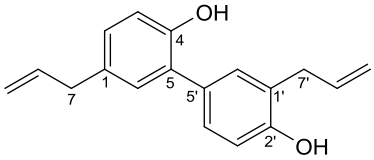

6.5

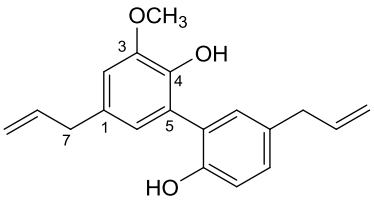

6.6

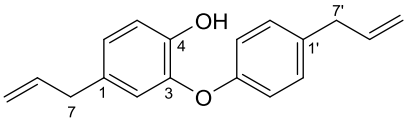

6.7

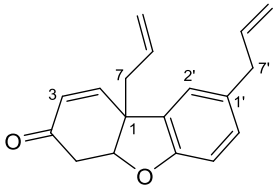

6.8

6.2.2 Structure elucidation of isolated compounds

Compound **6.1** was isolated as a colorless oil and was assigned the molecular formula $C_{18}H_{20}O_2$ based on its sodiated molecular ion peak at *m/z* 291.1352 $[M + Na]^+$ in its HRESIMS. Its ^{1}H NMR data (Table **6-1**) displayed three aromatic protons of an ABX system at δ_H 6.73 (1H, *J* = 8.0 Hz, H-2), 6.96 (1H, *J* = 8.0, 1.8 Hz, H-3), and 6.98 (1H, *J* = 1.8 Hz, H-5). Signals for two allyl groups were present at δ_H 3.34 (2H, d, *J* = 6.6 Hz, H-7), 2.49 (1H, d, *J* = 7.8 Hz, H-7´a), 2.56 (1H, m, H-7´b), H-5.93 (1H, m, H-8), 5.70 (1H, m, H- H-8´), 5.06 (2H, m, H-9), and 5.09 (2H, m, H-9´). Proton shifts at δ_H 5.62 (1H, d, *J* = 10.0 Hz) and 5.98 (1H, m) were assigned to H-5´ and H-6´, respectively. Moreover, two oxygenated methine and two methylene protons were also observed at chemical shift values of δ_H 4.14 (1H, dq, *J* = 8.4, 4.5 Hz, H-1´), δ_H 4.71 (1H, broad t, *J* = 3.9 Hz, H-3´), δ_H 2.04 (1H, m, H-2´a) and δ_H 2.45 (1H, m, H-2´b). Its ^{13}C NMR spectrum (Table **6-1**) showed the presence of 18 carbon signals. An HSQC experiment in combination with ^{13}C NMR data identified five methylenes at δ_C 31.8, 39.9, 41.6, 115.8 and 118.7, two sp^3-methines at δ_C 62.4 and 85.6, and seven sp^2-methines at δ_C 110.3, 123.4, 128.2, 128.7, 131.6, 133.7, and 138.0.

Table 6-1. NMR Spectroscopic Data for Compounds **6.1** in $CDCl_3$ (500 MHz)

position	δ_H, *J* in Hz	δ_C, type	position	δ_H, *J* in Hz	δ_C, type
1		156.3, C	2′a	2.04 m	31.8, CH_2
2	6.73 d 8.0	110.3, CH	2′b	2.45 m	
3	6.96 dd 8.0, 1.8	128.7, CH	3′	4.71 brt 3.9	85.6, CH
4		133.4, C	4′		47.9, C
5	6.98 d 1.8	123.4, CH	5′	5.62 d 10.0	131.6, CH
6		133.5, C	6′	5.98 m	128.2, CH
7	3.34 d 6.6	39.9, CH_2	7′a	2.49 d 7.8	41.6, CH_2
8	5.93 m	138.0, CH	7′b	2.56 m	
9	5.06 m	115.8, CH_2	8′	5.70 m	133.7, CH
1′	4.14 dq 8.4, 4.5	62.4, CH	9′	5.09 m	118.7, CH_2

The remaining 4 carbon signals were classified as quaternary carbons with resonances at δ_C 47.9, 133.2, 133.4, and 156.3. The NMR data (Table **6-1**) of **6.1** is similar to that of Pumerer's ketone (**6.8**)[10, 11] except for the presence of a hydroxymethine at δ_C 62.4 (C-1′) instead of the ketone carbonyl at δ_C 195.2 (C-1′). An HMBC experiment on **6.1** (Figure **6-1**) indicated correlations of H-7 (δ_H 3.34) with C-4 (δ_C 133.4), C-3 (δ_C 128.7) and C-5 (δ_C 123.4) confirming the presence of an allyl group on the aromatic ring. The presence of a second allyl group at C-4′ was validated from correlations between H-7′ (δ_H 2.56) to C-4′ (δ_C 47.9), and C-3′(δ_C 85.6). The position of the double bond was fixed between C-5′ and C-6′ by the correlations of H-5′(δ_H 5.62) with C-4′, C-1′, and C-3′. The position of C-3′ (δ_C 85.6) was confirmed on the basis of its correlations to H-5′ (δ_H 5.62) and H-7′ (δ_H 2.56). A COSY spectrum (Figure **6-1**) was also obtained for compound **6.1**, and cross peaks were located for H-1′ to H-2′a/b and H-6′ and H-2′a/b to H-3′, indicating the presence of a cyclohexene ring (C-1′ through C-6′) in **6.1**. Compound **6.1** was thus identified as 4,4′-diallyl-1,2,6,4′-tetrahydrodibenzo[*b*,*d*]furan-3′-ol.

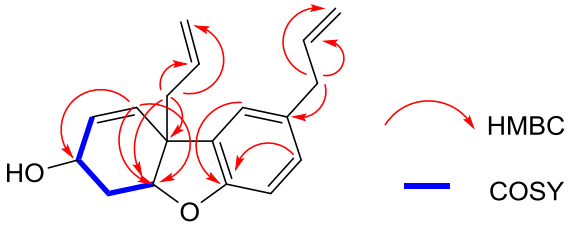

Figure 6-1. Key HMBC and COSY correlations of compound **6.1**

Compound **6.2**, a colorless oil, was assigned the molecular formula $C_{26}H_{27}NO_2$ (*m/z* 386.2107 $[M + H]^+$, calcd. 386.2115) on the basis of its HRESIMS. ^{1}H NMR data (Table **6-2**) exhibited the presence of two ABX substituted benzene rings and a 1,4-disubstituted benzene ring. Protons of the two ABX aromatic rings were assigned chemical shift values of δ_H 7.11 (1H, m, overlapped, H-2'), 7.02 (1H, m, overlapped, H-2), 6.89 (1H, m, H-5), 6.77 (1H, d, *J* = 8.2 Hz, H-5´), 7.03 (1H,dd, *J* = 8.8, 2.3 Hz, H-6), and 7.24 (1H, dd, *J* = 8.2, 2.2 Hz, H-6´). The 1,4-disubstituted third aromatic ring had proton signals at δ_H 7.11 (2H, d, *J* = 8.4 Hz, H-2" and H-6") and 6.80 (2H, d, *J* = 8.4 Hz, H-3" and H-5"). Chemical shifts of 3.34 (2H, dt, *J* = 6.7, 1.7 Hz, H-7), 3.21 (2H, dt, *J* = 6.3, 1.7 Hz, H-7´), 5.97 (1H, ddt, *J* = 16.8, 10.0, 6.7 Hz, H-8), 5.82 (1H, ddt, *J* = 16.6, 10.2, 6.3 Hz, H-8´), 5.04 (1H, dq, *J* = 10.0, 1.7, H-9a), 5.08 (1H, dq, *J* = 17.0, 1.7, H-9b), 4.99 (1H, dq, *J* = 17.0, 1.7, H-9a') and 5.01 (1H, dq, *J* = 10.2, 1.7, H-9b') were assigned to two allyl groups on the separate aromatic rings. Additional signals characteristic of an ethylamino group[12] were observed at δ_H 2.90 (2H, t, *J* = 6.9 Hz, H-7") and 3.41 (2H, dt *J* = 6.9, 6.9 Hz, H-8"). ^{13}C NMR data (Table **6-2**) for compound **6.2** displayed a total of 26 carbon atoms. An HSQC NMR experiment in combination with ^{13}C NMR data classified these carbon atoms into 6 methylenes (δ_C 34.6, 36.6, 39.6, 45.1, 115.6, and 116.8), 12 methines (δ_C 111.2, 115.4, 115.5, 115.6, 128.4, 128.5, 130.1, 130.1, 130.3,

130.6, 135.5, and 138.0) and 7 quaternary carbons (δ_C 124.8, 125.3, 128.0, 131.3, 132.2, 146.1, 151.0, and 154.3.

Table 6-2. NMR Spectroscopic Data for Compounds **6.2** in $CDCl_3$ (500 MHz)

position	δ_H, *J* in Hz	δ_C, type
1		128.0, C
2	7.02 d 2.3	130.3, CH
3		132.2, C
4		151.0, C
5	6.89 d 8.8	115.4, CH
6	7.03 dd 8.8, 2.3	128.4, CH
7	3.34 dt 6.7, 1.7	39.6, CH_2
8	5.97 ddt 16.8, 10.0, 6.7	138.0, CH
9a	5.04 dq 10.0, 1.7	115.6, CH_2
9b	5.08 dq 17.0, 1.7	
1′		125.3, C
2′	7.11 d 2.2	130.6, CH
3′		124.8, C
4′		146.1, C
5′	6.77 d 8.2	111.2, CH
6′	7.24 dd 8.2, 2.2	128.5, CH
7′	3.21 dt 6.3, 1.7	36.6, CH_2
8′	5.82 ddt 16.6, 10.2, 6.3	135.5, CH
9′a	4.99 dq 17.0, 1.7	116.8, CH_2
9′b	5.01 dq 10.2, 1.7	
1″		131.3, C
2″	7.11 d 8.4	130.1, CH
3″	6.80 d 8.4	115.6, CH
4″		154.3, C
5″	6.80 d 8.4	115.5, CH
6″	7.11 d 8.4	130.1, CH
7″	2.90 t 6.9	34.6, CH_2
8″	3.41dt 6.9, 6.9	45.1, CH_2
NH	3.85, br s	
OH	5.21, s	
OH	4.70, s	

Assignment of the ^{13}C NMR spectrum of **6.2** was made on the basis of its HSQC spectrum and by comparison with the ^{13}C NMR spectra of honokiol analogs.[13] An HMBC NMR spectrum (Figure **6-2**) showed key correlations for **6.2**, including cross-peaks for the three-bond correlation H-2"/H-6" to C-7" (δ_C 34.6), for the two-bond correlation H-7" to C-8"

(δ_C 45.1), and for the three bond correlations H-2 to C-1' (δ_C 125.3) and to C-4 (δ_C 151.0), H-7 to C-2 (δ_C 130.3), and H-7' to C-2' (δ_C 130.6) and C-4' (δ_C 146.1). These correlations established the structure of **6.2** as 3,3'-diallyl-4'-((4-hydroxyphenethyl)amino)-[1,1'-bi-phenyl]-4-ol.

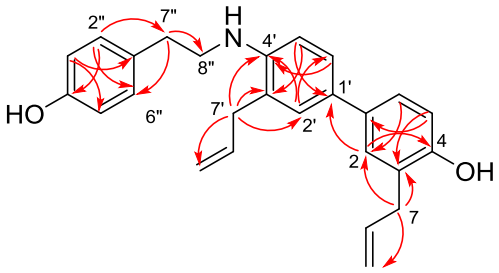

Figure 6-2. Key HMBC correlations of compound **6.2**

Compounds **6.3**–**6.4** were identified as 4′-*O*-methyl honokiol (**6.3**),[14] and magnolol (**6.4**),[15] as reported in Tables **6-3**.

Table 6-3. NMR Spectroscopic Data for Compounds **6.3**–**6.4** in $CDCl_3$ (500 MHz)

	6.3	**6.4**
position	δ_H, *J* in Hz	δ_H, *J* in Hz
2	7.28 dd 8.4, 2.3	7.13 dd 8.3, 2.2
3	6.96 d 8.4	6.95 d 8.3
6	7.23 d 2,3	7.07 d 2.2
7	3.43 dt 6.7, 1.5	3.36 dt 6.8, 1.4
8	5.99 ddt 16.8, 10.0, 6.7	5.96 ddt 16.9, 10.0, 6.8
9a	5.09 ddt 16.8, 1.5, 1.5	5.09 ddt 16.9, 1.8, 1.4
9b	5.05 ddt 10.0, 1.5, 1.5	5.06 ddt 10.0, 1.8, 1.4
2'	7.05 dd 8.1, 2.3	
3'	6.90 d 8.1	
6'	7.02 d 2.3	
7'	3.35 dt 6.7, 1.5	
8'	5.99 ddt 16.8, 10.0, 6.7	
9'a	5.09 ddt 16.8, 1.5, 1.5	
9'b	5.05 ddt 10.0, 1.5, 1.5	
OMe	3.88 s	
OH	5.14 s	

Compounds **6.5**–**6.6** were identified as honokiol (**6.5**),[16] and 3-methoxymagnolol (**6.6**),[15] as reported in Tables **6-4**.

Table 6-4. NMR Spectroscopic Data for Compounds **6.5**–**6.6** in $CDCl_3$ (500 MHz)

	6.5	**6.6**
position	δ_H, *J* in Hz	δ_H, *J* in Hz
2	7.23 dd 8.3, 2.3	7.77 d 1.9
3	6.92 d 8.3	7.74 d 1.9
6	7.21 d 2.3	
7	3.46 dt 6.5, 1.6	3.37 dt 6.7, 1.5
8	6.61 ddt 16.8, 10.0, 6.5	5.98 ddt 17.0, 10.1, 6.7
9a	5.21 ddt 16.8, 1.6, 1.6	5.11 ddt 17.0, 1.5, 1.5
9b	5.19 ddt 10.0, 1.6, 1.6	5.08 ddt 10.1, 1.5, 1.5
2'	7.05 dd 8.1, 2.3	7.11 dd 8.3, 2.2
3'	6.90 d 8.1	6.97 d 8.3
6'	7.02 d 2.3	7.08 d 2.2
7'	3.35 dt 6.5, 1.6	3.37 dt 6.7, 1.6
8'	5.99 ddt 16.8, 10.0, 6.7	5.98 ddt 17.0, 10.1, 6.7
9'a	5.08 ddt 16.8, 1.6, 1.6	5.09 ddt 17.0, 1.5, 1.5
9'b	5.05 ddt 10.0, 1.6, 1.6	5.05 ddt 10.1, 1.5, 1.5
OMe		3.94

Compounds **6.7**–**6.8** were identified as isomagnolol (**6.7**),[17] and Pumerer's ketone (**6.8**)[10, 11] as reported in Tables **6-5**.

Table 6-5. NMR Spectroscopic Data for Compounds **6.7**–**6.8** in $CDCl_3$ (500 MHz)

	6.7		**6.8**
position	δ_H, *J* in Hz	position	δ_H, *J* in Hz
2	6.71 d 2.0	2	6.50 dd 10.2, 1.8
5	6.85 dd 8.2, 2.0	3	6.01 dd 10.2, 0.9
6	6.96 d 8.2	5a	2.76 dd 17.6, 4.4
7	3.37 dt 6.7, 1.5	5b	3.00 ddd 17.6, 2.8, 0.9
8	5.96 ddt 16.0, 10.5, 6.7	6	4.82 ddd 4.4, 2.8, 1.8
9a	5.09 ddt 16.0, 1.5, 1.5	7a	2.80 ddt 14.2, 6.7, 1.4
9b	5.08 ddt 10.5, 1.5, 1.5	7b	2.64 ddt 14.2, 8.2, 1.0
2'	6.94 dd 8.5, 1.5	8	5.79 dddd 16.9, 10.1, 8.1, 6.7
3'	7.15 dd 8.5, 1.5	9	5.19 m
5'	7.15 dd 8.5, 1.5	2'	7.02 d 1.8
6'	6.94 dd 8.5, 1.5	5'	6.74 d 8.0
7'	3.35 dt 6.7, 1.5	6'	7.00 dd 8.0, 1.8
8'	5.89 ddt 17.5, 9.5, 6.7	7'	3.35 dt 6.8, 1.5
9'a	5.00 ddt 17.5, 1.5, 1.5	8'	5.94 ddt 17.8, 9.4, 6.8
9'b	5.01 ddt 9.5, 1.5, 1.5	9'	5.07 m
OH	5.45 s		

6.2.3 Bioactivities of isolated compounds

The isolated compounds **6.1**–**6.8** were evaluated for their antiplasmodial activity against the Dd2 strain of *P. falciparum*. Compounds **6.3** and **6.4** showed moderate antimalarial activity with IC_{50} values of 2.8 ± 0.06 and 3.4 ± 0.08 μM, respectively. Compounds **6.1**, **6.2**, **6.5**, **6.6**, **6.7**, and **6.8** had weaker activities with IC_{50} values of 37.5 ± 2.00, 22.7 ± 1.81, 16.6 ± 0.2, 86.1 ± 0.6, 44.4 ± 4.1 and 114 ± 9 μM, respectively.

The fact that simple lignans show moderate antiplasmodial activity is not unprecedented. Thus several lignans with antiplasmodial activity from African medicinal plants are reported in the review by Ntie-Kang et al.,[18] and lignans with antiplasmodial activity have been reported from *Asparagus africanus*[19] and *Carrisa edulis*.[20] Neolignans have also shown good antiplasmodial activity.[21] One point of interest is that antiplasmodial activity appears to be strongly dependent on the substitution pattern of simple lignans. Thus compounds **6.3** and **6.4** were active at the single digit micromolar level, but compound **6.5**, isomeric with **6.4**, was fivefold less potent, and compound **6.6**, with an extra hydroxyl group, was thirtyfold less potent than **6.3**.

6.3 Experimental Section

6.3.1 General Experimental Procedures

UV spectra were measured on Shimadzu a UV-1201 spectrophotometer. ^{1}H- and ^{13}C NMR spectra were recorded on a Bruker Avance 500 spectrometer in $CDCl_3$ with TMS as internal standard. An Agilent 6220 mass spectrometer was used to obtain high resolution mass spectra. Solid phase extraction was performed using RP-18 silica gel (40–63μm, EM Science, Germany). Semi-preparative HPLC was performed on a semipreparative

Phenomenex C18 column (5μm, 250 × 10 mm), using Shimadzu LC-10AT pumps coupled with a Shimadzu SPD M10A diode array detector, and a SCL-10A system controller.

6.3.2 Plant Material.

The plant material was collected in Santa Barbara, CA on September 11, 1995 by Cori Morenberg and Jan Wienpahl (NYBG) in the Santa Barbara Alice Keck Memorial Park, along Arrelaga St. 34º25' N, 119º42' W. http://sweetgum.nybg.org/science/vh/specimen_details.php?irn=284841. Voucher specimen CM00144c.

6.3.3 Antiplasmodial Bioassays.

The effect of each fraction or compound on parasite growth of the Dd2 strain of *P. falciparum* was measured in a 72 h growth assay in the presence of compound as descibed previously [22, 23]. Briefly, ring stage parasite cultures (100 μL per well, with 1% hematocrit and 1% parasitemia) were grown for 72 h in the presence of increasing concentration of the drug in a 5% CO_2, 5% O_2, and 90% N_2 gas mixture at 37 ^oC. After 72 h in culture, parasite viability was determined by DNA quantitation using SYBR Green I assay [23]. The half-maximum inhibitory concentration (IC_{50}) calculation was performed with KaleidaGraph software using a nonlinear regression curve fitting. IC_{50} values are the average of three independent determinations with each determination in duplicate and are expressed ± SEM. Artemisinin was used as the positive control with an IC_{50} of 6 ± 2 nM.

6.3.4 Extraction and Isolation.

The dried and powdered twigs and fruit of *M. grandiflora* (175 g) were exhaustively extracted with MeOH in two 24-hour percolation steps followed by partition into hexane, methylene chloride and an aqueous methanolic fractions. The latter was detanninized by

passage through a column of polyvinyl pyrrolidone to give the active methanolic fraction 0038279-03C, X-4568 (about 10 g). For purposes of fractionation and purification, 1.5 g of extract was shipped to Virginia Tech for bioassay-guided isolation.

The crude extract (1.3 g) was first detanninized again by dissolving in MeOH and passing it through a polyamide column. A total of 932 mg detanninized extract was collected after elution and evaporation. It was dissolved in 200 mL of 90% aquous methanol and extracted with hexanes (200 × 5 mL). A total of 69 mg hexanes fraction was obtained. The 90 % aqeous methanol extact was evaporated, suspended in 200 mL water, and then extracted with EtOAc (200 × 5 mL); evaporation of this EtOAc-soluble fraction gave 317 mg residue. The water layer was concentrated to a brown reside (530 mg). The EtOAc fraction had the highest antiplasmodial activity, with an IC_{50} value between 5 and 2.5 μg/mL. It was separated into seven sub-fractions (**C6-2.1**–**C6-2.7**) by open column chromatography over RP-18 silica gel with a MeOH/H_2O gradient. Sub-fraction **C6-2.5** (eluted with 90% MeOH/H_2O) was the most active fraction with an IC_{50} value between 2.5 and 1.5 μg/mL. Semi-preparative C_{18} HPLC (MeOH/H_2O sovent system) on **C6-2.5** yielded nine subfractions (**C6-2.5.1** to **C6-2.5.9**). Fraction **C6-2.5.8** was further purified on HPLC using a C_{18} column with a MeOH/H_2O solvent system to give compound **6.3** (3.2 mg, t_R 19.2 min). Fraction **C6-2.5.6** was subjected to HPLC purification on a C_{18} column using MeCN/H_2O as solvent system to afford compounds **6.4** (2.0 mg, t_R 12.76 min) and **6.6** (0.3 mg, t_R 14.5 min). **C6-2.5.5** was purified by HPLC on a C_{18} column using the MeCN/H_2O solvent system to obtain compound **6.1** (0.5 mg, t_R 12.1 min). The seventh fraction **C6-2.5.7** yieded compounds **6.2** (0.6 mg, t_R 14.2 min) and **6.7** (0.3 mg, t_R 18.8 min) on HPLC separation on a C_{18} column using the

MeCN/H_2O solvent system. HPLC of fraction **C6-2.5.3** on a C_{18} column (MeCN/H_2O solvent system) resulted in the isolation of compounds **6.5** (2.7 mg, t_R 10.1 min) and **6.8** (0.3 mg, t_R 14.4 min).

6.3.5 Compound Information

4,4´-Diallyl-1,2,6,4´-tetrahydrodibenzo[b,d]furan-3´-ol **6.1**. Colorless oil. $[\alpha]_D^{21}$ –33.8º (*c* = 0.020, MeOH), LC-UV [(acetonitrile in H_2O)] λ_{max} 225, 285 nm. ^{1}H NMR ($CDCl_3$, 500 MHz) and ^{13}C NMR ($CDCl_3$, 125 MHz), see Table **6-1**. ESI-HRMS *m/z* 291.1352 $[M + Na]^+$; $C_{18}H_{20}O_2Na$ (calc. 291.1361).

3,3'-Diallyl-4'-((4-hydroxyphenethyl)amino)-[1,1'-biphenyl]-4-ol **6.2** LC-UV [(acetonitrile in H_2O)] λ_{max} 219, 280 nm. ^{1}H NMR ($CDCl_3$, 500 MHz) and ^{13}C NMR ($CDCl_3$, 125 MHz), see Table **6-2**. ESI-HRMS *m/z* 386.2107 $[M + H]^+$; $C_{26}H_{28}NO_2$ (calc. 386.2120).

6.4 References

1. Latif, A. D., Y.; Dalal, S. R.; Fernández-Murga, M. L.; Merino, E. F.; Cassera, M. B.; Goetz, M.; Kingston, D. G. I. Bioactive Neolignans and Other Compounds from *Magnolia grandiflora* L.: Isolation and Antiplasmodial Activity. *Chem. Biodiversity* **2017**, doi: 10.1002/cbdv.201700209.

2. Wu, Z.; Zhou, T.; Xiao, P. *Compendium of Xinhua Herbal Book*. 1988.

3. Clark, A. M.; El-Feraly, A. S.; Li, W. S. Antimicrobial Activity of Phenolic Constituents of *Magnolia grandiflora*. L. *J. Pharm. Sci.* **1981,** *70* (8), 951–952.

4. Rao, K. V. Glycosides of *Magnolia grandiflora*. *Planta Med.* **1975,** *27* (01), 24–30.

5. Rao, K. V.; Wu, W. N. Glycosides of Magnolia III. Structural Elucidation of Magnolenin C. *Lloydia* **1978,** *41*, 56–62.

6. El-Feraly, F. S. Melampolides from *Magnolia grandiflora*. *Phytochemistry* **1984,** *23* (10), 2372–2374.

7. Li, H.-M.; Zhao, S.-R.; Huo, Q.; Ma, T.; Liu, H.; Lee, J. K.; Hong, Y.-S.; Wu, C.-Z. A New Dimeric Neolignan from *Magnolia grandiflora* L. Seeds. *Arch. Pharm. Res.* **2015,** *38*, 1066–1071.

8. Yang, M.; Blunden, G.; Patel, A.; O'Neill, M.; Lewis, J. Coumarins and Sesquiterpene Lactones from *Magnolia grandiflora* Leaves. *Planta Med.* **1994,** *60* (04), 390–390.

9. Morshedloo, M. R.; Quassinti, L.; Bramucci, M.; Lupidi, G.; Maggi, F. Chemical Composition, Antioxidant Activity and Cytotoxicity on Tumour Cells of the Essential Oil from Flowers of *Magnolia grandiflora* Cultivated in Iran. *Nat. Prod. Res.* **2017,** *31*, 2857–2864.

10. Sy, L.-K.; Brown, G. D. Biomimetic Synthesis of *Illicium* Oligomeric Neolignans. *J. Chem. Res., Synop.* **1998,** (8), 476–477.

11. Tzeng, S.-C.; Liu, Y.-C. Peroxidase-catalyzed Synthesis of Neolignan and its Anti-inflammatory Activity. *J. Mol. Catal. B: Enzym.* **2004,** *32* (1–2), 7–13.

12. Liu, Y.; Chen, L.; Ji, Y. Quantification and Structural Elucidation of Potential Impurities in Agomelatine Active Pharmaceutical Ingredient. *J. Pharm. Biomed. Anal.* **2013,** *81–82*, 193–201.

13. Lin, J. M.; Gowda, A. S. P.; Sharma, A. K.; Amin, S. In Vitro Growth Inhibition of Human Cancer Cells by Novel Honokiol Analogs. *Bioorg. Med. Chem.* **2012,** *20*, 3202–3211.

14. Denton, R. M.; Scragg, J. T.; Saska, J. A Concise Synthesis of 4′-O-Methyl Honokiol. *Tetrahedron Lett.* **2011,** *52* (20), 2554–2556.

15. Kijjoa, A.; Pinto, M. M. M.; Tantisewie, B.; Herz, W. A Biphenyl Type Neolignan and a Biphenyl Ether from *Magnolia henryi*. *Phytochemistry* **1989,** *28* (4), 1284–1286.

16. Denton, R. M.; Scragg, J. T.; Galofré, A. M.; Gui, X.; Lewis, W. A Concise Synthesis of Honokiol. *Tetrahedron* **2010,** *66* (40), 8029–8035.

17. El-Feraly, F. S.; Cheatham, S. F.; Breedlove, R. L. Antimicrobial Neolignans of *Sassafras randaiense* Roots. *J. Nat. Prod.* **1983,** *46* (4), 493–498.

18. Ntie-Kang, F.; Onguéné, P. A.; Lifongo, L. L.; Ndom, J. C.; Sippl, W.; Mbaze, L. M. a. The Potential of Anti-malarial Compounds Derived from African Medicinal Plants, Part II: A Pharmacological Evaluation of Non-alkaloids and Non-terpenoids. *Malaria J.* **2014,** *13* (1), 81.

19. Oketch-Rabah, H. A.; Dossaji, S. F.; Christensen, S. B.; Frydenvang, K.; Lemmich, E.; Cornett, C.; Olsen, C. E.; Chen, M.; Kharazmi, A.; Theander, T. Antiprotozoal Compounds from *Asparagus africanus*. *J. Nat. Prod.* **1997,** *60* (10), 1017–1022.

20. Kebenei, J. S.; Ndalut, P. K.; Sabah, A. O. Anti-plasmodial Activity of Nortrachelogenin from the Root Bark of *Carissa edulis* (Vahl). *Int. J. Appl. Res. Nat. Prod.* **2011,** *4* (3), 21.

21. Rakotondraibe, H. L.; Graupner, P. R.; Xiong, Q.; Olson, M.; Wiley, J. D.; Krai, P.; Brodie, P., J.; Callmander, M. W.; Rakotobe, E.; Ratovoson, F.; Rasamison, V. E.; Cassera, M. B.; Hahn, D. R.; Kingston, D. G. I.; Fotso, S. Neolignans and Other Metabolites from *Ocotea cymosa* from the Madagascar Rain Forest and their Biological Activities. *J. Nat. Prod.* **2015,** *78*, 431–440.

22. Bennett, T. N.; Paguio, M.; Gligorijevic, B.; Seudieu, C.; Kosar, A. D.; Davidson, E.; Roepe, P. D. Novel, Rapid, and Inexpensive Cell-based Quantification of Antimalarial Drug

Efficacy. *Antimicrob. Agents Chemother.* **2004,** *48* (5), 1807–1810.

23. Smilkstein, M.; Sriwilaijaroen, N.; Kelly, J. X.; Wilairat, P.; Riscoe, M. Simple and Inexpensive Fluorescence-based Technique for High-throughput Antimalarial Drug Screening. *Antimicrob. Agents Chemother.* **2004,** *48* (5), 1803–1806.

Chapter 7: Structure Reassignment of New Bicyclic Tetrahydro-α-pyrones

This chapter is a slightly expanded version of a published note.[1] (Du, Y.; Kingston, D. G. I., Structure Reassignment of Cryptorigidifoliols E and K. *J. Nat. Prod.* **2018**, 81, 414-417.) Author contributions of the articles are described as follows in the order of the names listed. The author of this dissertation (Mr. Yongle Du) redetermined the structures of compounds cryptorigidifoliol E and K. Dr. David G. I. Kingston was a mentor for this work and the corresponding author for the published article. He also edited the final manuscript.

7.1 Introduction

The isolation and structure elucidation of the antimalarial compounds cryptorigidifoliols A – K from an ethanolic extract of the root wood of *Cryptocarya rigidifolia* was reported in 2015.[2] The structures of cryptorigidifoliols A,[3] B,[4] and I,[5] were confirmed by synthesis, but syntheses of cryptorigidifoliols E[6] (**7.1a**) and K[7] (**7.2a**) failed to confirm these structures. In this study cryptorigidifoliols E and K are reassigned as **7.1** and **7.2**.

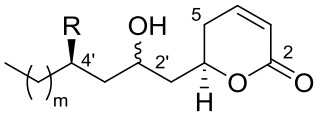

A (2'*R*) R = H, m = 10
B (2'*S*) R = OH, m = 14

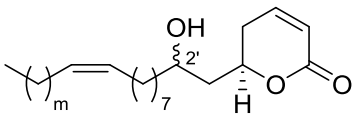

C (2'*R*) m = 5
D (2'*S*) m = 7

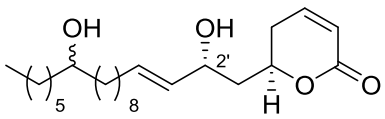

7.1a (E)

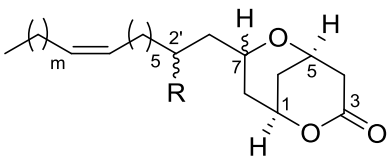

F R = OH, m = 7
G R = H, m = 10
J (7*R*) R = H, m = 5

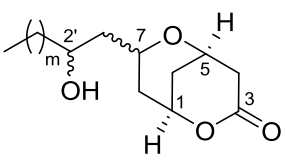

H m = 11
I (2'*R*,7*S*) m = 14

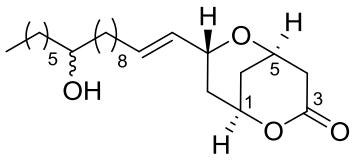

7.2a (K)

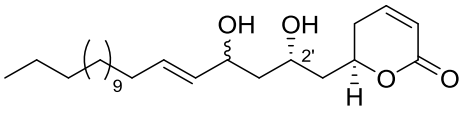

7.1

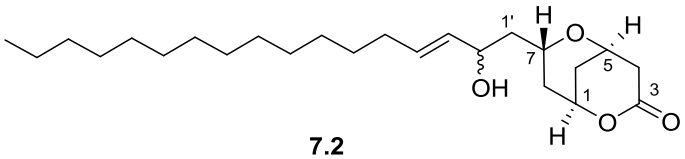

7.2

7.2 Structure reassignment of Cryptorigidifoliol K from *Cryptocarya rigidifolia*

7.2.1 Structure elucidation of a new bicyclic tetrahydro-α-pyrone derivative

The position of the distal hydroxyl group in the structure of cryptorigidifoliol E (**7.1a)** and thus also in the structure of cryptorigidifoliol K (**7.2a**), into which cryptorigidifoliol E is converted on treatment with acid, was originally assigned based on its ESIMS.[2] Since the only sample available for study was 1 mg of cryptorigidifoliol K, this sample was used for a detailed NMR investigation. Based on this additional information, the structure of cryptorigidifoliol K is reassigned as **7.2** on the basis of the following evidence.

7.2.2 Structure reassignment of the new bicyclic tetrahydro-α-pyrone derivative

The positive ion HRESIMS for **7.2** revealed a peak for a protonated dehydrated molecular ion at *m/z* 377.3060, and for a sodium adduct ion at *m/z* 417.2981, both corresponding to a molecular formula of $C_{24}H_{42}O_4$ for **7.2**. Its IR spectrum exhibited bands at 3431 and 1732 cm^{-1}, indicating the presence of hydroxyl and ester carbonyl groups. The presence of a 2,6-dioxabicyclo[3.3.1]nonan-3-one system was indicated by ^{1}H NMR signals at δ_H 4.88 (br, H-1), 2.87 (dt 19.3, 1.9, H-4a), 2.79 (dd 19.3, 5.0, H-4b), 4.39 (br, H-5), 2.04-2.00 (m, H-6a), 1.93 (ddt 13.9, 4.0, 1.9, H-6b), 3.98 (ddt, 12.0, 9.4, 2.5, H-7), 2.03 (ddd 14.0, 4.0, 2.5, H-8a), and 1.64 (ddd 14.0, 12.0, 1.9, H-8b) and the ^{13}C NMR signals at δ_C 72.7 (C-1), 169.2 (C-3), 36.5 (C-4), 65.8 (C-5), 29.7 (C-6), 65.9 (C-7) and 37.1 (C-8), as shown in Table **7-1**.

Table 7-1. NMR Spectroscopic Data for Compounds 7.2 in $CDCl_3$ (500 MHz)

position	δ_H, *J* in Hz	δ_C, type	position	δ_H, *J* in Hz	δ_C, type
1	4.88 br	72.7, CH	5'	2.03–1.99 m	32.4, CH_2
3		169.2, C	6'	1.39–1.33 m	29.2, CH_2
4	2.87 ddd 19.3, 1.9, 1.9	36.5, CH_2	7'	1.28–1.22 m	29.8, CH_2
	2.79 dd 19.3, 5.0		8'	1.28–1.22 m	29.8, CH_2
5	4.39 br	65.8, CH	9'	1.28–1.22 m	29.8, CH_2
6	2.04-2.00 m	29.7, CH_2	10'	1.28–1.22 m	29.8, CH_2
	1.93 dddd 13.9, 4.0, 1.9, 1.9		11'	1.28–1.22 m	29.8, CH_2
7	3.98 ddt 12.0, 9.4, 2.5	65.9, CH	12'	1.28–1.22 m	29.8, CH_2
8	2.03 ddd 14.0, 4.0, 2.5	37.1, CH_2	13'	1.28–1.22 m	29.8, CH_2
	1.64 ddd 14.0, 12.0, 1.9		14'	1.28–1.22 m	29.8, CH_2
1'	1.78 ddd 14.3, 9.4, 7.8	43.0, CH_2	15'	1.27–1.23 m	32.2, CH_2
	1.61 ddd 14.3, 4.3, 2.5		16'	1.31–1.28 m	22.9, CH_2
2'	4.27 ddd 7.8, 7.1, 4.3	72.0, CH	17'	0.88 t 6.9	14.1, CH_3
3'	5.42 ddt 15.0, 7.1, 1.5	131.8, CH	OH	2.77	
4'	5.67 dt 15.0, 6.8	132.5, CH			

These assignments were confirmed by ^2J-HMBC correlations between H-4 and C-3, H-4 and C-5, and by ^3J-HMBC correlations between H-1 and C-7, H-5 and C-1/C-3/C-7, H-6 and C-4/C-8 (Figure **7-1**). The long 2'-hydroxyheptadec-3-en-1-yl side chain was indicated by ^{1}H NMR signals at δ_H 1.78 (ddd 14.3, 9.4, 7.8, H-1'a), 1.61 (ddd 14.3, 4.3, 2.5, H-1'b), 4.27 (ddd 7.8, 7.1, 4.3, H-2'), 5.42 (ddt 15.0, 7.1, 1.5, H-3'), 5.67 (dt 15.0, 6.8, H-4'), 2.03 – 1.99 (m, H-5'), 1.39 – 1.22 (m, 24H, H-6' – H-15'), 1.31 – 1.28 (m, 2H, H-16'), and 0.88 (t, 6.9, H-17'). Crucially, ^3J-HMBC correlations were observed between H-2' and C-7, between H-3' and C-1'/C-5', between H-4' and C-2'/C-6', and between the hydroxyl proton and C-1'/C-3'. These correlations uniquely assign the hydroxyl group to C-2' and the double bond to C-3'. The side chain was connected at C-7 based on ^2J-HMBC correlations between H-7 and C-1' and ^3J-HMBC correlations between H-8 and C-1' and H-2' and C-7 (Figure **7-1**). In addition, COSY correlations defined the H-7 to H-4' spin system (Figure **7-1**).

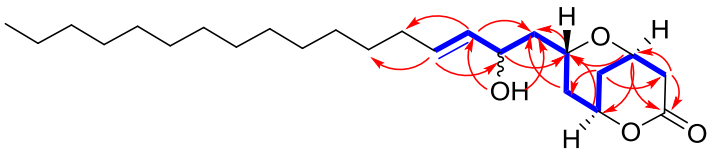

Figure 7-1. Selected HMBC (red) and COSY (blue) correlations of cryptorigidifoliol K **7.2**

As reported in the original paper,[2] compound **7.2** had no significant Δδ (H) difference between its *R*- and *S*-MPA derivatives, so its absolute configuration at C-2' could not be determined.

Regrettably no sample of cryptorigidifoliol E (**7.1**) was available, but since it can be converted to its isomer cryptorigidifoliol K (**7.2**) on treatment with acid,[2] its structure can be reassigned as **7.1**.

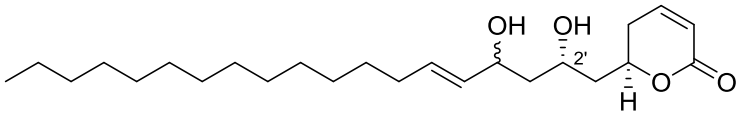

7.1

7.2.3 Compound Information

Cryptorigidifoliol K (**7.2**). colorless oil; $[\alpha]^{21}_{D}$ –8º (*c* 0.6, MeOH); UV (MeOH) λ_{max} (log ε): 204 (3.10) nm; IR ν_{max} 3431, 2956, 2867, 1732, 1036 cm^{-1}; ^{1}H and ^{13}C NMR data, see Table **7-1**; HRESIMS *m/z* $[M+Na]^+$ 417.2981 (calcd for $C_{24}H_{42}O_4Na$, 417.2975), $[M+H-H_2O]^+$ 377.3060 (calcd for $C_{24}H_{41}O_3$, 377.3050).

7.3 References

1. Du, Y. K., D. G. I. Structure Reassignment of Cryptorigidifoliols E and K. *J. Nat. Prod.* **2018,** *81*, 414–417.

2. Liu, Y.; Rakotondraibe, L. H.; Brodie, P. J.; Wiley, J. D.; Cassera, M. B.; Miller, J. S.; Ratovoson, F.; Rakotobe, E.; Rasamison, V. E.; Kingston, D. G. I. Antimalarial 5,6-Dihydro-alpha-pyrones from Cryptocarya rigidifolia: Related Bicyclic Tetrahydro-α-Pyrones Are Artifacts. *J. Nat. Prod.* **2015,** *78* (6), 1330–1338.

3. Raju, A.; Yugendar Reddy, A.; Sabitha, G. First total synthesis of antimalarial (+)-cryptorigidifoliol A. *Tetrahedron Lett.* **2015,** *56* (40), 5474–5476.

4. Perla, R.; Ramisetti, A.; Atla, R. First total synthesis of the proposed structure of cryptorigidifoliol B. *Tetrahedron Lett.* **2016,** *57* (19), 2100–2102.

5. Padhi, B.; Reddy, G. S.; Mohapatra, D. K. Total Synthesis of Tetraketide and Cryptorigidifoliol I via a Sequential Allylation Strategy. *J. Nat. Prod.* **2016,** *79* (11), 2788–2796.

6. Radha Krishna, P.; Manikanta, G.; Nagaraju, T. Total Synthesis of the Proposed Structures of the Novel Antimalarial Pyranone Cryptorigidifoliol E. *Synthesis* **2016,** *48* (23), 4213–4220.

7. Reddy, G. S.; Padhi, B.; Bharath, Y.; Mohapatra, D. K. Total Synthesis of Four Isomers of the Proposed Structures of Cryptorigidifoliol K. *Org. Lett.* **2017,** *19*, 6506–6509.

Chapter 8: Isolation of Known Bioactive Compounds

This chapter is a summary of the isolation of known bioactive compounds from crude extracts and of work on other antimalarial extracts from which no bioactive compounds were isolated. Author contributions of this chapter are described as follows in the order of the names listed. The author of this dissertation (Mr. Yongle Du) isolated and determined the structures of all the compounds, and performed A2780 bioassays on these compounds. Dr. Yumin Dai was a mentor, and provided some important suggestions for the isolation and structural elucidation of the known compounds from *Trichocladus grandiflorus*. Dr. Michael Goetz provided all the NPDI extracts. Dr. Priscilla Krai, Dr. Seema Dalal and Dr. Ana Lisa Valenciano carried out the antiplasmodial bioassays on the fractions and the isolated compound under the direction of Maria B. Cassera. Dr. David G. I. Kingston was a mentor for this work.

8.1 Introduction

The extracts discussed in this chapter were selected on the basis of their antimalarial activity. Two of them only yielded known compounds and the other four extracts did not yield any bioactive compounds.

8.2 Two known glucosides from *Trichocladus grandiflorus*

8.2.1 Isolation of active compounds

A crude extract of stems of *Trichocladus grandiflorus* 60070-8H (550 mg) was suspended in aqueous methanol (methanol:water 9:1, 100 mL), and extracted with hexane (3 × 100 mL

portions). The aqueous methanol layer was diluted to 60% methanol (v/v) with water and extracted with DCM (3 × 100 mL portions). The hexane fraction was evaporated in vacuo to leave 29 mg of material with IC_{50} > 10 μg/mL. The residue from the dichloromethane fraction (50 mg) was the most active fraction with an IC_{50} value of l.25 ~ 2.5 μg/mL. The remaining aqueous methanol fraction was evaporated to give a supernatant (464 mg) with an IC_{50} of 5 ~ 10 μg/mL. The DCM fraction was directly applied to a Sephadex LH-20 open column to afford five fractions with masses of 5, 6, 7, 3, and 20 mg. The fifth fraction was the most active with an IC_{50} value of 5 ~ 2.5 μg/mL, and was separated by HPLC on a C-18 column using an acetonitrile and water gradient from 10% acetonitrile to 40% acetonitrile over 20 min to yield two known compounds, norbergenin **8.1** (1 mg) and bergenin **8.2** (2 mg) with retention times of 9.0 and 15.5 min.

8.2.2 Structure elucidation of isolated compounds

The molecular formulas of norbergenin **8.1** and bergenin **8.2** were determined as $C_{13}H_{14}O_9$ and $C_{14}H_{16}O_9$ from their positive ion HRESIMS. Their structures were confirmed by comparing their ^{1}H NMR and ^{13}C NMR data with those of known compounds.[1] This work indicated that the ^{13}C NMR chemical shifts of C-2' and C-3' had been assigned as the reverse of the correct assignments; the correct data is shown in Table **8-1**.

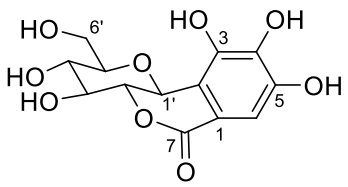

8.1

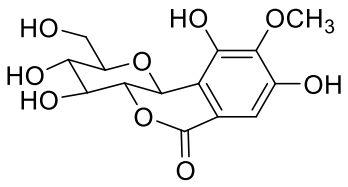

8.2

Table 8-1. NMR Spectroscopic Data for Compounds **8.1** and **8.2** in Acetone-d6 (500 MHz)

	8.1		**8.2**	
position	δ_H, *J* in Hz	δ_C, type	δ_H, *J* in Hz	δ_C, type
1		116.9, C		119.6, C
2		114.9, C		113.3, C
3		143.3, C		143.8, C
4		139.9, C		141.1, C
5		146.8, C		149.1, C
6	7.10 s	110.6, CH	7.07 s	110.2, CH
7		164.2, C		163.4, C
1'	5.00 d 10.4	73.9, CH	5.04 d 10.4	73.9, CH
2'	4.04 dd 10.4, 9.4	80.9, CH	4.08 dd 10.4, 9.4	80.9, CH
3'	3.87 dd 9.4, 8.5	75.6, CH	3.88 dd 9.4, 8.5	75.5, CH
4'	3.50 dd 9.7, 8.5	72.1, CH	3.50 dd 9.7, 8.5	72.0, CH
5'	3.78 ddd 9.7, 7.3, 2.3	82.7, CH	3.79 ddd 9.7, 7.3, 2.3	82.9, CH
6'	4.10 dd 11.7, 2.3	62.7, CH_2	4.12 dd 11.7, 2.3	62.7, CH_2
	3.70 dd 11.7, 7.3		3.71 dd 11.7, 7.3	
-OMe			3.89 s	60.7, CH_3

8.2.3 Bioactivities of isolated compounds

Both norbergenin **8.1** and bergenin **8.2** showed only weak antiplasmodial activities, with IC_{50} values of ~ 30 μM. These two compounds had previously shown potent anti-arthritic activities.[2]

8.3 A known lignan and three known canthinone alkaloids from *Leitneria floridana*

8.3.1 Isolation of active compounds

An extract of the whole plant of *Leitneria floridana* 38275-04G (1500 mg) was suspended in aqueous methanol (methanol:water 9:1, 100 mL), and extracted with hexane (3 × 100 mL portions). The aqueous methanol layer was diluted to 60% methanol (v/v) with water and extracted with dichloromethane (3 × 100 mL portions). The hexane fraction was evaporated in vacuo to leave 250 mg of material with IC_{50} 5 ~ 10 μg/mL. The residue from the dichloromethane fraction (200 mg) was the most active fraction with an IC_{50} value of <<

l.25 μg/mL. The remaining aqueous methanol fraction was evaporated to give 608 mg of material, with an IC_{50} of 5 ~ 10 μg/mL. The dichloromethane fraction was directly applied to a silica gel open column with elution by a dichloromethane and methanol gradient from 20:1 to 100 % methanol to afford twenty-two fractions. Fraction twelve with an IC_{50} value of 5 ~ 2.5 μg/mL was separated by HPLC on a C-18 column using an acetonitrile and water gradient from 40% acetonitrile to 100% acetonitrile over 40 min to yield two known compounds, canthin-6-one **8.3** (1 mg) and 1-methoxycanthin-6-one **8.4** (1 mg) with retention times of 16.4 and 19.5 min. Fraction sixteen from the silica gel column with an IC_{50} value of 5 ~ 2.5 μg/mL was separated by HPLC on a C-18 column using an acetonitrile and water gradient from 50% acetonitrile to 87.5% acetonitrile over 30 min to yield the known compound 5-methoxycanthin-6-one **8.5** (1 mg) with a retention time of 21.8 min. Fraction twenty with an IC_{50} value of << 1.25 μg/mL was separated by HPLC on a C-18 column using an acetonitrile and water gradient from 40% acetonitrile to 60% acetonitrile over 30 min to yield the known compound, (+)-lariciresinol **8.6** (1 mg) with a retention time of 15.0 min.

8.3.2 Structure elucidation of isolated compounds

The molecular formulas of the four known compounds, canthin-6-one **8.3**, 1-methoxycanthin-6-one **8.4**, 5-methoxycanthin-6-one **8.5** and (+)-lariciresinol **8.6** were determined from their positive ion HRESIMS. Their structures were confirmed by comparing their ^{1}H NMR spectra with ^{1}H NMR data of the corresponding known compounds.[3-6] Their ^{1}H NMR data is shown in Tables **8-2** and **8-3**.

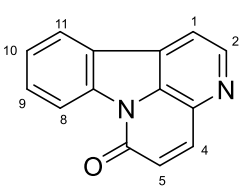

8.3

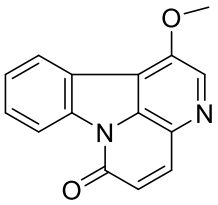

8.4

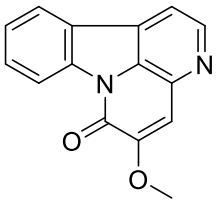

8.5

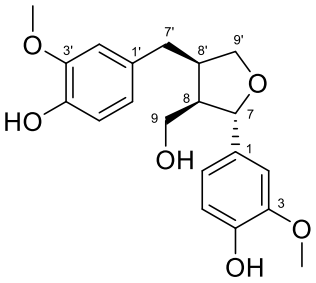

8.6

Table 8-2. NMR Spectroscopic Data for Compounds **8.3**–**8.5** in $CDCl_3$ (500 MHz)

	8.3	**8.4**	**8.5**
position	δ_H, *J* in Hz	δ_H, *J* in Hz	δ_H, *J* in Hz
1	8.06 d 5.2		7.86 d 5.2
2	8.83 d 5.2	8.51 s	8.78 d 5.2
4	8.18 d 9.8	8.01 d 9.8	7.22 s
5	7.05 d 9.8	6.87 d 9.8	
8	8.17 d 7.8	8.25 d 7.7	8.11 dd 8.0, 1.0
9	7.77 t 7.8	7.69 t 7.7	7.72 td 8.0, 1.0
10	7.68 t 7.8	7.54 t 7.7	7.55 td 8.0, 1.0
11	8.71 d 7.8	8.70 d 7.7	8.73 dd 8.0, 1.0
-OMe		4.28 s	4.07 s

Table 8-3. NMR Spectroscopic Data for Compounds **8.6** in $CDCl_3$ (500 MHz)

position	δ_H, *J* in Hz	position	δ_H, *J* in Hz
1		1'	
2	6.90 d 1.8	2'	6.79 d 1.9
3		3'	
4		4'	
5	6.76 m	5'	6.71 d 8.0
6	6.75 m	6'	6.64 dd 8.0, 1.9
7	4.74 d 7.0	7'	2.48 dd 13.4, 11.1
8	2.37 m		2.92 dd 13.4, 4.8
9	3.62 dd 10.9, 6.5	8'	2.73 m
	3.83 dd 10.9, 8.0	9'	3.72 dd 8.4, 5.8
3-OMe	3.84 s		3.97 dd 8.4, 6.5
		3'-OMe	3.82 s

8.3.3 Bioactivities of isolated compounds

The two known compounds 1-methoxycanthin-6-one **8.4** and 5-methoxycanthin-6-one **8.5** had very only weak antiplasmodial activities, with IC_{50} values of > 30 μM, and canthin-6-one **8.3** showed no antiplasmodial activity. Canthin-6-one **8.3** did however have better antiproliferative activity than 1-methoxycanthin-6-one **8.4** and 5-methoxycanthin-6-one **8.5**, with an IC_{50} value of 22 μM. In previous work 1-methoxycanthin-6-one **8.4** had shown good anti-HIV activity, so the canthin-6-one type alkaloids might provide a useful lead for anti-AIDS drug development.[7] The known compound (+)-lariciresinol **8.6** showed good antiplasmodial and antiproliferative activities with IC_{50} values of 3.7 and 7.8 μM.

8.4 Investigations of other antimalarial extracts

8.4.1 The whole plant extract of *Juncellus serotinus*

An extract of the whole plant *Juncellus serotinus* (NPDI 1000585-6C, 560 mg) had weak antiplasmodial activity with an IC_{50} value of > 10 μg/mL. After liquid liquid partition and separation on a Sephadex LH-20 open column, only 30 mg of a bioactive fraction was obtained. It was separated by HPLC on a C-18 column, but no pure compounds could be isolated, and the bioactivity was lost. Work on this extract was thus discontinued.

8.4.2 The whole plant extract of *Cymbopogon citratus*

An extract of the whole plant extract of *Cymbopogon citratus* (NPDI 0013101-09G, 108 mg) had weak antiplasmodial activity with an IC_{50} value of > 10 μg/mL. After liquid liquid partition, the hexane fraction had improved activity with an IC_{50} value of ~ 5 μg/mL.

Separation on a Sephadex LH-20 open column failed to yield any active fractions, so this extract was dropped.

8.4.3 The whole plant extract of *Melloa quadrivalvis*

An extract of the whole plant extract of *Melloa quadrivalvis* (NPDI 29676-11F, 145 mg) had weak antiplasmodial activity with an IC_{50} value of > 10 μg/mL. After separation on a Sephadex LH-20 open column, no active fraction was obtained, so this extract was dropped.

8.4.4 The whole plant extract of *Metroxylon vitiense*

An extract of the whole plant extract of *Metroxylon vitiense* (NPDI 0039966-07G, 280 mg) had weak antiplasmodial activity with an IC_{50} value of 2.5 ~ 5 μg/mL. After separation on a Sephadex LH-20 open column, three moderately active fractions were obtained. They were separated on a silica gel open column or by HPLC on a C-18 column, but no pure compounds could be isolated, and the bioactivity was lost. Work on this extract was thus discontinued.

8.5 References

1. Taneyama, M.; Yoshida, S.; Kobayashi, M.; Hasegawa, M. Studies on C-Glycosides in Higher-plants.3. Isolation of Norbergenin from *Saxifraga stolonifera*. *Phytochemistry* **1983,** *22* (4), 1053–1054.

2. Nazir, N.; Koul, S.; Qurishi, M. A.; Taneja, S. C.; Ahmad, S. F.; Ani, S. B.; Qazi, G. N. Immunomodulatory Effect of Bergenin and Norbergenin against Adjuvant-induced Arthritis - A Flow Cytometric Study. *J. Ethnopharmacol.* **2007,** *112* (2), 401–405.

3. Cordell, G. A.; Ogura, M.; Farnsworth, N. R. Alkaloid Constituents of *Ailanthus excelsa* (Simaroubaceae). *Lloydia* **1978,** *41* (2), 166–168.

4. Crespiperellino, N.; Guicciardi, A.; Malyszko, G.; Arlandini, E.; Ballabio, M.; Minghetti, A. Occurrence of Indole Alkaloids in *Ailanthus altissima* Cell-cultures. *J. Nat. Prod.* **1986,** *49* (6), 1010–1014.

5. Hagen, T. J.; Narayanan, K.; Names, J.; Cook, J. M. DDQ Oxidations in the Indole Area. Synthesis of 4-Alkoxy-*β*-carbolines Including the Natural Prodcuts Crenatine and 1-Methoxycanthin-6-one. *J. Org. Chem.* **1989,** *54* (9), 2170–2178.

6. Nishiwaki, H.; Kumamoto, M.; Shuto, Y.; Yamauchi, S. Stereoselective Syntheses of All Stereoisomers of Lariciresinol and Their Plant Growth Inhibitory Activities. *J. Agric. Food Chem.* **2011,** *59* (24), 13089–13095.

7. Xu, Z.; Chang, F.-R.; Wang, H.-K.; Kashiwada, Y.; McPhail, A. T.; Bastow, K. F.; Tachibana, Y.; Cosentino, M.; Lee, K.-H. Anti-HIV Agents 45 and AntitumorAgents 205. Two New Sesquiterpenes, Leitneridanins A and B, and the Cytotoxic and Anti-HIV Principles from *Leitneria floridana*. *J. Nat. Prod.* **2000,** *63* (12), 1712–1715.

.

Chapter 9: Synthesis and Evaluation of Doxorubicin-Loaded Gold Nanoparticles for Tumor-Targeted Drug Delivery

This chapter is a slightly abbreviated version of a published article. (Du, Y.; Xia, L.; Jo, A.; Davis, R. M.; Bissel, P.; Ehrich, M. F.; Kingston, D. G. I. Synthesis and Evaluation of Doxorubicin-Loaded Gold Nanoparticles for Tumor-Targeted Drug Delivery. *Bioconjugate Chem.* **2018,** 29, 420−430.) Author contributions of the articles are described as follows in the order of the names listed. The author of this dissertation (Mr. Yongle Du) synthesized one of the new thiolated doxorubicin analogs and the gold nanoparticles, loaded and released the drug−loaded gold nanoparticles and drafted part of the manuscript. Mr. Long Xia synthesized five new thiolated doxorubicin analogs, studied the stability of the analogs, and prepared the doxorubicin loaded gold nanoparticles for mouse studies, which are not included in this chapter. Ms. Ami Jo evaluated the doxorubicin loaded gold nanoparticles by TEM under the direction of Dr. Richey Davis. Philippe Bissel and Dr. Marion Ehrich performed the mouse experiments. Dr. David G. I. Kingston was a mentor for this work and the corresponding author for the published article. He also edited the final manuscript.

9.1 Introduction

9.1.1 Abstract

Doxorubicin is an effective and widely used cancer chemotherapeutic agent, but its application is greatly compromised by its cumulative dose-dependent side effect of cardiotoxicity. A gold nanoparticle-based drug delivery system has been designed to

overcome this limitation. One novel thiolated doxorubicin analog was synthesized and its biological activities evaluated. Different concentrations of this doxorubicin analog and PEG stabilizing ligand were then conjugated to gold nanoparticles, and the resulting Au-Dox constructs were evaluated by TEM. The results show that release of native drug can be achieved by the action of reducing agents such as glutathione under acidic conditions, and that reductive drug release gave the cleanest drug release.

9.1.2 Investigations of doxorubicin and gold nanoparticles for drug delivery

The anthracycline antibiotic doxorubicin (**9.1**) was discovered in the late 1960's as a minor component of the fermentation broth used to produce its analog daunorubicin (**9.2**).[1] Daunorubicin itself was discovered in the 1950's from a strain of *Streptomyces peucetius* isolated from a soil sample collected near the Adriatic Sea;[2] it had good bioactivity against mouse tumors, and was eventually marketed for treatment of leukemia.[3] Doxorubicin was identified as a hydroxylated analog of daunorubicin and was initially named adriamycin after the source of the original soil sample, but was later renamed doxorubicin by the World Health Organization.

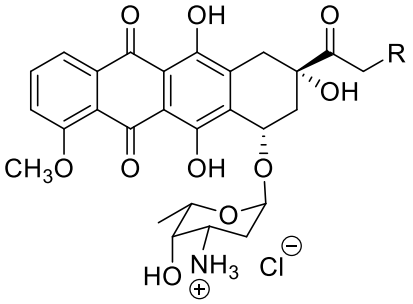

9.1 R = OH
9.2 R = H

Doxorubicin has a wide spectrum of activity and is used today, either alone or in combination with other drugs, for the treatment of a variety of cancers, including acute

leukemias and ovarian and breast cancers. It is one of the most effective cancer chemotherapeutic agents available,[4-7] and is on the World Health Organization list of essential medicines for both adults and children.[8] Regrettably its use is severely limited by various side effects, including myelosuppression, vomiting, diarrhea, and especially life-threatening cardiotoxicity.[9, 10] Two liposomal formulations of doxorubicin have been approved for clinical use. Doxil®, available in the U.S., is a pegylated liposomal formulation of doxorubicin that is approved for treatment of Kaposi's sarcoma, ovarian cancer, and multiple myeloma; it is much less cardiotoxic than native doxorubicin, but it does have some new side-effects.[11] Myocet® (liposome encapsulated doxorubicin citrate), available in the U.K., also is less cardiotoxic than doxorubicin and can be better tolerated by patients, while having an equivalent therapeutic efficacy.[12] While these formulations of doxorubicin are an improvement over the native drug, there is still room for further improvement, and it is a measure of doxorubicin's clinical effectiveness that it is so widely used in spite of its very significant side effects. Clearly however a selective targeted drug delivery method would offer the opportunity to make doxorubicin an even better option for cancer treatment.

The basic idea of targeting cancer chemotherapeutic agents is well known, and several approaches to targeting doxorubicin have been published. These include targeted delivery to hepatocarcinoma cells by laponite nanodiscs,[13] the use of magnetoliposomes,[14] and the use of doxorubicin-loaded poly(lactic-co-glycolic acid) hollow microcapsules.[15] The nanoparticle approach to drug delivery is attractive, since the enhanced permeability and retention effect assures a measure of selectivity,[16] although the magnitude of this effect has been questioned by a meta-analysis which showed that only 0.7% of the administered dose of nanoparticle

drugs is delivered to solid tumors.[17] Even this relatively low number is however higher than that of naked drug molecules,[18] and in the particular case of doxorubicin even this low delivery efficiency could be significant if the remaining drug never reached the heart.

The use of gold nanoparticles (AuNP) for drug delivery is particularly attractive since they can be generated in a range of sizes and can readily be functionalized with a variety of ligands,[19] and numerous studies have been made of AuNPs conjugated with doxorubicin. In some cases protonated doxorubicin was absorbed directly onto the surface of negatively charged AuNP under acidic conditions,[20] and a one-pot synthesis of doxorubicin-loaded AuNP was achieved in the presence of oxygen to generate radicals.[21] Several studies used various polymers to link doxorubicin to AuNP. Thus doxorubicin was loaded onto anionic polyaspartic acid AuNP by ionic complexation,[22] or it was bound to DNA which was itself bound to the AuNP.[23] Another study used DNA-caged AuNP that allowed T7 exonuclease and pH responsive controlled release of doxorubicin.[24] A study of doxorubicin-loaded PEG-AuNPs and their further antibody targeting showed that toxicity was reduced and therapeutic efficacy increased for the antibody targeted system.[25] On the other hand, a study of PEGylated gold nanoparticles with doxorubicin attached by covalent peptide or pH-active hydrazone linkers revealed that gold nanostructures modified with doxorubicin were more toxic to A549 and HeLa cells than free doxorubicin.[26] The use of folate-modified pegylated AuNP to conjugate doxorubicin gave a drug system that showed a much higher cytotoxicity than that of free doxorubicin, as well as an increased water-solubility.[27] Another study of folic acid-coated AuNP gave a construct with enhanced drug accumulation and retention in multidrug resistant hepG2-R cancer cells compared with free doxorubicin.[28] Grafting a

thiolated doxorubicin onto AuNPs via a cleavable disulfide linkage (Au-PEG-SS-DOX) improved drug uptake as compared with native doxorubicin, although the drug released was a doxorubicin derivative.[29] A study of a formulation with a pH-sensitive hydrazone bond as linker between doxorubicin and pegylated AuNP showed greatly enhanced solubility and an excellent pH response profile of drug release for the drug construct.[30] A variation of this approach grafted doxorubicin by a cleavable hydrazone linker onto the hydrophobic inner shell of a folate-conjugated poly(L-aspartate-doxorubicin)-*b*-poly(ethylene glycol) copolymer to give a drug construct that released doxorubicin readily at pH 5.3.[31] Ultrasmall gold-doxorubicin conjugates were found to target apoptosis-resistant cancer cells.[32] The use of AuNPs for targeted drug delivery[19] has been reviewed, as has the use of iron and gold nanoparticles for doxorubicin delivery,[19, 33] and the cytotoxicity of AuNPs has recently been evaluated, with the finding that PEG-coated nanospheres, nanorods, and nanostars show low cytotoxicity to U87 cells and fibroblasts.[34]

The use of AuNPs conjugated with the cytokine tumor necrosis factor (TNF) is a particularly powerful approach to drug targeting, since TNF not only targets the nanoparticle to tumors but also reduces the interstitial fluid pressure, allowing for enhanced uptake of the chemotherapeutic payload.[35] In the present study we investigated the conjugation of doxorubicin to AuNPs in preparation for future studies to add TNF to the drug construct.

9.2 Results and Discussion

9.2.1 Design and Synthesis of one New Thiolated Doxorubicin Analog.

A key consideration in any approach to drug delivery by AuNPs is whether the drug payload is released from the nanoparticle, and if so how this will occur. Release of the native

drug from the nanoparticle is preferable, since it allows the drug to interact with its target unhindered by any linker, and so we prepared the new doxorubicin analogs **9.3** that were designed to release free doxorubicin in the tumor cell.

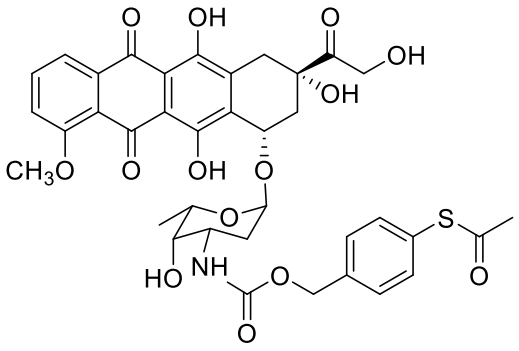

9.3

The 7-*O*-thiobenzyl derivative **9.3** was designed to undergo reductive cleavage from the AuNP by glutathione in the reducing tumor environment and to release native doxorubicin, as previously described for a similar paclitaxel derivative.[35] The proposed mechanism of doxorubicin release is shown in Figure **9-1**, with glutathione displacing analog **9.3** from the gold surface to give deacetyl **9.3**, which undergoes self-immolation (arrows) leading to doxorubicin, a thioquinone methide, and carbon dioxide. The thioquinone methide then undergoes hydration to (4-mercaptophenyl)methanol.

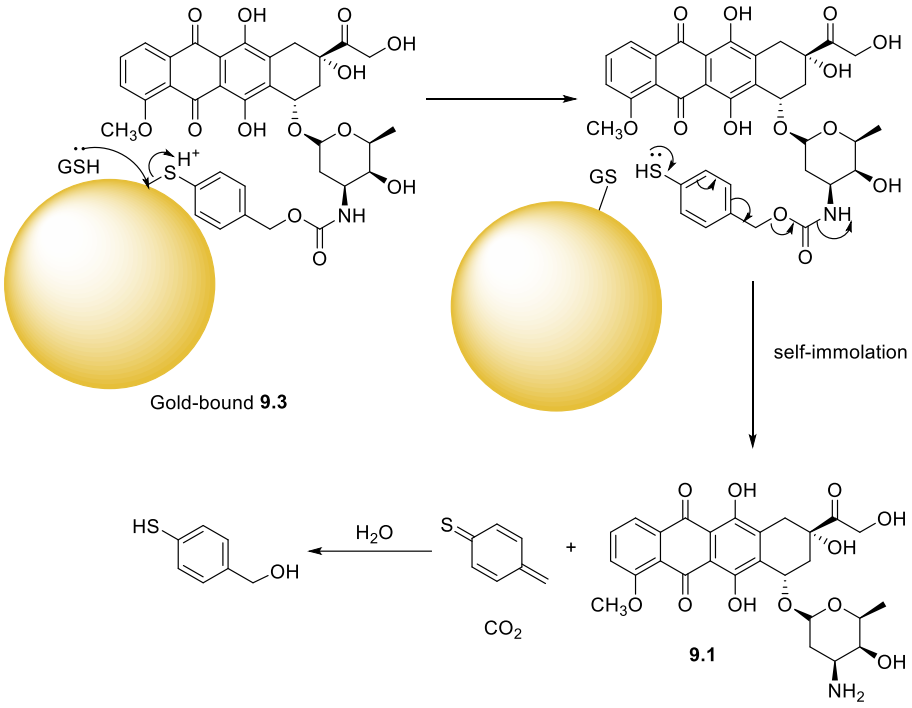

Figure 9-1. Proposed mechanism of doxorubicin release from gold-bound analog **9.3** by glutathione (GSH).

The synthesis of analog **9.3** is shown in Scheme **9-1**. Commercially available 4-mercaptobenzoic acid (**9.4**) underwent acetylation, reduction and acylation with 4-nitrophenyl chloroformate to obtain compound **9.7**, which was then reacted directly with doxorubicin hydrochloride (**9.1**) to give final product **9.3** in 63% overall yield.

Scheme 8-1. Synthesis of doxorubicin derivative 9.3[a]

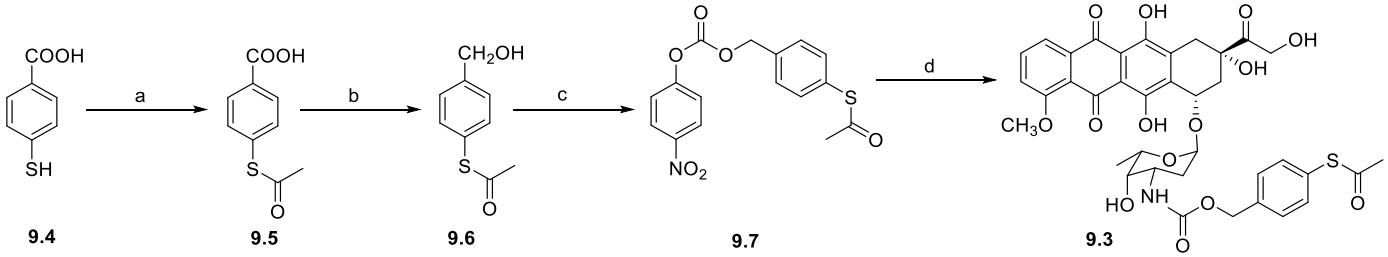

[a](a) Ac_2O, pyridine, CH_2Cl_2, 6 h 0 ºC to rt, 98%; (b) $Me_2S.BH_3$, THF, -10 ºC to rt, 4 h, 85%: (c) 4-nitrophenyl chloroformate, pyridine, CH_2Cl_2, 4 h 0 ºC to rt, 88%; (d) Et_3N, DMF, **9.1**, 0 ºC to rt, 2 h, 86%;

9.2.2 Preparation of AuNPs.

Gold nanoparticles (AuNPs) were prepared by two variations of the Wang method without added $AgNO_3$.[36] The citrate concentration was adjusted to produce approximately spherical nanoparticles with an average diameter of 34.6 ± 0.1 nm as determined by TEM (Figures **9-2** and **9-3**).

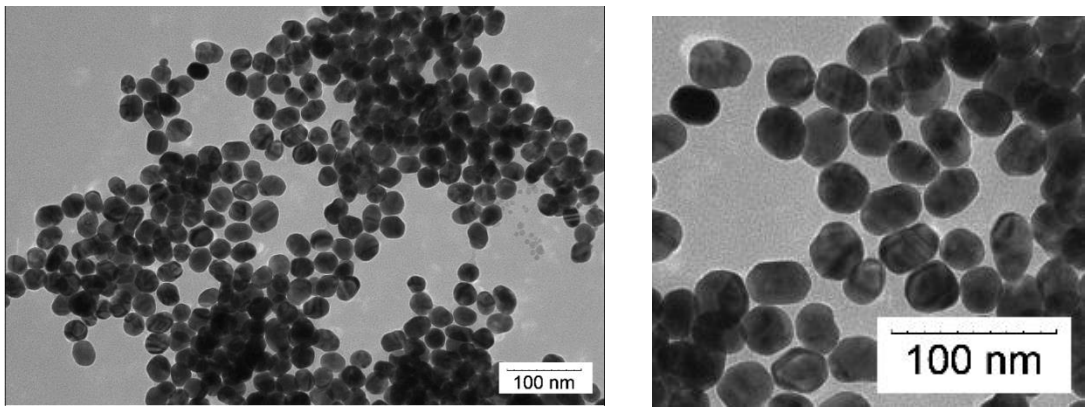

Figure **9-2**. TEM images of naked AuNPs.

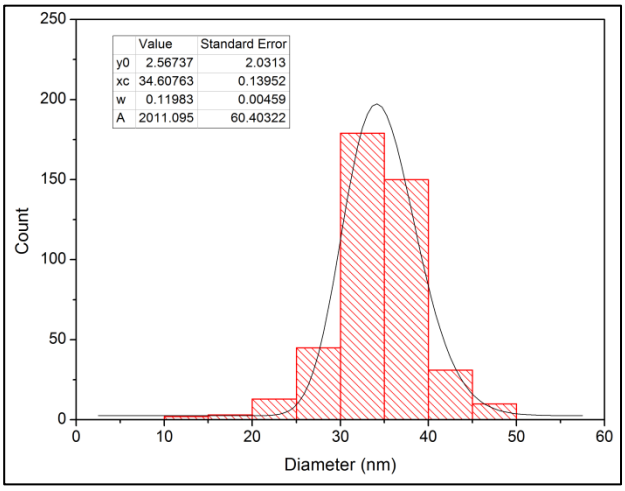

Figure **9-3**. Image analysis of > 400 AuNP, 5 nm bins fit to a LogNormal distribution

9.2.3 Standard curve for concentration of doxorubicin and area of absorption at 478 nm

Pure doxorubicin and pure doxorubicin analog **9.3** were analyzed by HPLC on a C-18 column using a gradient from 30:70 acetonitrile:water to 100% acetonitrile over 30 mins. The retention time of doxorubicin (Figure **9-4**) was 7.7 min and of doxorubicin analog **9.3** (Figure **9-5**) was 14.8 min. The Standard curve for concentration of doxorubicin and area of

absorption at 478 nm was made by different concentrations of doxorubicin, as shown in Table **9-1** and Figure **9-6**.

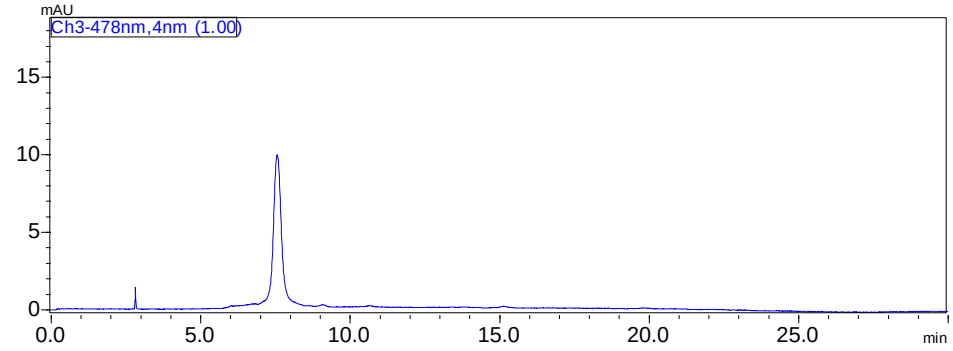

Figure 9-4. The HPLC of doxorubicin

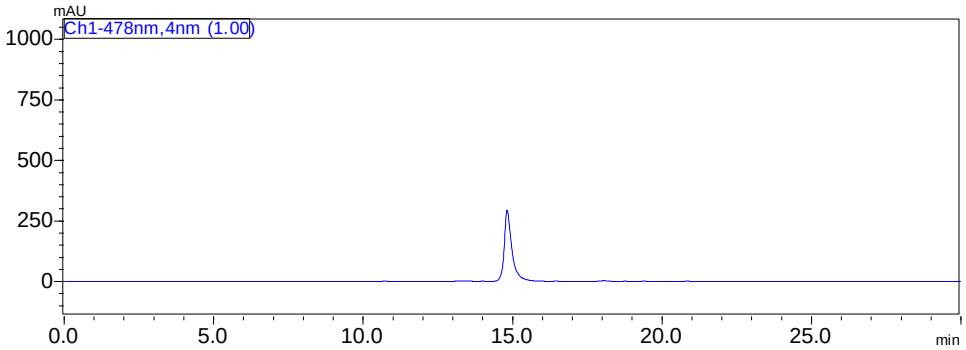

Figure 9-5. The HPLC of doxorubicin analog **9.3**

Table 9-1. Standard curve for concentration of doxorubicin and area of absorption at 478 nm	
Concentration of Doxorubicin (mg/100 μL)	AUC at 478 nm
0	0
0.00104	62553
0.00208	143701
0.00312	216531
0.00416	272159

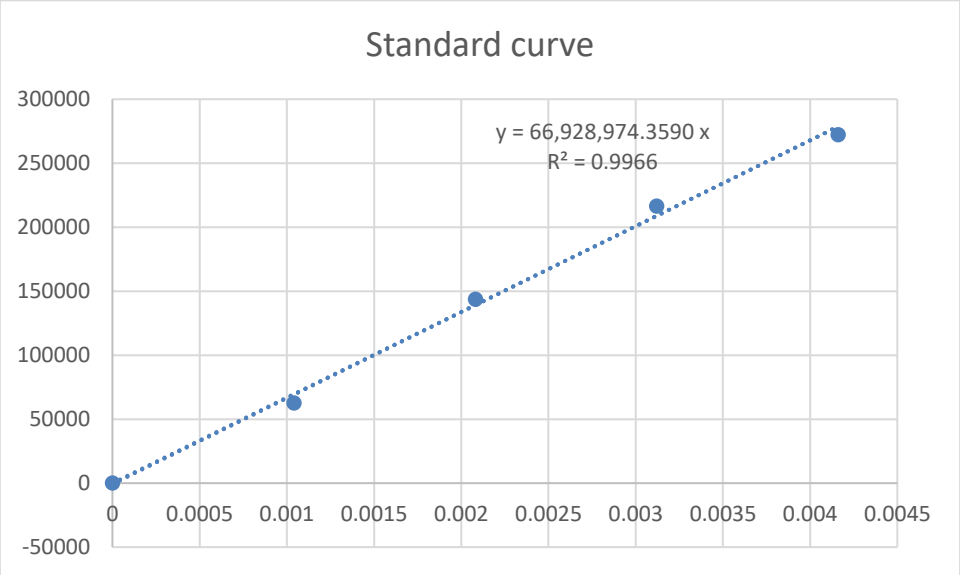

Figure 9-6. Standard curve for concentration of doxorubicin

9.2.4 Drug loading and release of nanoparticles as a function of the concentration of PEG.

Doxorubicin-functionalized nanoparticles were prepared by treating 50 mL of a solution of AuNP containing 2.5 mg AuNP with 6.67 mg of **9.3** in 100 mL CH_3OH and either 13.3 mg or 26.6 mg of PEG methyl ether thiol (mPEG thiol) in 1.0 mL water with stirring for 48 h, followed by repeated centrifugation and resuspension to remove excess reagents. The residue was dissolved in 1 mL water to give soluble doxorubicin-loaded nanoparticles **Au-9.3-1** and **Au-9.3-2** respectively, with gold contents of 1.05 and 1.70 mg as determined by ICP-MS; the low recovery of AuNP reflects handling losses during the repeated centrifugation and resuspension purification procedure. **Au-9.3-1** and **Au-9.3-2** were then incubated with glutathione as described above for 72 h to ensure complete drug release, and the resulting solutions were analyzed by HPLC, showed in Figure **9-7** and Figure **9-8**. Both **Au-9.3-1** and **Au-9.3-2** gave a major peak which matched that of doxorubicin. The areas of the peaks (128639 for **Au-9.3-1** and 139427 for **Au-9.3-2**) combined with ICP-MS data indicated that **Au-9.3-1** had a loading of 0.018 mg per mg AuNP, while **Au-9.3-2** had a loading of 0.012

mg per mg AuNP. This result indicates that the concentration of mPEG thiol affects drug loading, with the higher concentration of mPEG thiol reducing drug loading.

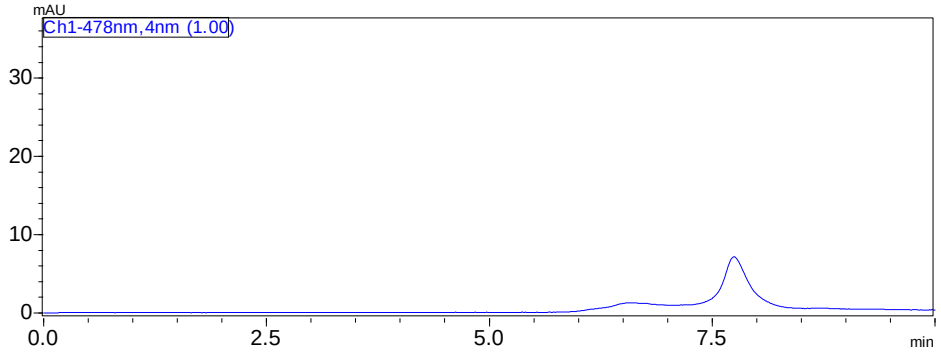

Figure 9-7. The HPLC of release of doxorubicin from **Au-9.3-1**

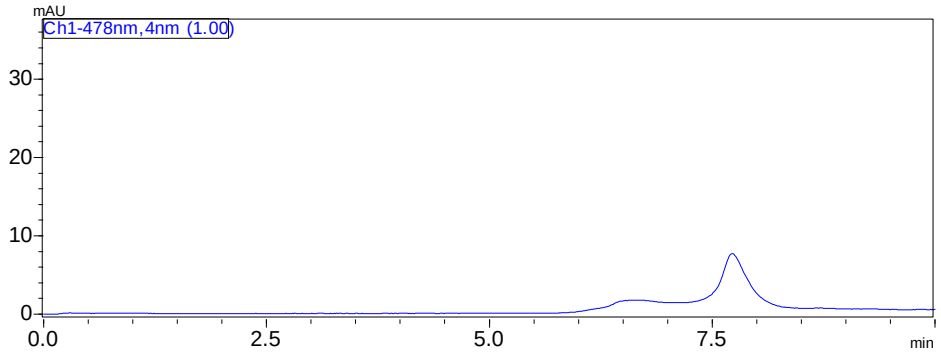

Figure 9-8. The HPLC of release of doxorubicin from **Au-9.3-2**

9.2.5 Drug loading and release of nanoparticles as a function of doxorubicin concentration.

Doxorubicin-functionalized nanoparticles were prepared by treating a solution of AuNP prepared as described above with a fixed concentration of mPEG thiol of 88.67 μg/mL (17.7 μM) and concentrations of **9.3** of 6.67, 13.34 and 20 μg/mL (8.87, 17.7, and 26.6 μM) in CH_3OH, followed by centrifugation and resuspension to remove excess reagents. This gave soluble doxorubicin-loaded nanoparticles **Au-9.3-1**, **Au-9.3-3** and **Au-9.3-4** with gold contents of 1.05, 0.39 and 1.79 mg as determined by ICP-MS. Samples of each of the three doxorubicin-loaded nanoparticles were incubated in the presence of 5 mM glutathione and analyzed as described above, and the resulting chromatograms of each exhibited a major peak which matched that of doxorubicin, showed in Figure **9-7**, Figure **9-9** and Figure **9-10**. The

area of the peak (128639 for **Au-9.3-1**, 88179 for **Au-9.3-3** and 601830 for **Au-9.3-4**) and the ICP-MS data indicated that **Au-9.3-1** had a loading of 0.018 mg per mg AuNP, while **Au-9.3-3** had a loading of 0.034 mg per mg AuNP and **Au-9.3-4** had a loading of 0.050 mg per mg AuNP. These data indicated unsurprisingly that the doxorubicin loading increased as the initial concentration of doxorubicin analog **9.3** increased.

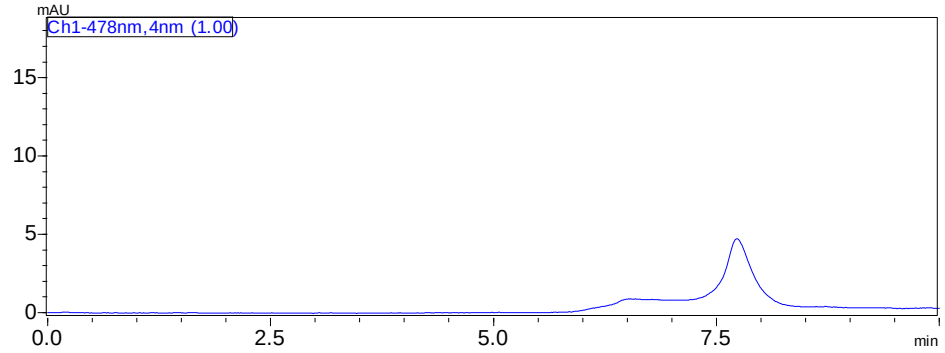

Figure 9-9. The HPLC of release of doxorubicin from **Au-9.3-3**

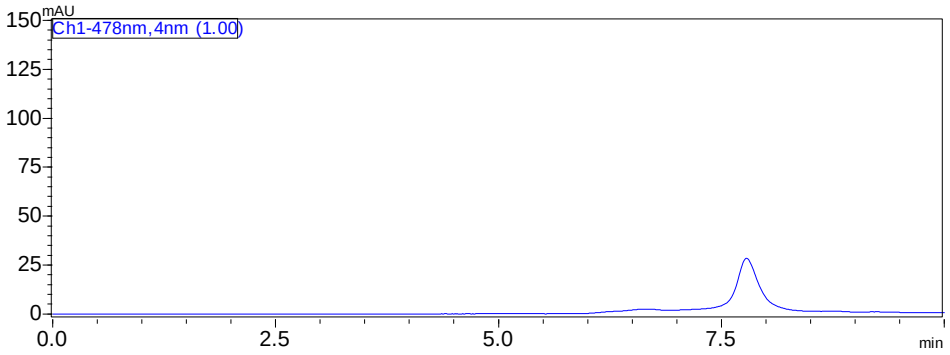

Figure 9-10. The HPLC of release of doxorubicin from **Au-9.3-4**

9.3 Experimental Section

9.3.1 General experimental procedures

The following standard conditions apply unless other stated. All chemicals were purchased from Sigma-Aldrich and used as received unless otherwise stated. Doxorubicin hydrochloride was purchased from Wonda Science Inc, USA, amino-dPEG™4 acid was obtained from QuanatBioDesign, Ltd., Powell, OH, and methoxypolyethylene glycol thiol (5

kDa) was obtained from Creative PEGworks. All glassware was oven-dried and all reactions were conducted under nitrogen. Dichloromethane (CH_2Cl_2) was distilled from $CaCl_2$, tetrahydrofuran (THF) was distilled from CaH_2, anhydrous methanol (MeOH) was purchased directly from Sigma-Aldrich. Thin layer chromatography (TLC) was used to monitor the reaction progress on silica gel UV_{254}. Purification was achieved either by column chromatography over silica gel 60 (220–240 mesh), or preparative thin layer chromatography (PTLC) on glass-backed plates coated with silica UV_{254}. HPLC was performed on Shimadzu SCL-10AVP system using a column purchased from Phenomenex (Luna 5μ C18 (2) 25 x 4.6 mm). ^{1}H and ^{13}C NMR spectra were obtained on an Agilent U4-DD2 spectrometer at 400 MHz for ^{1}H and 100 MHz for ^{13}C or a Bruker Avance II spectrometer at 500 MHz for ^{1}H and 125 MHz for ^{13}C. All chemical shifts were referenced to the solvent peaks of $CDCl_3$ (7.26 ppm for ^{1}H and 77.16 ppm for ^{13}C) unless otherwise stated. An Agilent 6220 accurate-mass TOF LC/MS instrument was used to obtain high-resolution mass spectra of pure compounds, an ICP-MS (Thermo Electron X-Series) following APHA Standard Method 3125-B (American Public Health Association et al., 1998) was used for analysis of concentrations of gold content in the Civil and Environmental Engineering Department at Virginia Tech..

8.3.2 Compounds information.

4-(Acetylthio)benzoic acid (9.5). A 25 mL round bottom flask was oven-dried, cooled to room temperature and charged with a magnetic stirring bar, 4-mercaptobenzoic acid **9.4** (154 mg, 1.0 mmol), and a rubber septum. Dry CH_2Cl_2 (5 mL) was added via syringe to dissolve the solid and followed by adding C_5H_5N (0.323 mL, 4.0 mmol). An ice bath was used to cool the solution to 0 ºC, followed by vigorous stirring for 5 min. After the solid was

dissolved completely, Ac_2O (0.1 mL, 1.06 mmol) was added over a period of 10 min via syringe. The resulting mixture was warmed to room temperature and stirred for 6 h under nitrogen (balloon). The reaction was diluted with EtOAc (100 mL), washed with 0.6 M HCl solution (2 x 10 mL), brine (2 x 20 mL), and dried with anhydrous Na_2SO_4. After evaporating the solvent by rotary evaporation (25 ºC), a white crude product was obtained and purified by PTLC (eluted with $CHCl_3$:MeOH, 13:1) to yield **9.5** (192 mg, 0.98 mmol) as a white powder in a yield of 98%. ^{1}H NMR (CD_3OD, 500 MHz, δ): δ 8.05 (dd, *J* = 8.5, 2 Hz, 2H), 7.54 (dd, *J* = 8.5, 2 Hz, 2H), 2.44 (s, 3H); ^{13}C NMR (125 MHz, δ): δ 194.2, 169.0, 135.2, 135.0, 132.7, 131.2, 30.3; HRESIMS: (*m/z*) $[M - H]^-$ calcd for $C_9H_7O_3S$, 195.0121; found 195.0124.

S-(4-(hydroxymethyl)phenyl) ethanethioate (9.6). A 10 mL round bottom flask was oven-dried, cooled to room temperature and charged with a magnetic stirring bar, compound **9.5** (192 mg, 0.98 mmol), and a rubber septum. The flask was evacuated for 5 min and flushed with nitrogen. Dry THF (3 mL) was added to dissolve the solid. An ice-salt bath was used to cool the solution to –10 ºC, followed by vigorous stirring for 5 min. A solution of $(CH_3)_2S{\bullet}BH_3$ in THF (1.0 mL, 2.0 mmol) was added over a period of 10 min via syringe. The resulting mixture was warmed to room temperature and stirred for 4 h under nitrogen (balloon). H_2O (2 mL) was added to remove unreacted $(CH_3)_2S{\bullet}BH_3$, the solution was diluted with EtOAc (100 mL), washed with brine (2 x 20 mL), and dried with anhydrous Na_2SO_4. After evaporating the solvent by rotary evaporation (30 ºC), a liquid crude product was obtained, which was purified by PTLC (eluted with $CHCl_3$:MeOH, 15:1) to yield **9.6** (151 mg, 0.83 mmol) as a colorless liquid in a yield of 85%. ^{1}H NMR (CD_3OD, 500 MHz, δ): δ 7.36 (m, 4H), 4.60 (s, 2H), 2.34 (s, 3H); ^{13}C NMR (126 MHz, δ): 195.8, 144.5, 135.6, 128.5, 127.9

64.5, 30.0; HRESIMS: (*m/z*) $[M + H]^+$ calcd for $C_9H_{11}O_2S^+$, 183.0474; found 183.0466.

S-4-((((4-nitrophenoxy)carbonyl)oxy)methyl)-phenyl ethanethioate (9.7). A 50 mL round bottom flask was oven-dried, cooled to room temperature and charged with a magnetic stirring bar, compound **9.6** (151 mg, 0.83 mmol), and a rubber septum. Dry CH_2Cl_2 (10 mL) was added via syringe to dissolve the liquid followed by adding C_5H_5N (0.202 mL, 2.5 mmol). An ice bath was used to cool the solution to 0 ºC, followed by vigorous stirring for 5 min. A solution of 4-nitrophenyl chloroformate (168 mg, 0.83 mmol) in 5 mL CH_2Cl_2 was added over a period of 10 min via syringe. The resulting mixture was warmed to room temperature and stirred for 4 h under nitrogen (balloon). The reaction was diluted with EtOAc (100 mL), washed with saturated $NaHCO_3$ solution (2 x 10 mL), H_2O (2 x 10 mL) and brine (2 x 10 mL), and dried with anhydrous Na_2SO_4. The solid crude obtained after evaporation was purified by column chromatography (silica gel, 100 g, eluted with hexane:CH_2Cl_2, 5:1) to yield **9.7** (253 mg, 0.73 mmol) as a white powder in a yield of 88%. ^{1}H NMR ($CDCl_3$, 500 MHz, δ): 8.27 (dd, *J* = 9, 2 Hz, 2H), 7.47 (m, 4H), 7.38 (dd, *J* = 9, 2 Hz, 2H), 5.31 (s, 2H), 2.44 (s, 3H); ^{13}C NMR (126 MHz, δ): 193.7, 155.5, 152.5, 145.5, 135.6, 134.8, 129.3, 129.0, 125.4, 121.9, 70.2, 30.4; HRESIMS (*m/z*) $[M + NH_4]^+$ calcd for $C_{16}H_{17}N_2O_6S^+$, 365.0807; found 365.0795.

Doxorubicin Analog 9.3: *S*-(4-(((((2*S*,3*S*,4*S*,6*R*)-3-hydroxy-2-methyl-6-(((1*S*,3*S*)-3,5,12-trihydroxy-3-(2-hydroxyacetyl)-10-methoxy-6,11-dioxo-1,2,3,4,6,11-hexahydrotetracen-1-yl)oxy)tetrahydro-2H-pyran-4yl)carbamoyl)oxy) methyl)phenyl) ethanethioate. A 10 mL round bottom flask was oven-dried, cooled to room temperature and charged with a magnetic stirring bar, doxorubicin hydrochloride (20 mg, 0.0345 mmol), compound **9.7** (20

mg, 0.0576 mmol), and a rubber septum. Anhydrous DMF (5 mL) was added by syringe to dissolve the solids. An ice bath was used to cool the solution to 0 ºC, followed by vigorous stirring for 5 min. Then Et_3N (0.013 mL, 0.0988 mmol) was added to the solution over a period of 5 min via syringe. The resulting mixture was warmed to room temperature and stirred for 2 h under nitrogen (balloon). The reaction was diluted with EtOAc (30 mL), washed with 0.6 M HCl solution (2 x 5 mL), saturated sodium $NaHCO_3$ (2 x 5 mL), brine (2 x 10 mL), and dried with anhydrous Na_2SO_4. The crude product was purified by PTLC (eluted with $CHCl_3$:MeOH, 13:1) to yield **9.3** (22.3 mg, 0.0297 mmol) as a red solid in a yield of 86%. ^{1}H NMR ($CDCl_3$, 500 MHz, δ): 13.95 (s, 1H, -OH), 13.21 (s, 1H, -OH), 8.02 (dd, *J* = 8.0, 1.1 Hz, 1H), 7.78 (t, *J* = 8.0 Hz, 1H), 7.39 (dd, *J* = 8.0, 1.1 Hz, 1H), 7.34 (m, 4H), 5.50 (d, *J* = 4.0 Hz, 1H), 5.27 (d, *J* = 3.5 Hz, 1H), 5.19 (d, *J* = 8.6 Hz, 1H, -OH), 5.04 (s, 2H), 4.75 (dd, *J* = 5.0, 2.0 Hz, 2H), 4.53 (s, 1H, -OH), 4.13 (q, *J* = 6.5 Hz, 1H), 4.07 (s, 3H), 3.86 (m, 1H), 3.66 (d, *J* = 5.6 Hz, 1H), 3.25 (dd, *J* = 18.8, 2.0 Hz, 1H), 3.02 (t, *J* = 5.0 Hz, 1H, -OH), 3.00 (d, *J* = 18.8 Hz, 1H), 2.39 (s, 3H), 2.32 (dt, *J* = 14.7, 2.0 Hz, 1H), 2.16 (dd, *J* = 14.7, 3.5 Hz, 1H), 2.05 (d, *J* = 7.5 Hz, 1H, -OH), 1.87 (dd, *J* = 13.2, 5.1 Hz, 1H), 1.77 (td, *J* = 13.2, 4.0 Hz, 1H), 1.25 (d, *J* = 6.5 Hz, 3H); ^{13}C NMR (126 MHz, δ): 214.0, 194.0, 187.2, 186.8, 161.2, 156.3, 155.8, 155.5, 138.0, 135.9, 135.6, 134.7, 133.7, 133.7, 128.8, 127.8, 121.0, 120.0, 118.6, 111.7, 111.6, 100.8, 76.7, 69.8, 69.7, 67.4, 66.2, 65.7, 56.8, 47.2, 35.8, 34.1, 30.3, 30.3 17.0; HRESIMS: (*m/z*) $[M + Na]^+$ calcd for $C_{37}H_{37}NO_{14}SNa^+$, 774.1832: found 774.1840.

9.3.3 Preparation of monodisperse spherical AuNPs.

A 25 mL round bottom flask was charged with 1.5 mL sodium citrate aqueous solution

(1 wt %) and a magnetic stirring bar. Aqueous $HAuCl_4$ (5.0 mL containing 12.5 mg Au as) was added, and H_2O (6.0 mL) was added to bring the volume of the solution to 12.5 mL. This mixture was incubated for 5 min before rapid addition to 237.5 mL of boiling H_2O in a 500 mL two-necked round bottom flask with vigorous stirring. The color of the reaction solution changed quickly from colorless, grayish blue to purple and then to ruby red within 1 min. The reaction solution was refluxed for 30 min under stirring to promote formation of uniform quasi-spherical AuNPs.

Excess sodium citrate and other small molecules were removed by dialysis using dialysis tubing with a MW cutoff of 3,500 Da and immersing it in 4 L water with vigorous stirring. The water was changed every 2 hours over an 8 hour period and the resulting solution (250 mL) was used for the following steps.

9.3.4 Transmission Electron Microscopy.

Aliquots of 0.01 mL of the AuNP suspensions were deposited on carbon-coated 200-mesh copper grids. The aqueous droplet was left to dry in ambient conditions, typically for ~1 hour. Grids were imaged using a Philips EM420 electron microscope with an accelerating voltage of 120 kV to enhance the contrast of the electron-dense gold. Enough frames were collected to capture at least 400 particles per replicate. Nanoparticle diameter (d) was estimated using the formula $d = A/\pi$, where A is the cross-sectional area of a particle measured using ImageJ software.

9.3.5 **Synthesis of Doxorubicin Loaded AuNPs**.

A 50 mL aqueous solution of AuNPs containing 2.5 mg AuNP as described above, a 100 mL solution of 1 mg doxorubicin analog **9.3** in CH_3OH, and a 1 mL aqueous solution of

either 13.3 mg or 26.6 mg mPEG thiol (5 kDa) were mixed and stirred for 48 h at room temperature. Unbound drugs and mPEG thiol were removed by centrifugation on an Eppendorf Centrifuge 5810 R with a rotor diameter of 10 cm at 14,000 rpm (10,956 x g) for 20 min at room temperature, pipetting of the supernatant and re-dispersal of the nanoparticle pellet in water. This process was repeated three times to remove the unbound material completely. The residue was dissolved in 1.0 mL water to make **Au-9.3-1** and **Au-9.3-2** respectively. Repetition of this process with 2 mg of **9.3** and 13.3 mg mPEG thiol gave **Au-9.3-3**, and with 3 mg of **9.3** and 13.3 mg mPEG thiol gave **Au-9.3-4**. Four batches of each sample were prepared.

9.3.6 ICP-MS of Doxorubicin Loaded AuNPs.

A 10 μL aliquot of a 1.0 mL solution of **Au-9.3-1** and 25 μL aliquots of solutions of **Au-9.3-2**, **Au-9.3-3** and **Au-9.3-4** in 10 mL water were used to determine the concentration of Au by ICP-MS. The results were 1054, 4256, 982, and 4473 ppb respectively, corresponding to 0.53, 0.85, 0.196 and 0.895 mg Au in 500 μL.

9.3.7 Drug Release Studies of Analogs **9.3-1** – **9.3-4** from AuNP.

A 500 μL portion of each of the four AuNP solutions prepared above was mixed with 500 μL sodium acetate buffer containing 10 mM GSH, and the pH was adjusted to 4.6. The solution was stirred vigorously at 37 ºC for 72 h. The solution was then centrifuged at a speed of 14,000 rpm for 20 min. The four different supernatants were evaporated and dissolved in 450 μL MeCN and 50 μL 0.6 M HCl, and aliquots (100 μL) of the solution were injected onto an HPLC column and analyzed by quantitative HPLC. **Au-9.3-1**, **Au-9.3-2**, **Au-9.3-3** and **Au-9.3-4** each gave a single peak which matched that of doxorubicin. The areas of the

peaks were compared with those of the standard curve, and corresponding to masses of 0.00192, 0.00208, 0.00132 and 0.00899 mg per injection, corresponding to 0.0096, 0.0104, 0.0066 and 0.045 mg per sample. After adjustment for the differing masses of nanoparticles in each sample, these loadings correspond to drug loadings of 0.018, 0.012, 0.034, and 0.050 mg doxorubicin per 1 mg of AuNP for **Au-9.3-1** to **Au-9.3-4**, respectively.

9.4 References

1. Arcamone, F.; Cassindelli, G.; Fantini, G.; Orezzi, P.; Pol, C.; Spalla, C. Adriamycin, 14-hydroxydaunomycin, a new antitumor antibiotic from *S. peucetius* var. *caesius*. *Biotechnol. Bioeng.* **1969,** *11* (6), 1101−1110.

2. Arcamone, F.-M.; Gaetani, M.; Scotti, T.; Dimarco, A. Isolamento ed Attivita Antitumorale di un Antibiotico da *Streptomyces sp. Giorn. Microbiol.* **1961,** *9* (2), 83−90.

3. Arcamone, F.-M., Fifty Years of Chemical Research at Farmitalia. *Chem. Eur. J.* **2009,** *16* (11), 7774.

4. Arcamone, F.-M. Anthracyclines. In *Anticancer Agents from Natural Products*, 2nd ed.; Cragg, G. M.; Kingston, D. G. I.; Newman, D. J. Eds. CRC Press: Boca Raton, FL, 2012; pp 383−406.

5. Lown, J. W. Discovery and Development of Anthracycline Antitumour Antibiotics. *Chem. Soc. Rev.* **1993,** *22* (3), 165−176.

6. Minotti, G.; Menna, P.; Salvatorelli, E.; Cairo, G.; Gianni, L. Anthracyclines: Molecular Advances and Pharmacologic Developments in Antitumor Activity and Cardiotoxicity. *Pharmacol. Rev.* **2004,** *56* (2), 185−229.

7. Weiss, R. B. The Anthracyclines: will We ever Find a better Doxorubicin? *Sem. Oncol.*

1992, *19* (6), 670–686.

8. Hill, S. WHO Model Lists of Essential Medicines. http://www.who.int/medicines/publications/essentialmedicines/en/ (accessed January 20, 2017).

9. Carvalho, F. S.; Burgeiro, A.; Garcia, R.; Moreno, A. J.; Carvalho, R. A.; Oliveira, P. J. Doxorubicin-induced Cardiotoxicity: From Bioenergetic Failure and Cell Death to Cardiomyopathy. *Med. Res. Rev.* **2014,** *34* (1), 106–135.

10. Menna, P.; Salvatorelli, E.; Gianni, L.; Minotti, G. Anthracycline Cardiotoxicity. *Top. Curr. Chem.* **2008,** *283*, 21–44.

11. Barenholz, Y. Doxil® — The First FDA-approved Nano-drug: Lessons Learned. *J. Controlled Release* **2012,** *160*, 117–134.

12. Batist, G.; Barton, J.; Chaikin, P.; Swenson, C.; Welles, L. Myocet (Liposome-encapsulated Doxorubicin Citrate): a new Approach in Breast Cancer Therapy. *Expert Opin. Pharmacother.* **2002,** *3* (12), 1739–1751.

13. Chen, G.; Li, D.; Li, J.; Cao, X.; Wang, J.; Shi, X.; Guo, R. Targeted Doxorubicin Delivery to Hepatocarcinoma Cells by Lactobionic Acid-modified Laponite Nanodisks. *New J. Chem.* **2015,** *39*, 2847–2855.

14. Joniec, A.; Sek, S.; Krysinski, P. Magnetoliposomes as Potential Carriers of Doxorubicin to Tumours. *Chemistry* **2016,** *22* (49), 17715–17724.

15. Liu, W.; Wen, S.; Shen, M.; Shi, X. Doxorubicin-loaded Poly(lactic-co-glycolic acid) Hollow Microcapsules for Targeted Drug Delivery to Cancer Cells. *New J. Chem.* **2014,** *38*, 3917–3924.

16. Maeda, H. Macromolecular Therapeutics in Cancer Treatment: The EPR Effect and Beyond. *J. Controlled Release* **2012,** *164*, 138−144.

17. Wilhelm, S.; Tavares, A. J.; Dai, Q.; Ohta, S.; Audet, J.; Dvorak, H. F.; Chan, W. C. W. Analysis of Nanoparticle Delivery to Tumours. *Nat. Rev. Mater.* **2016,** *1*, 16014.

18. Torrice, M. Does Nanomedicine Have a Delivery Problem? *Chem. Eng. News* **2016,** *94 (25)*, 16−19.

19. Kumar, A.; Zhang, X.; Liang, X.-J. Gold Nanoparticles: Emerging Paradigm for Targeted Drug Delivery System. *Biotechnol. Adv.* **2013,** *31*, 593−606.

20. Mirza, A. Z.; Shamshad, H. Preparation and Characterization of Doxorubicin Functionalized Gold Nanoparticles. *Eur. J. Med. Chem* **2011,** *346*, 1857−1860.

21. Chaudhary, A.; Dwivedi, C.; Gupta, A.; Nandi, C. K. One Pot Synthesis of Doxorubicin Loaded Gold Nanoparticles for Sustained Drug Release. *RSC Adv.* **2015,** *5* (118), 97330−97334.

22. Khandekar, S. V.; Kulkarni, M. G.; Devarajan, P. V. Polyaspartic Acid Functionalized Gold Nanoparticles for Tumor Targeted Doxorubicin Delivery. *J. Biomed. Nanotechnol.* **2014,** *10* (1), 143−153.

23. Alexander, C. M.; Hamner, K. L.; Maye, M. M.; Dabrowiak, J. C. Multifunctional DNA-gold nanoparticles for targeted doxorubicin delivery. *Bioconjugate Chem.* **2014,** *25* (7), 1261−1271.

24. Zhang, Z.-M.; Gao, P.-C.; Wang, Z.-F.; Sun, B.-W.; Jiang, Y. DNA-caged Gold Nanoparticles for Controlled Release of Doxorubicin Triggered by a DNA Enzyme and pH. *Chem. Commun.* **2015,** *51*, 12996−12299.

25. Spadavecchia, J.; Movia, D.; Moore, C.; Maguire, C. M.; Moustaoui, H.; Casale, S.; Volkov, Y.; Prina-Mello, A. Targeted Polyethylene Glycol Gold Nanoparticles for the Treatment of PancreaticCancer: from Synthesis to Proof-of-concept in Vitro Studies. *Int. J. Nanomed.* **2016,** *11*, 791–822.

26. Swiech, O. A.; Opuchlik, L. J.; Wojciuk, G.; Stepkowski, T. M.; Kruszewski, M.; Bilewicz, R. Doxorubicin Carriers based on Au Nanoparticles - Effect of Shape and Gold-drug Linker on the Carrier Toxicity and Therapeutic Performance. *RSC Adv.* **2016,** *6* (38), 31960–31967.

27. Asadishad, B.; Vossoughi, M.; Alemzadeh, I. Folate-receptor-targeted Delivery of Doxorubicin Using Polyethylene Glycol-functionalized Gold Nanoparticles. *Ind. Eng. Chem. Res.* **2010,** *49* (4), 1958–1963.

28. Cheng, J.; Gu, Y.-J.; Cheng, S. H.; Wong, W.-T. Surface Functionalized Gold Nanoparticles for Drug Delivery. *J. Biomed. Nanotech.* **2013,** *9* (8), 1362–1369.

29. Gu, Y.-J.; Cheng, J.; Man, C. W.-Y.; Wong, W.-T.; Cheng, S. H. Gold-doxorubicin Nanoconjugates for Overcoming Multidrug Resistance. *Nanomedicine: Nanotechnology, Biology and Medicine* **2012,** *8* (2), 204–211.

30. Aryal, S.; Grailer, J. J.; Pilla, S.; Steeber, D. A.; Gong, S. DoxorubicinConjugated Gold Nanoparticles as Water-soluble and pH-responsive Anticancer Drug Nanocarriers. *J. Mater. Chem.* **2009,** *19* (42), 7879–7884.

31. Prabaharan, M.; Grailer, J. J.; Pilla, S.; Steeber, D. A.; Gong, S. Gold Nanoparticles with a Monolayer of Doxorubicin-conjugated Amphiphilic Block Copolymer for Tumor-targeted Drug Delivery. *Biomaterials* **2009,** *30* (30), 6065–6075.

32. Zhang, X.; Chibli, H.; Mielke, R.; Nadeau, J. Ultrasmall Gold-doxorubicin Conjugates Rapidly Kill Apoptosis-resistant Cancer Cells. *Bioconjugate Chem.* **2011,** *22*, 235–243.

33. Gautier, J.; Allard-Vannier, E.; Munnier, E.; Souce, M.; Chourpa, I. Recent Advances in Theranostic Nanocarriers of Doxorubicin Based on Iron Oxide and Gold Nanoparticles. *J. Controlled Release* **2013,** *169* (1-2), 48–61.

34. Bhamidipati, M.; Fabris, L. Multiparametric Assessment of Gold Nanoparticle Cytotoxicity in Cancerous and Healthy Cells: The Role of Size, Shape, and Surface Chemistry. *Bioconjug Chem* **2017,** *28* (2), 449–460.

35. Paciotti, G. F.; Zhao, J.; Cao, S.; Brodie, P. J.; Tamarkin, L.; Huhta, M.; Myer, L. D.; Friedman, J.; Kingston, D. G. I. Synthesis and Evaluation of Paclitaxel-loaded Gold Nanoparticles for Tumor-targeted Drug Delivery. *Bioconjugate Chem.* **2016,** *27* (11), 2646–2657.

36. Xia, H.; Bai, S.; Hartmann, J. R.; Wang, D. Synthesis of Monodisperse Quasi-spherical Gold Nanoparticles in Water via Silver (I)-assisted Citrate Reduction. *Langmuir* **2009,** *26* (5), 3585–3589.

Chapter 10: Conclusion

10.1 Summary of the structure elucidations

In five years of research on the isolation of antiplasmodial active natural products from plants, twenty-eight compounds were isolated, the structures of thirty compounds were elucidated, two structures were reassigned, and fourteen of the elucidated structures were novel. Among these fourteen new natural products, four of them (trichospirolides A–D **2.1**–**2.4**) were germacranolide-type sesquiterpenoids, four of them (petradoriolides A–D **3.1**–**3.4**) were labdanolide-type diterpenoids, one of them (petradoriolone I **3.5**) was a benzotropolone, one of them (anibomarin A **4.1**) was a coumarin, one of them (anibignan A **4.2**) was a norneolignan, one of them (malleastrumolide A **5.1**) was a long chain butanolide, one of them (compound **6.1**) was an alkaloid and the last one (cryptorigidifoliol K **7.2**) was a long chain bicyclic tetrahydro-α-pyrone derivative.

10.2 Summary of bioactivity of isolated natural products

Among the twenty-eight compounds isolated, there were three natural products with good antiplasmodial activities. These were trichospirolide A **2.1** with an IC_{50} value of 1.5 μM, malleastrumolide A **5.1** with an IC_{50} value of 2.7 μM, and (+)-lariciresinol **8.6** with an IC_{50} value of 3.7 μM. Trichospirolide A **2.1** also had a good antiproliferative activity with an IC_{50} value of 0.21 μM. Malleastrumolide A **5.1** had a weak antiproliferative activity with an IC_{50} value of 17.4 μM. (+)-Lariciresinol **8.6** had moderate antiproliferative activity with an IC_{50} value of 7.8 μM. The natural product with the best selectivity was malleastrumolide A **5.1**, followed by (+)-lariciresinol **8.6**. Trichospirolide A **2.1** showed the worst selectivity.

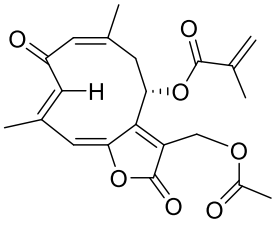

2.1

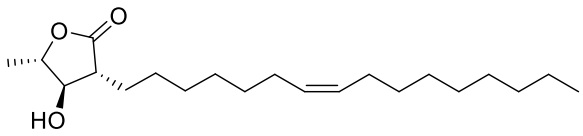

5.1

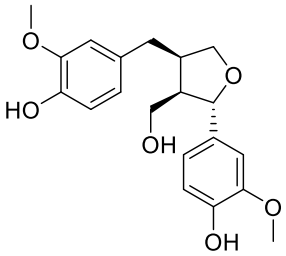

8.6

10.3 Discussion of lost bioactivity

In this dissertation, there were several highly active fractions and extracts, from which no highly active compounds with IC_{50} < 1 μM were isolated. There are three possible explanations for this loss of bioactivity. The first possible explantion is that the tannins in some extracts gave false positive results in the bioassay, since some of the early extracts mentioned in the dissertation was not detanninized before separation, and detanninized extracts turn out to be less active than crude extracts. A second possible explantion is synergism, in which a pure compound is less active than a mixture of compounds.. In the charpter 4 of this dissertation, compounds **4.1**–**4.8** were mixed and retested, but the reconstituted extract did not have improved activity, so synergism was eliminated as the cause of activity loss in that case.. The last reason is the decomposition or irreversible absorption of compounds on chromatographic columns.

Another factor in the evaluation of apparent activity loss is the conversion of the working units of μg/mL for fractions to units of μM fore the final iolated product. For natural products with molecular weights of less than 1000 Da, this conversion results in a numerical increase in the value. For example, trichospirolide A (**2.1**) was isolated from a fraction with an IC_{50} value of 2.5 ~ 5 μg/mL, and its bioactivity, with an IC_{50} value of ~ 600 ng/mL, looked very good. The molecular weight of trichospirolide A is 408 Da, so after unit conversion its

IC_{50} value was a less impressive 1.5 μM.

10.4 Future work

Future work in this area needs to focus on the isolation of natural prodacuts with very good antimalarial activity, with IC_{50} values of < 0.1 μM. This will most probably require improvements in the methods of bioguided isolation. Careful detanninization of crude plant extracts is the first step, because tannins do appear to contribute to the observed bioactivity of crude extracts. Alternatively bacterial, fungal or marine extracts can be selected, because while tannins are widely distributed in plants, they are uncommon in microorganisms or marine organisms. In previous isolations, fractions which were obtained with an IC_{50} value of < 10 μg/mL after liquid-liquid partition and those obtained after separation on an open column or by HPLC with an IC_{50} value of < 5 μg/mL were thought to be worth further study. In the future, the fractions after liquid-liquid partition need not be tested for their bioactivities. The hexanes and dichloromethane fractions can be separated by a Sephadex LH-20 open column, while the aqueous methanol fraction can be separated by a Diaion HP-20 open column directly. Then the subfractions will be tested in the bioassay and those with IC_{50} values of less than or equal to 1.25 μg/mL can be chosen for the next step. It is likely that compounds with vey good antimalarial activities will be isolated from these subfractions.

Appendix (1D and 2D NMR Spectra)

^{1}H NMR of Trichospirolide A (2.1) in $CDCl_3$

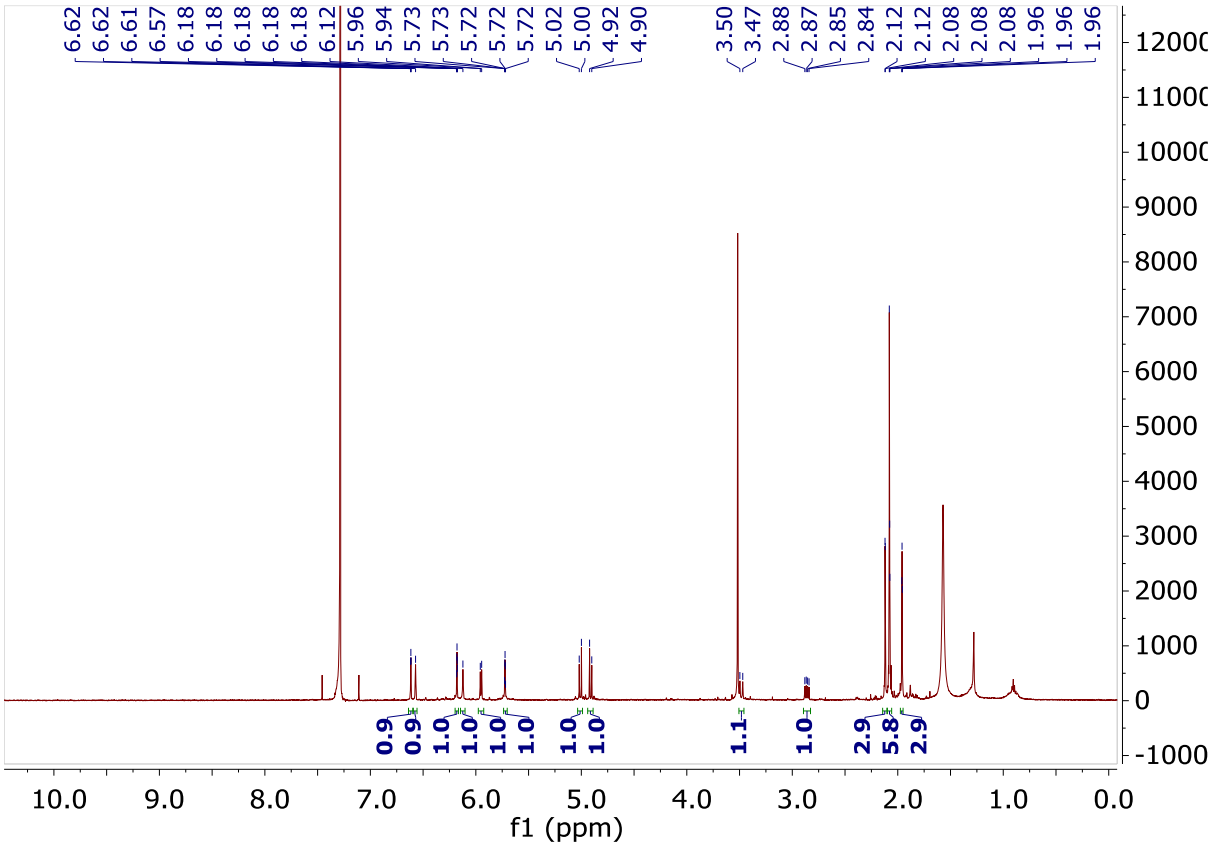

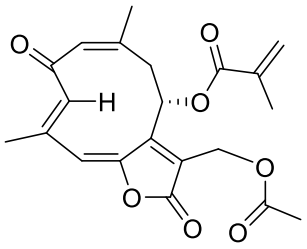

2.1

^{13}C NMR of Trichospirolide A (2.1) in $CDCl_3$

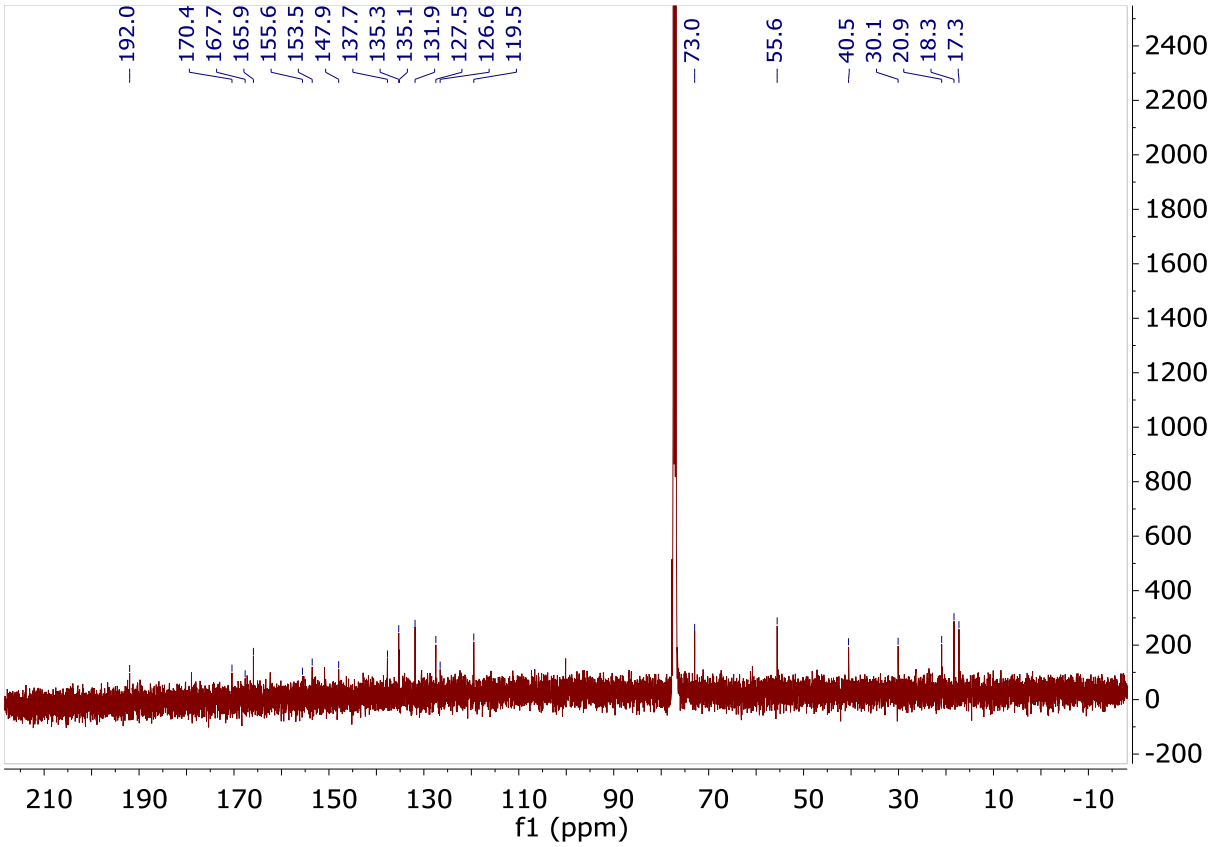

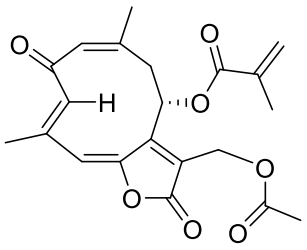

2.1

HSQC of Trichospirolide A (2.1) in $CDCl_3$

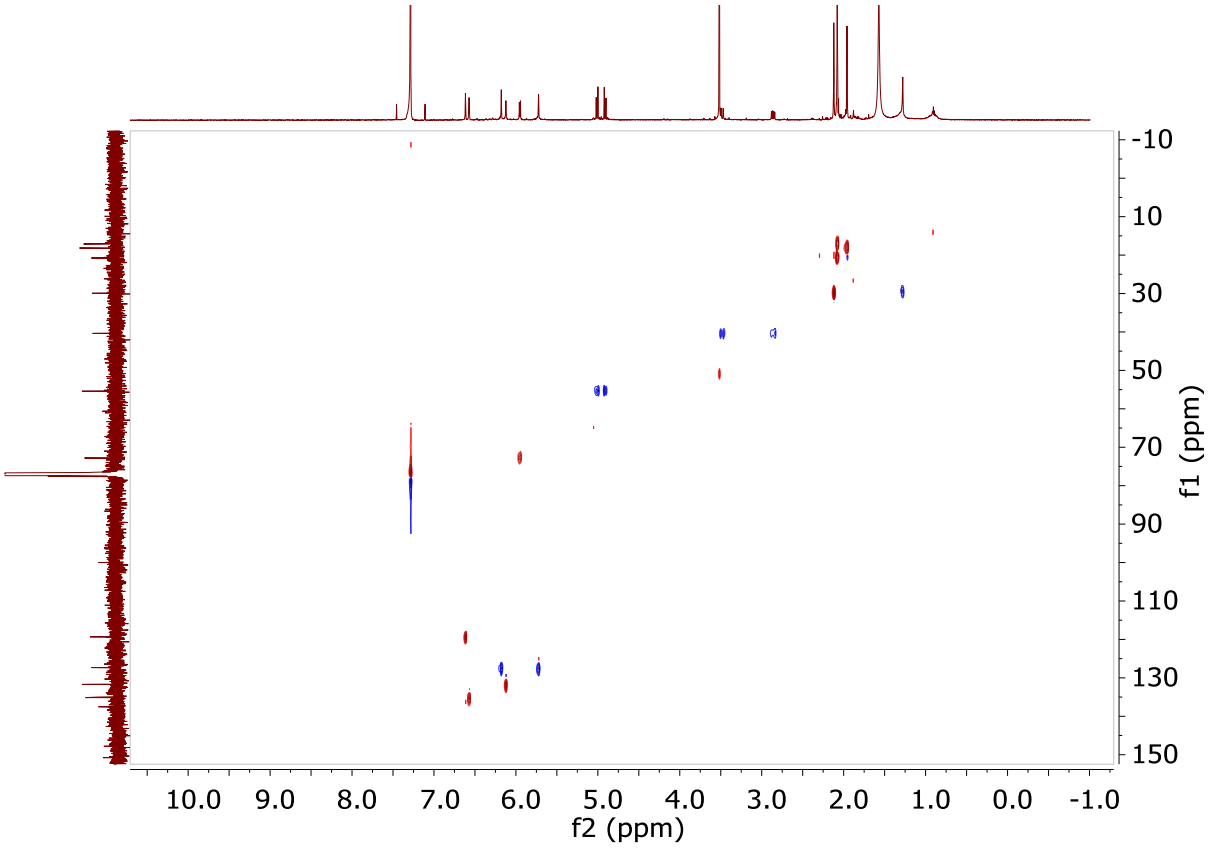

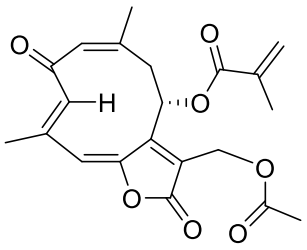

2.1

HMBC of Trichospirolide A (2.1) in $CDCl_3$

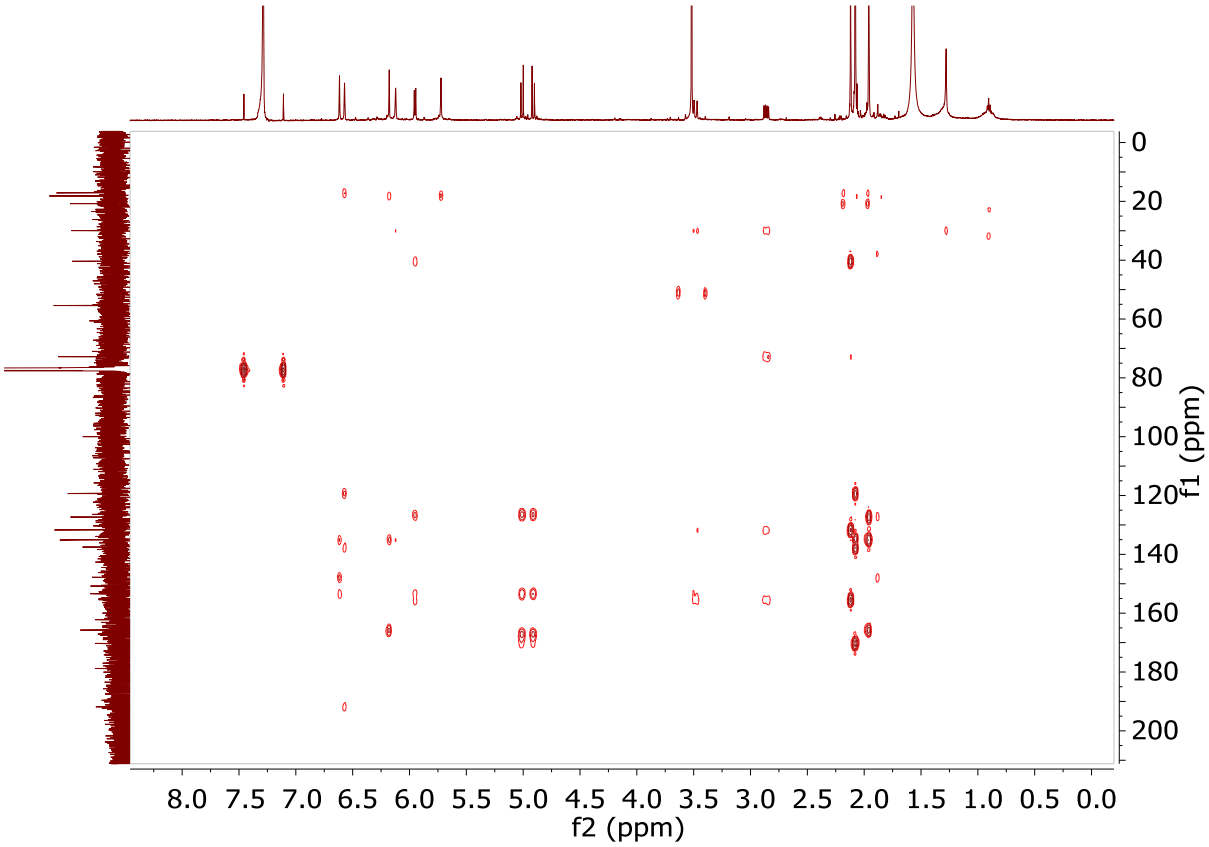

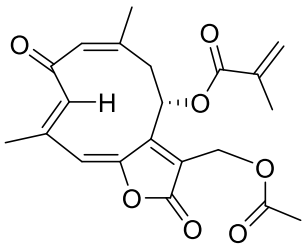

2.1

NOESY of Trichospirolide A (2.1) in $CDCl_3$

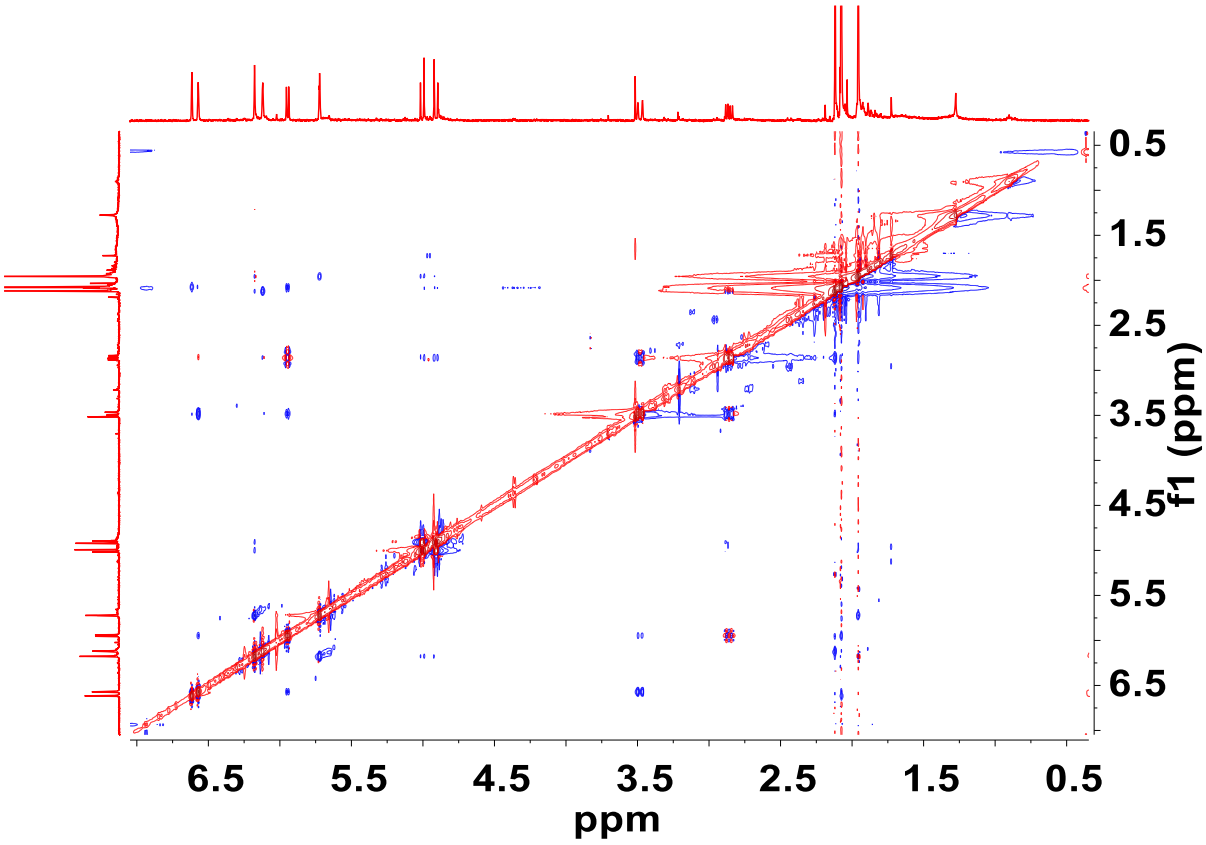

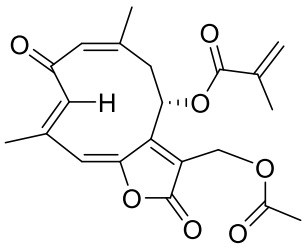

2.1

^{1}H NMR of Trichospirolide B (2.2) in $CDCl_3$

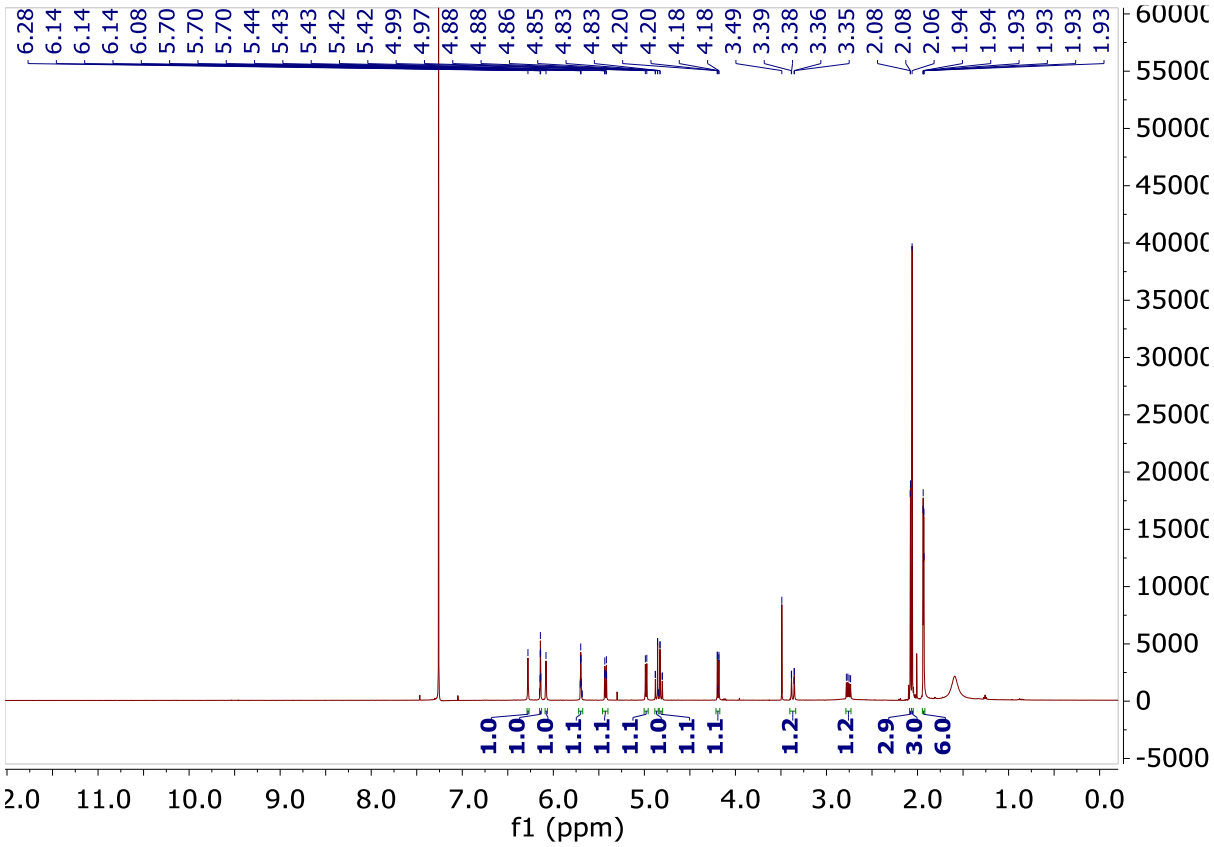

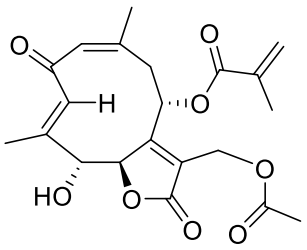

2.2

^{13}C NMR of Trichospirolide B (2.2) in $CDCl_3$

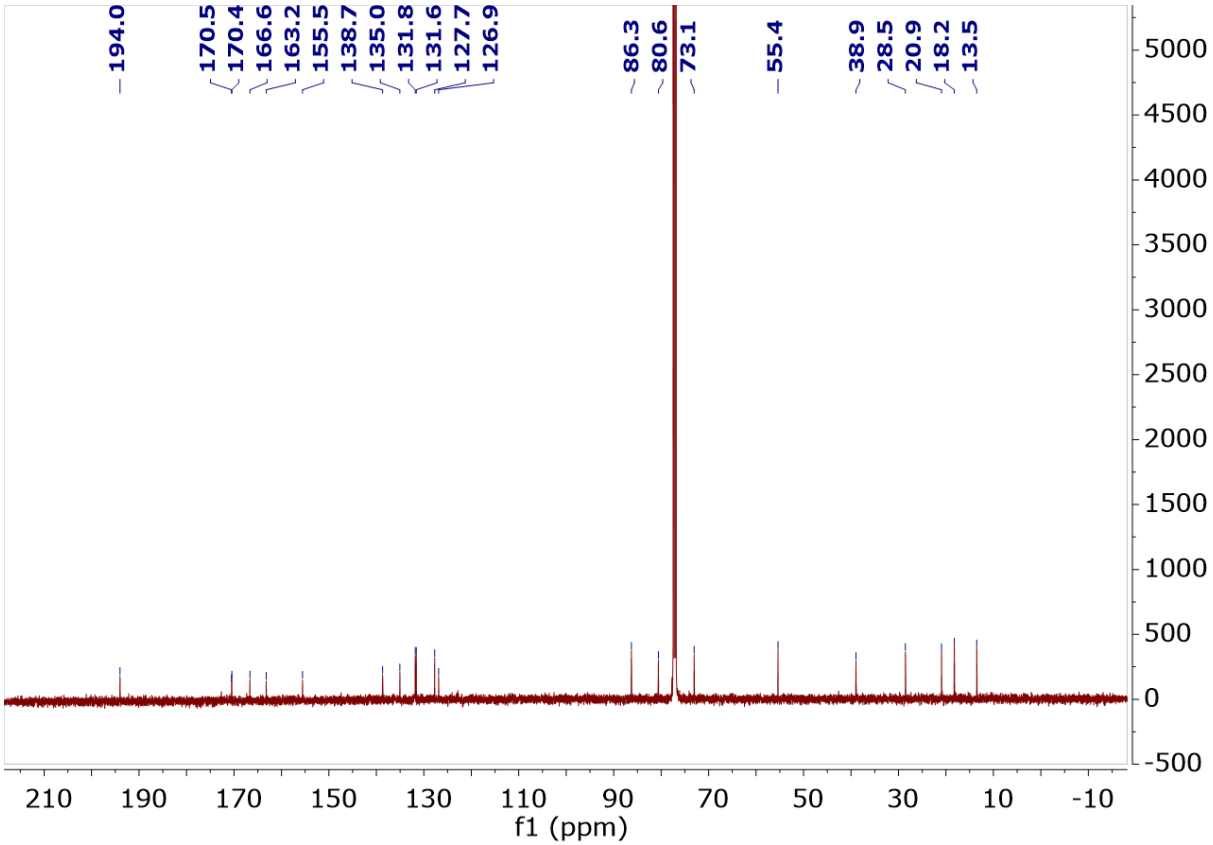

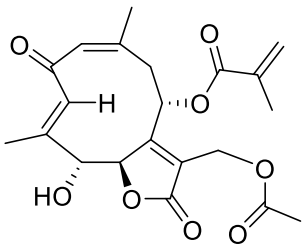

2.2

HSQC of Trichospirolide B (2.2) in $CDCl_3$

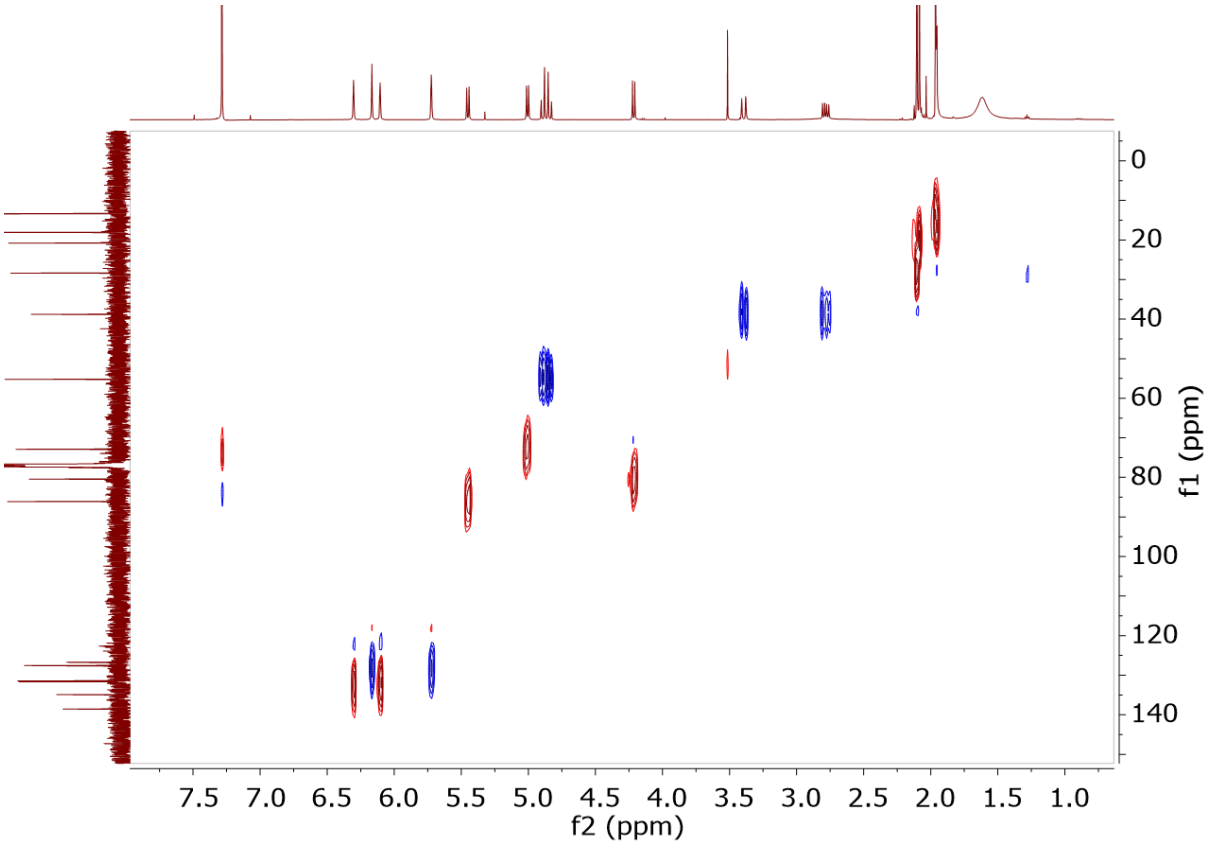

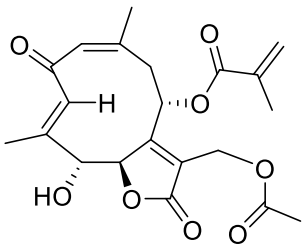

2.2

HMBC of Trichospirolide B (2.2) in $CDCl_3$

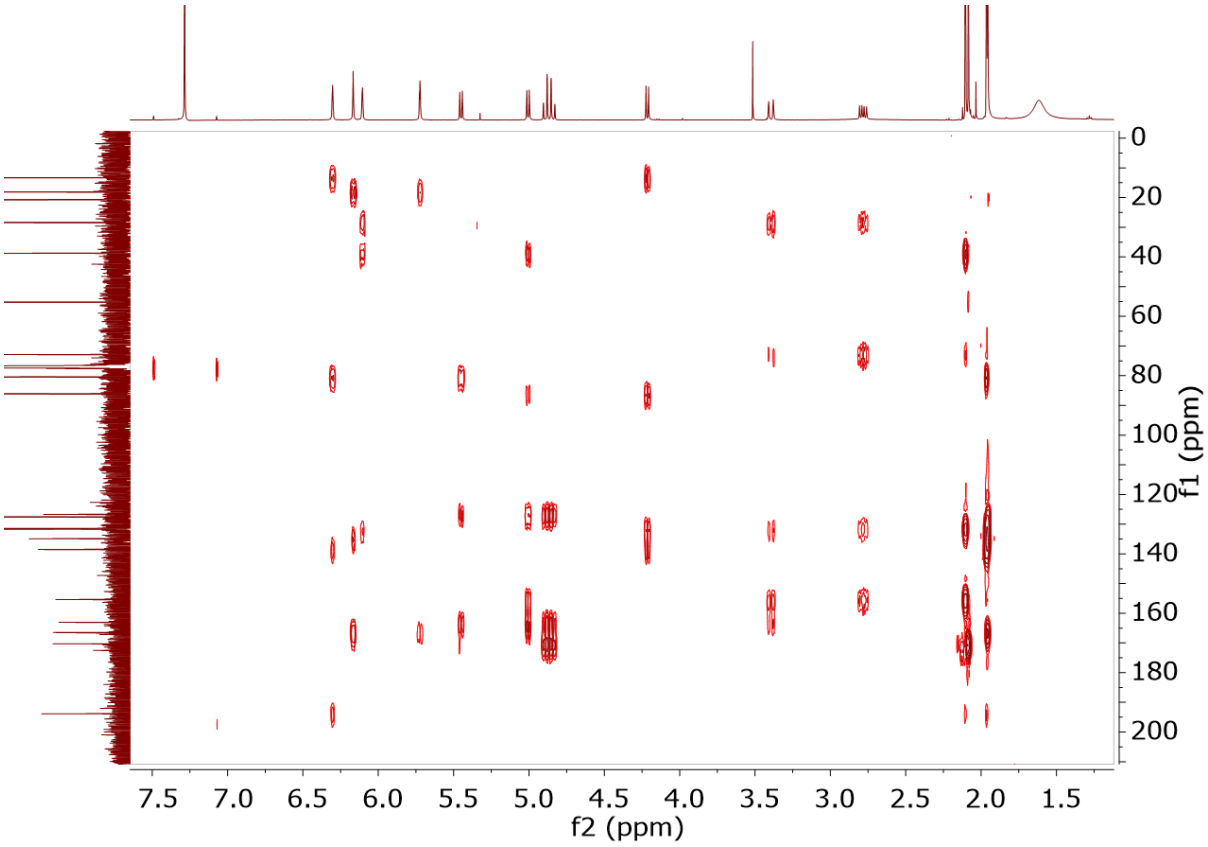

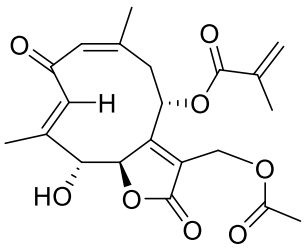

2.2

NOESY of Trichospirolide B (2.2) in $CDCl_3$

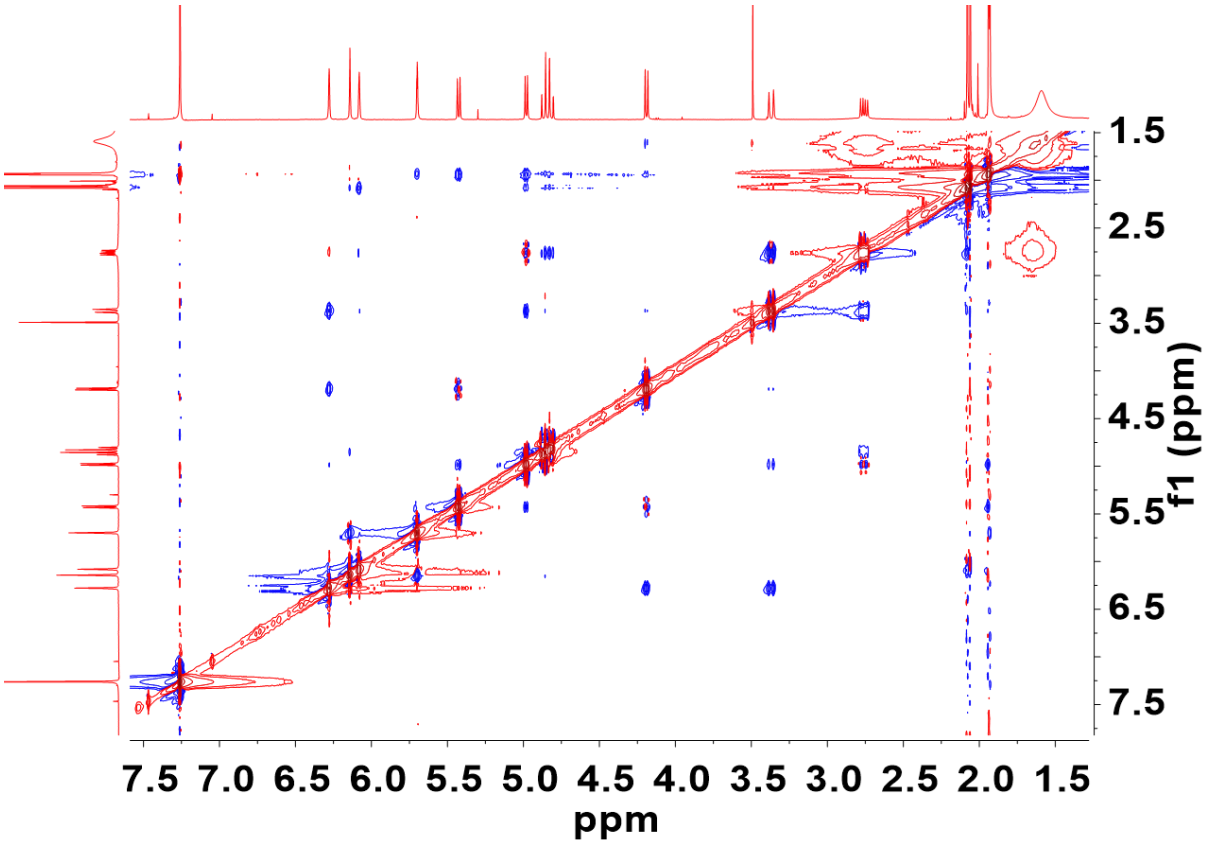

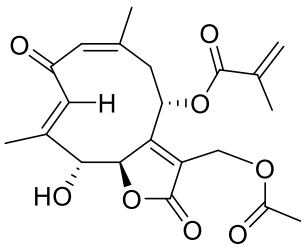

2.2

^{1}H NMR of Trichospirolide C (2.3) in $CDCl_3$

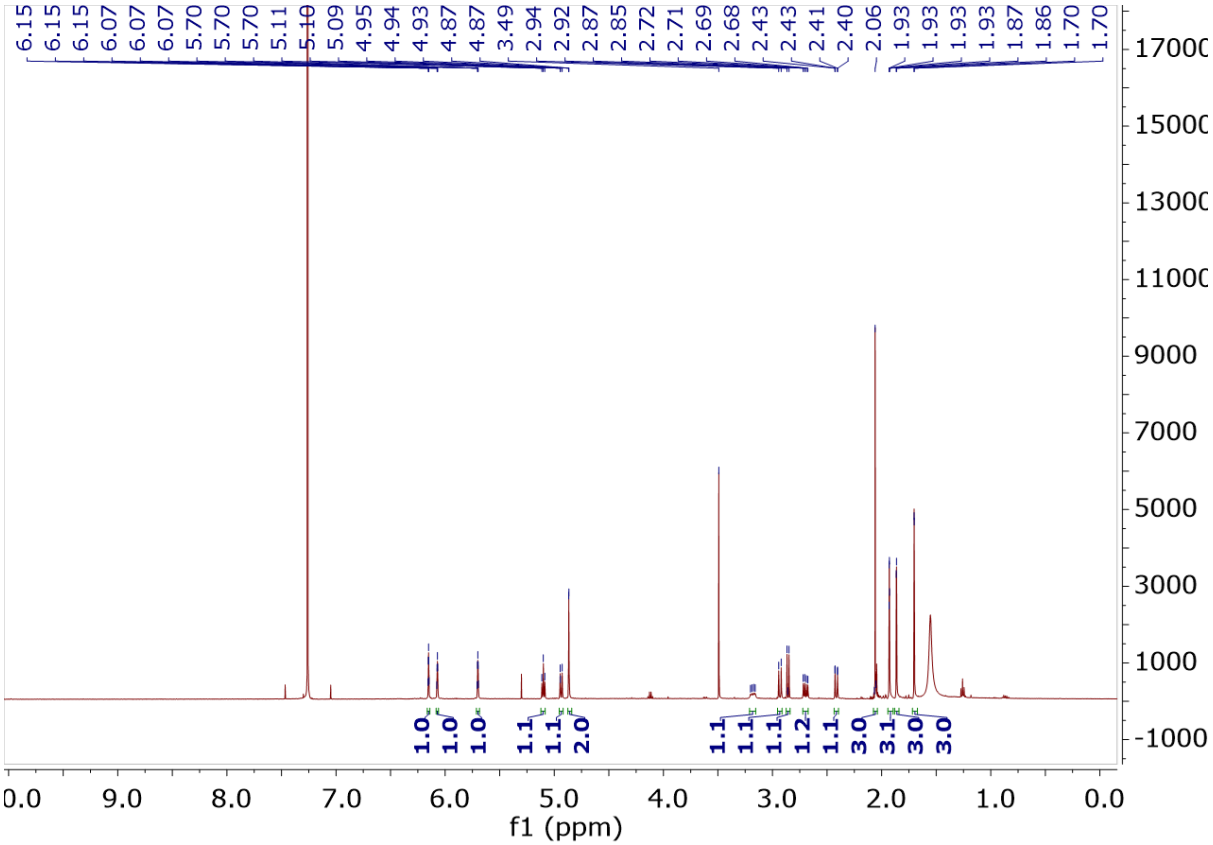

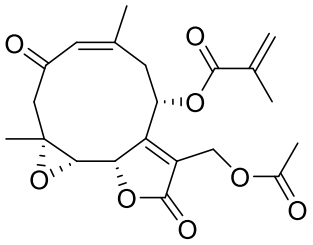

2.3

^{13}C NMR of Trichospirolide C (2.3) in $CDCl_3$

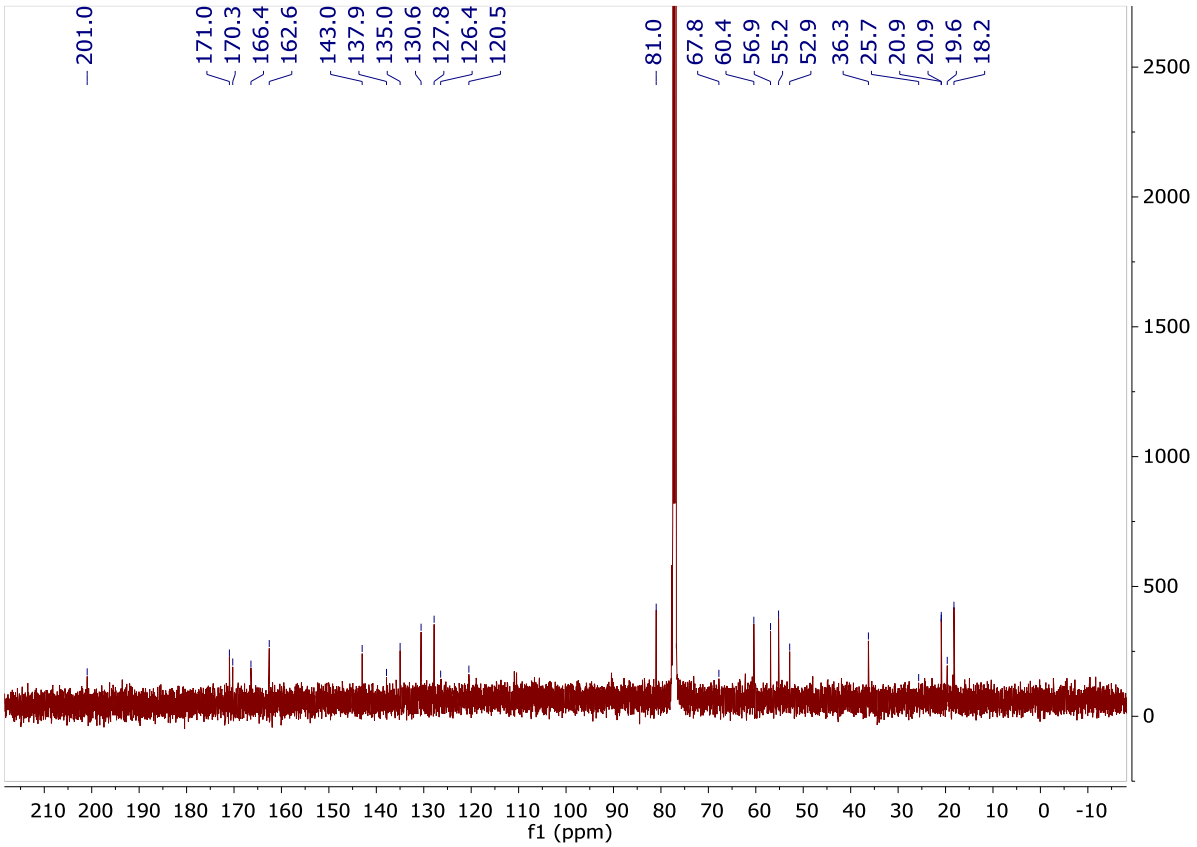

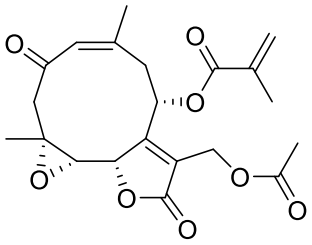

2.3

HSQC of Trichospirolide C (2.3) in $CDCl_3$

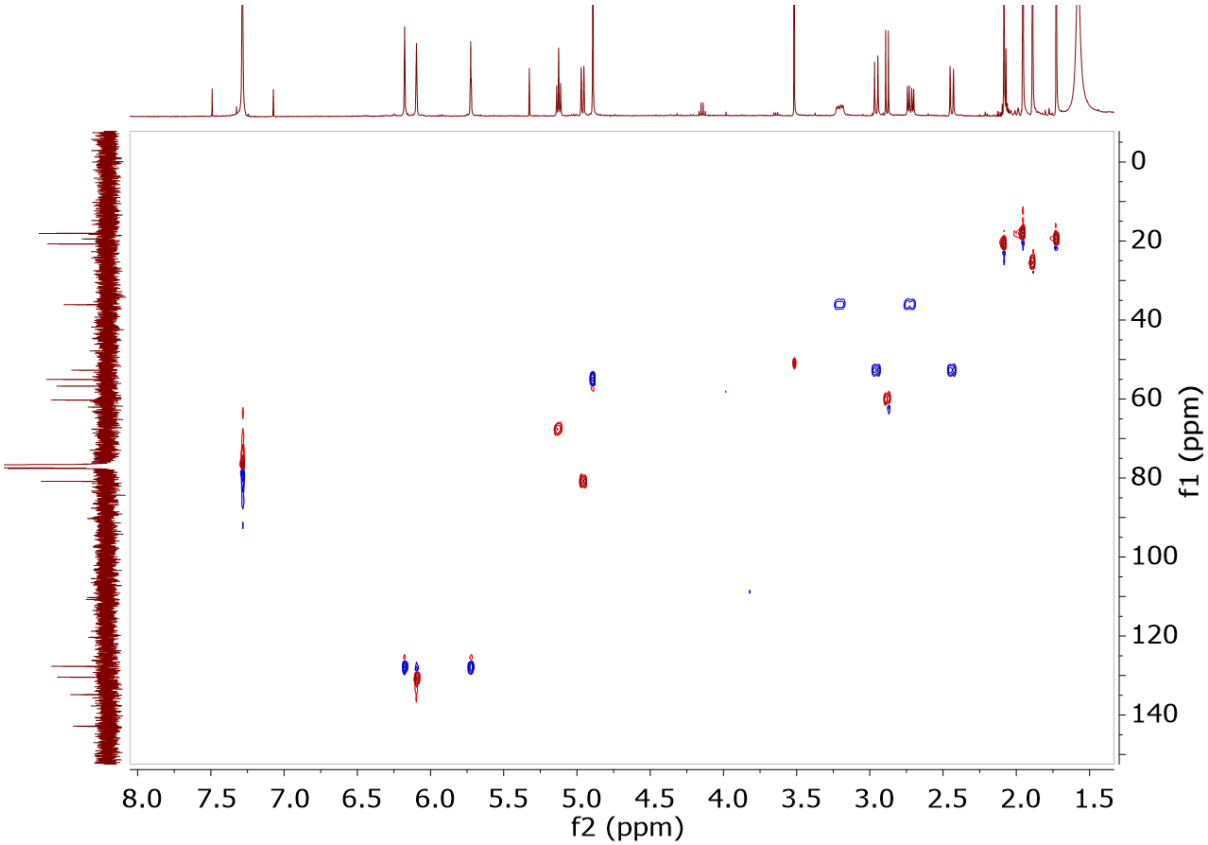

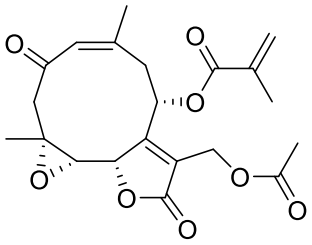

2.3

HMBC of Trichospirolide C (2.3) in $CDCl_3$

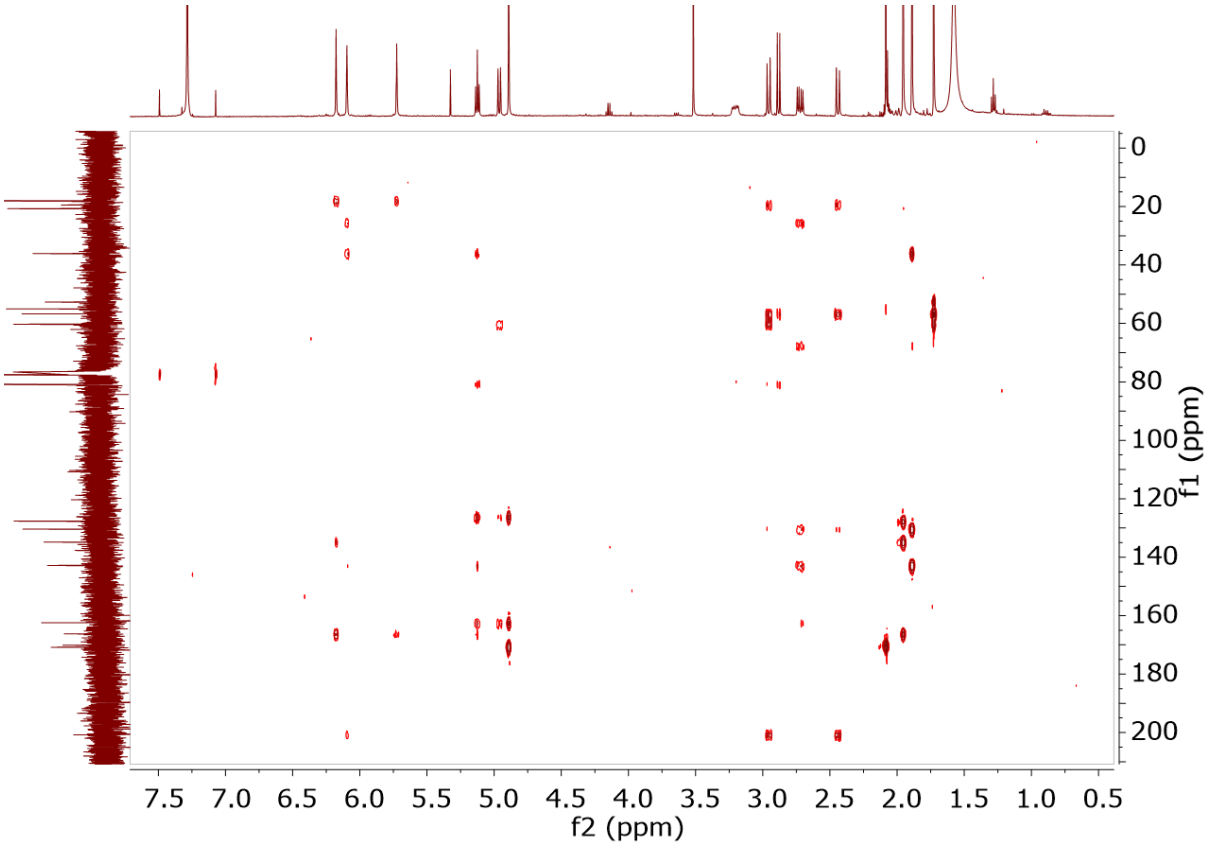

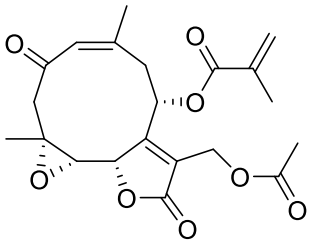

2.3

NOESY of Trichospirolide C (2.3) in $CDCl_3$

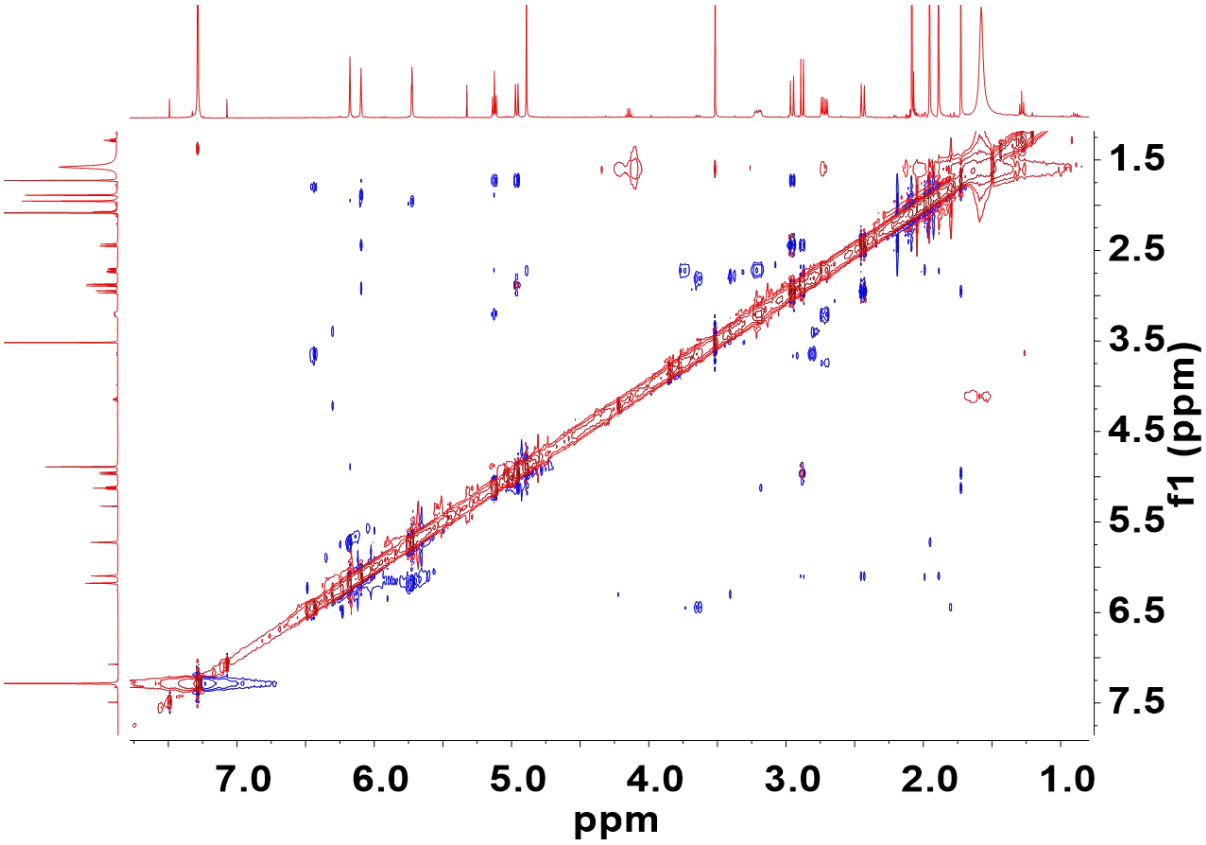

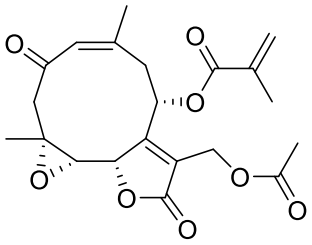

2.3

^{1}H NMR of Trichospirolide D (2.4) in $CDCl_3$

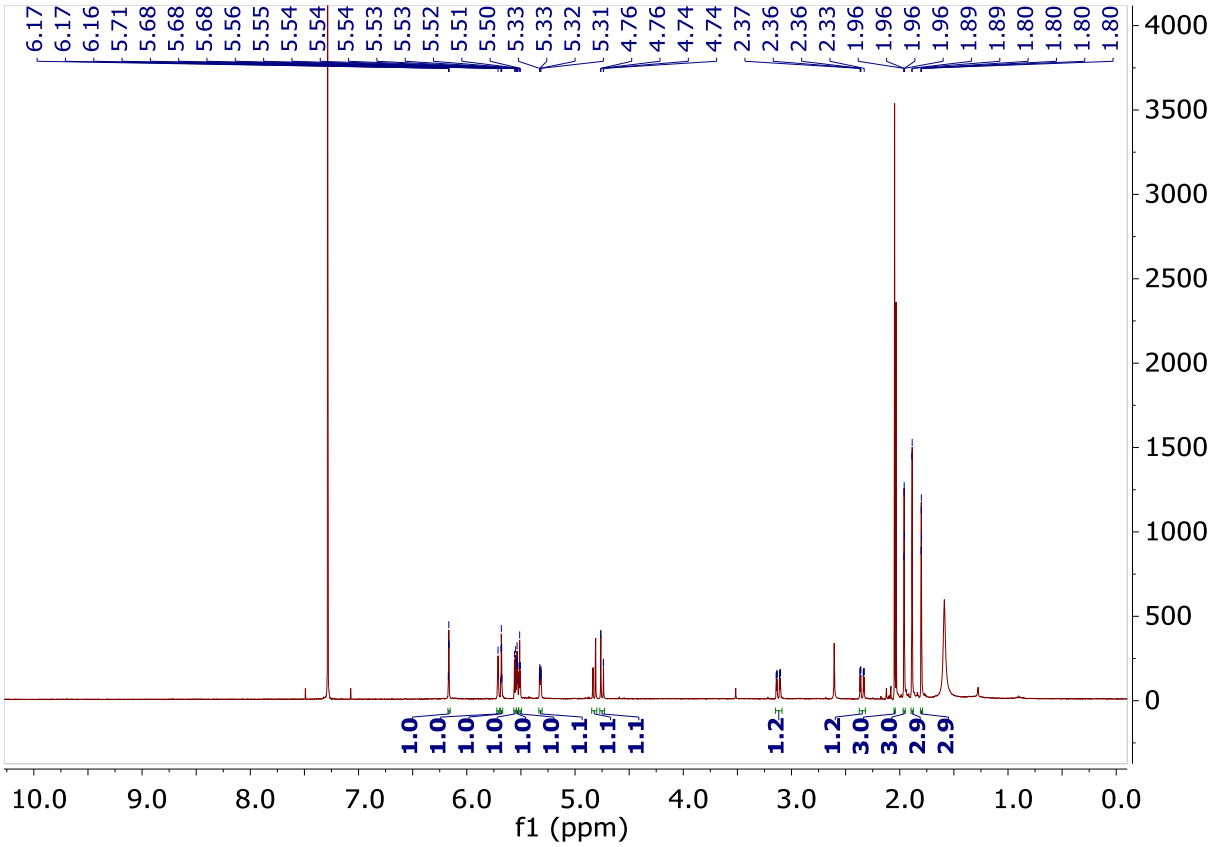

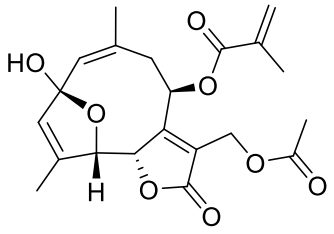

2.4

^{13}C NMR of Trichospirolide D (2.4) in $CDCl_3$

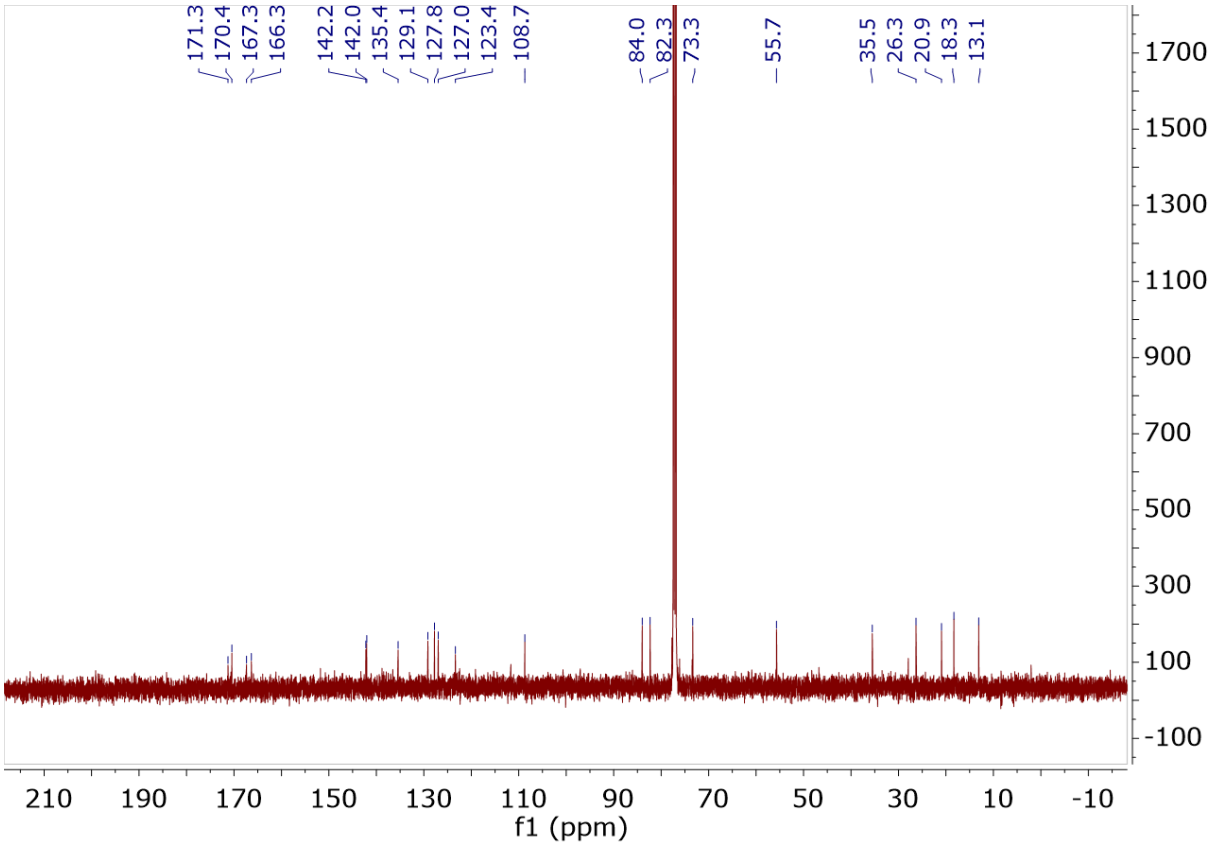

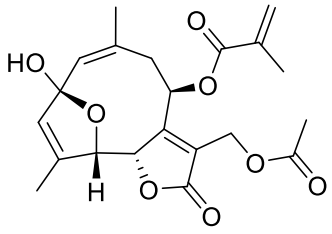

2.4

HSQC of Trichospirolide D (2.4) in $CDCl_3$

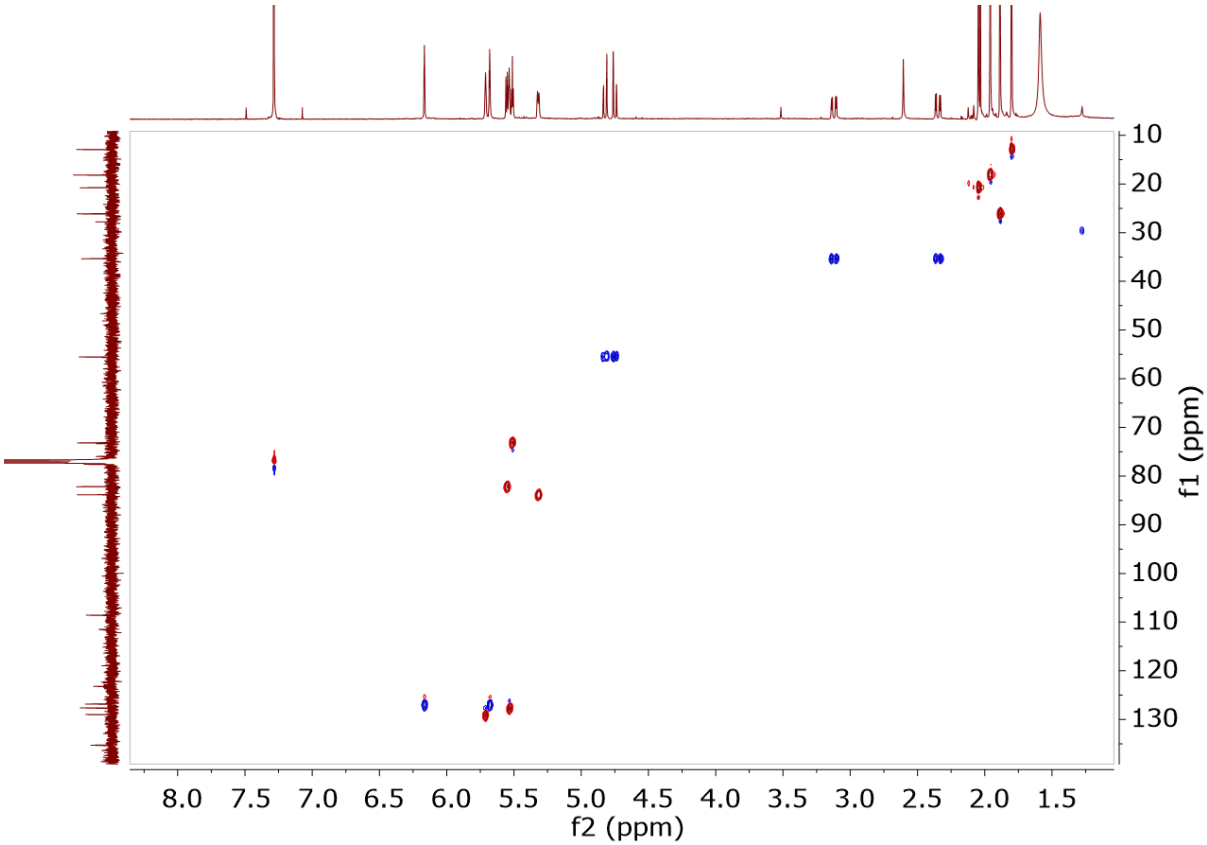

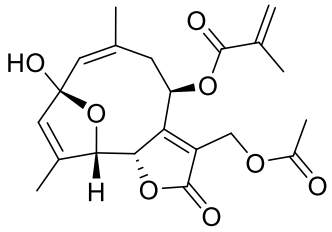

2.4

HMBC of Trichospirolide D (2.4) in $CDCl_3$

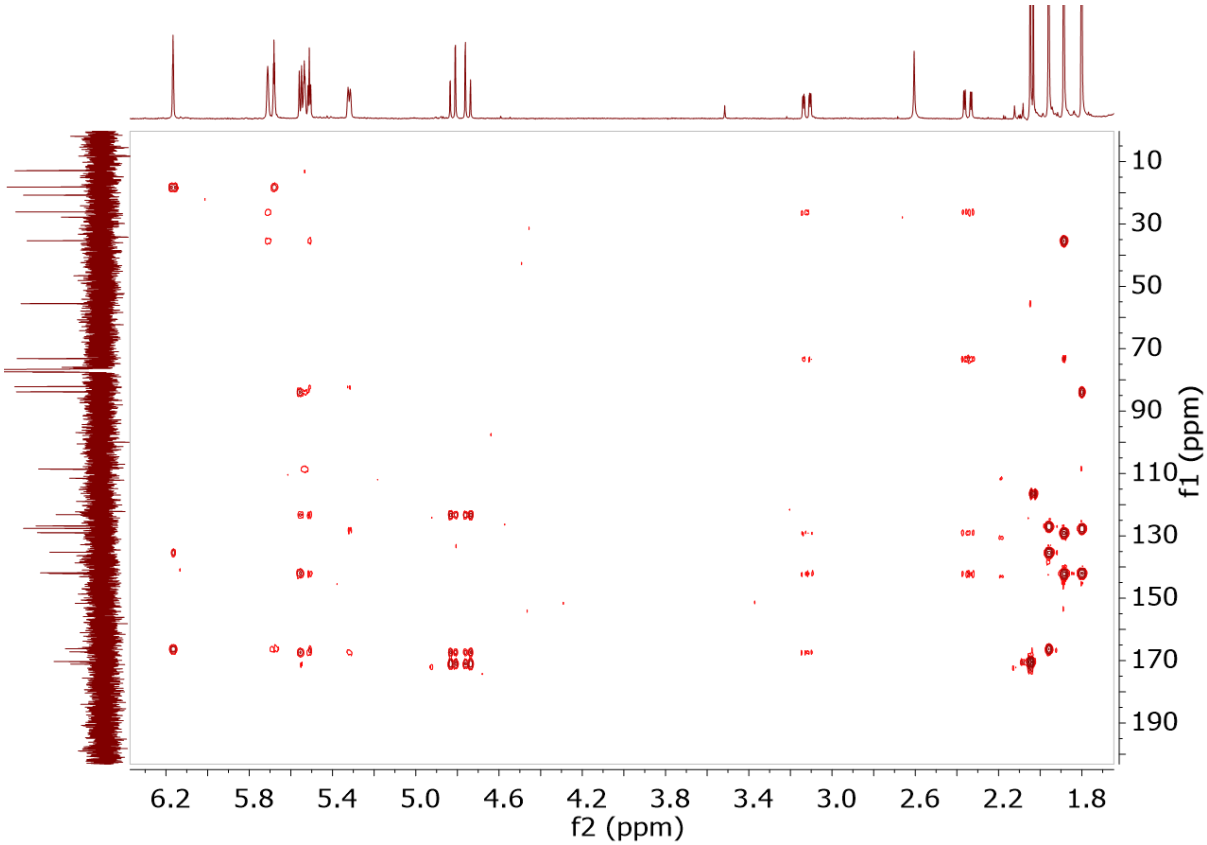

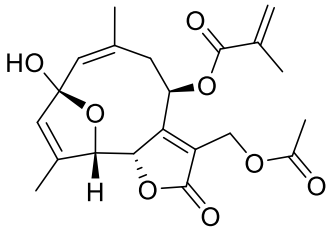

2.4

NOESY of Trichospirolide D (2.4) in $CDCl_3$

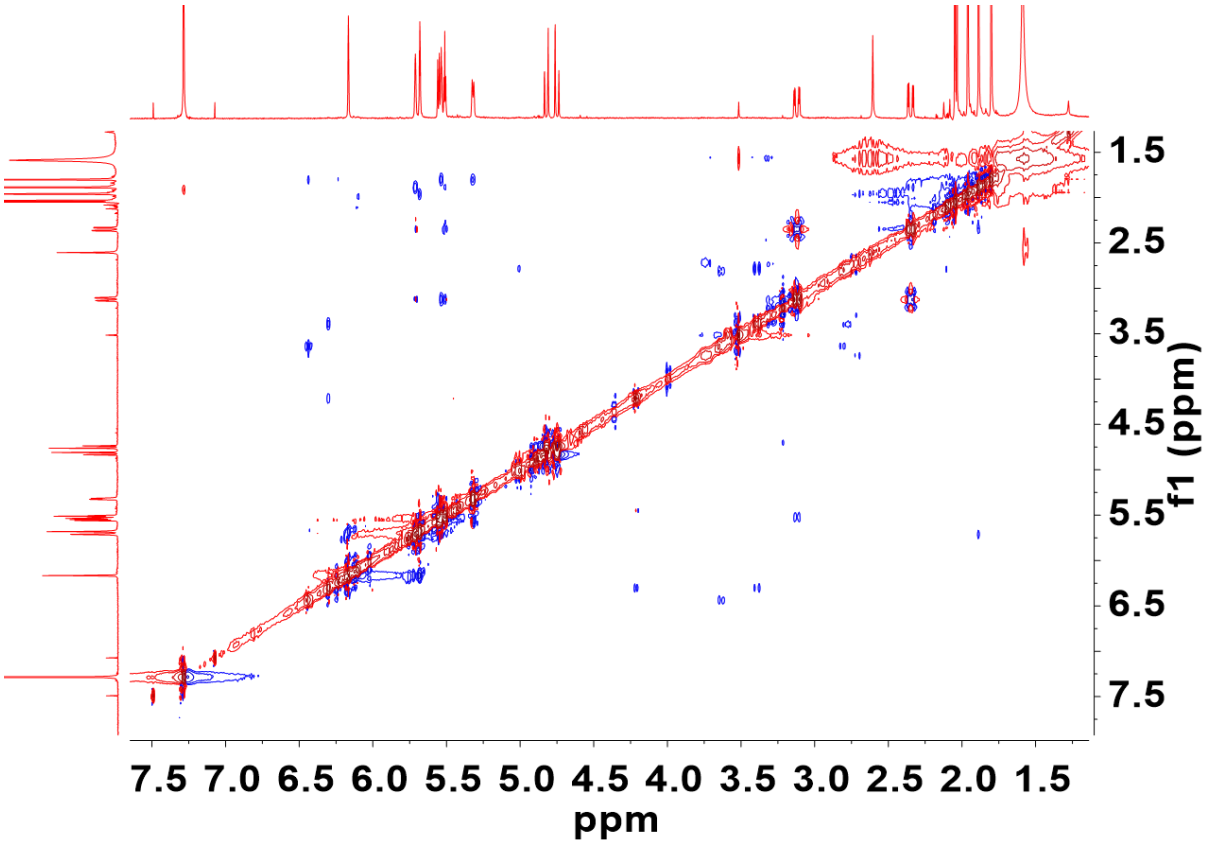

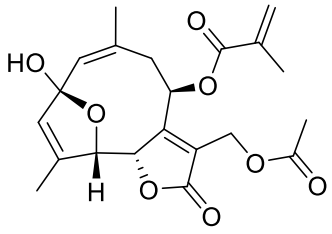

2.4

^{1}H NMR of Petradoriolide A (3.1) in $CDCl_3$

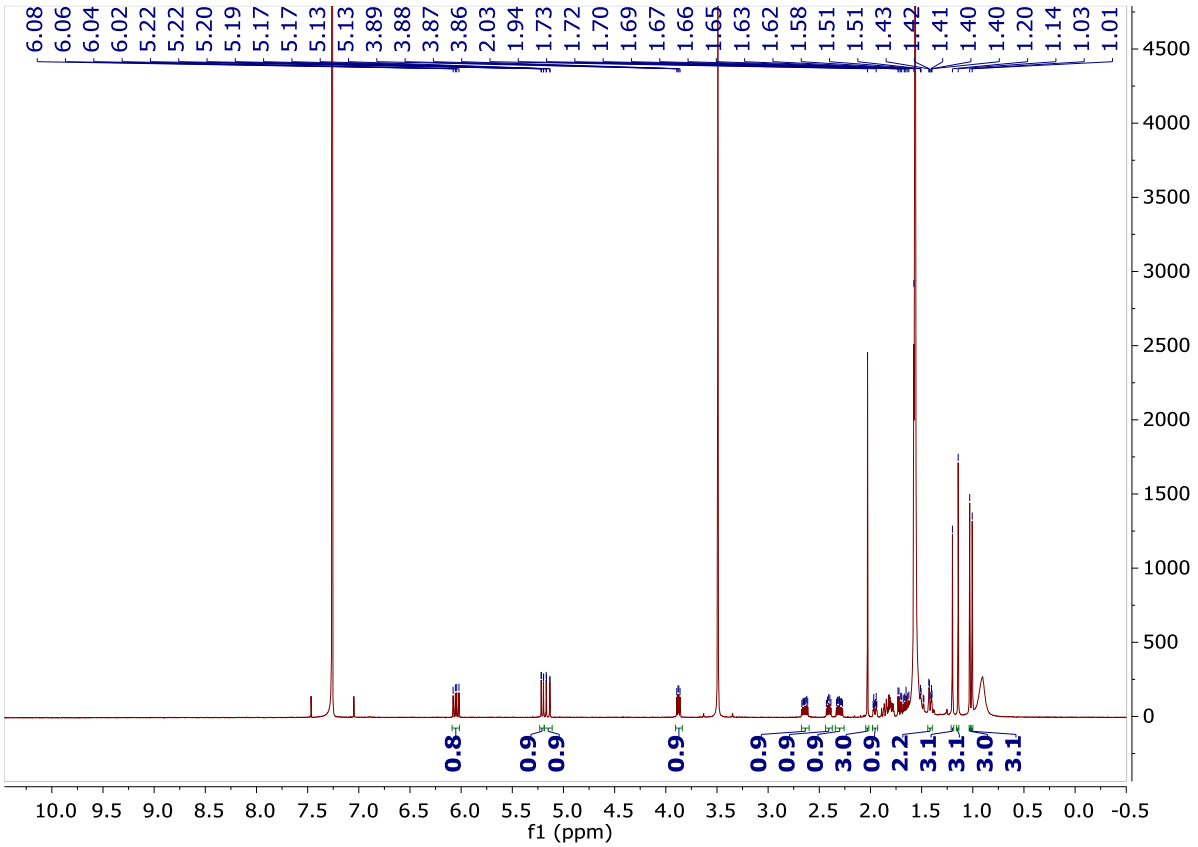

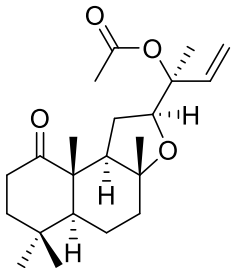

3.1

HSQC of Petradoriolide A (3.1) in $CDCl_3$

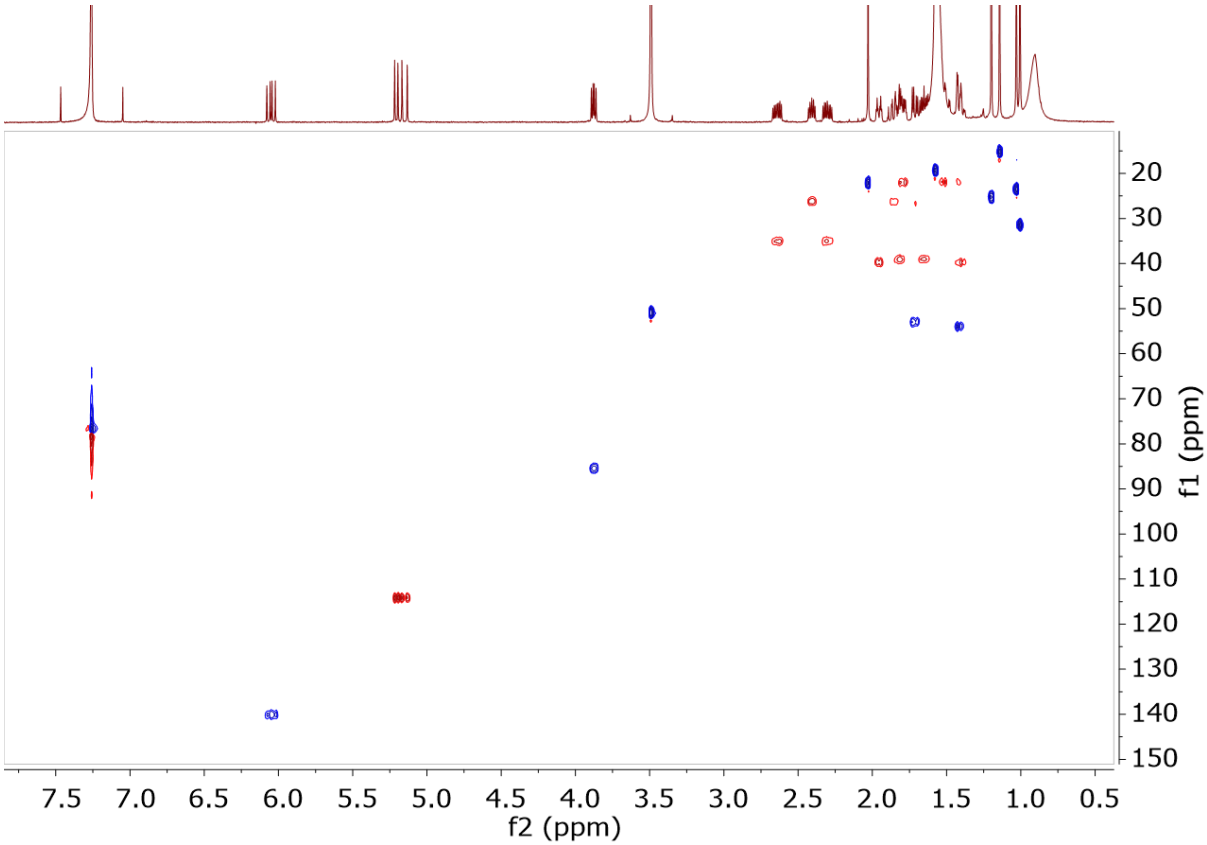

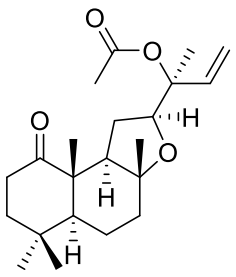

3.1

HMBC of Petradoriolide A (3.1) in $CDCl_3$

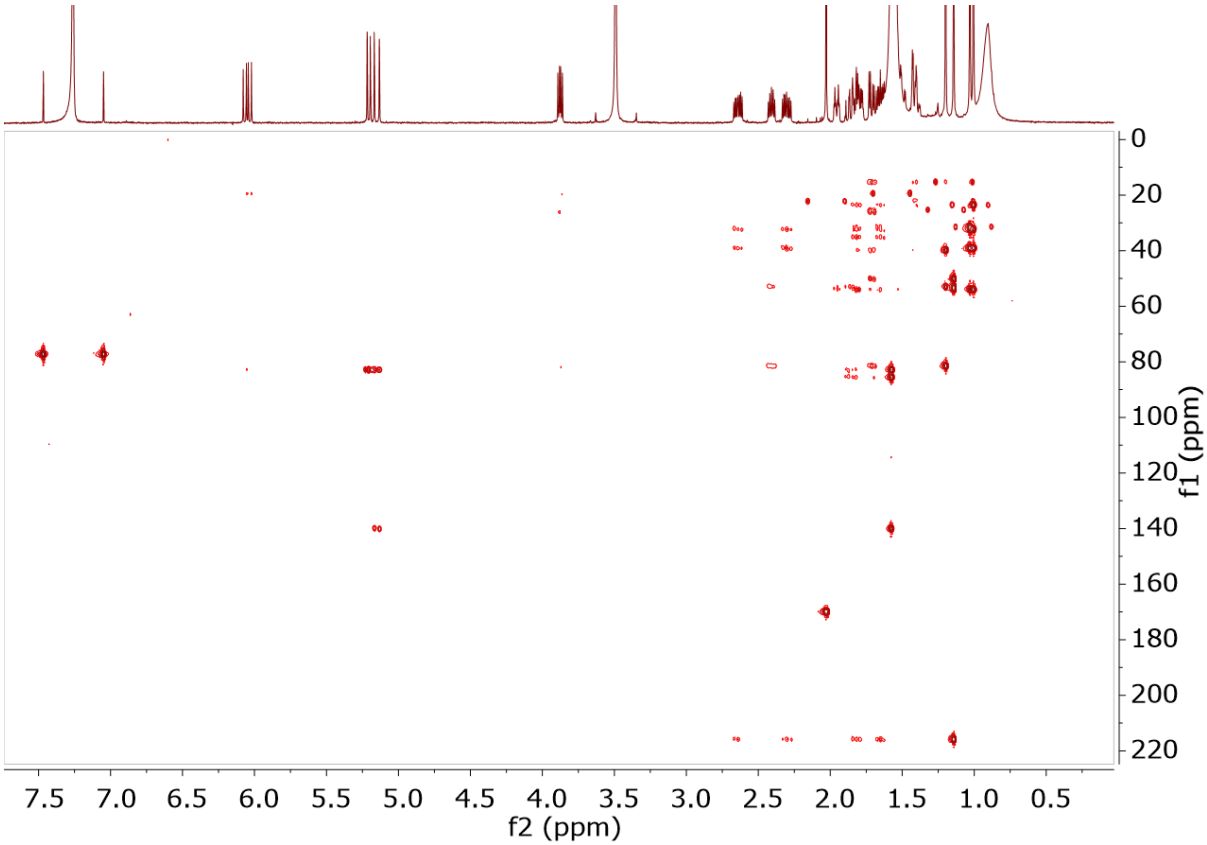

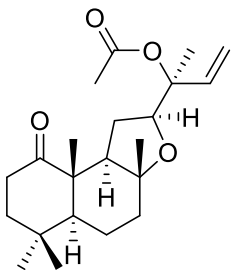

3.1

NOESY of Petradoriolide A (3.1) in $CDCl_3$

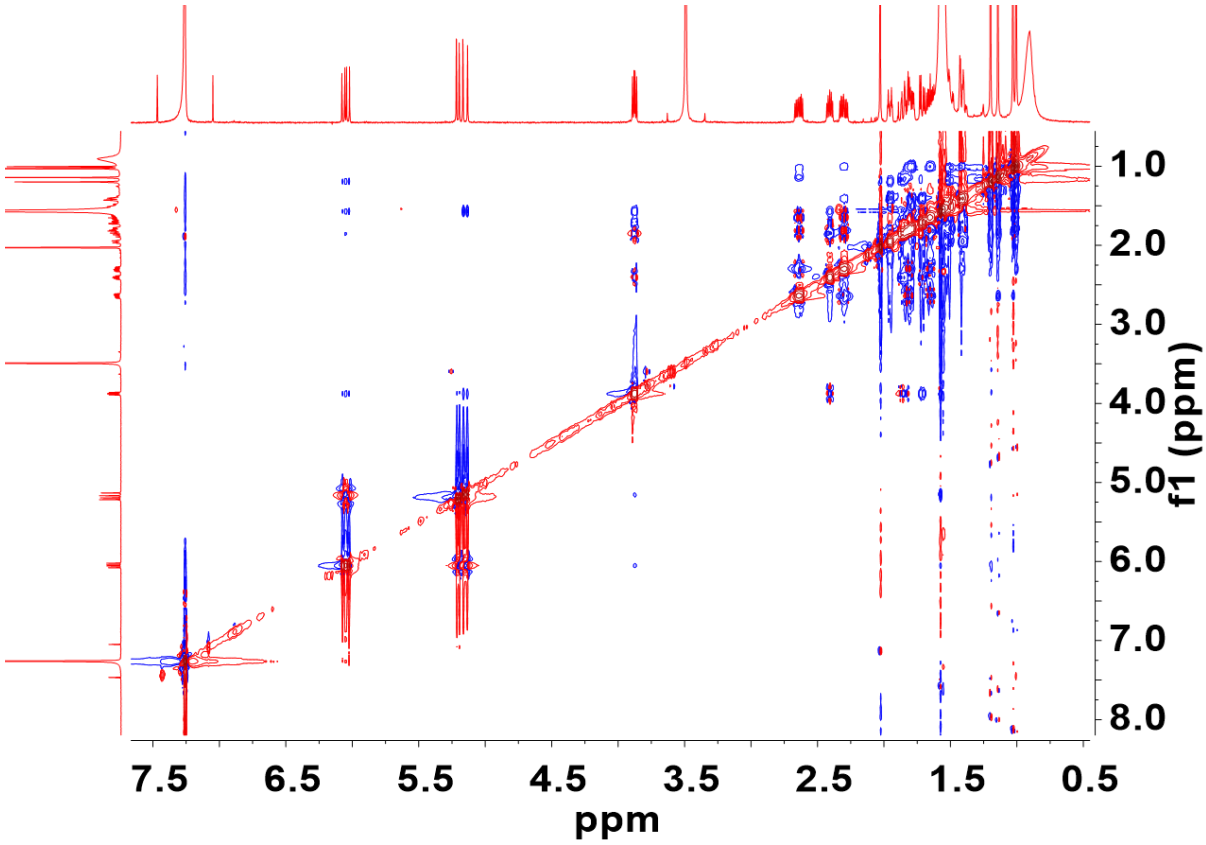

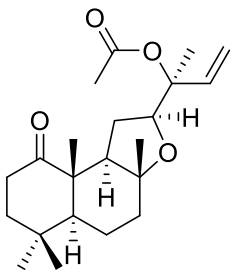

3.1

^{1}H NMR of Petradoriolide B (3.2) in $CDCl_3$

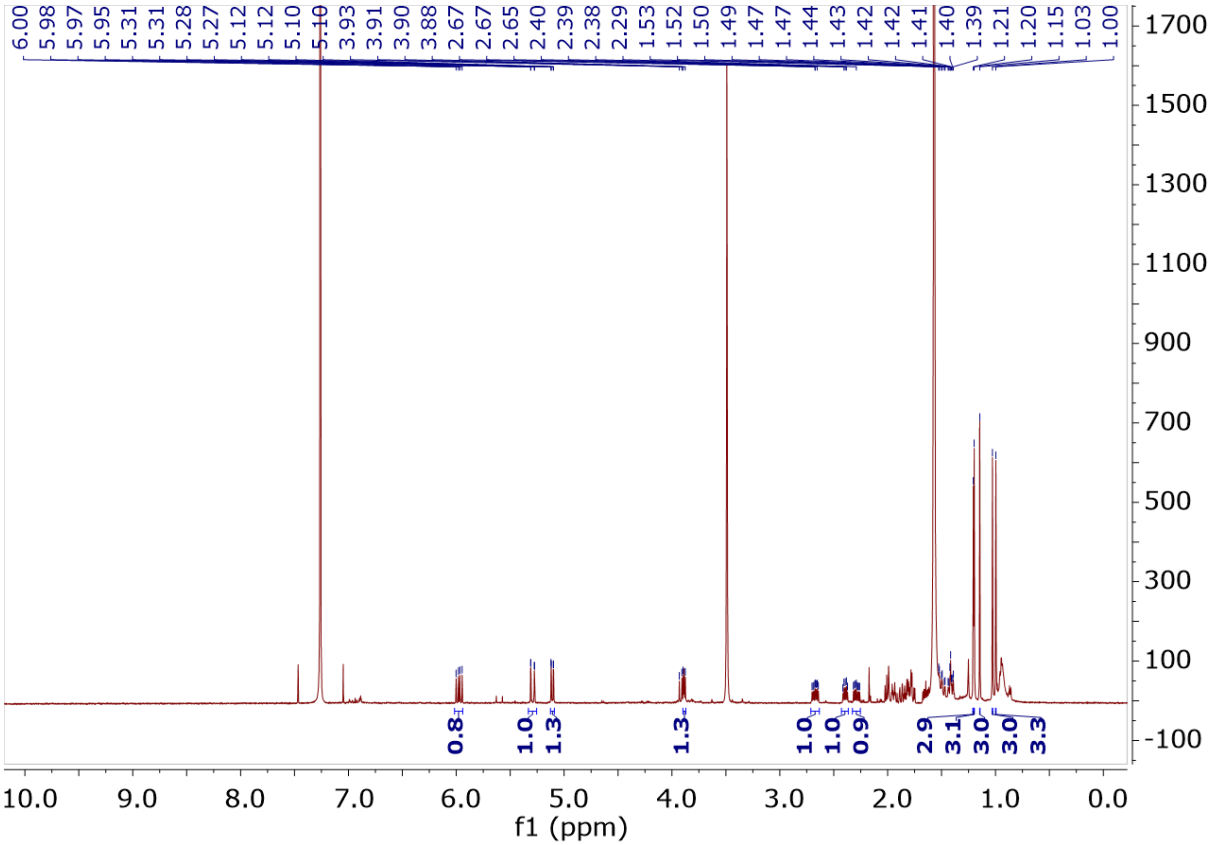

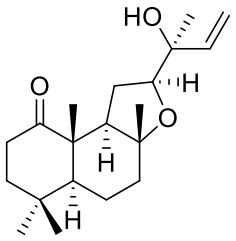

3.2

HSQC of Petradoriolide B (3.2) in $CDCl_3$

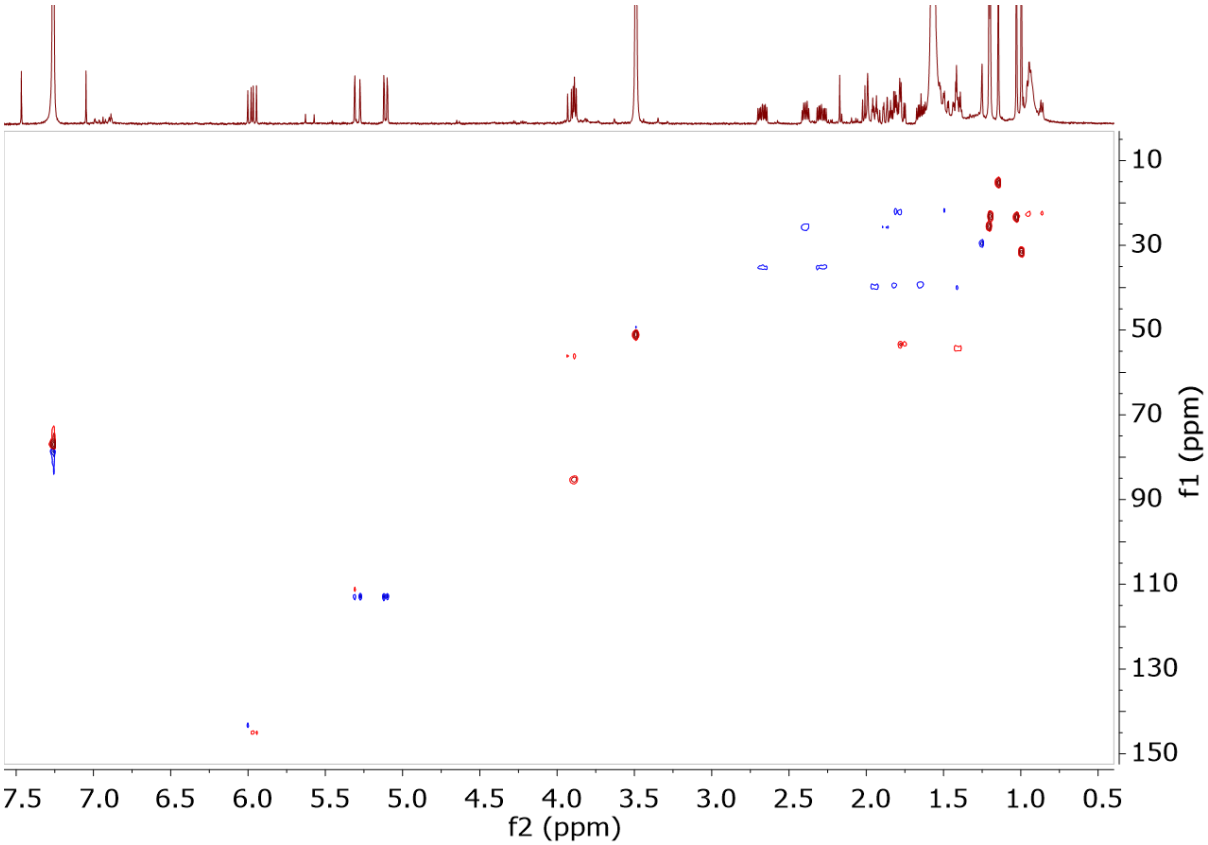

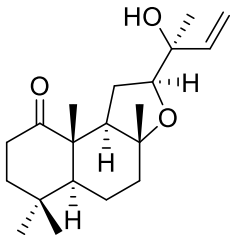

3.2

HMBC of Petradoriolide B (3.2) in $CDCl_3$

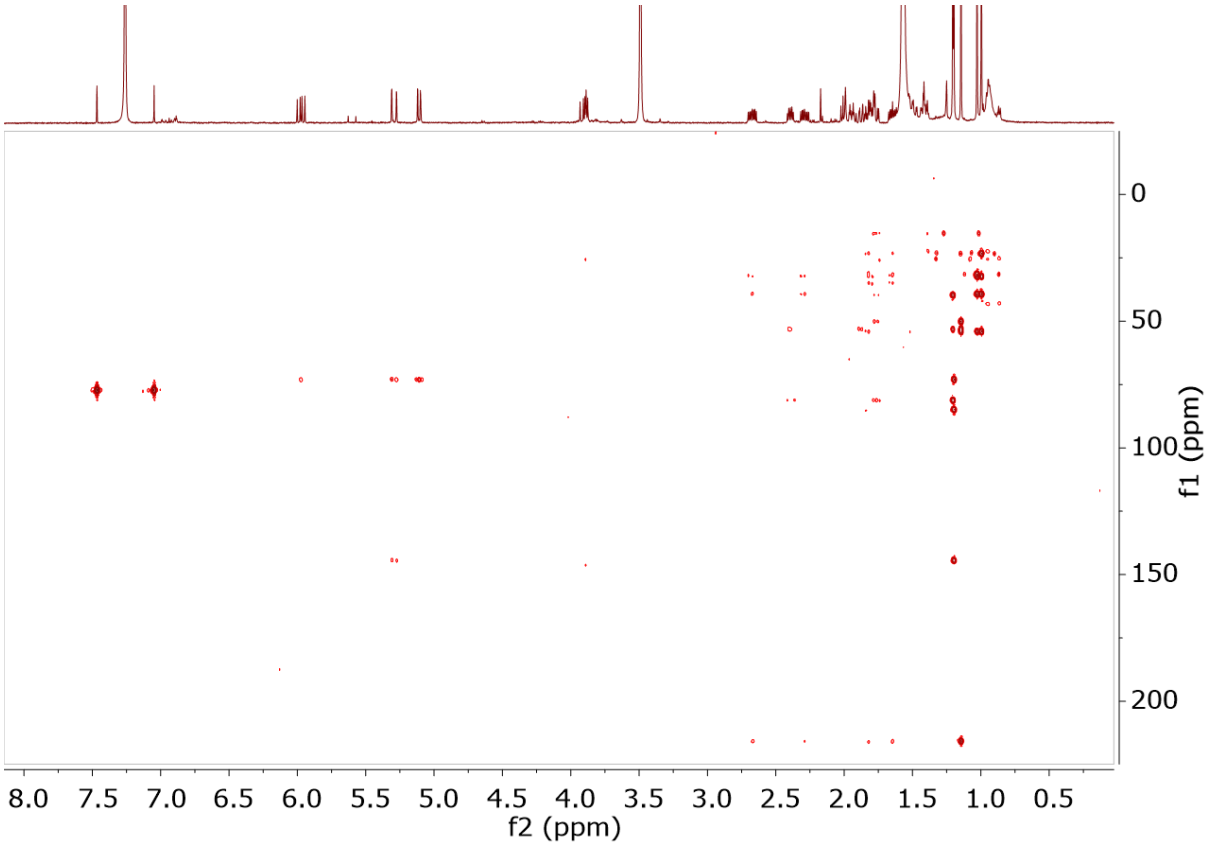

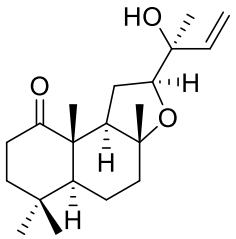

3.2

NOESY of Petradoriolide B (3.2) in $CDCl_3$

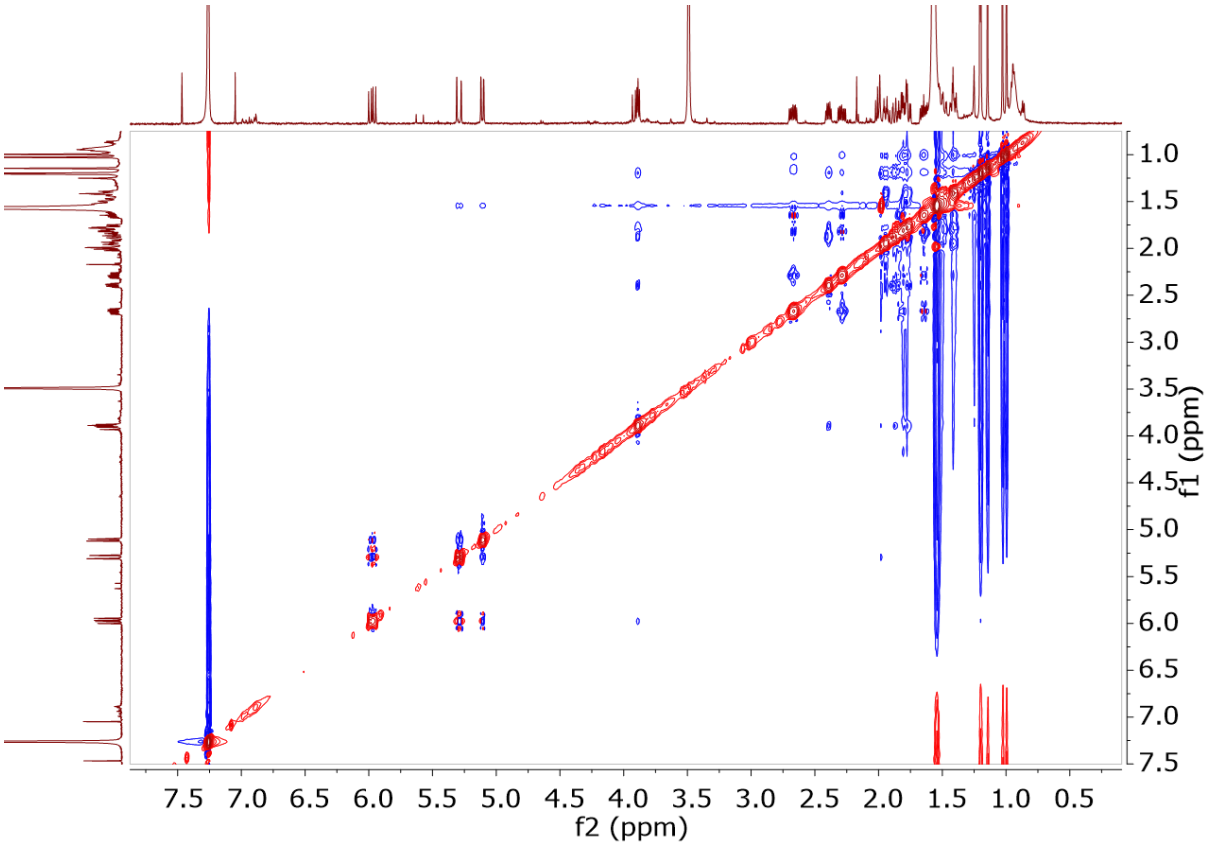

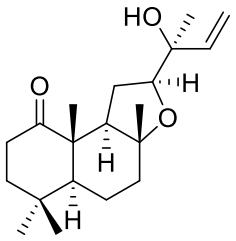

3.2

^{1}H NMR of Petradoriolide C (3.3) in $CDCl_3$

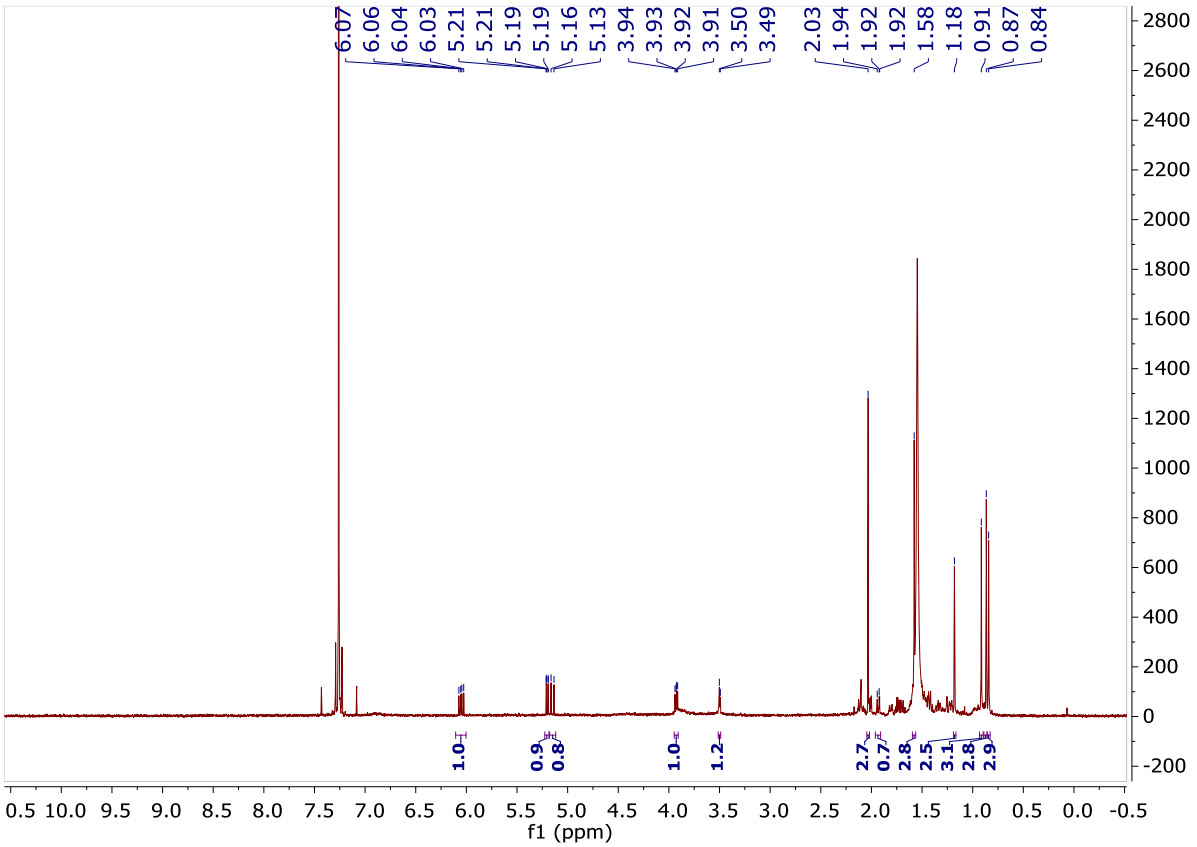

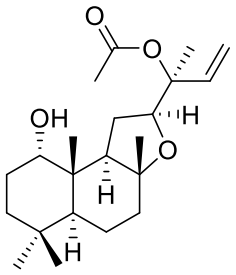

3.3

HSQC of Petradoriolide C (3.3) in $CDCl_3$

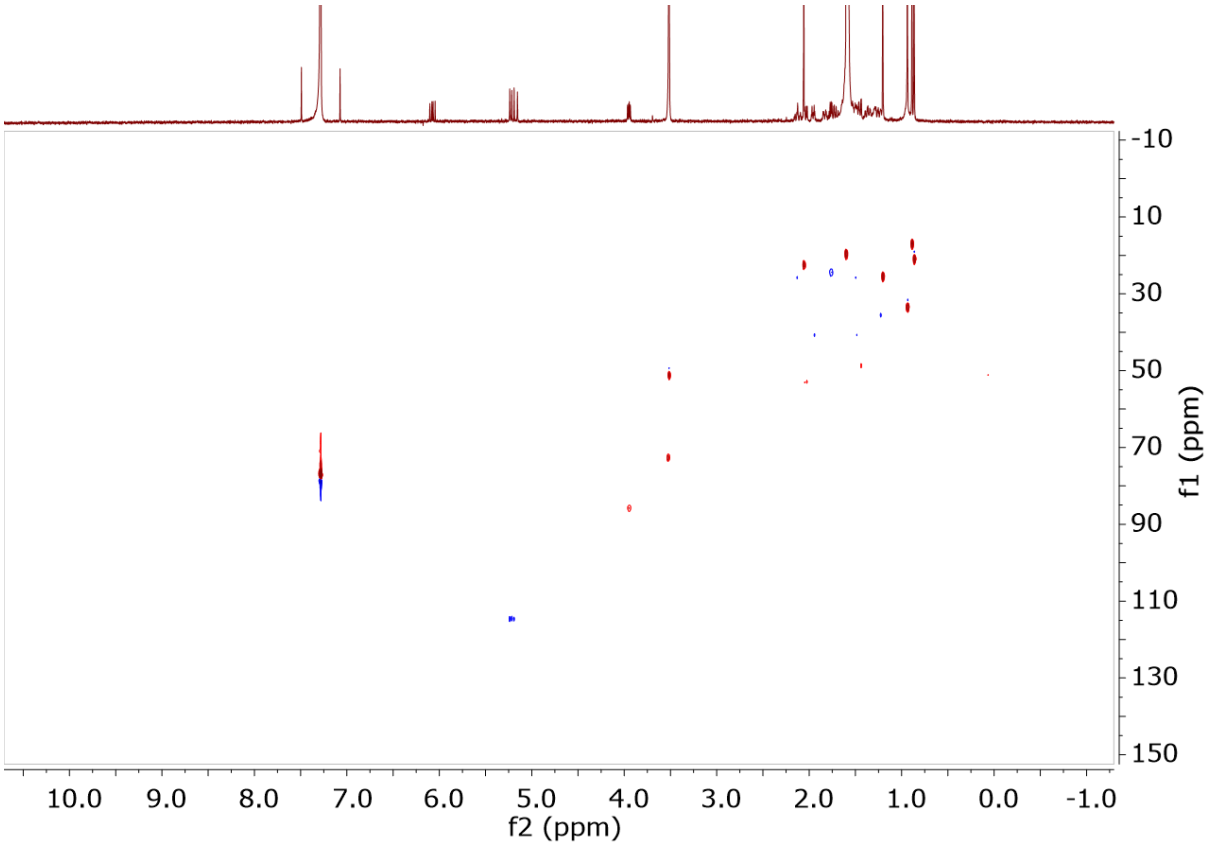

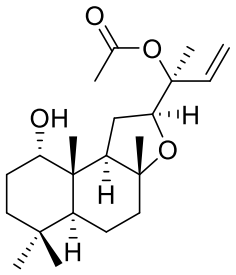

3.3

HMBC of Petradoriolide C (3.3) in $CDCl_3$

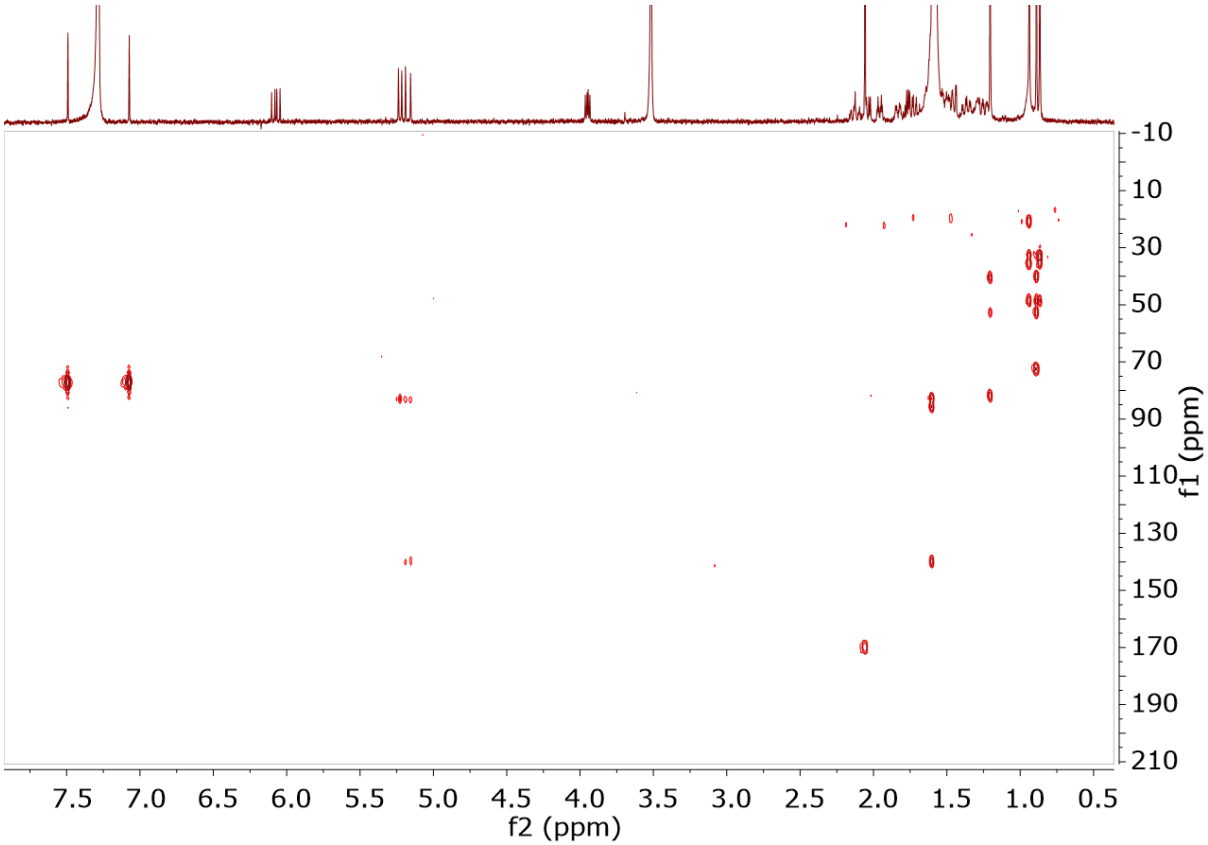

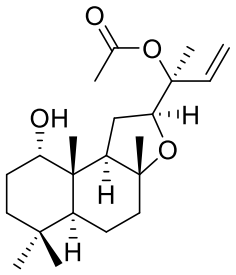

3.3

NOESY of Petradoriolide C (3.3) in $CDCl_3$

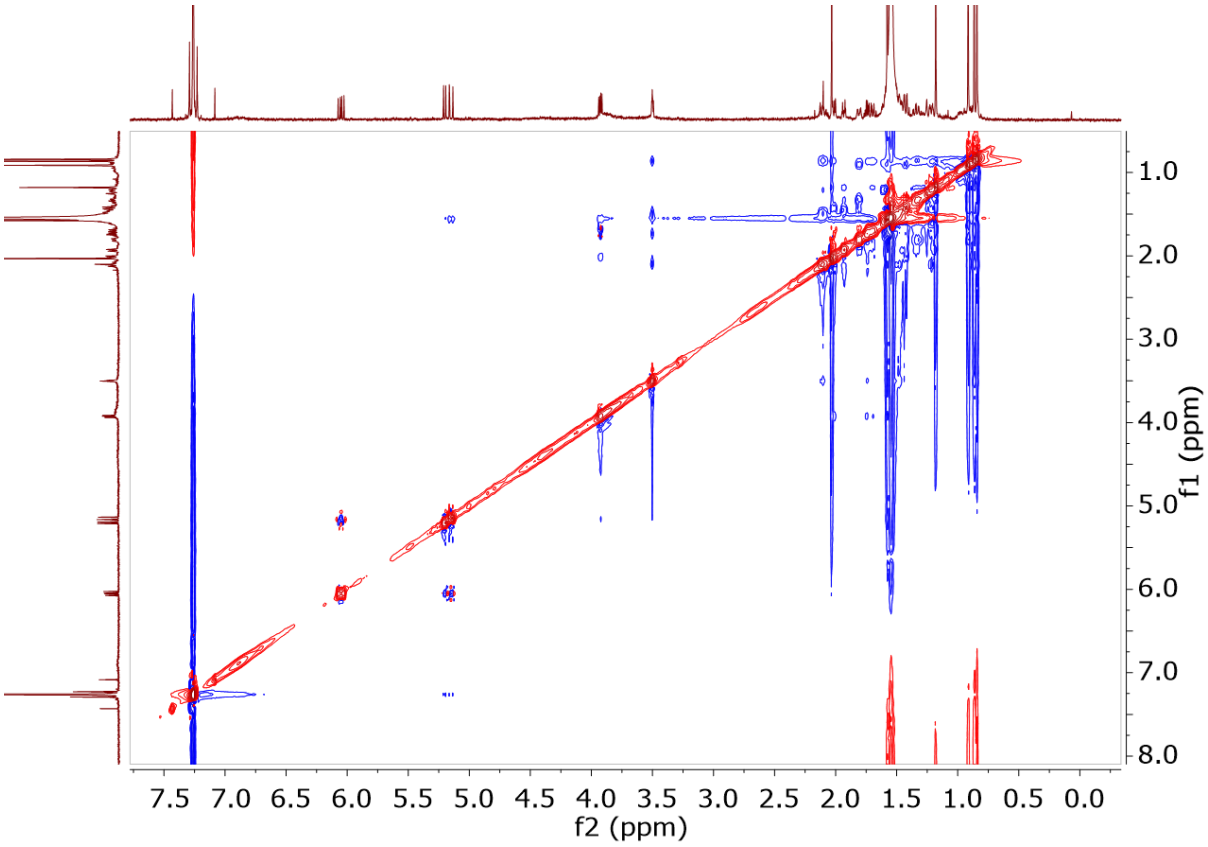

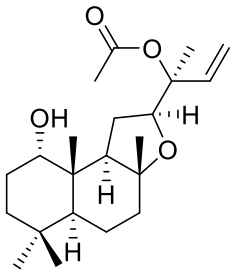

3.3

^{1}H NMR of Petradoriolide D (3.4) in $CDCl_3$

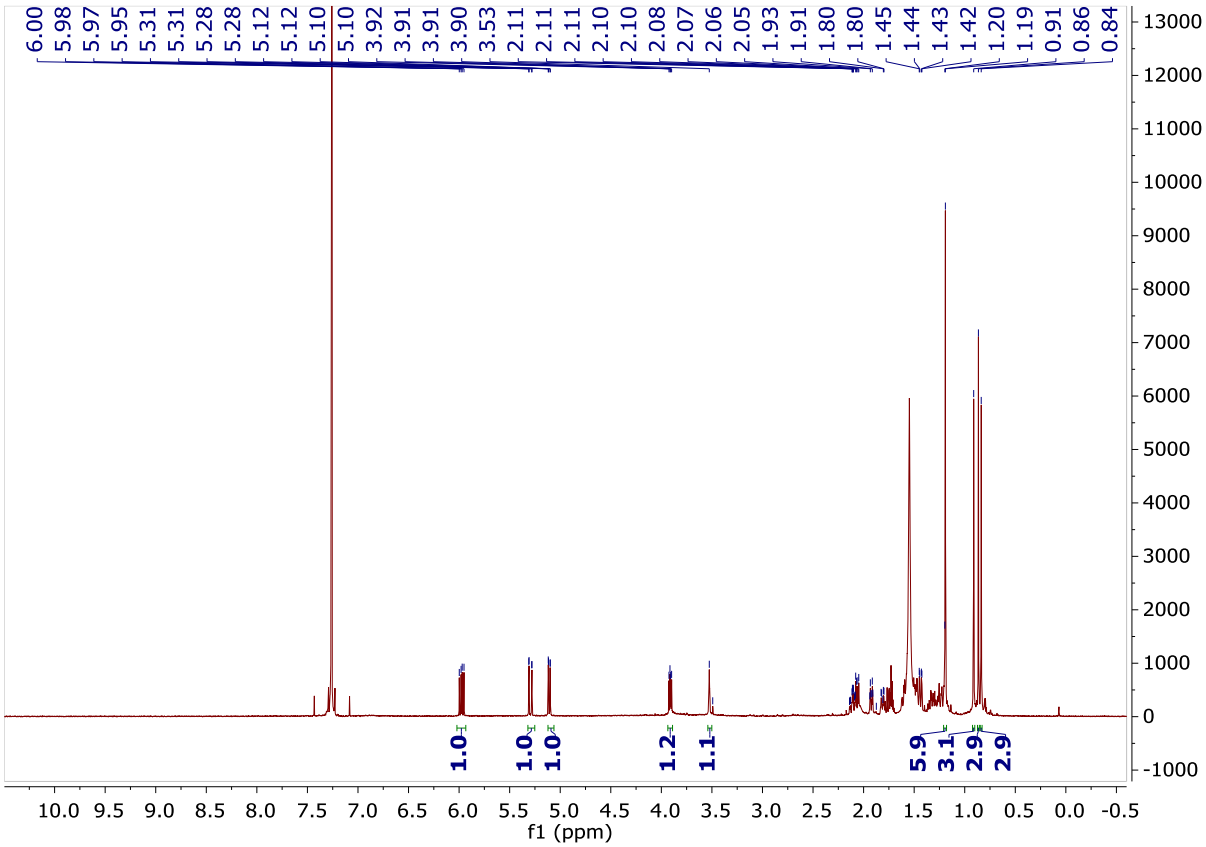

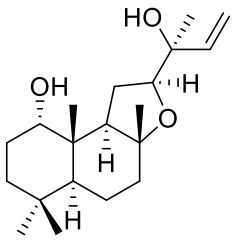

3.4

HSQC of Petradoriolide D (3.4) in $CDCl_3$

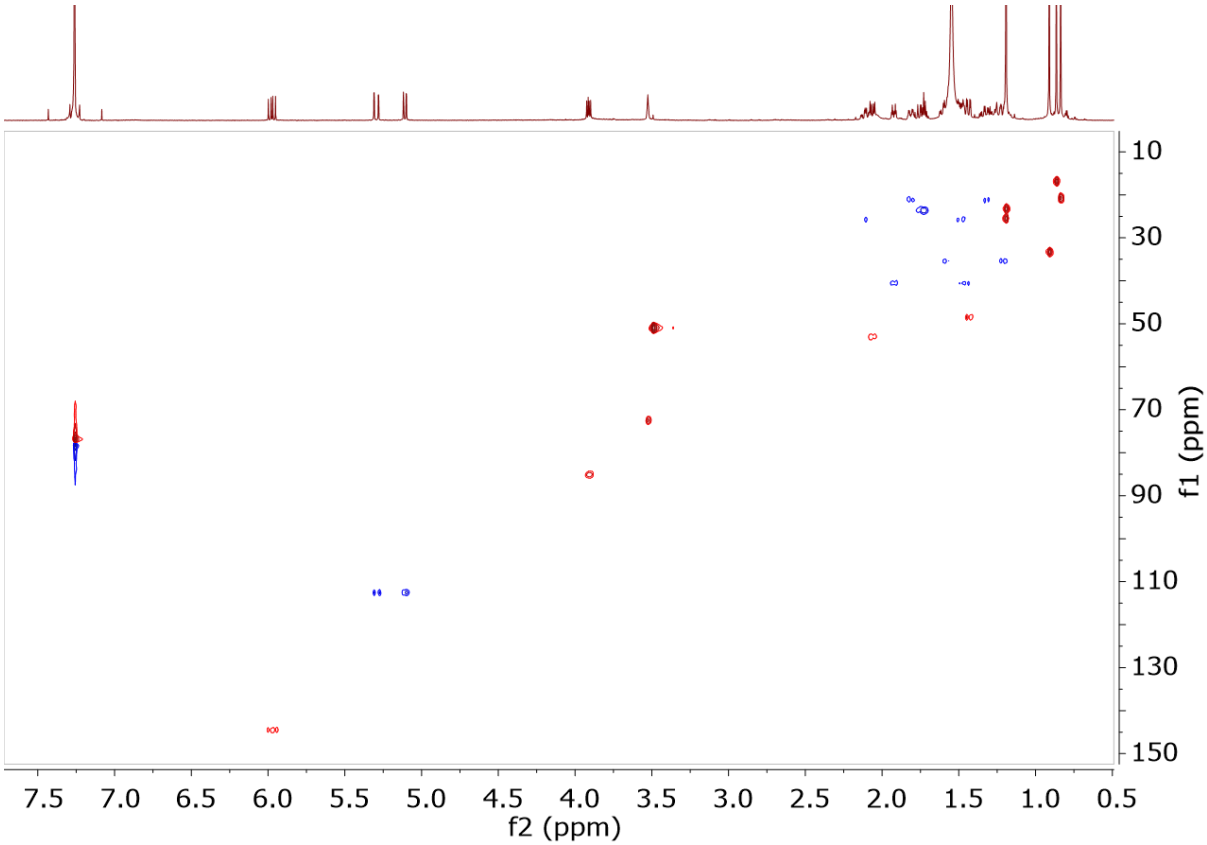

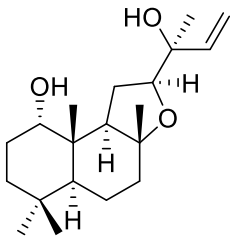

3.4

HMBC of Petradoriolide D (3.4) in $CDCl_3$

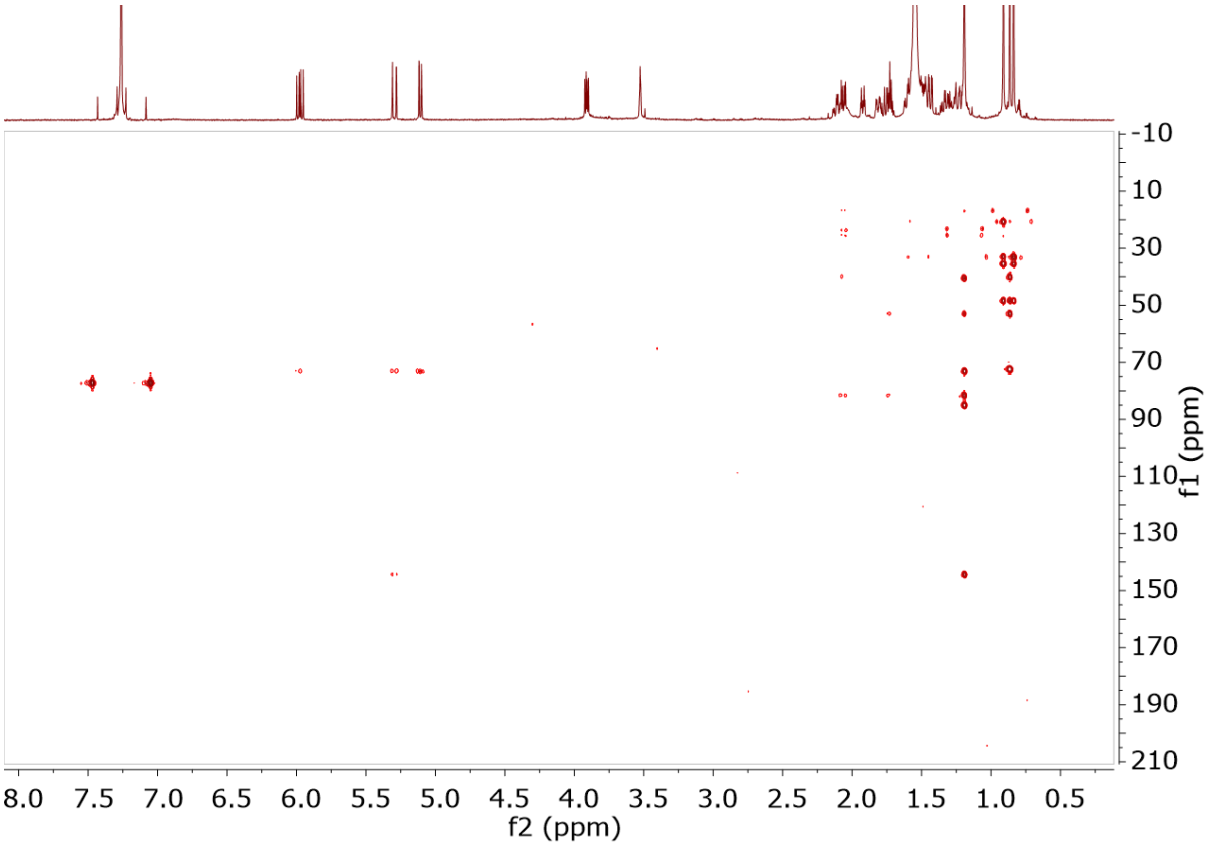

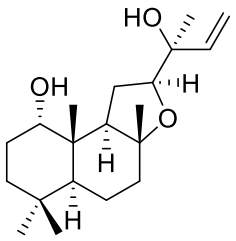

3.4

NOESY of Petradoriolide D (3.4) in $CDCl_3$

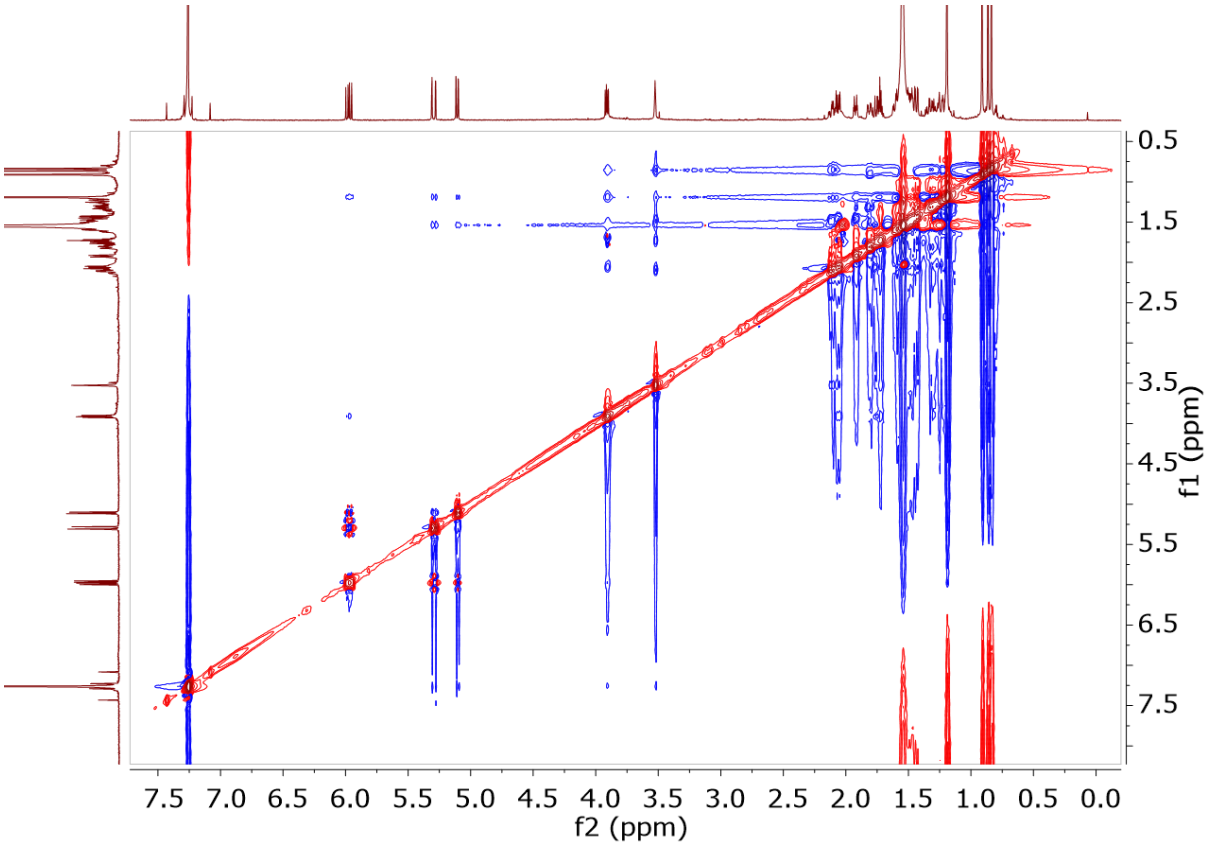

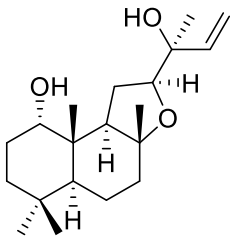

3.4

^{1}H NMR of Petradoriolone (3.5) in $CDCl_3$

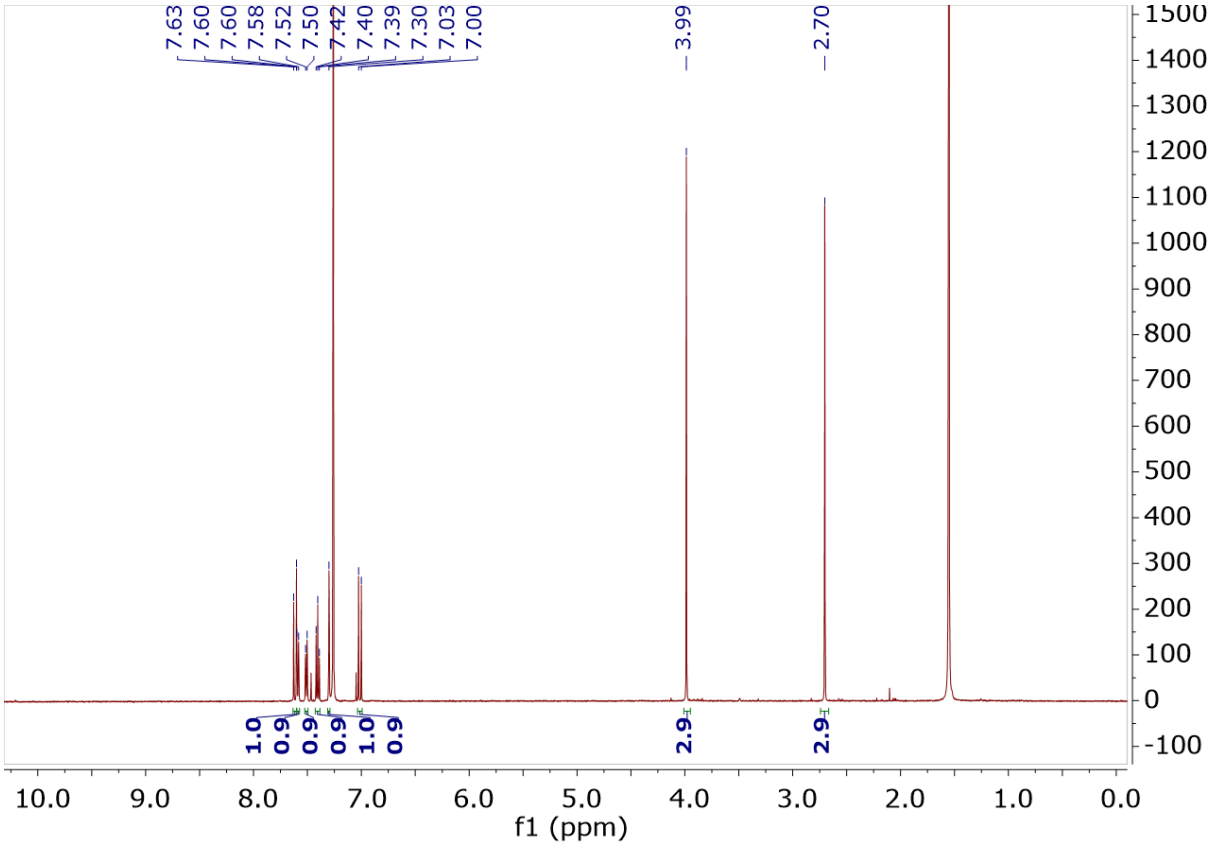

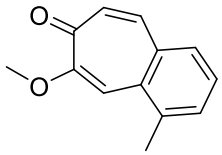

3.5

^{13}C NMR of Petradoriolone (3.5) in $CDCl_3$

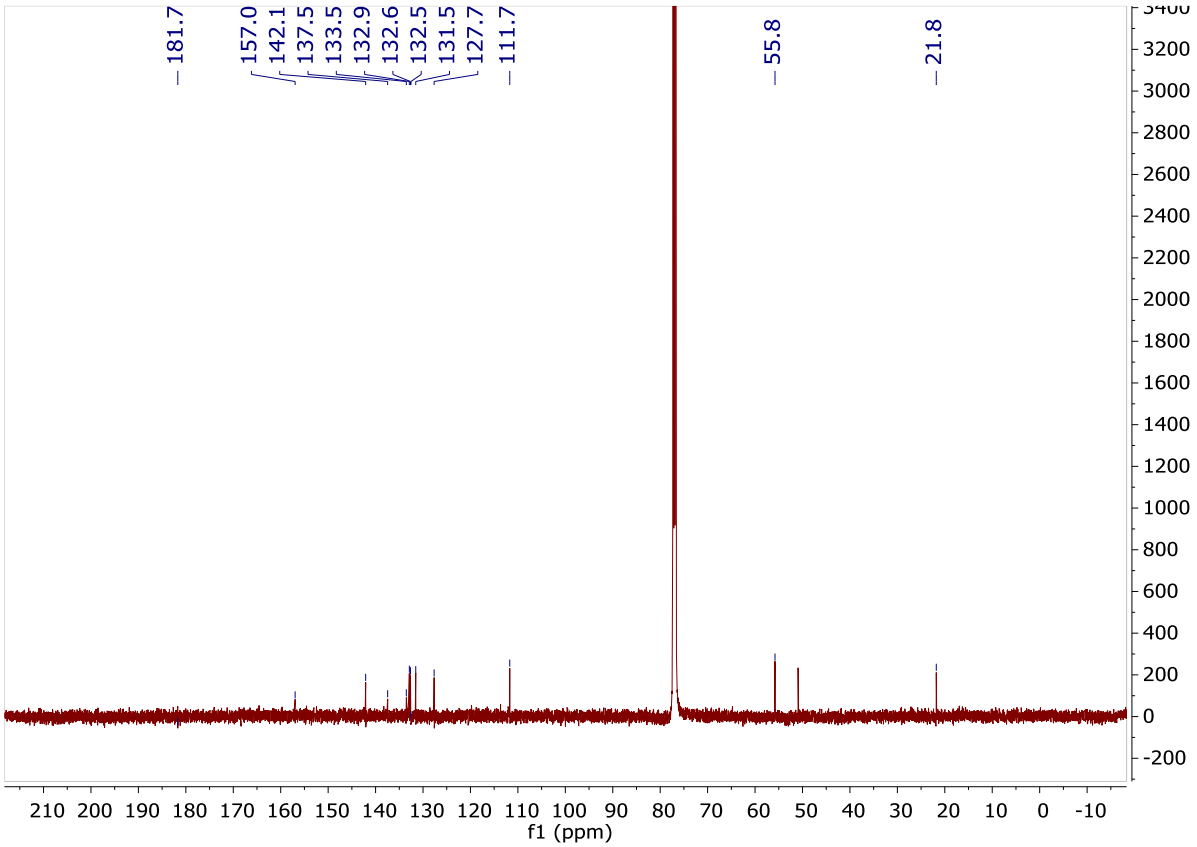

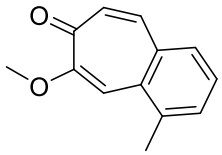

3.5

HSQC of Petradoriolone (3.5) in $CDCl_3$

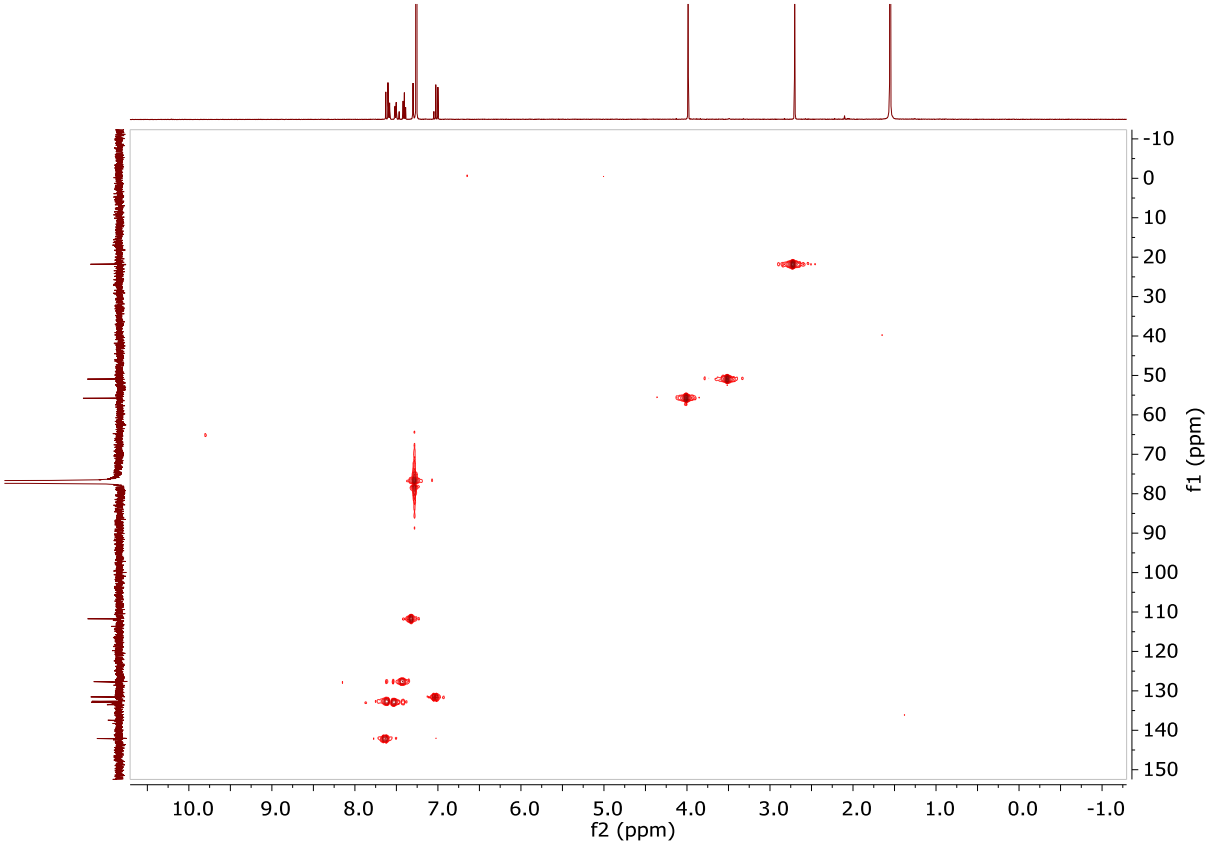

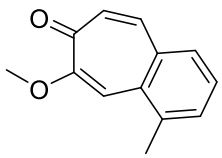

3.5

HMBC of Petradoriolone (3.5) in $CDCl_3$

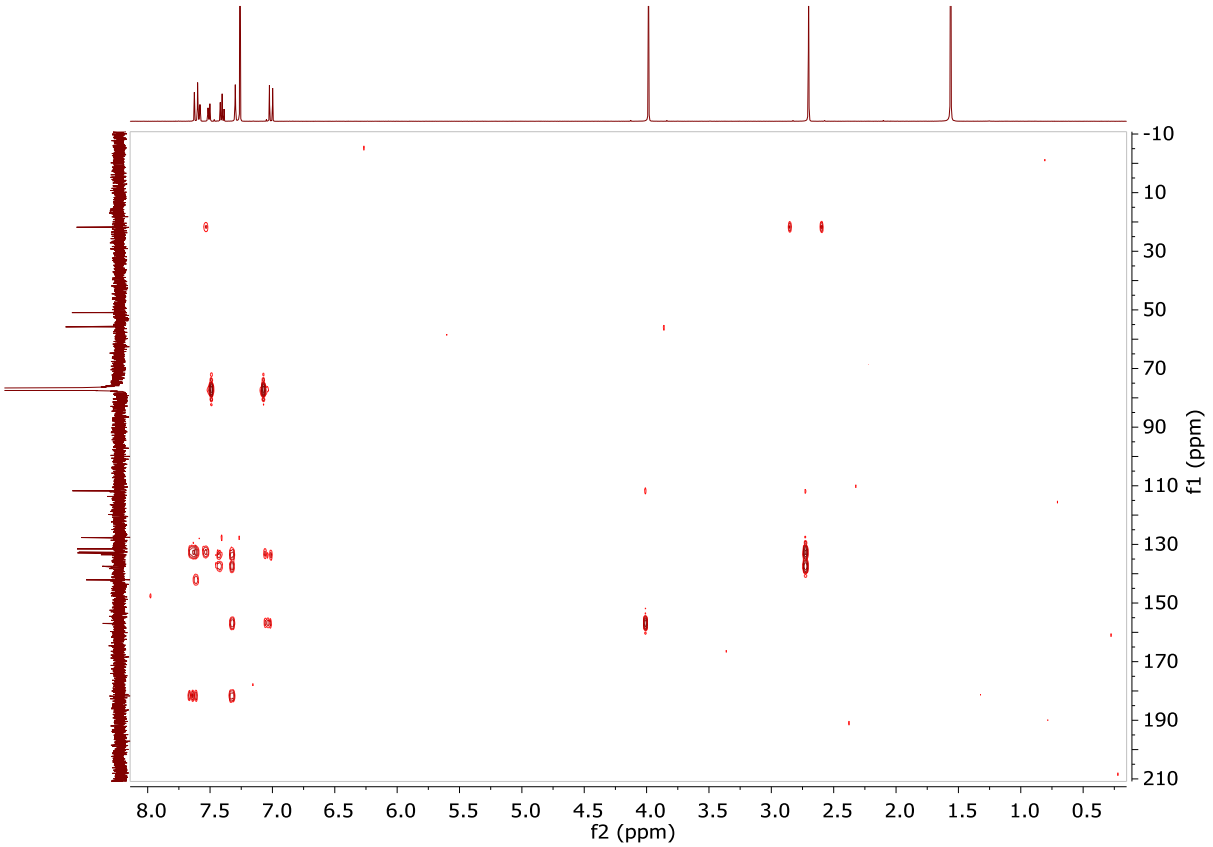

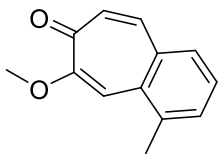

3.5

^{1}H NMR of (7E)-(7'*R*,*8*'S)-4'-hydroxy-3',5-dimethoxy-4,7'-epoxy-8',3-neolig-7-en-9,9'-diyl diacetate (3.6) in $CDCl_3$

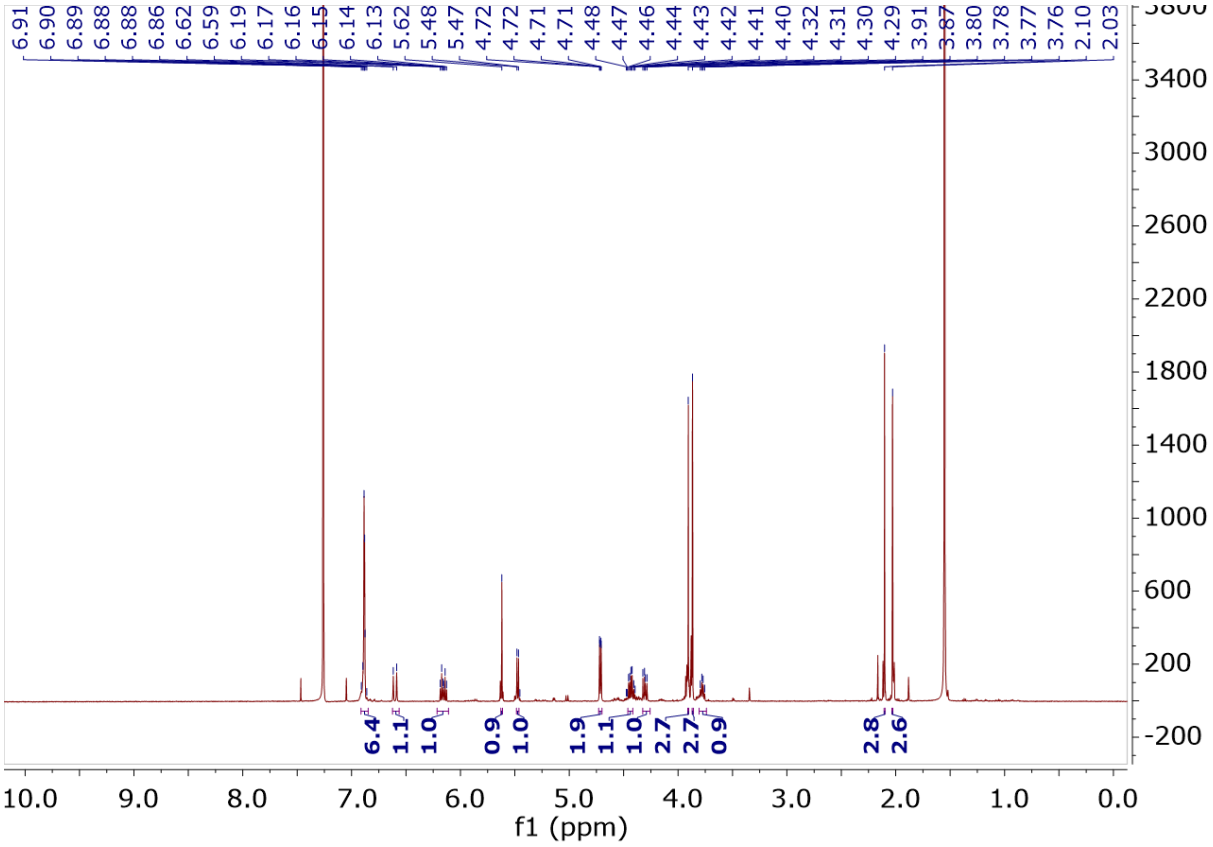

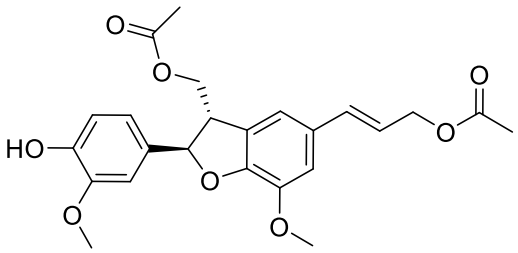

3.6

^{1}H NMR of (7*E*)-(7'*R*,8'*S*)-4'-hydroxy-3',5-dimethoxy-4,7'-epoxy-8',3-neolig-7-en-9,9'-diyl di-3-methylbutanoate (3.7) in $CDCl_3$

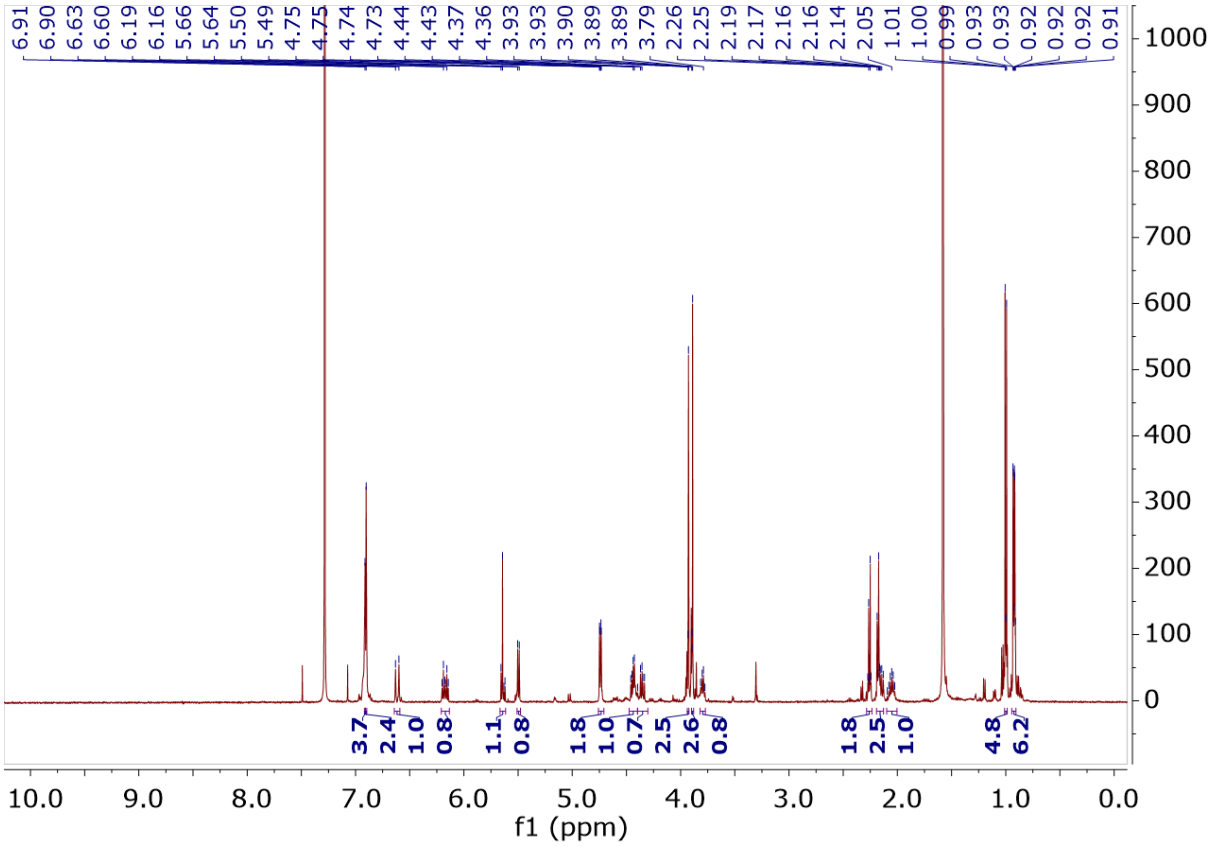

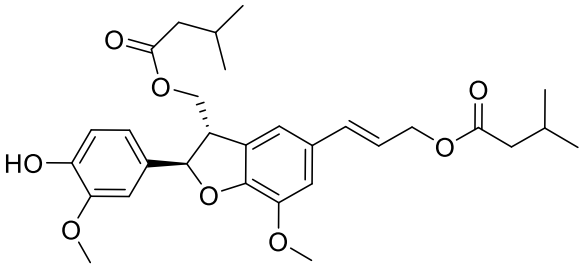

3.7

^{1}H NMR of Anibomarin A (4.1) in $CDCl_3$

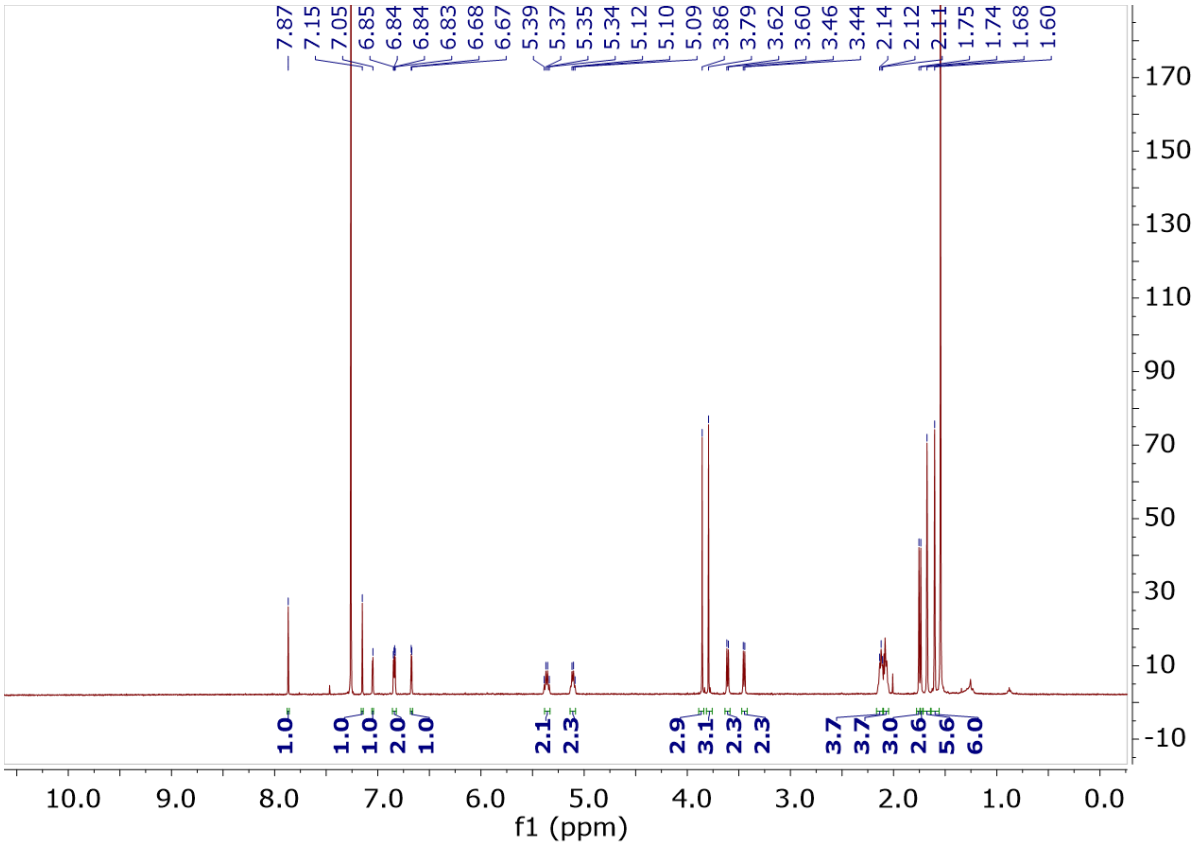

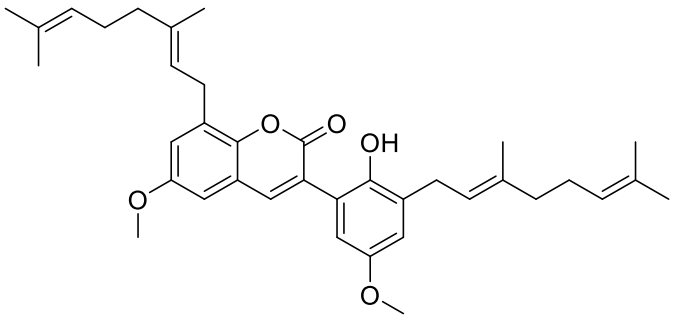

4.1

^{13}C NMR of Anibomarin A (4.1) in $CDCl_3$

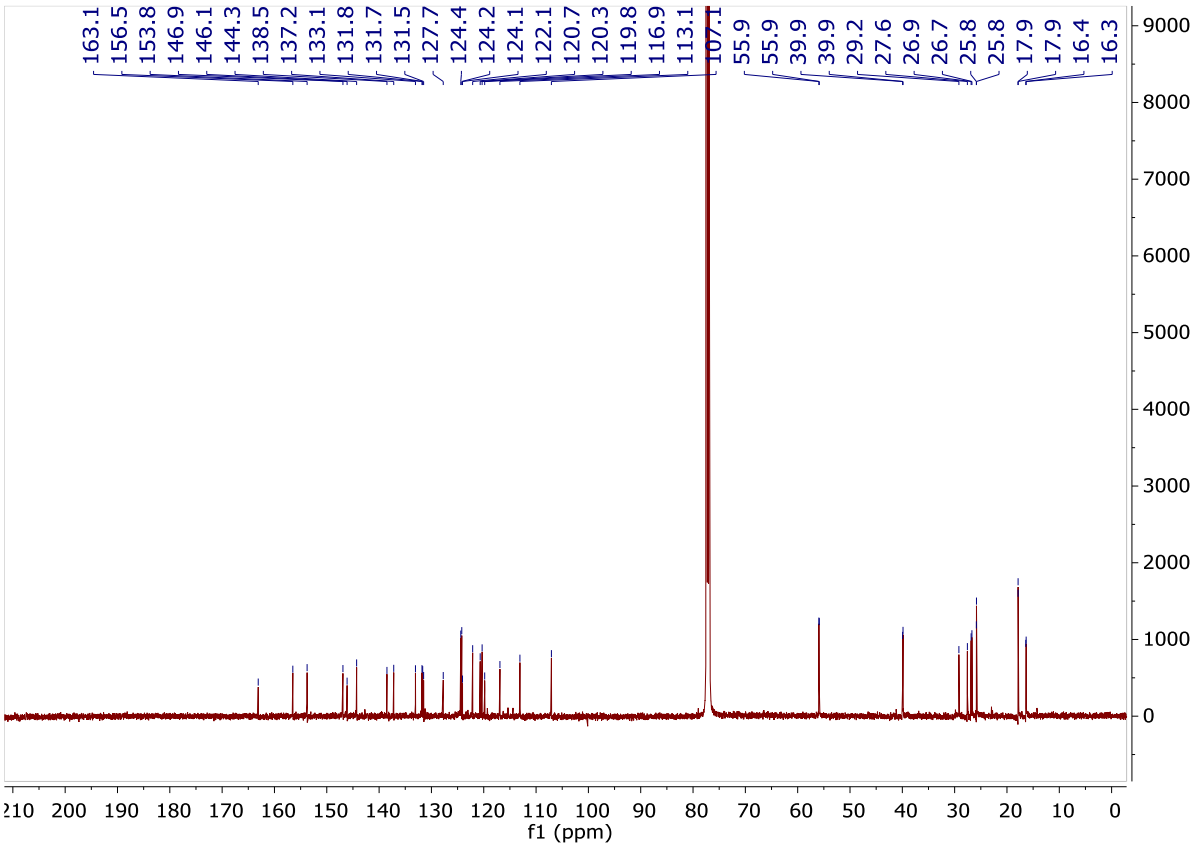

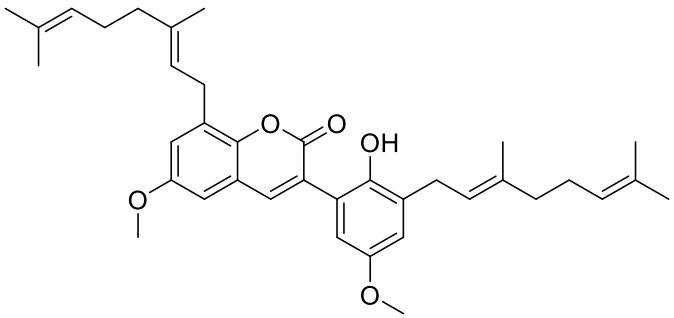

4.1

HSQC of Anibomarin A (4.1) in $CDCl_3$

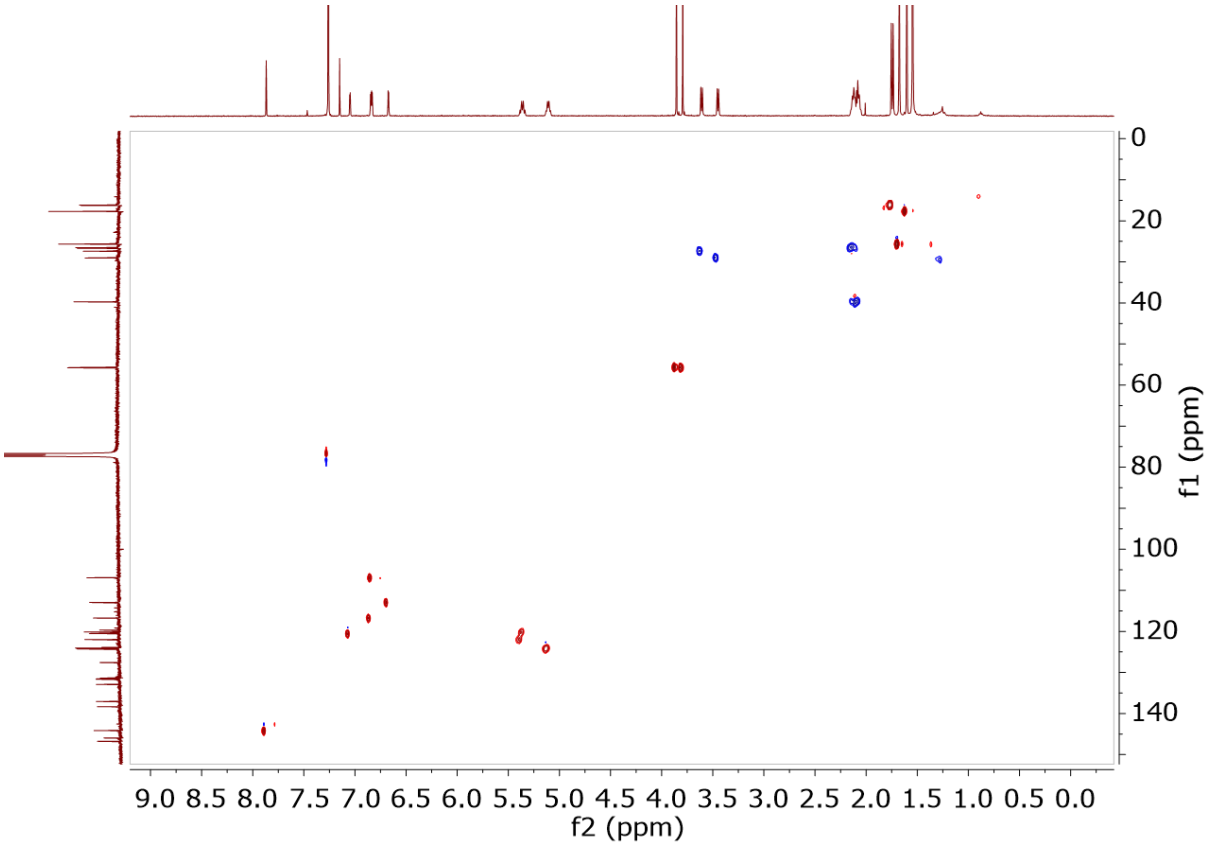

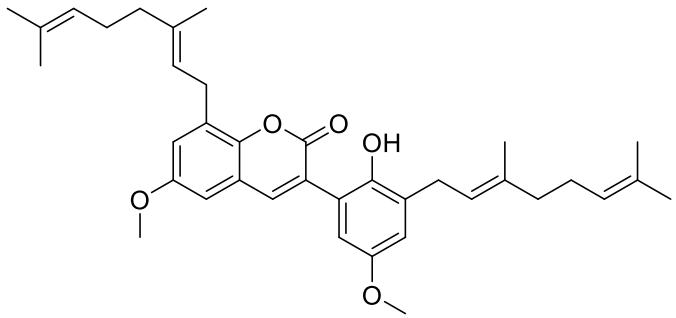

4.1

HMBC of Anibomarin A (4.1) in $CDCl_3$

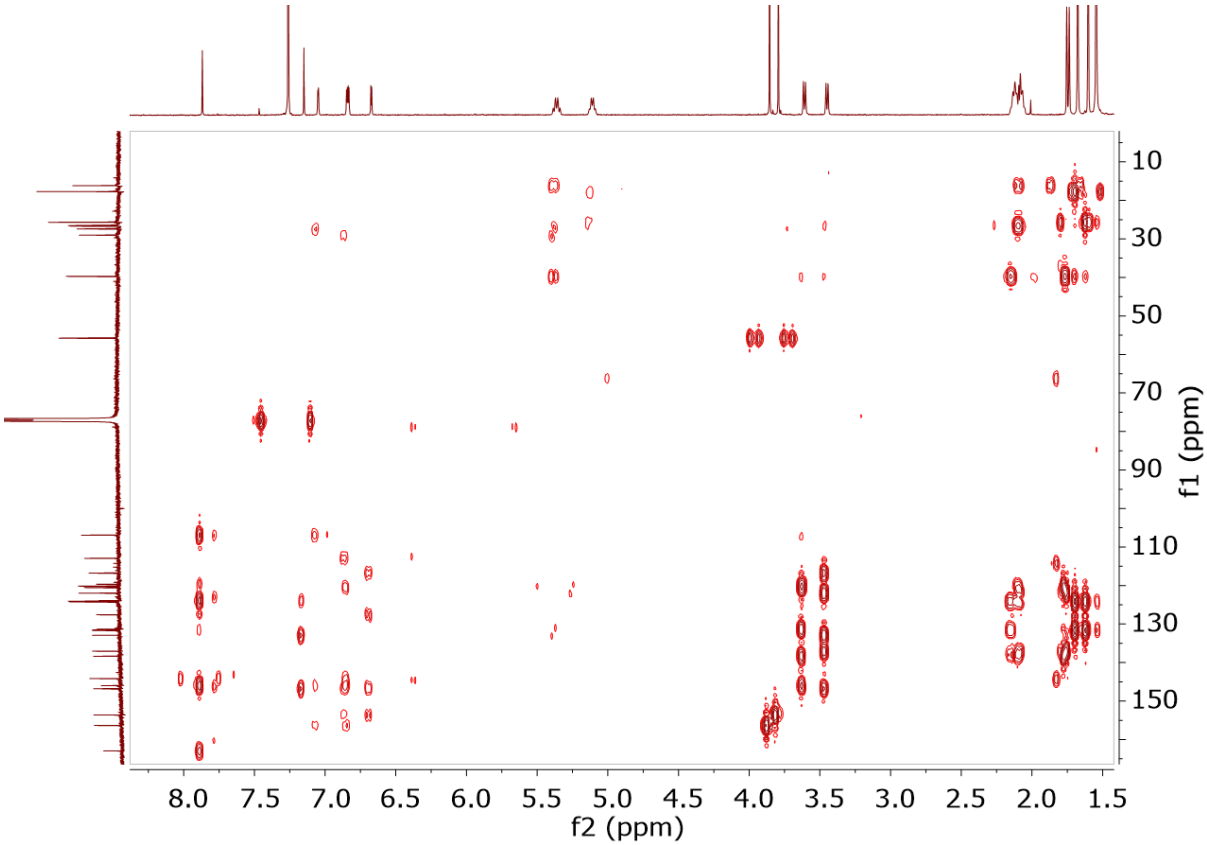

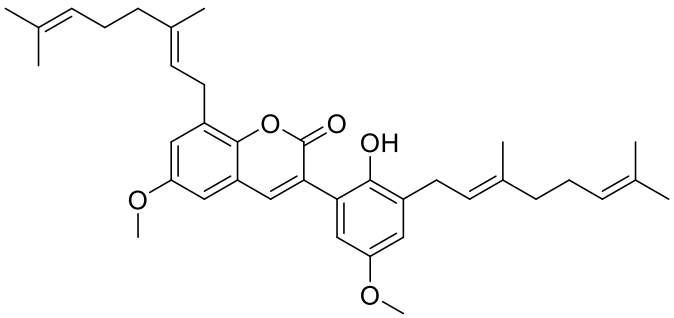

4.1

NOESY of Anibomarin A (4.1) in $CDCl_3$

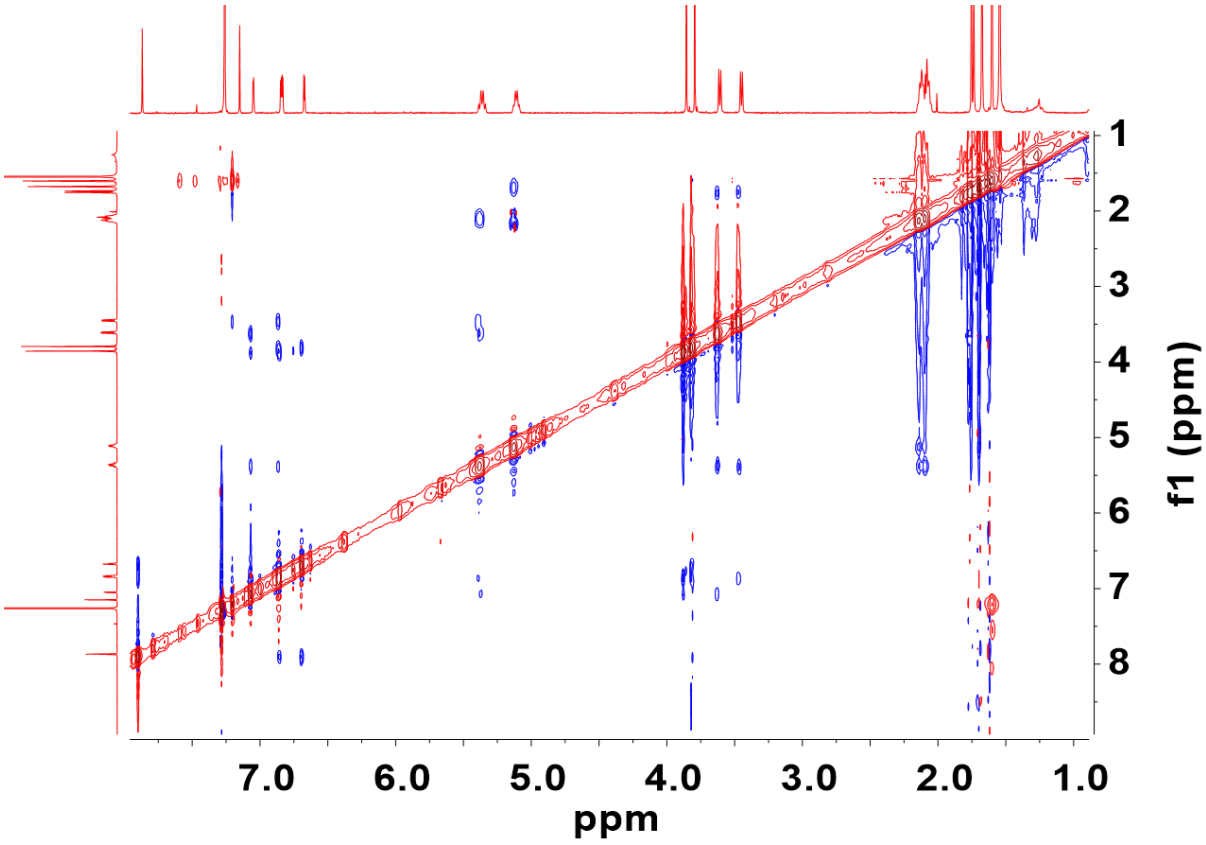

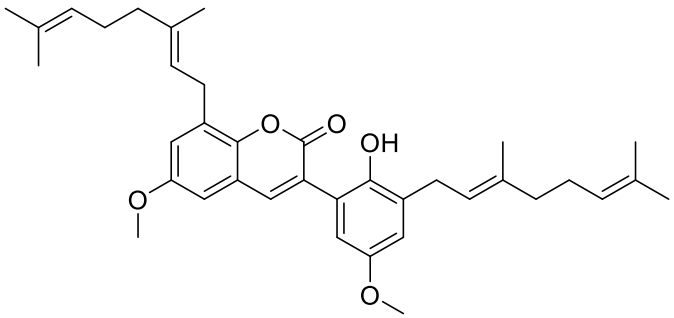

4.1

^{1}H NMR of Anibignan A (4.2) in $CDCl_3$

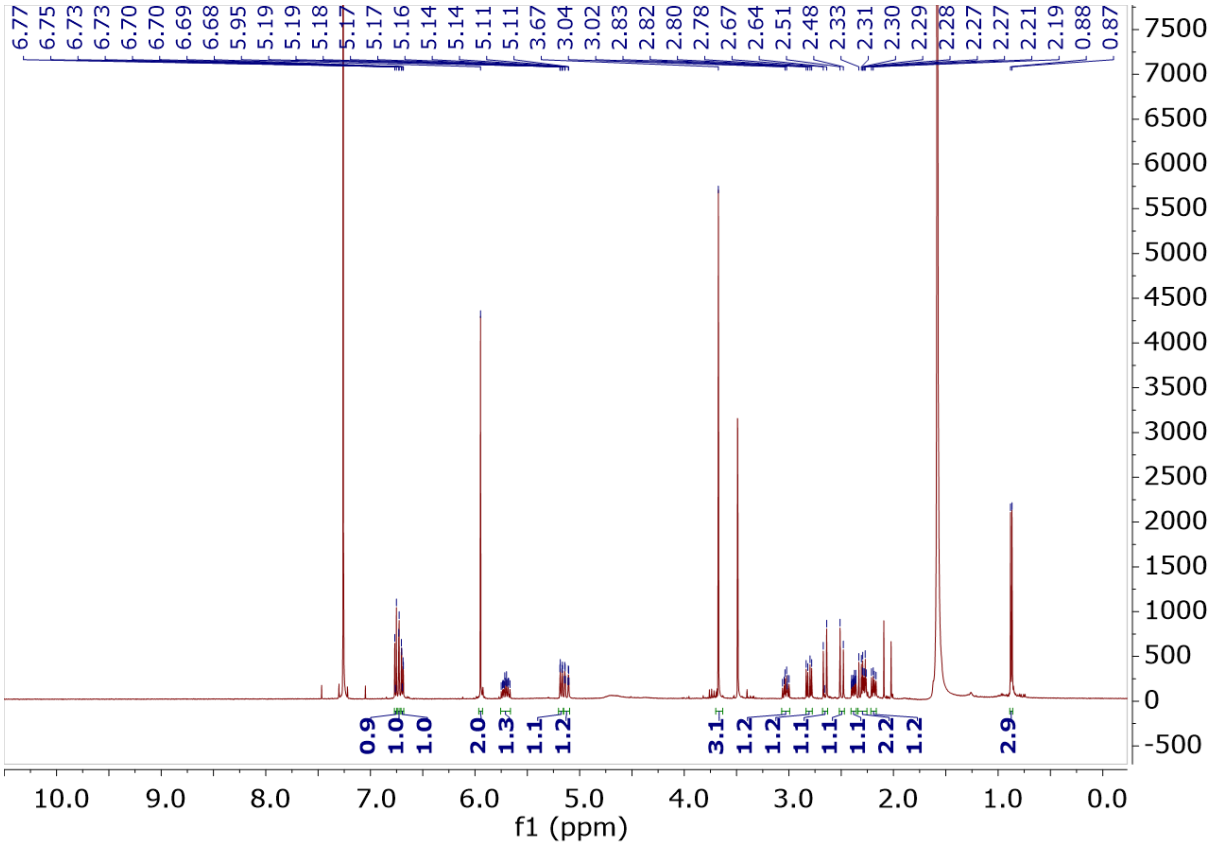

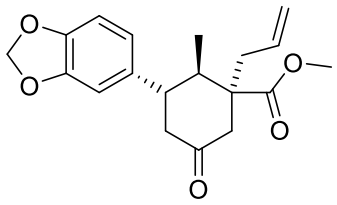

4.2

^{13}C NMR of Anibignan A (4.2) in $CDCl_3$

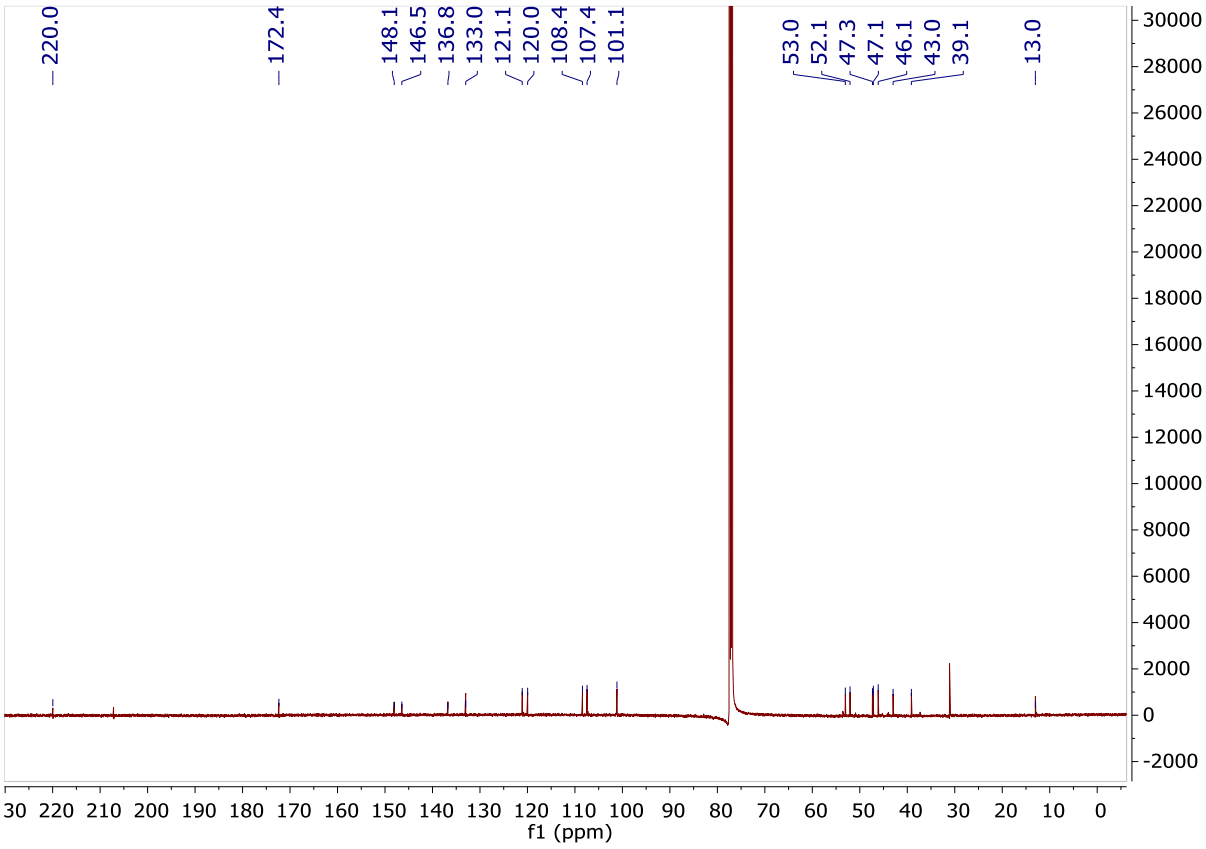

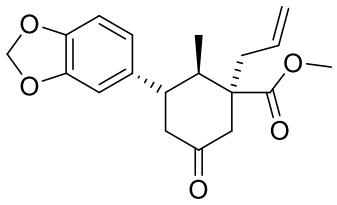

4.2

HSQC of Anibignan A (4.2) in $CDCl_3$

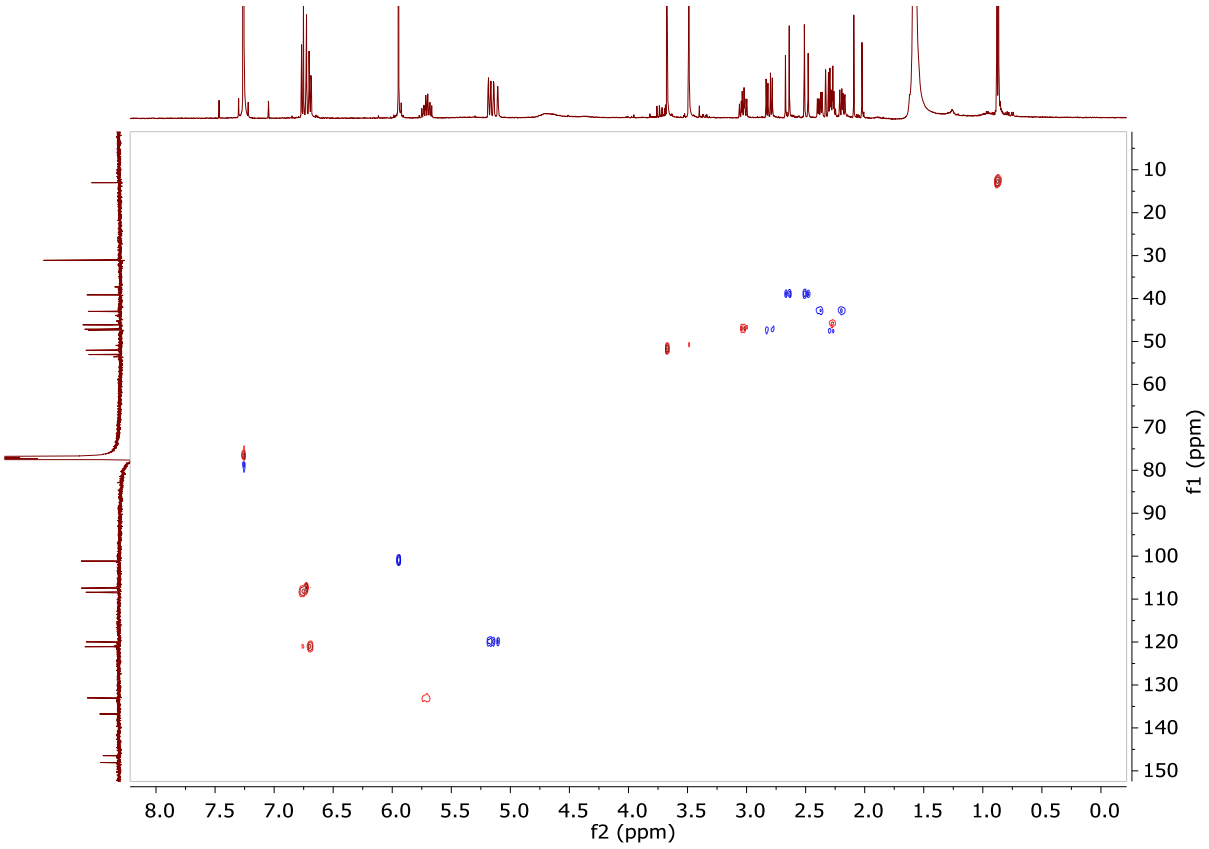

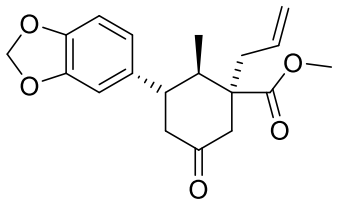

4.2

HMBC of Anibignan A (4.2) in $CDCl_3$

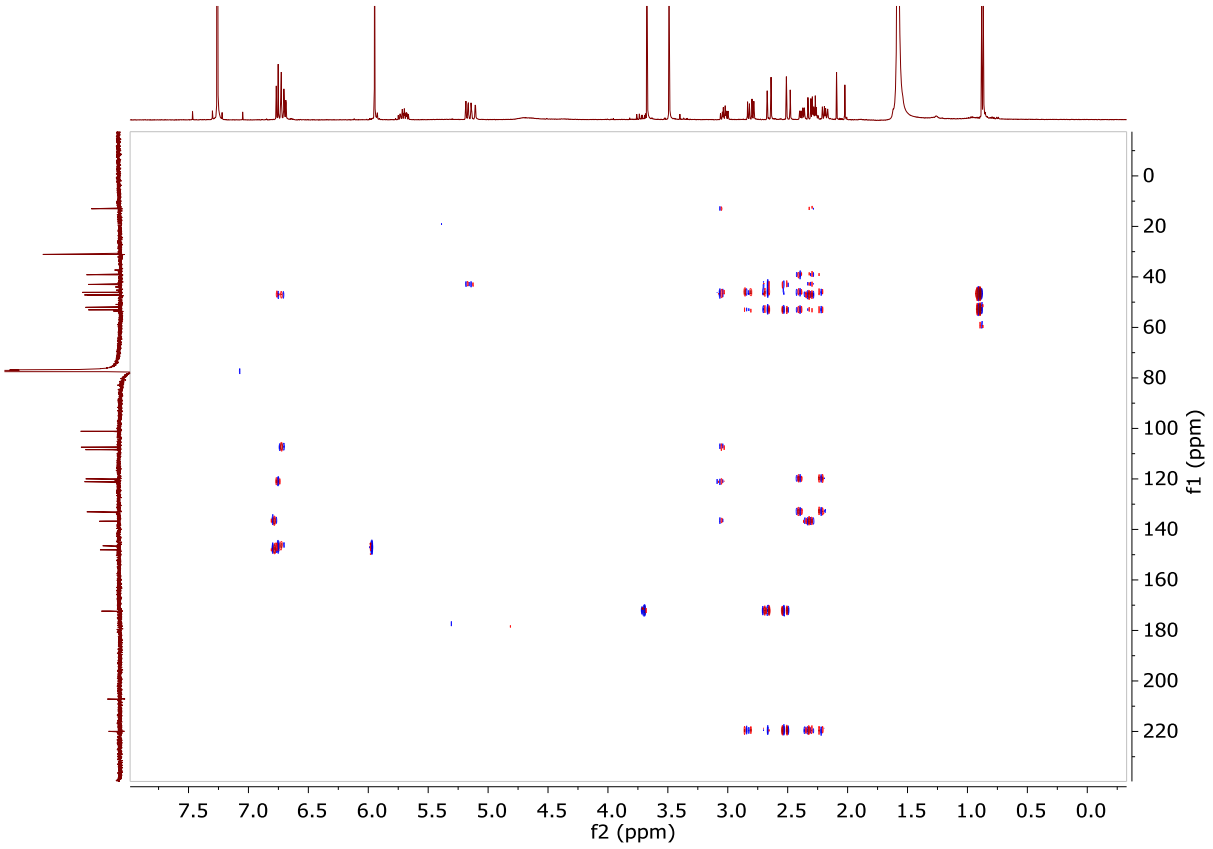

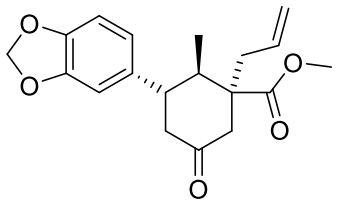

4.2

NOESY of Anibignan A (4.2) in $CDCl_3$

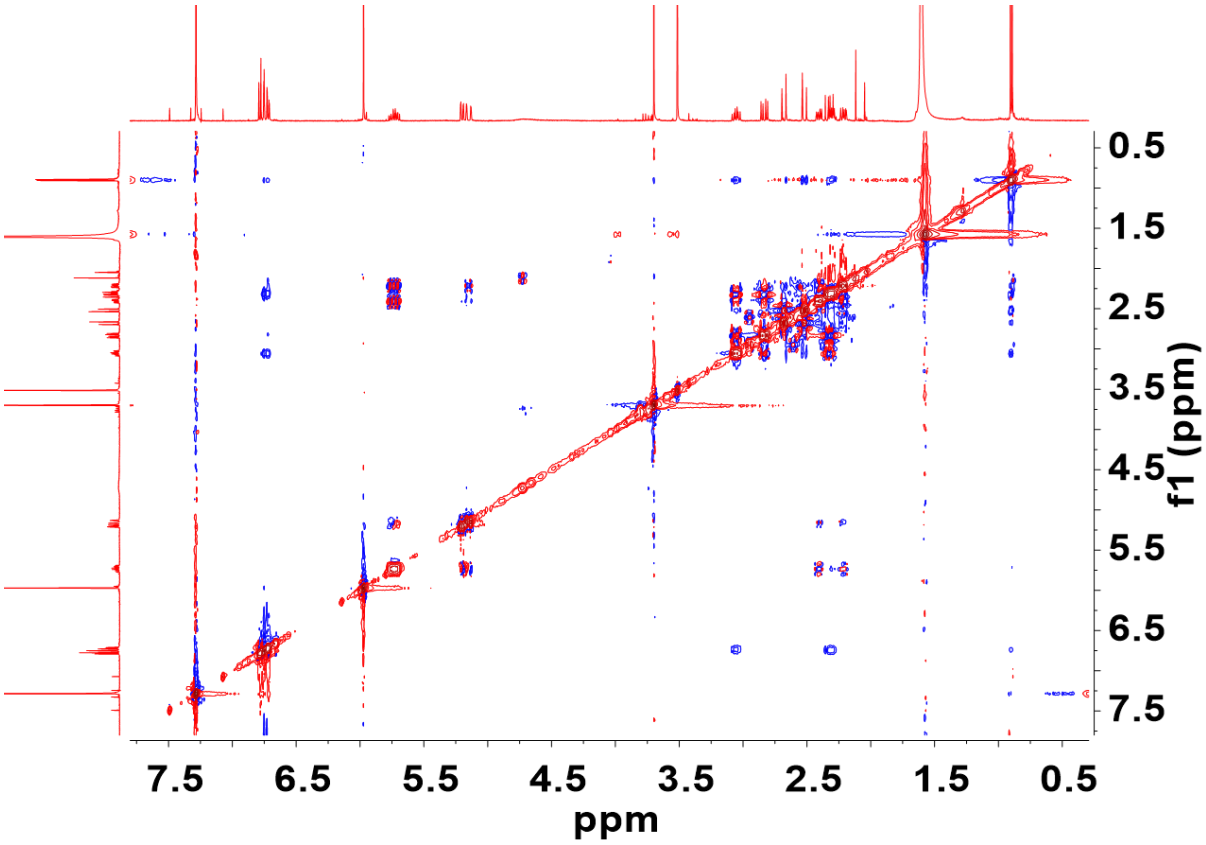

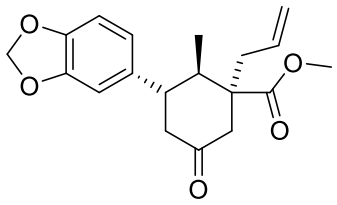

4.2

^{1}H NMR of (+)-Burchellin (4.3) in $CDCl_3$

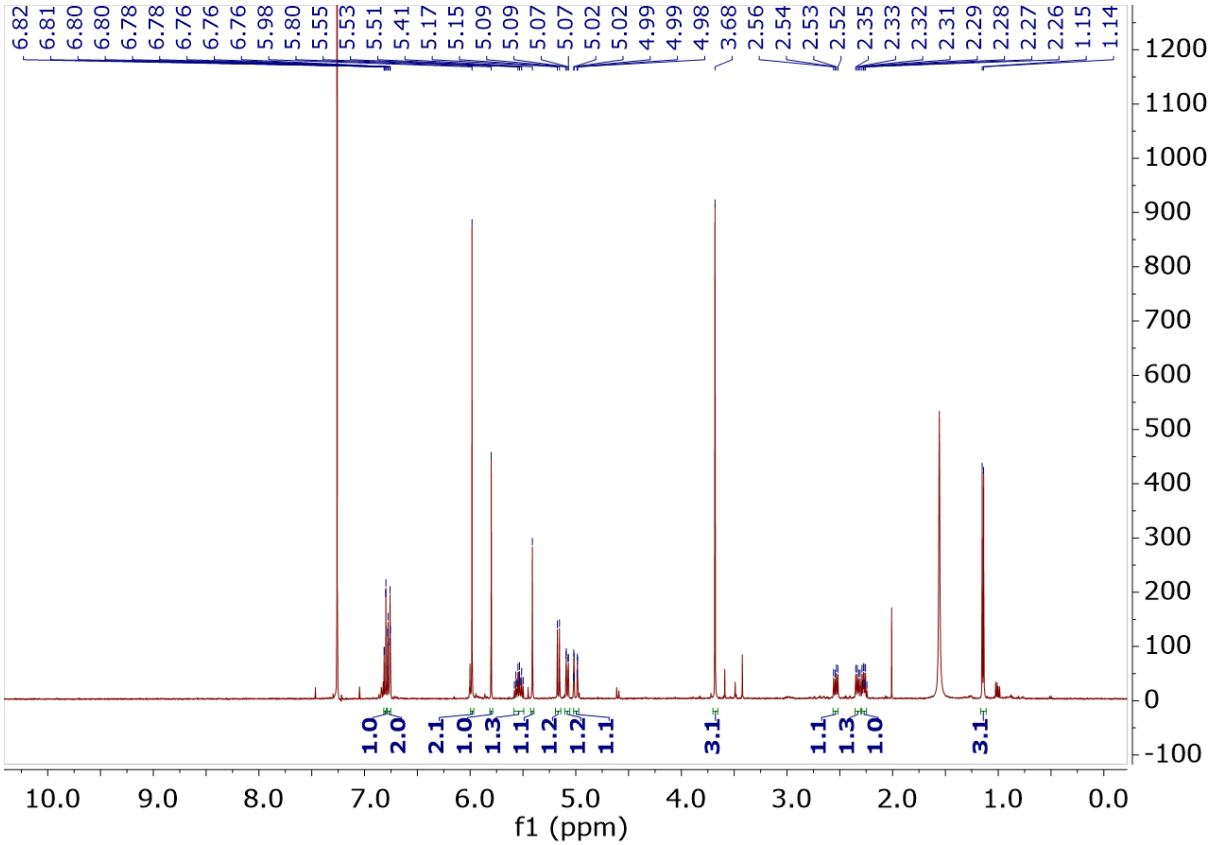

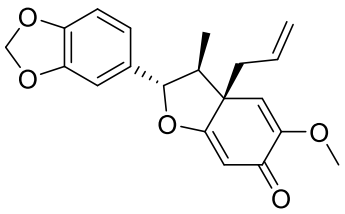

4.3

^{1}H NMR of (7*S*,8*S*,1'*R*)-D$^{8'}$-1'-methoxy-3,4-methylenedioxy-1',6'-dihydro-6'-oxo-7-*O*-4',8,3'-neolignan (4.4) in $CDCl_3$

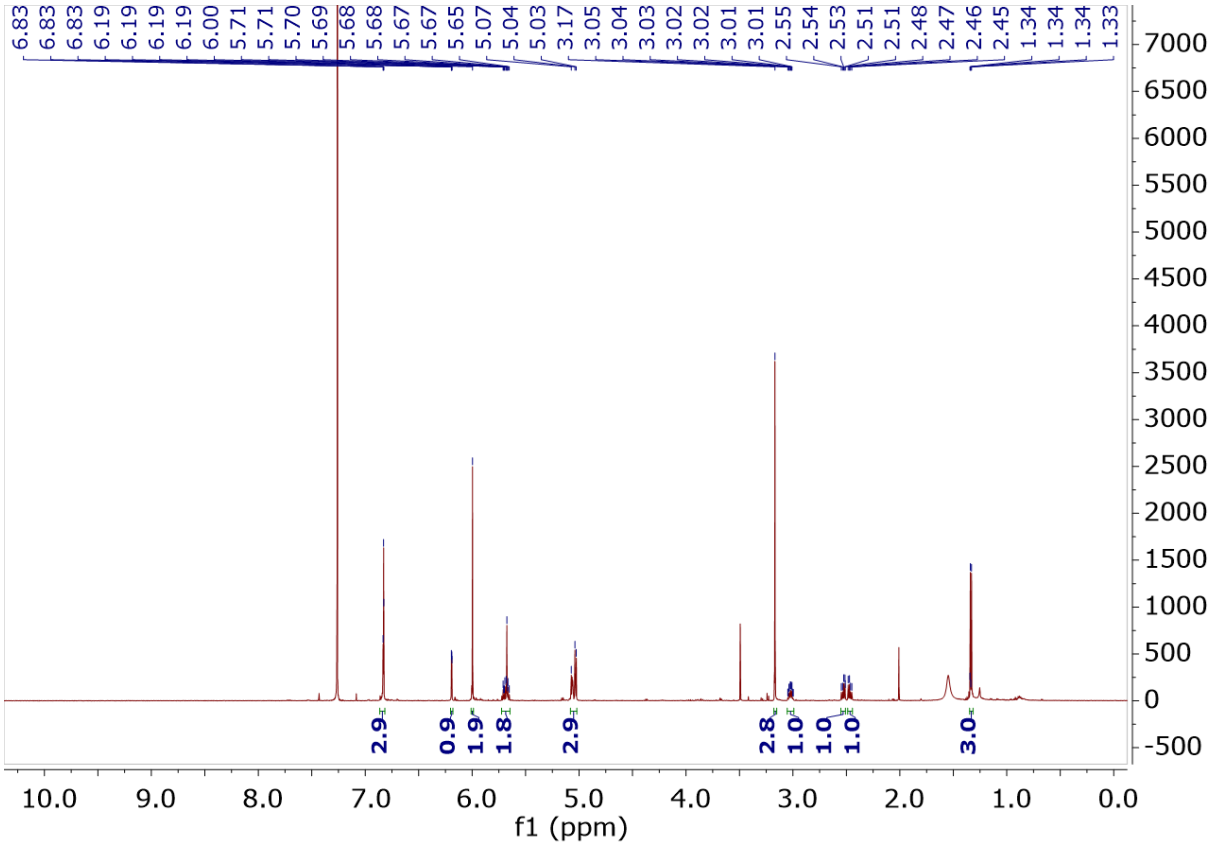

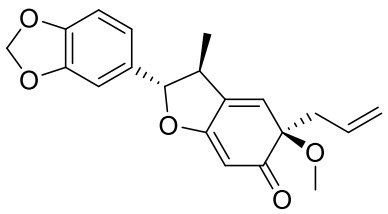

4.4

^{1}H NMR of (7*S*,8*S*)-D$^{8'}$-6'-methoxy- 3,4-methylenedioxy-7-*O*-3',8,4',1'-*O*-7'-neolignan (4.5) in $CDCl_3$

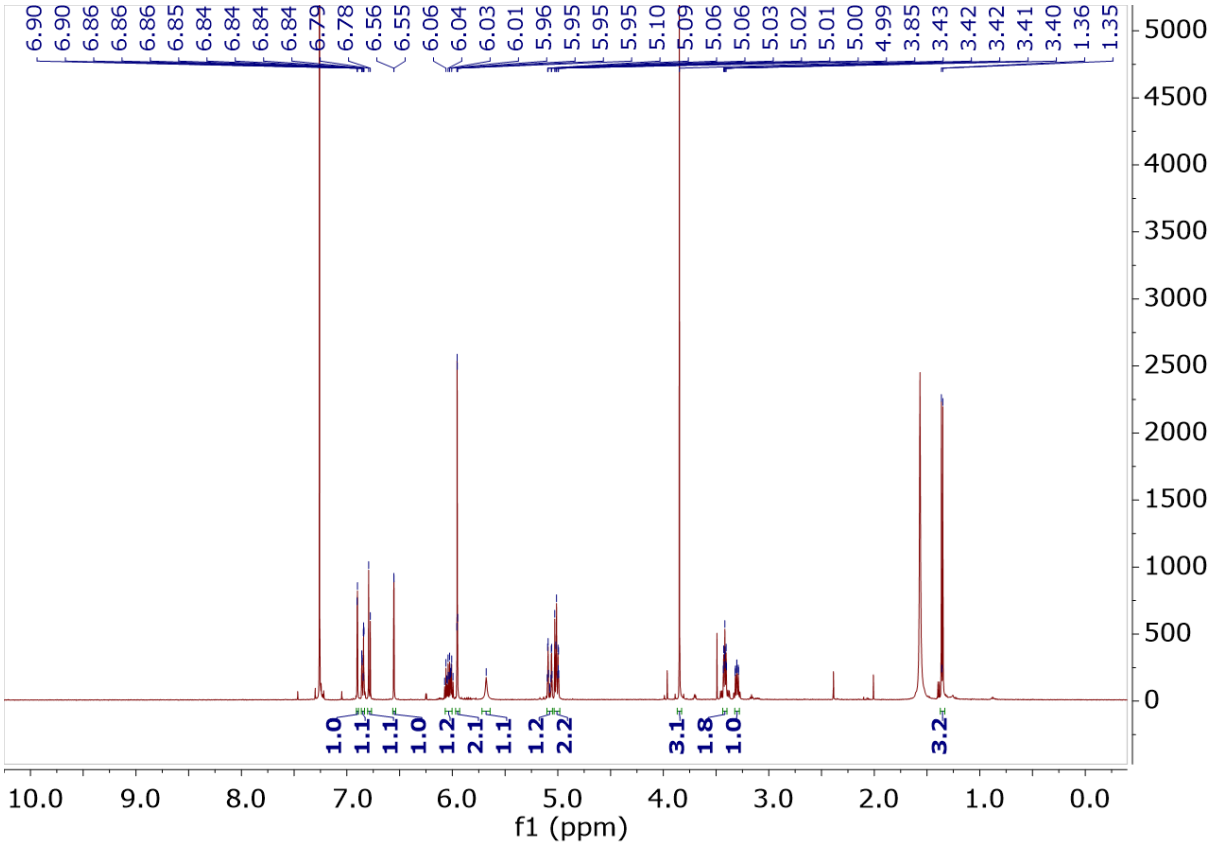

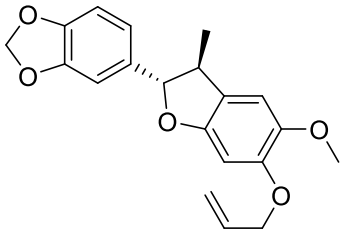

4.5

^{1}H NMR of *trans*-2,3-dihydro-7-allyl-6-hydroxy-5-methoxy-3-methyl-2-(3,4-methylene-dioxyphenyl)benzofuran (4.6) in $CDCl_3$

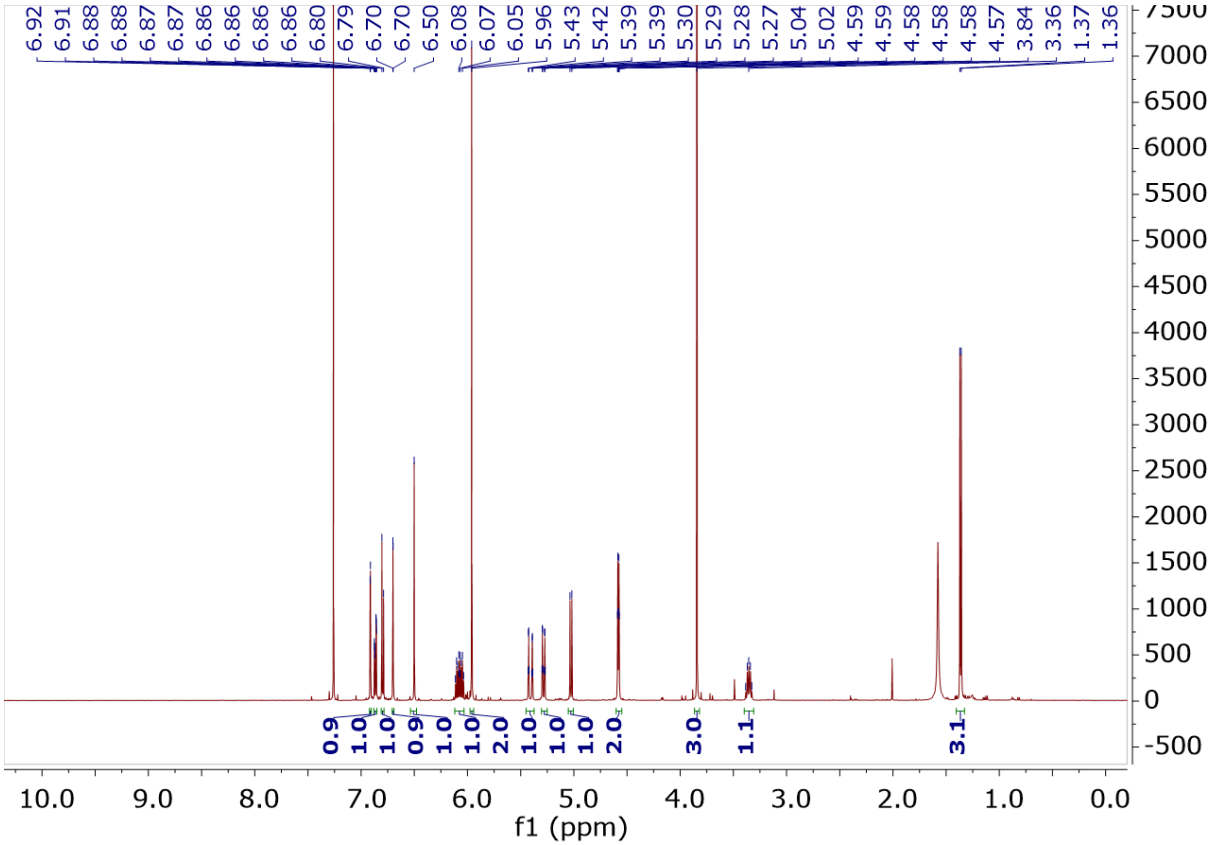

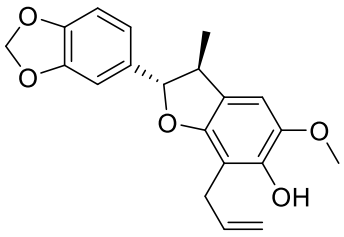

4.6

^{1}H NMR of (7*S*,8*S*,1'*S*,2'*S*,3'*S*)-D$^{5',8'}$-2'-hydroxy-5'-methoxy-3,4-methylenedioxy-4'-oxo-7,3',8,1'-neolignan (4.7) in $CDCl_3$

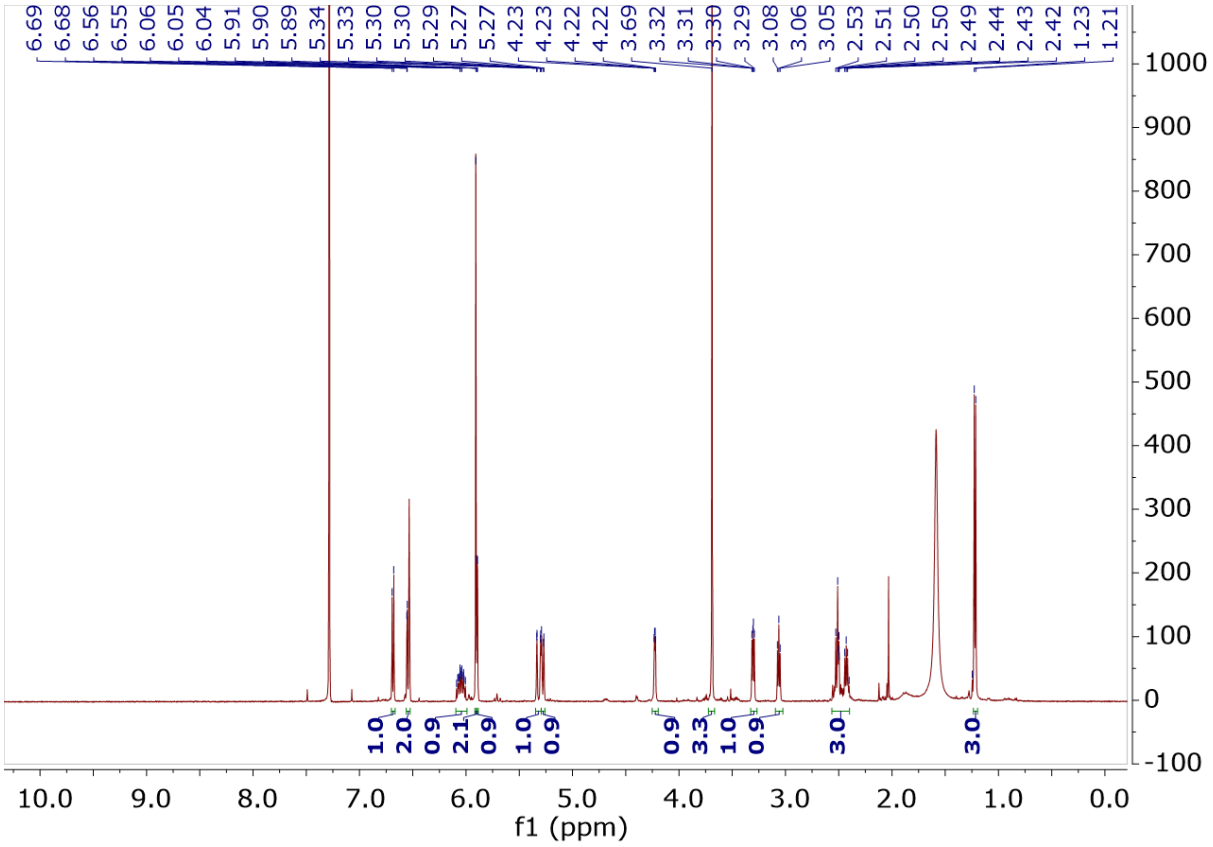

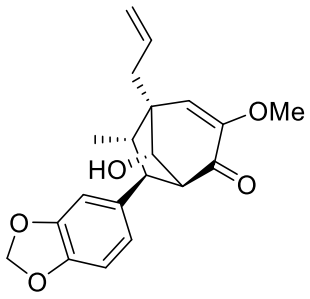

4.7

^{1}H NMR of (7*R*,8*R*,1'*S*,2'*R*,3'*S*)-D$^{5',8'}$-2'-hydroxy-6'-methoxy-3,4-methylenedioxy-4'-oxo-7.3',8.1'-neolignan (4.8) in $CDCl_3$

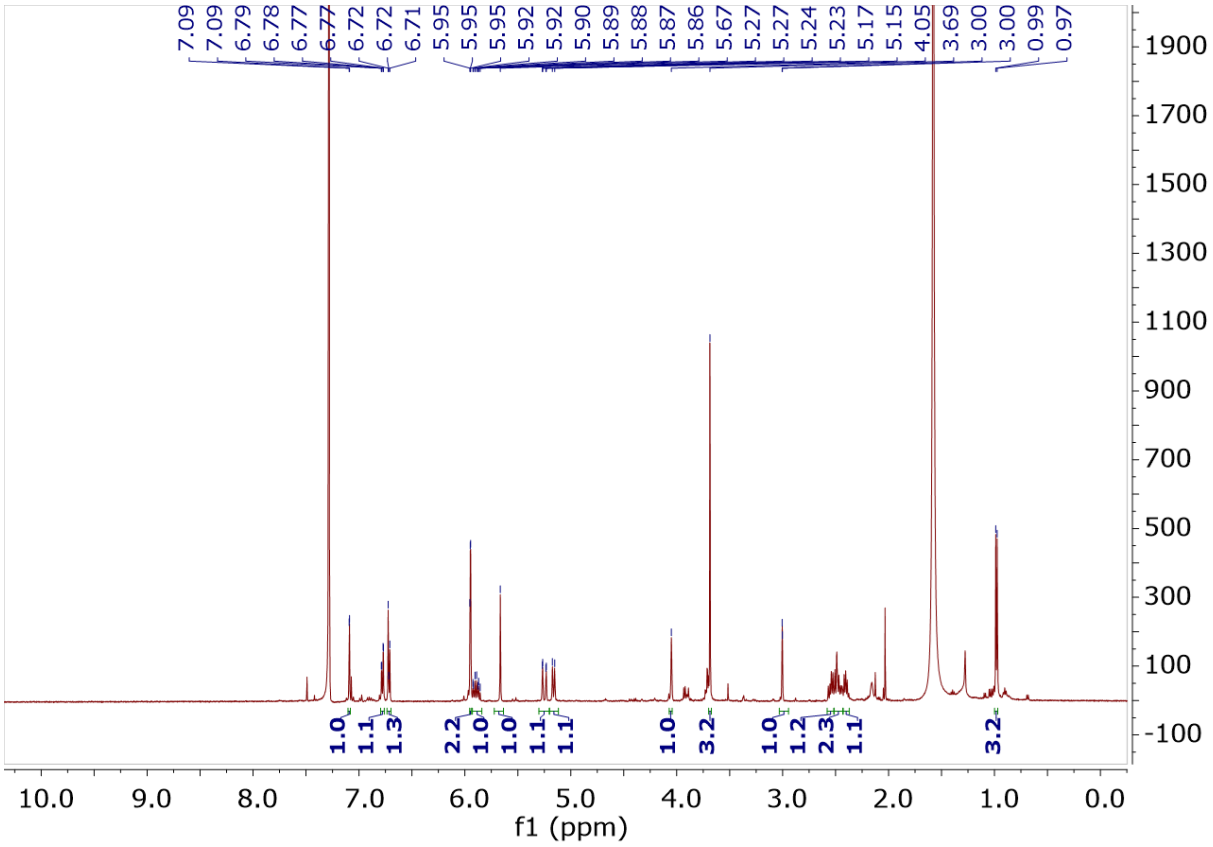

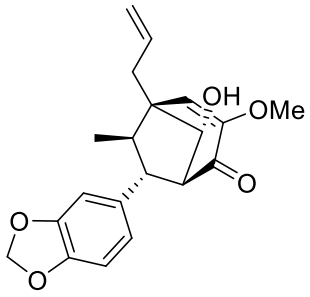

4.8

^{1}H NMR of Malleastrumolide A (5.1) in $CDCl_3$

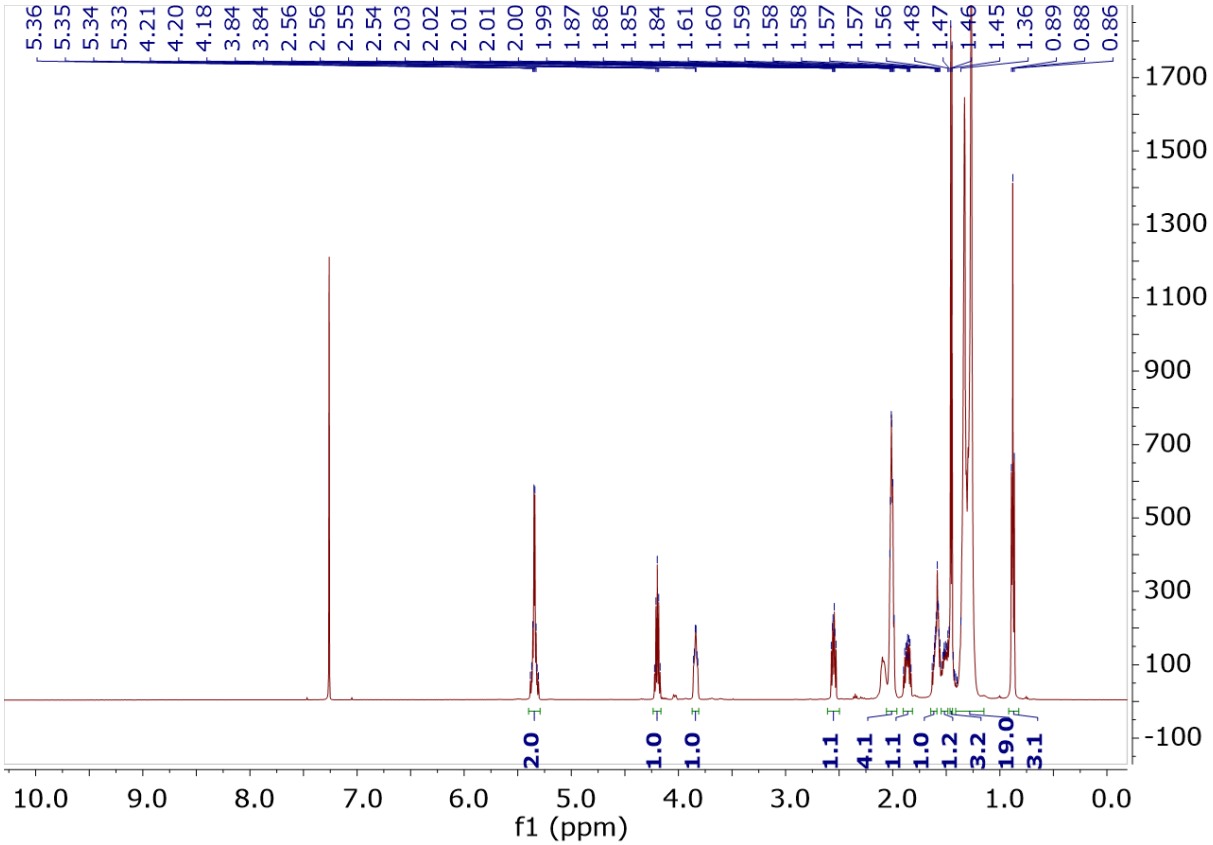

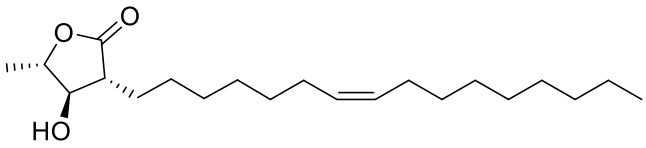

5.1

HSQC of Malleastrumolide A (5.1) in $CDCl_3$

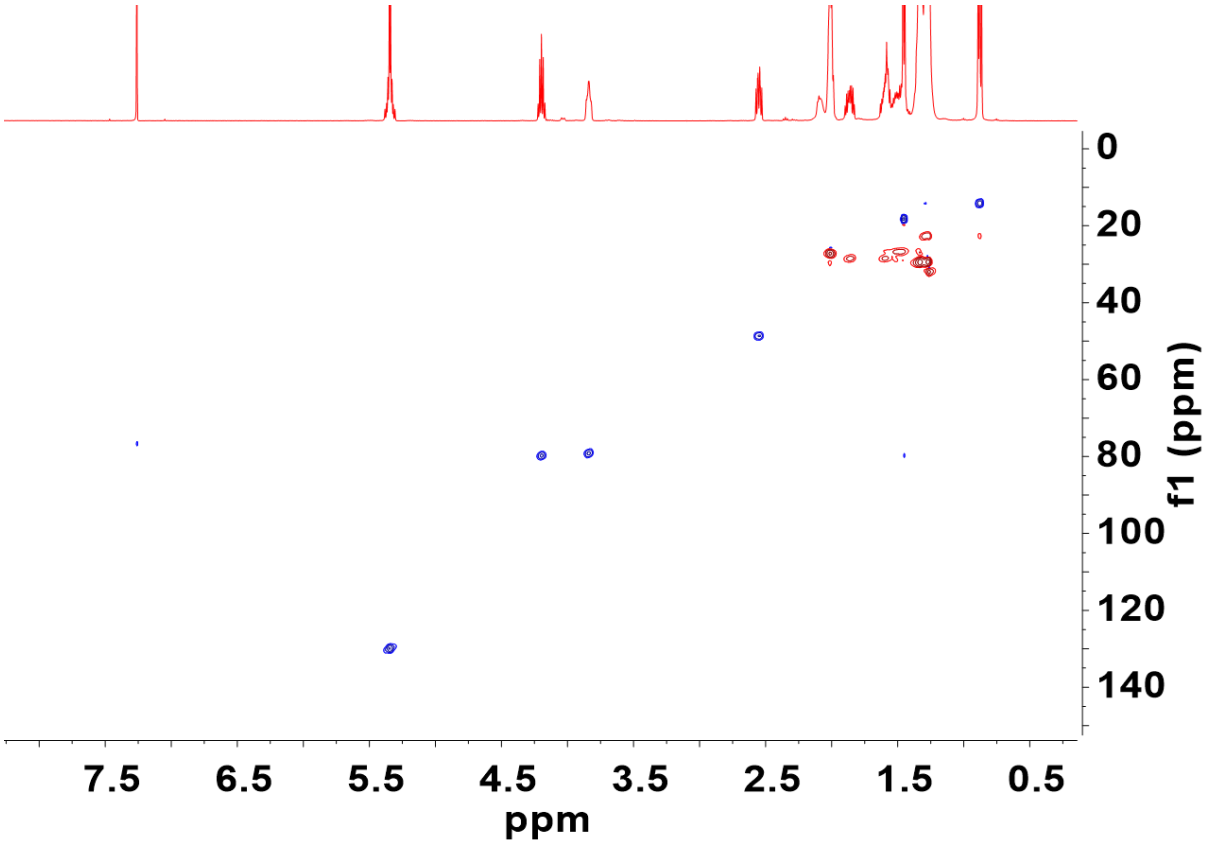

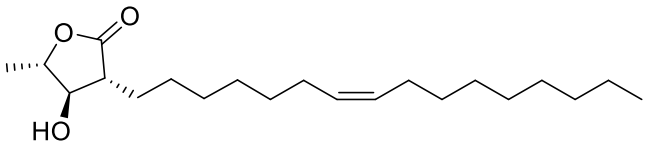

5.1

HMBC of Malleastrumolide A (5.1) in $CDCl_3$

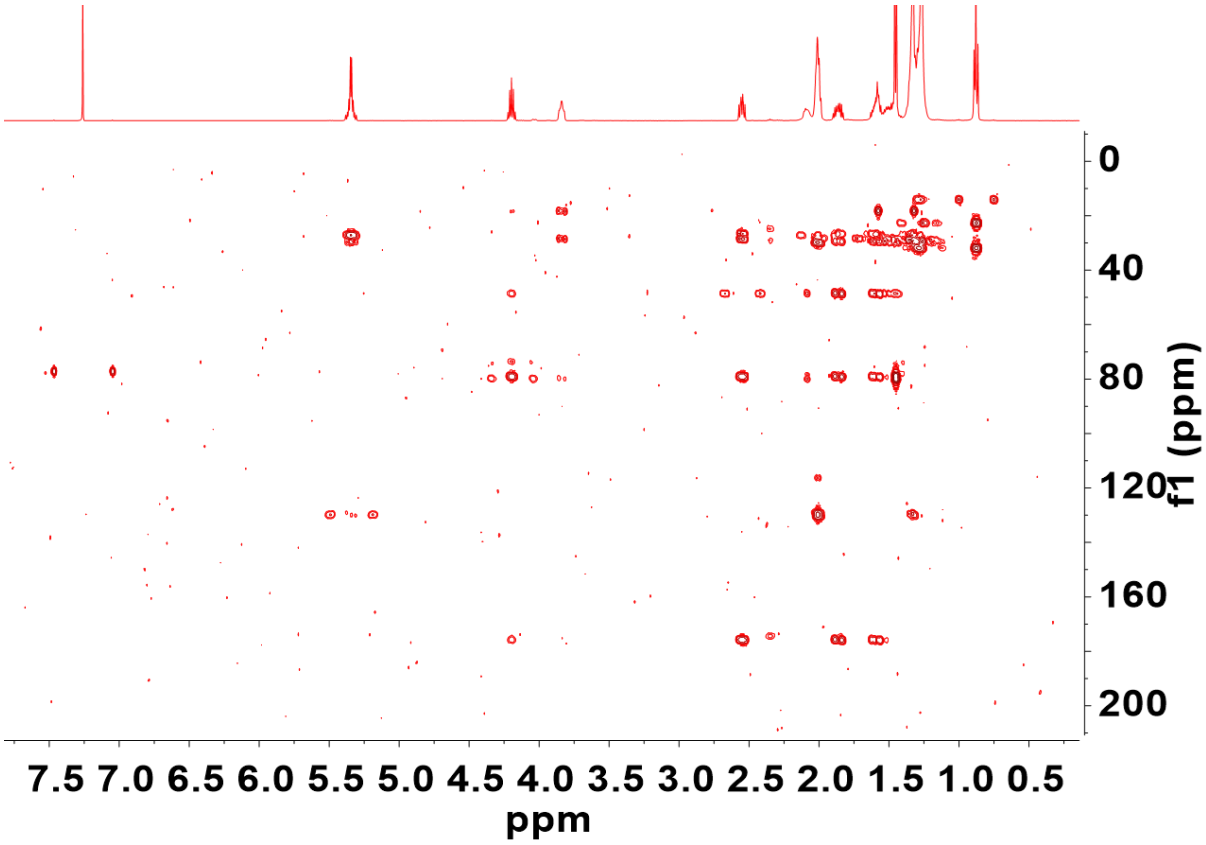

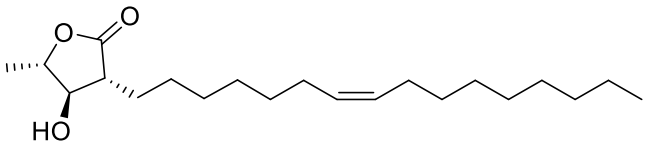

5.1

NOESY of Malleastrumolide A (5.1) in $CDCl_3$

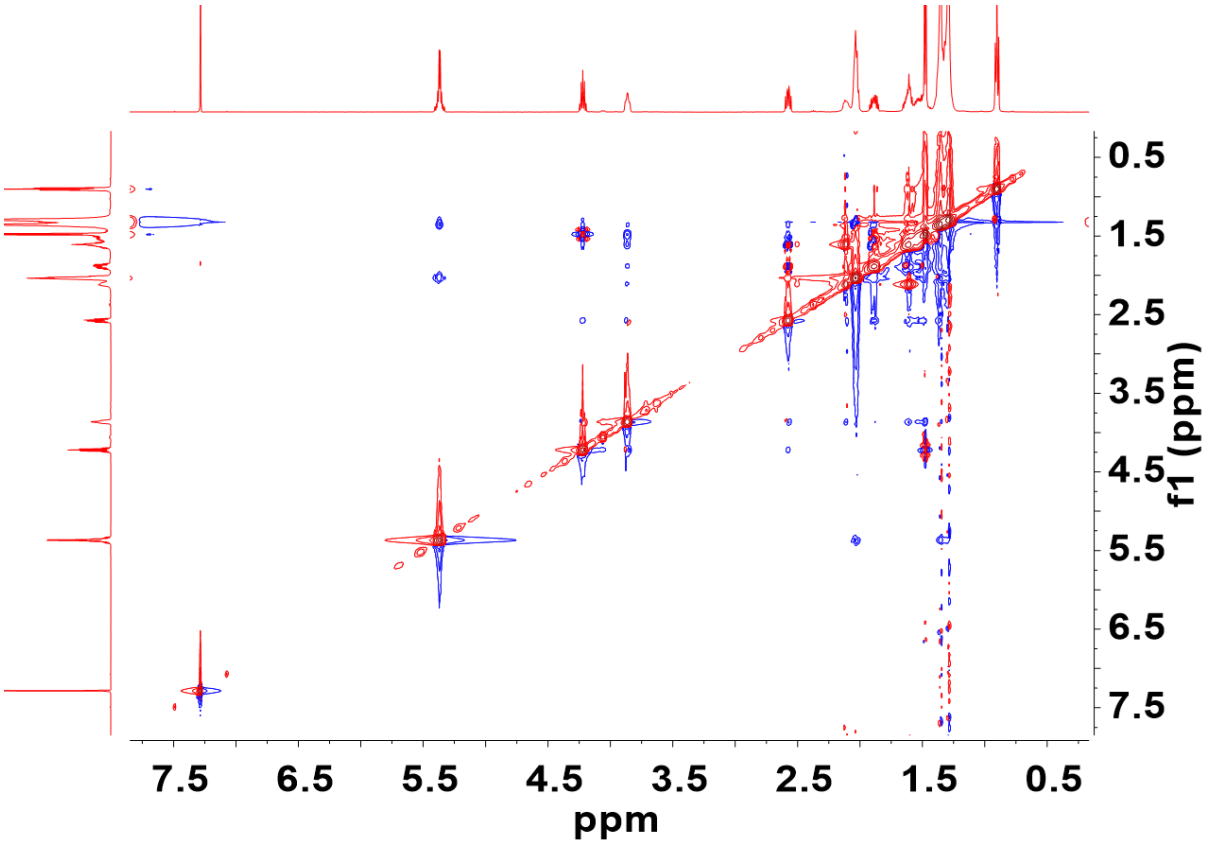

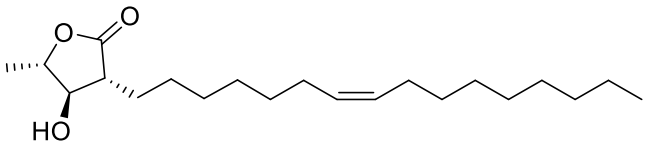

5.1

^{1}H NMR of 4,4'-diallyl-1,2,6,4'-tetrahydrodibenzo[*b*,*d*]furan-3'-ol (6.1) in $CDCl_3$

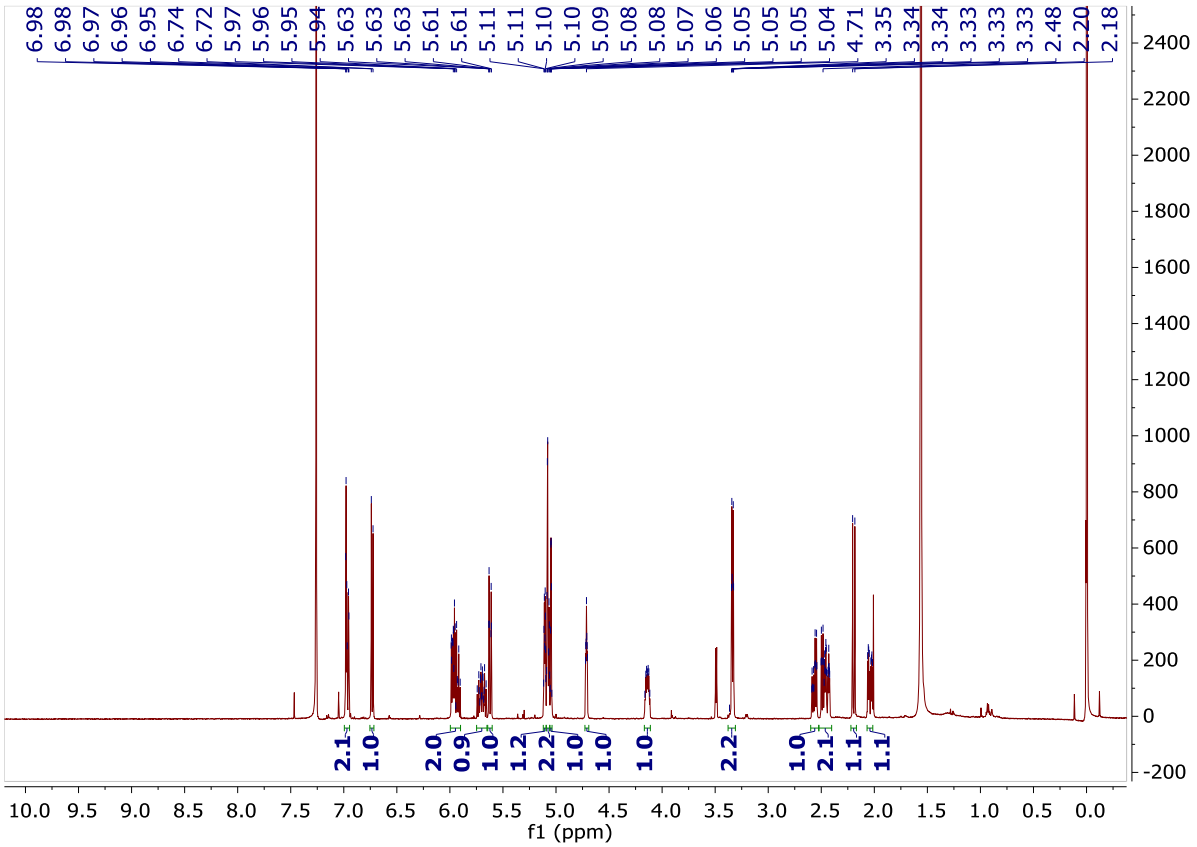

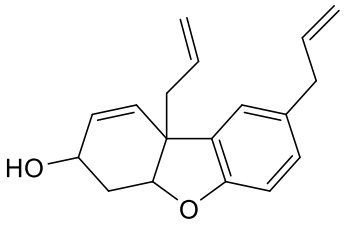

6.1

^{13}C NMR of 4,4'-diallyl-1,2,6,4'-tetrahydrodibenzo[*b,d*]furan-3'-ol (6.1) in $CDCl_3$

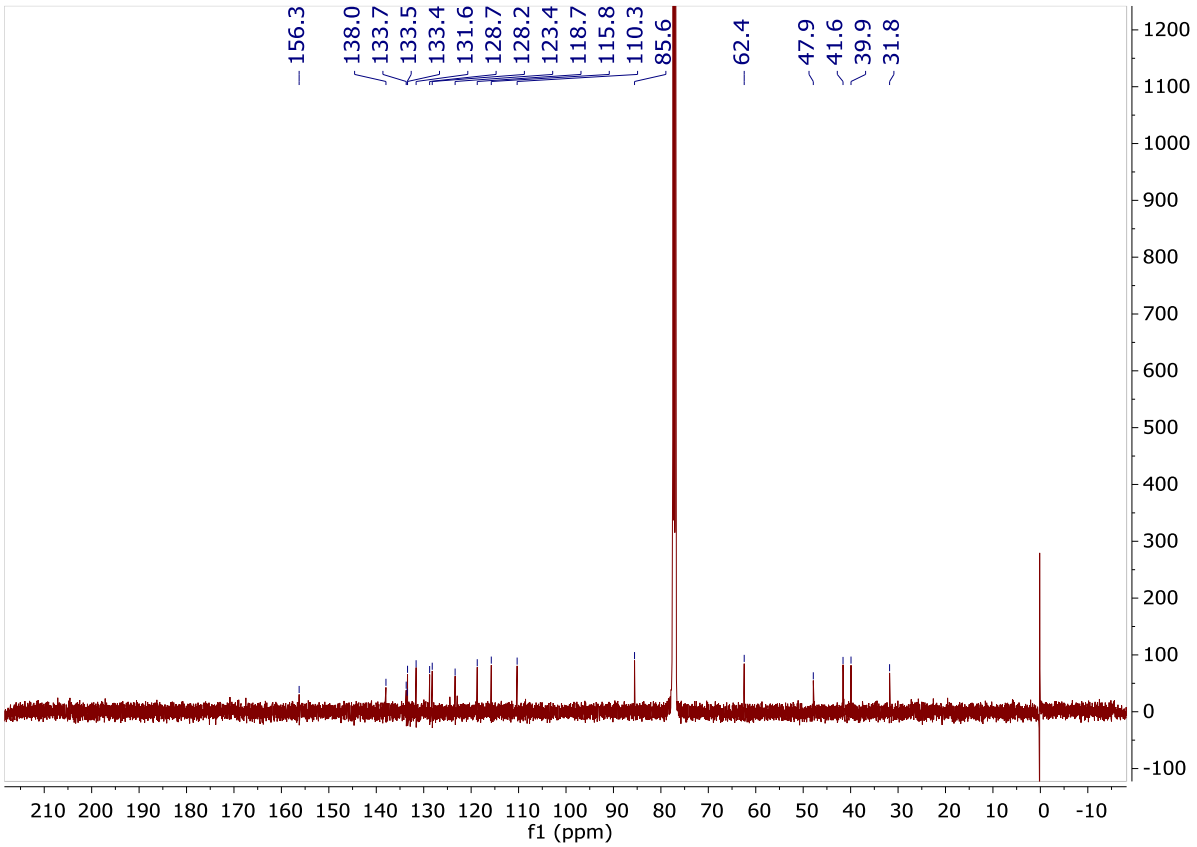

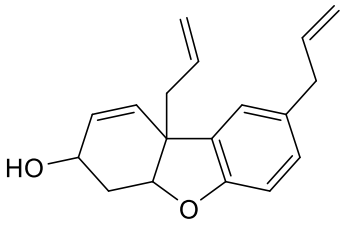

6.1

COSY of 4,4'-diallyl-1,2,6,4'-tetrahydrodibenzo[*b*,*d*]furan-3'-ol (6.1) in $CDCl_3$

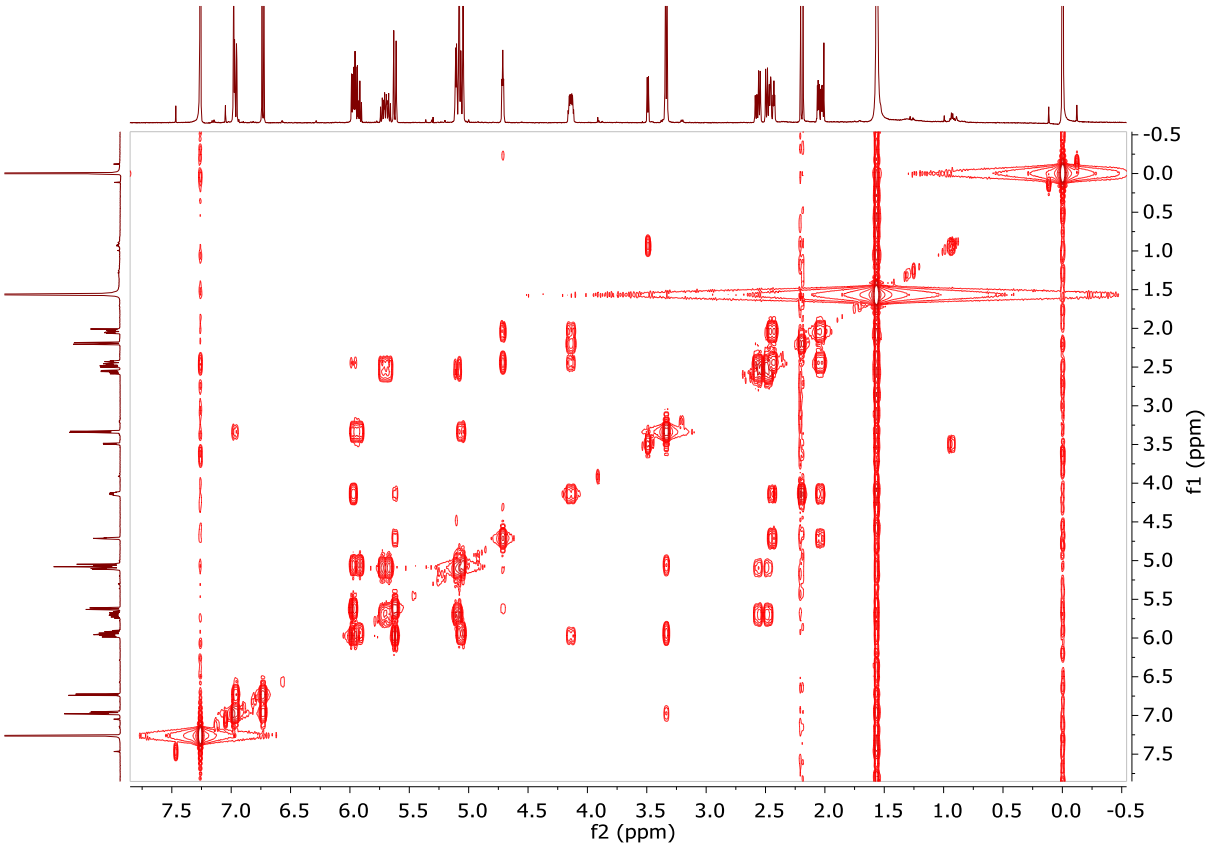

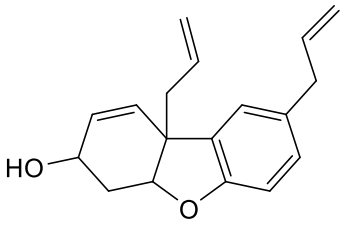

6.1

HSQC of 4,4'-diallyl-1,2,6,4'-tetrahydrodibenzo[*b*,*d*]furan-3'-ol (6.1) in $CDCl_3$

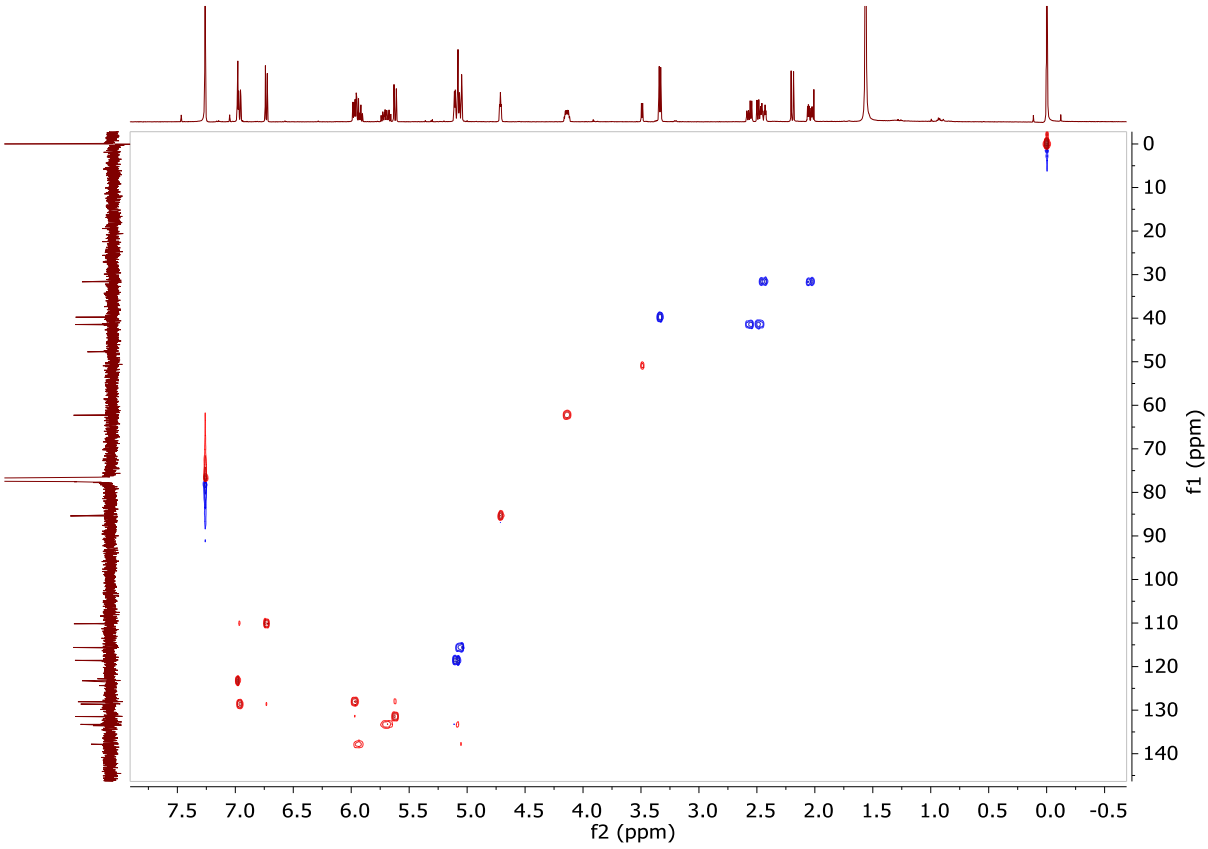

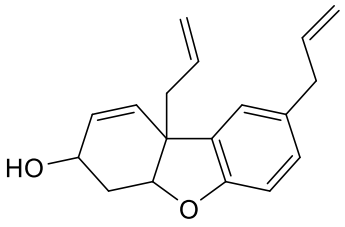

6.1

HMBC of 4,4'-diallyl-1,2,6,4'-tetrahydrodibenzo[*b,d*]furan-3'-ol (6.1) in $CDCl_3$

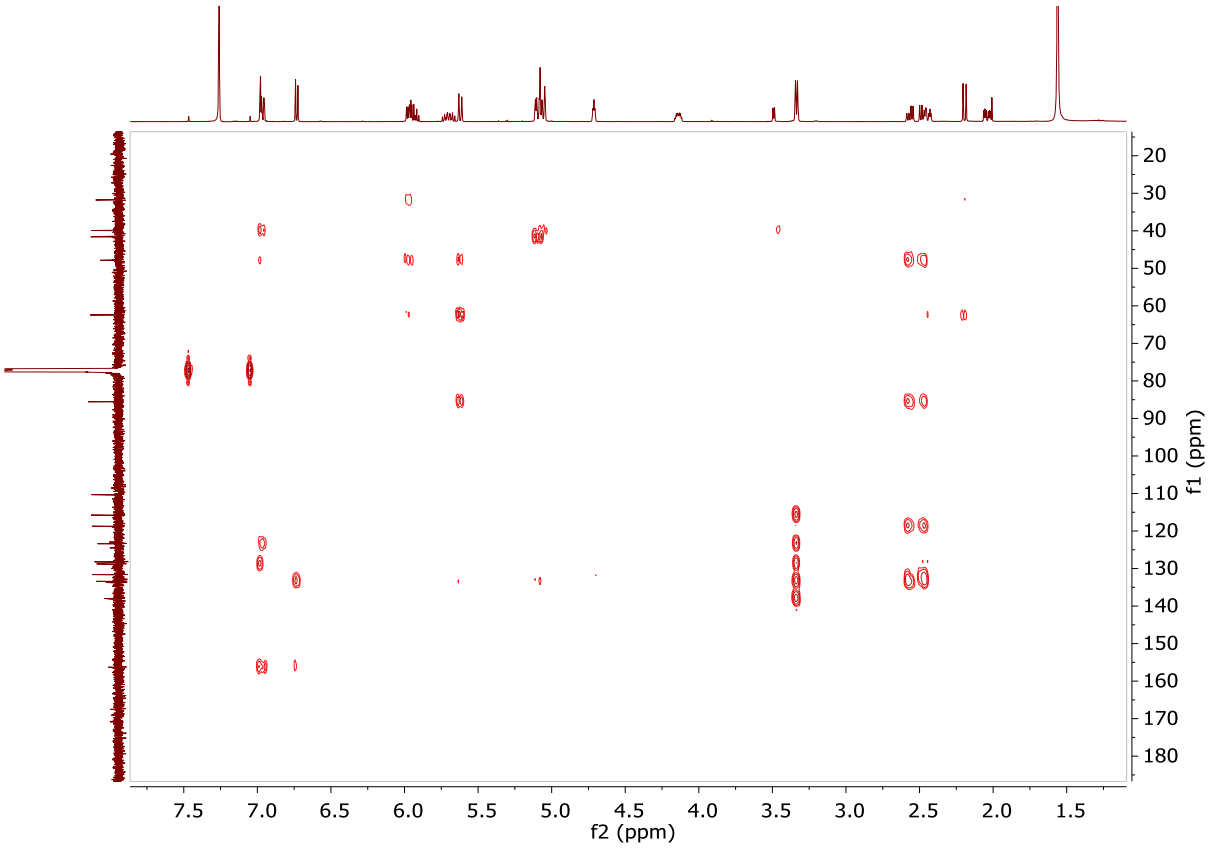

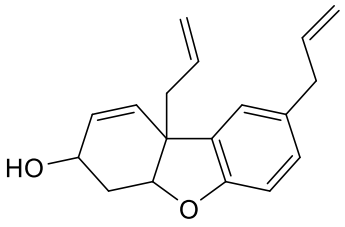

6.1

^{1}H NMR of 3,3'-diallyl-4'-((4-hydroxyphenethyl)amino)-[1,1'-bi- phenyl]-4-ol (6.2) in $CDCl_3$

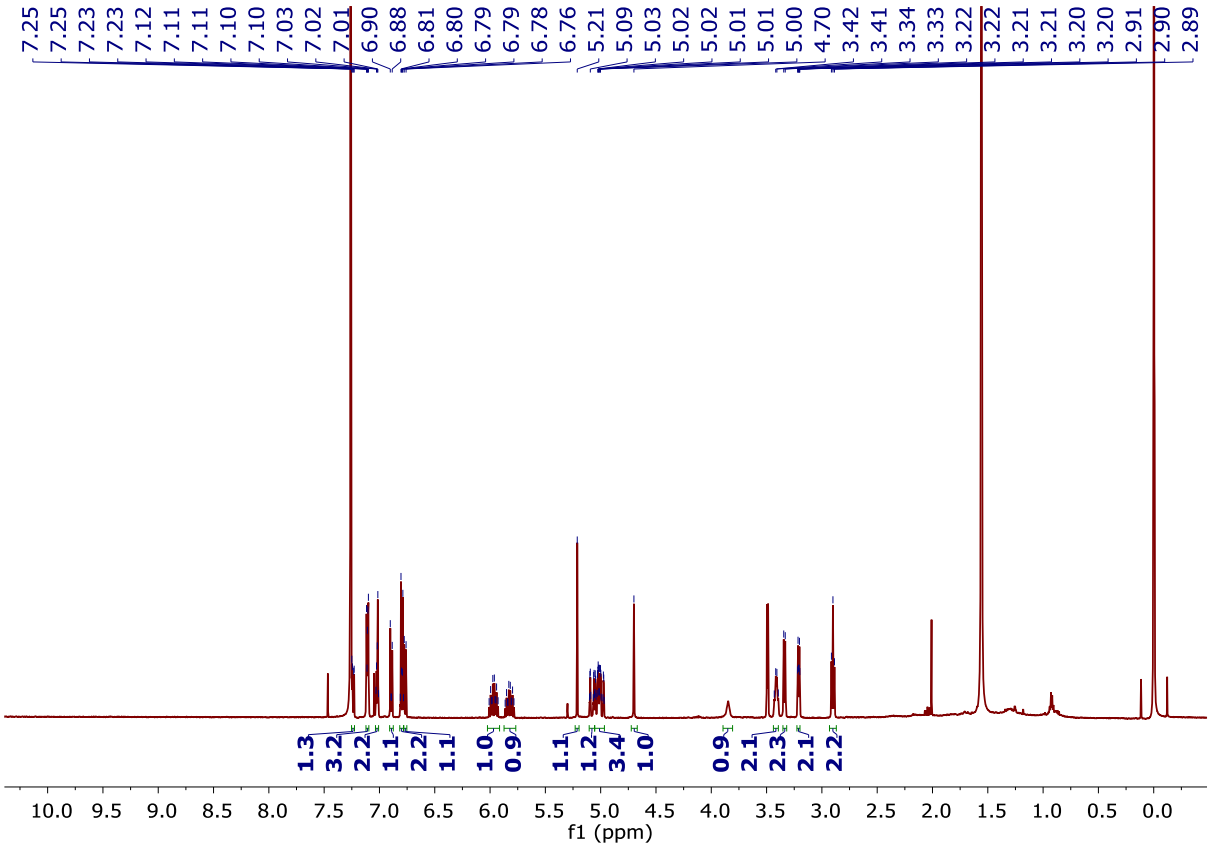

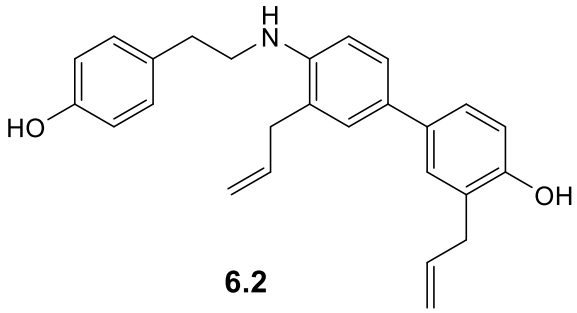

6.2

^{13}C NMR of 3,3'-diallyl-4'-((4-hydroxyphenethyl)amino)-[1,1'-bi- phenyl]-4-ol (6.2) in $CDCl_3$

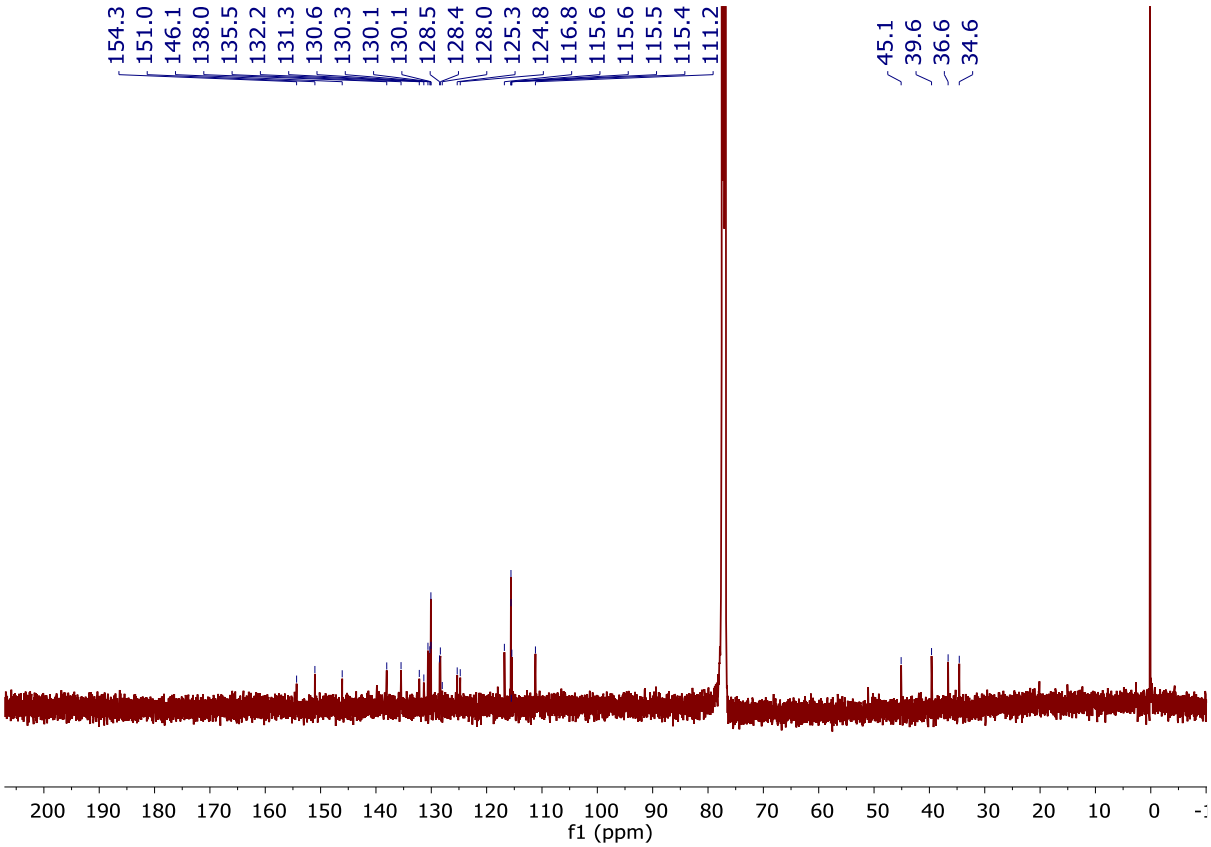

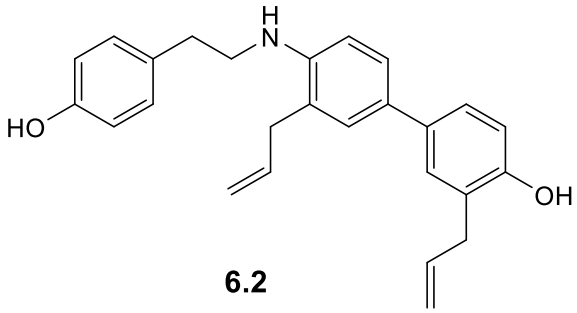

6.2

HSQC of 3,3'-diallyl-4'-((4-hydroxyphenethyl)amino)-[1,1'-bi- phenyl]-4-ol (6.2) in $CDCl_3$

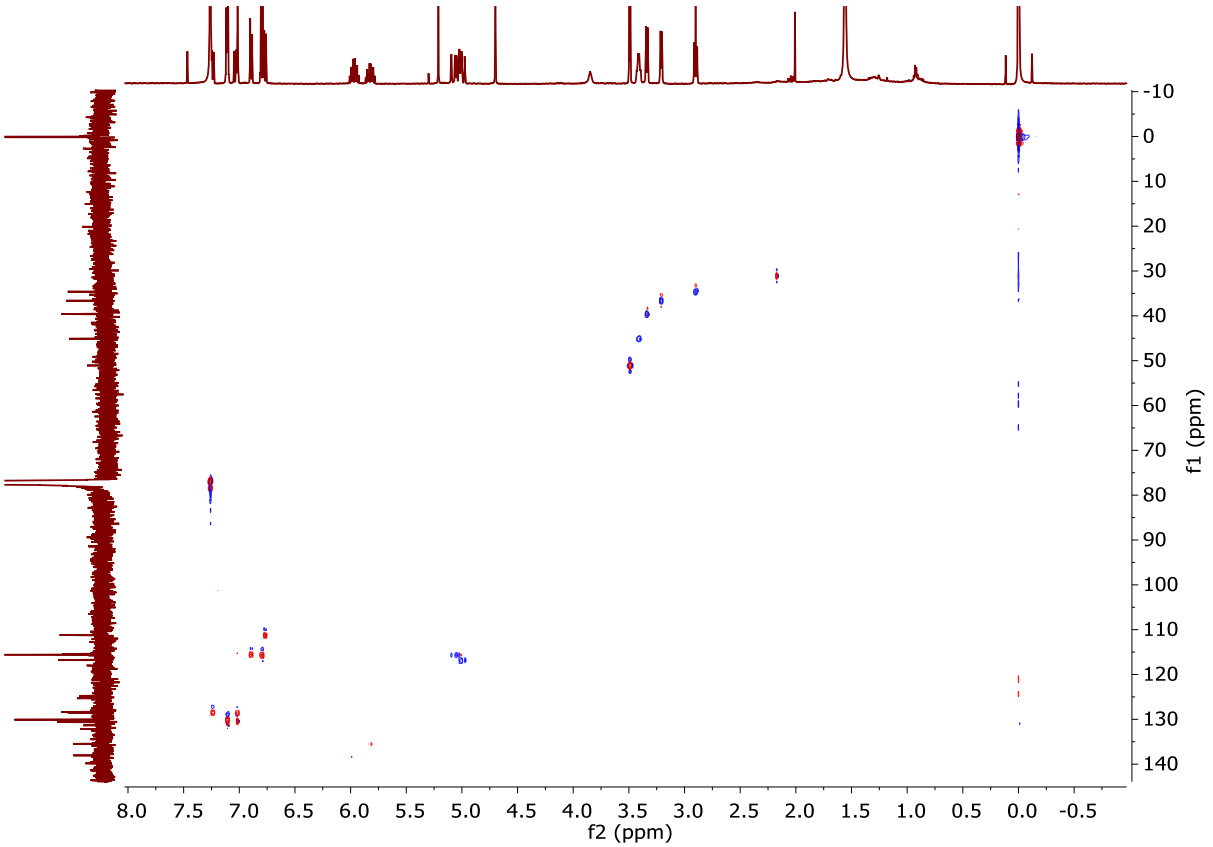

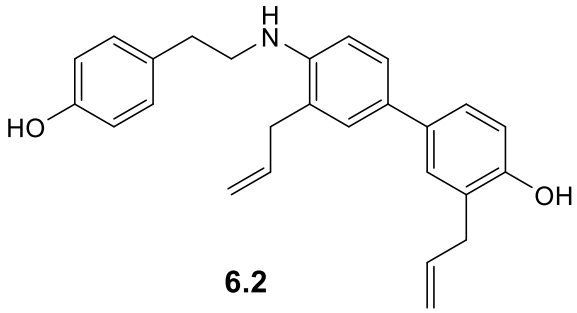

6.2

HMBC of 3,3'-diallyl-4'-((4-hydroxyphenethyl)amino)-[1,1'-bi- phenyl]-4-ol (6.2) in $CDCl_3$

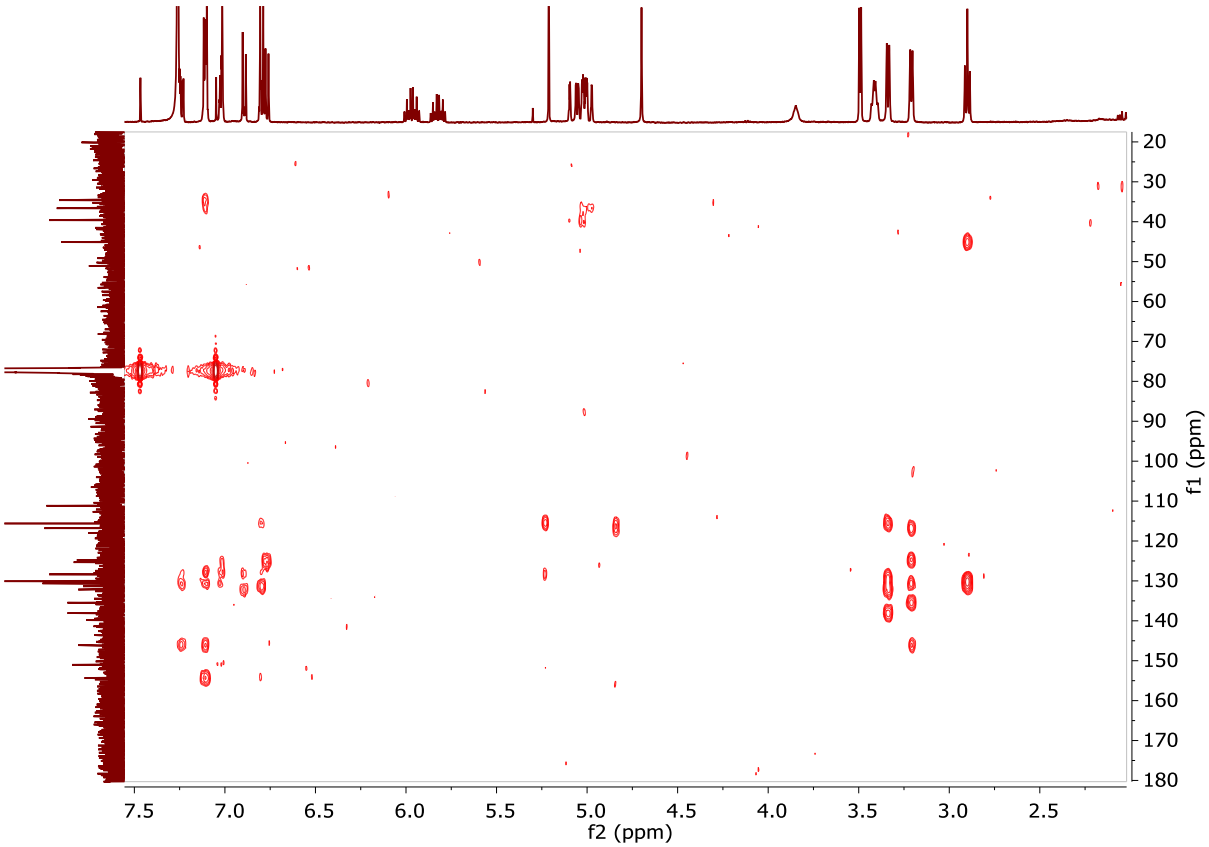

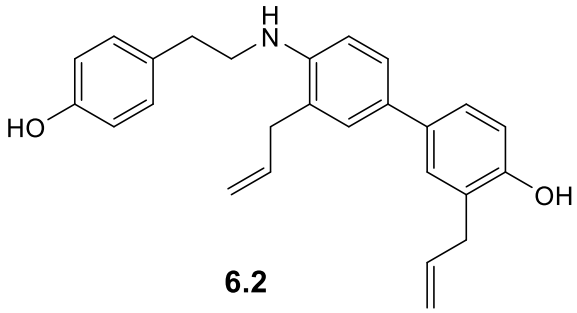

6.2

^{1}H NMR of 4′-*O*-methyl honokiol (6.3) in $CDCl_3$

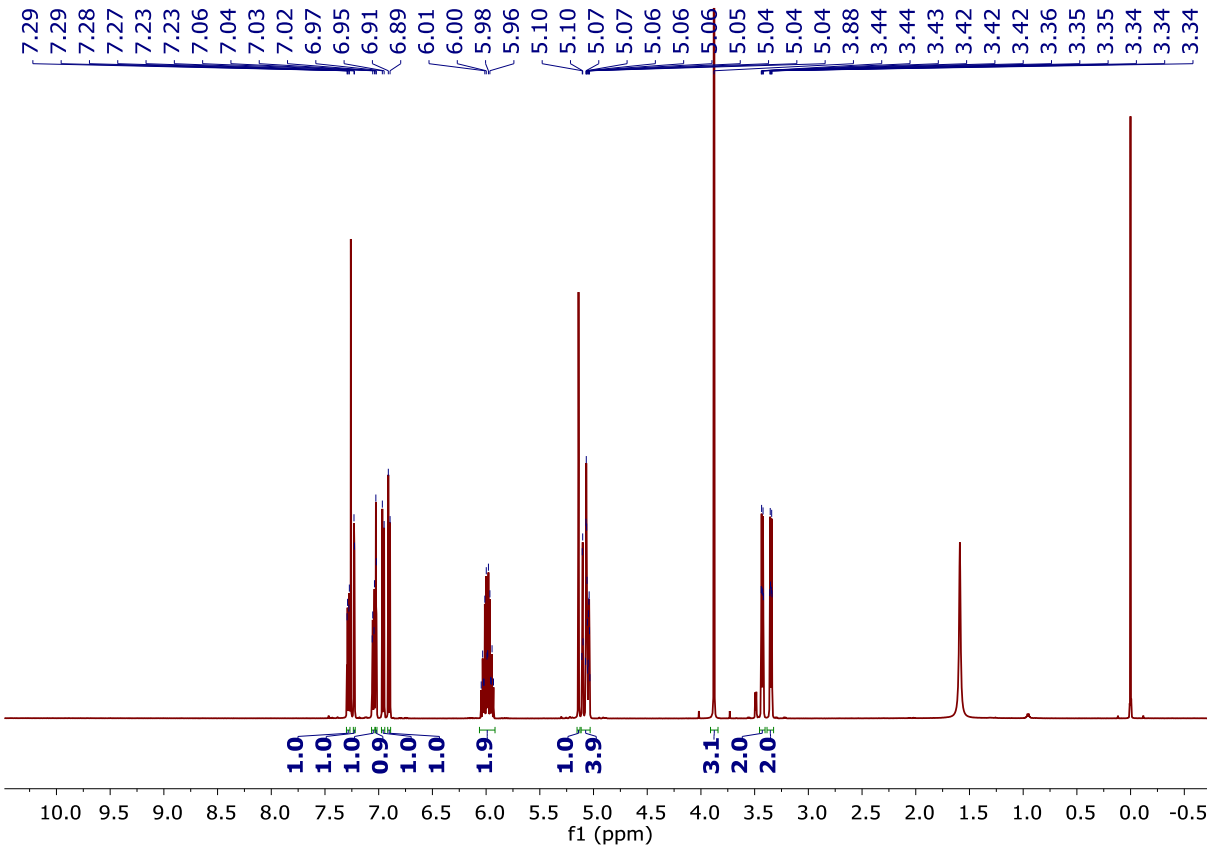

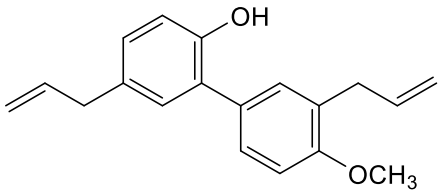

6.3

^{1}H NMR of magnolol (6.4) in $CDCl_3$

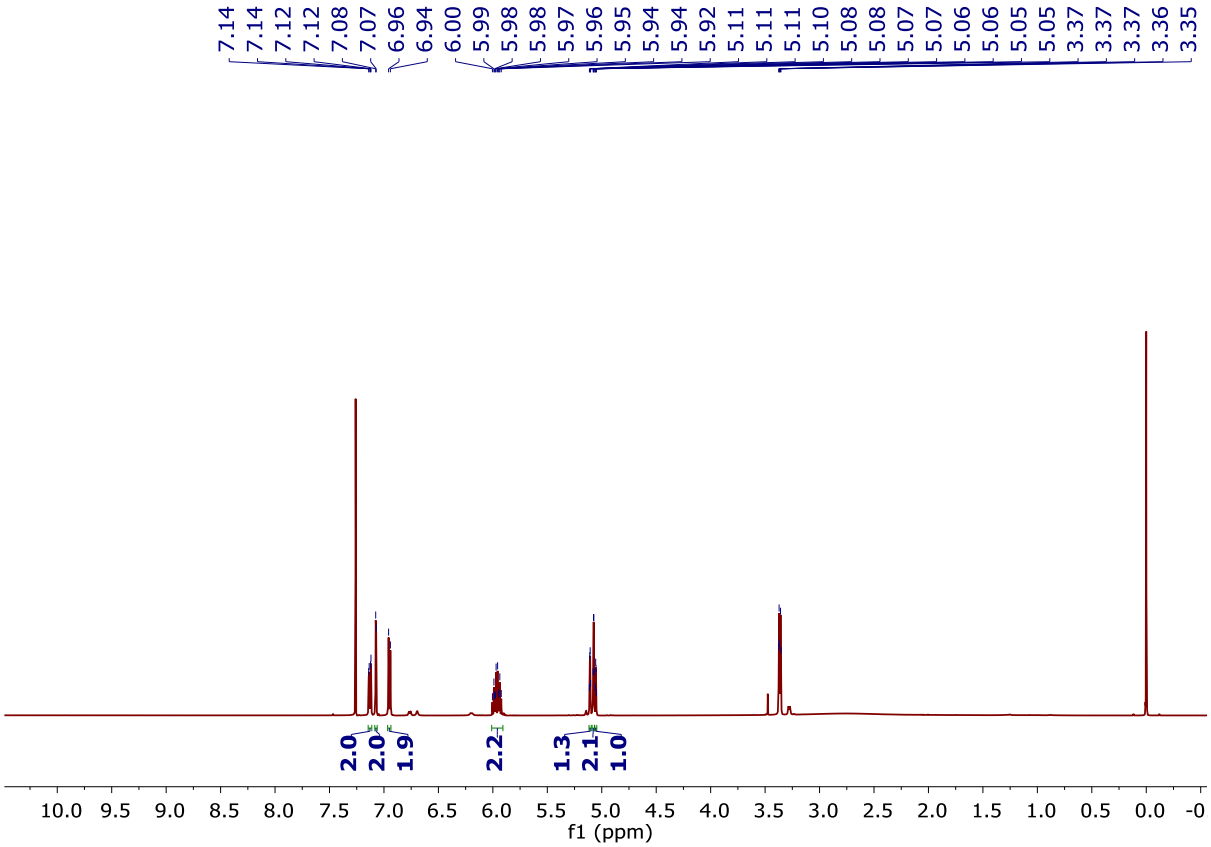

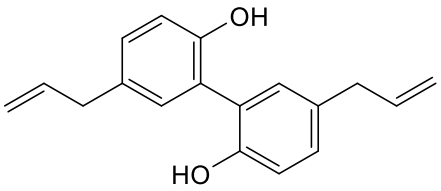

6.4

^{1}H NMR of honokiol (6.5) in $CDCl_3$

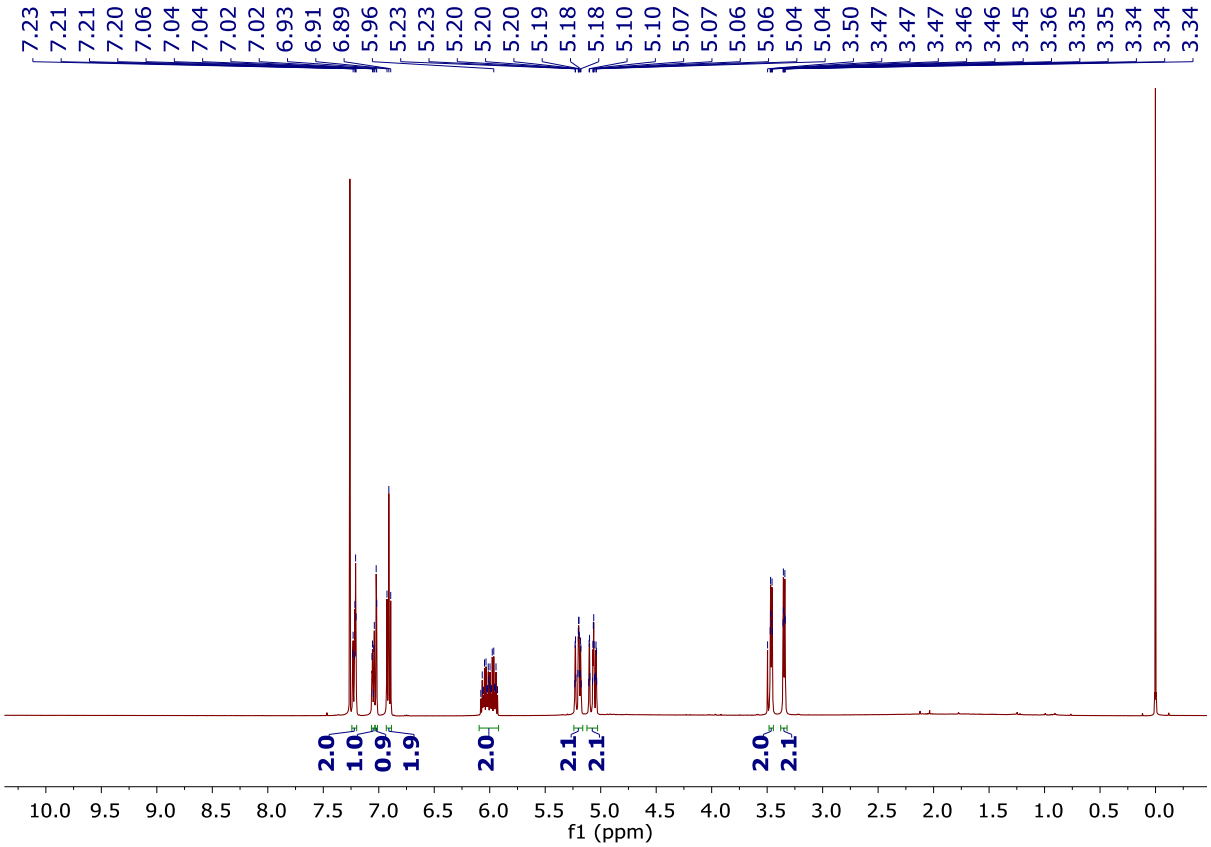

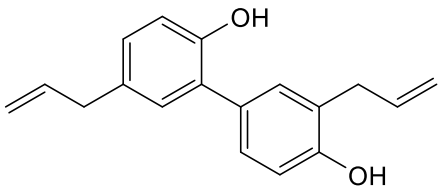

6.5

^{1}H NMR of 3-methoxymagnolol (6.6) in $CDCl_3$

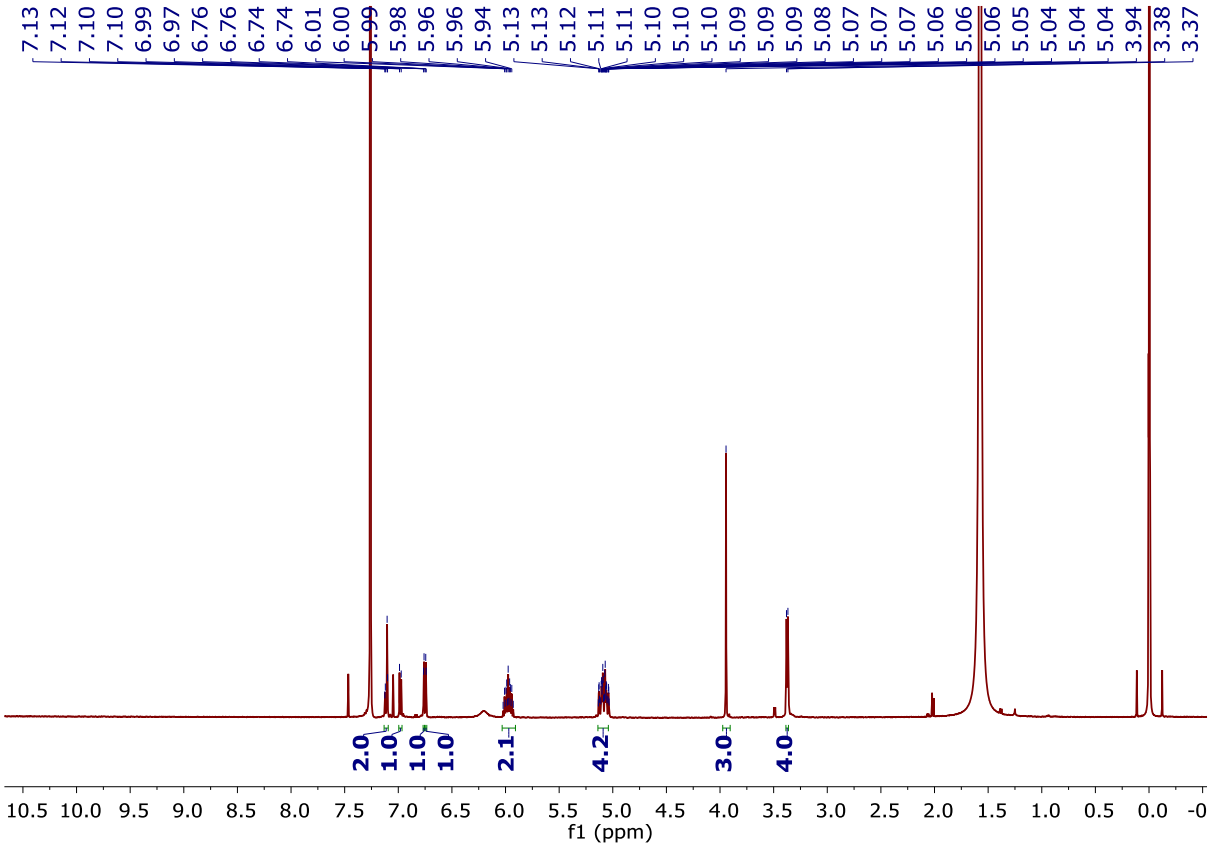

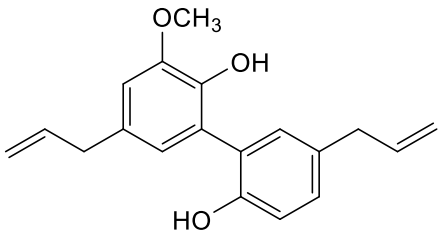

6.6

^{1}H NMR of isomagnolol (6.7) in $CDCl_3$

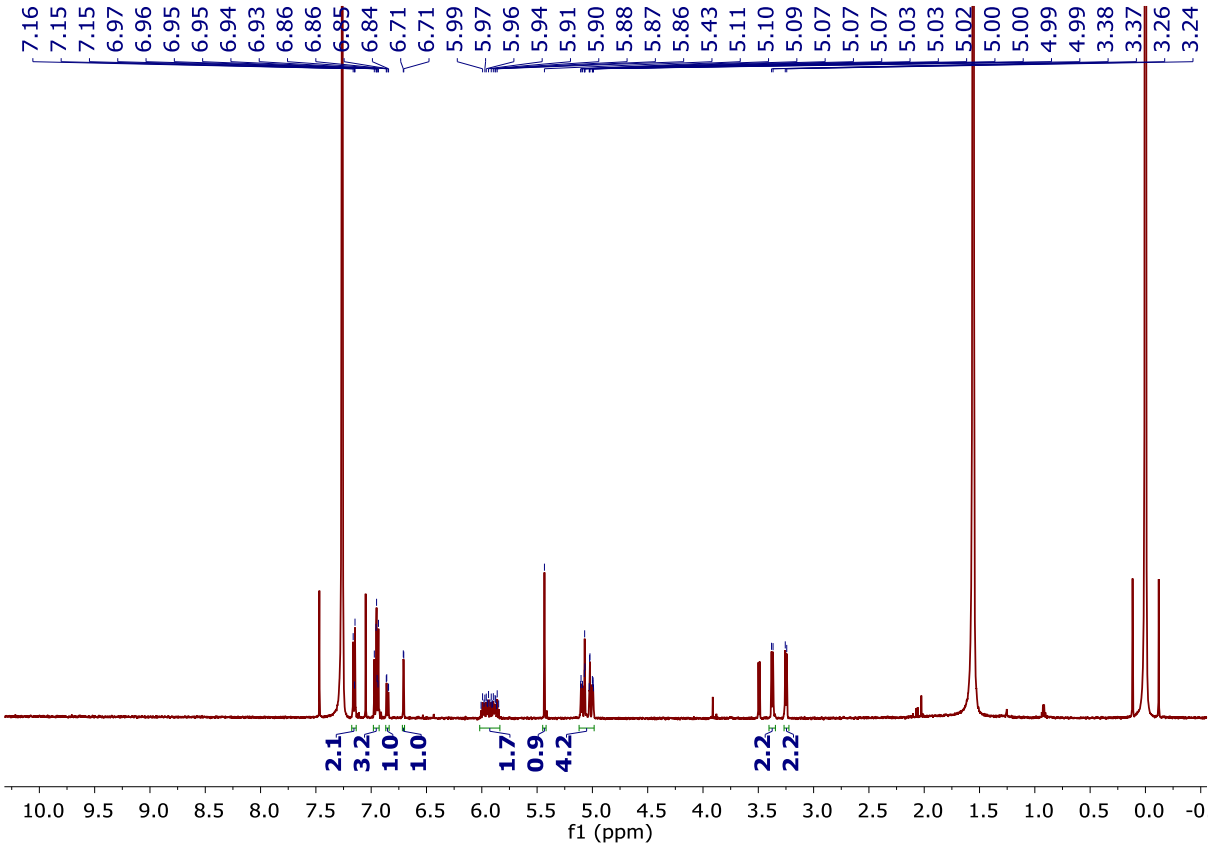

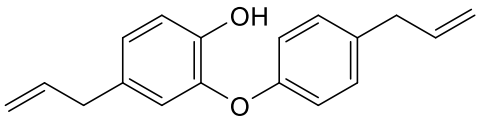

6.7

^{1}H NMR of Pumerer's ketone (6.8) in $CDCl_3$

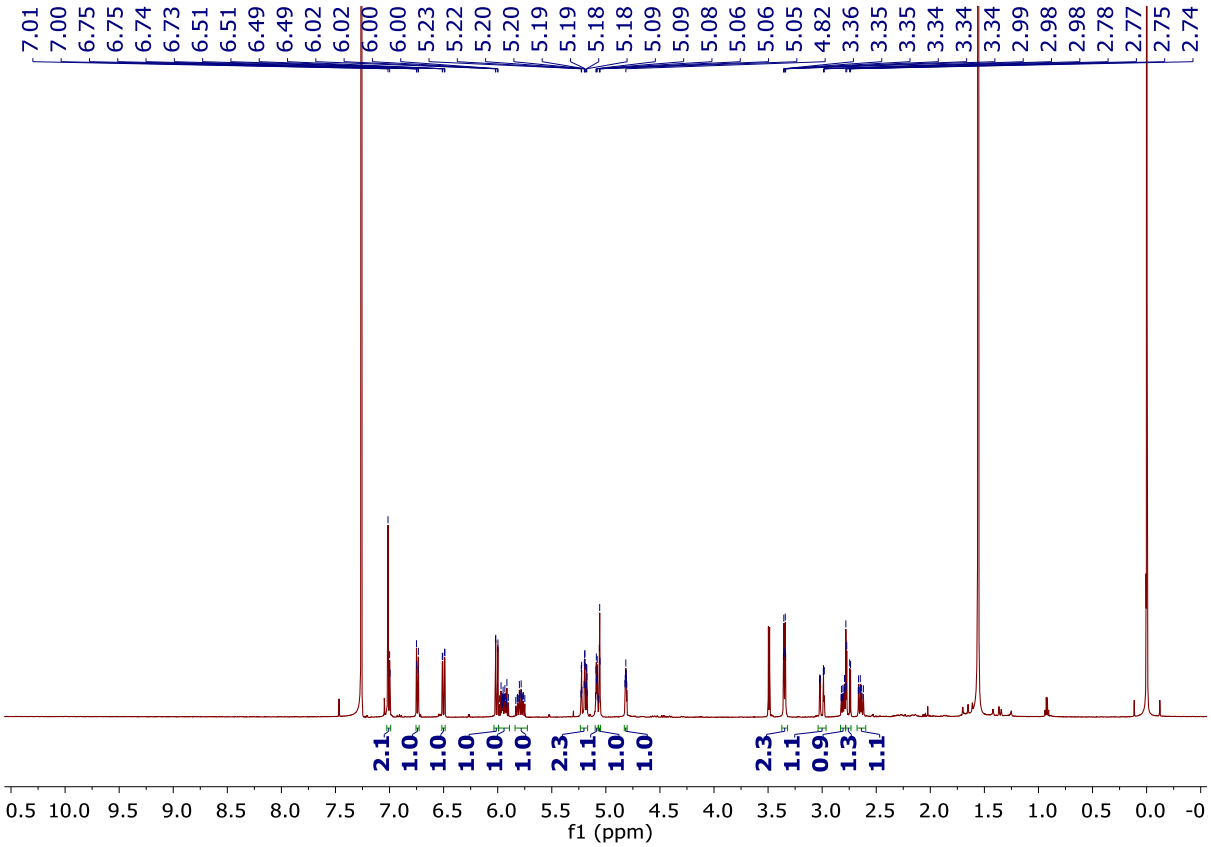

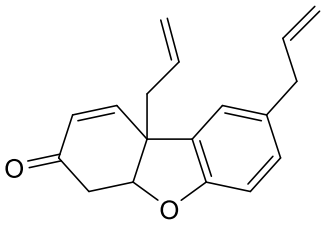

6.8

^{1}H NMR of Cryptorigidifoliol K (7.2) in $CDCl_3$

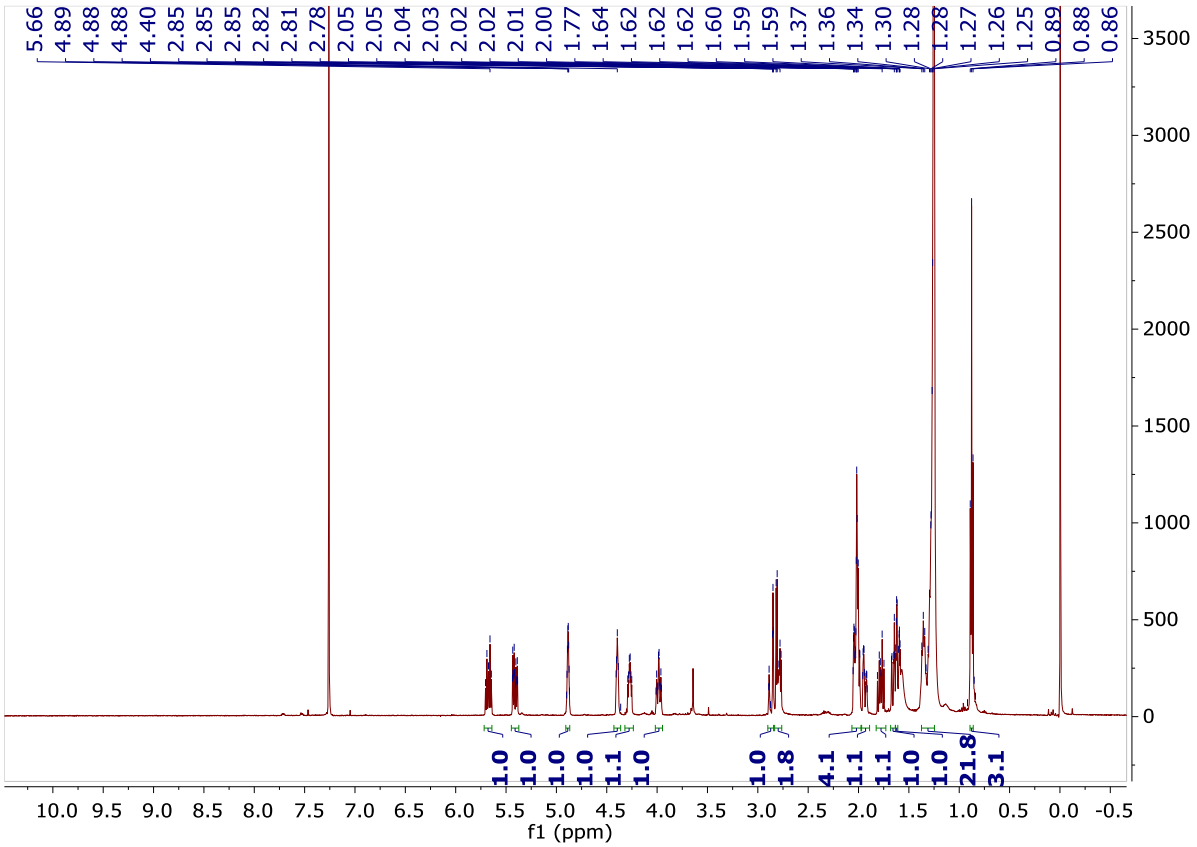

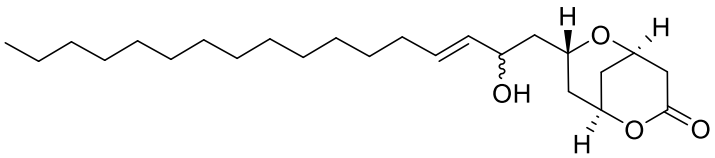

7.2

COSY of Cryptorigidifoliol K (7.2) in $CDCl_3$

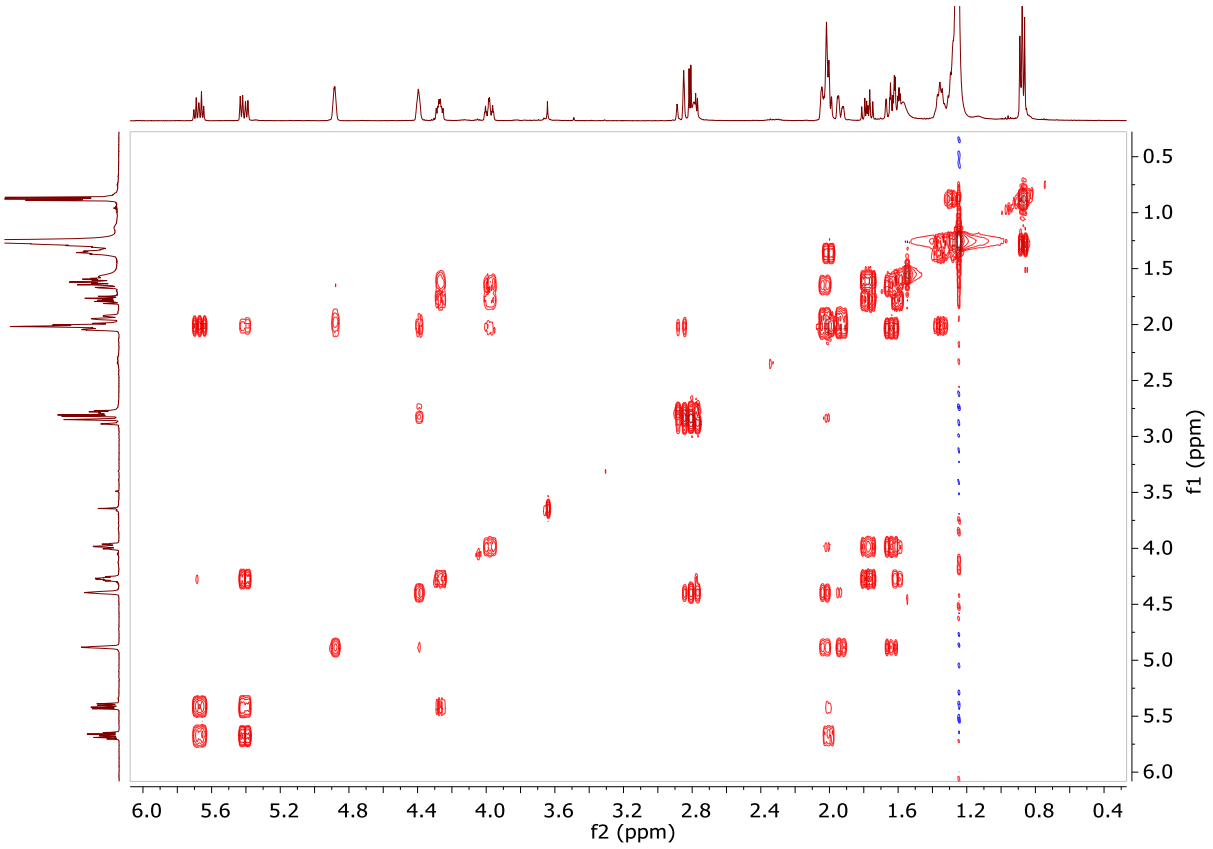

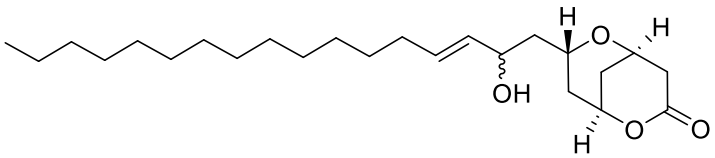

7.2

HSQC of Cryptorigidifoliol K (7.2) in $CDCl_3$

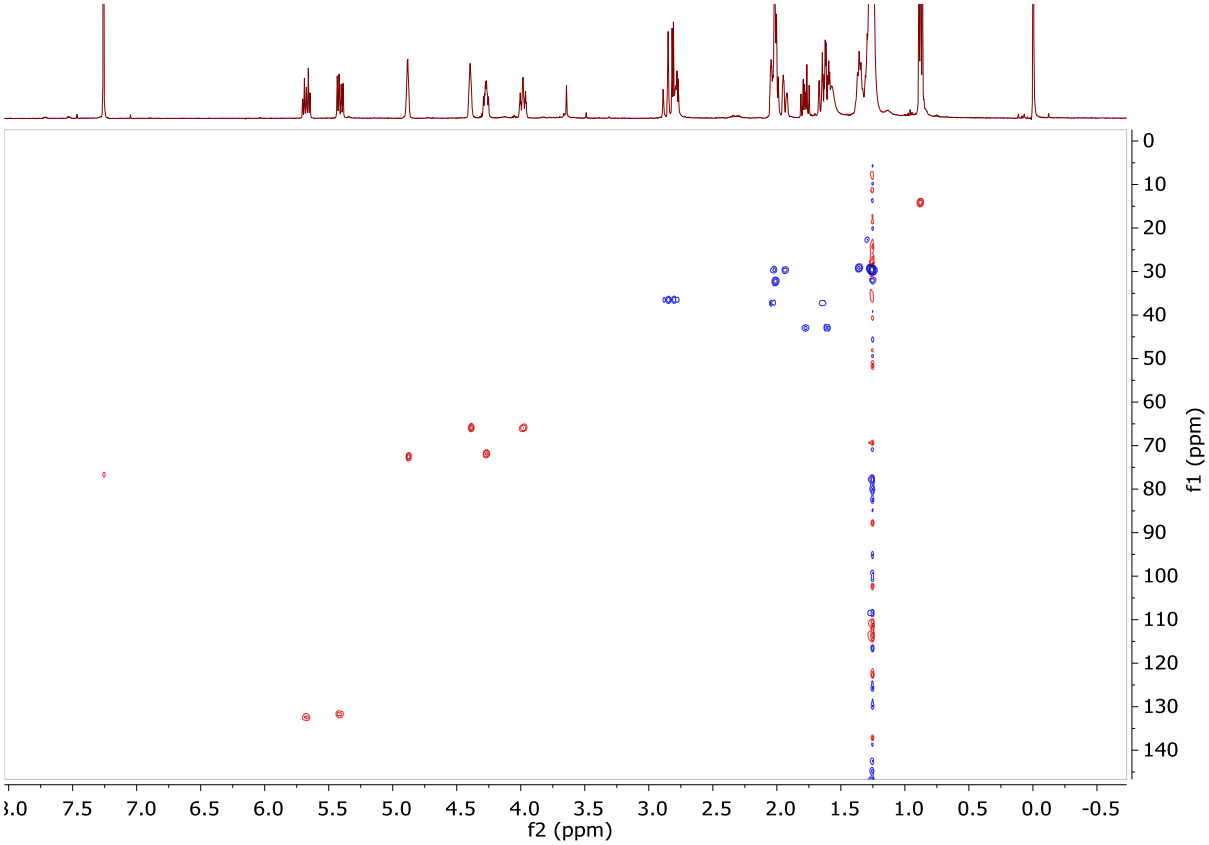

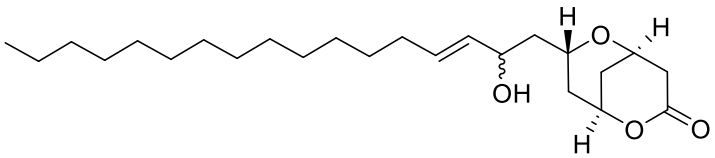

7.2

HMBC of Cryptorigidifoliol K (7.2) in $CDCl_3$

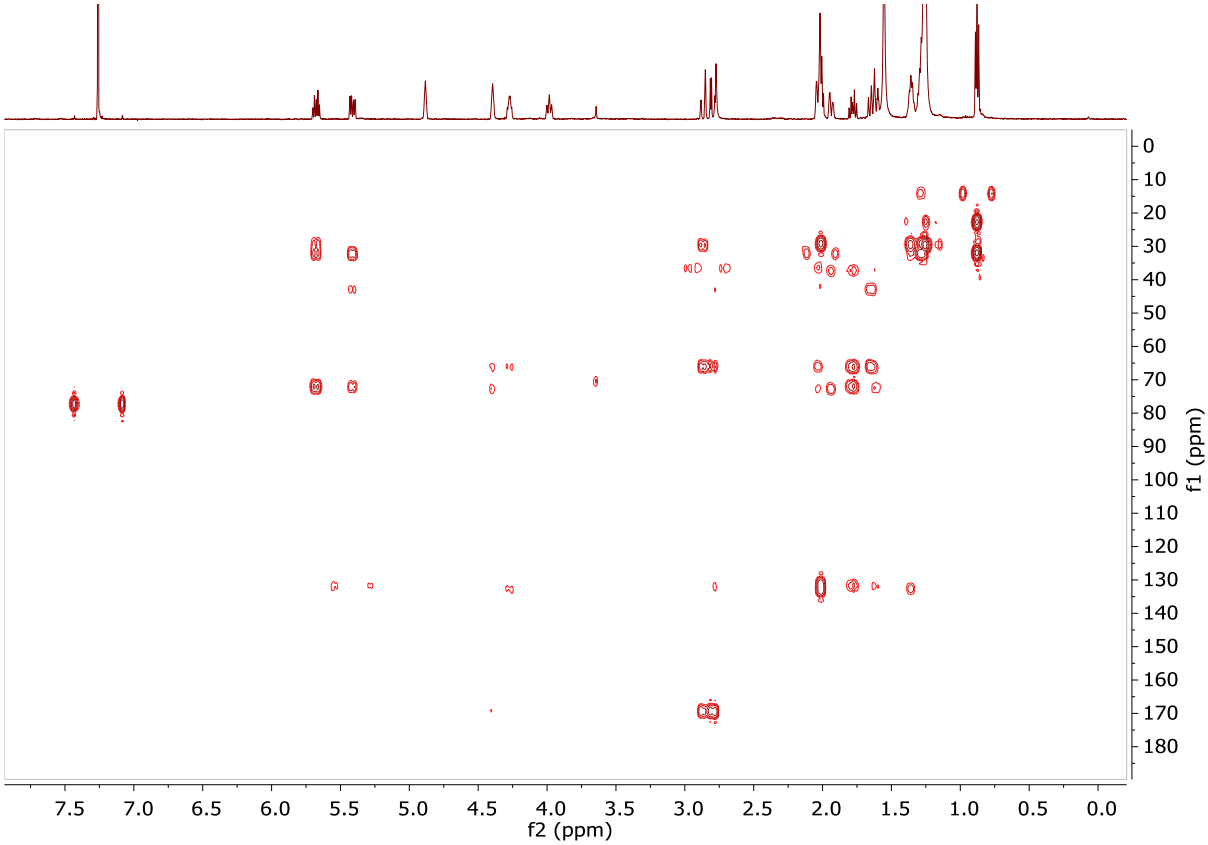

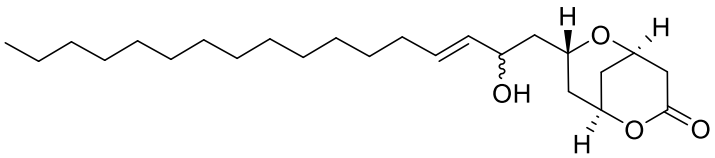

7.2

^{1}H NMR of Norbergenin (8.1) in Acetone-d6

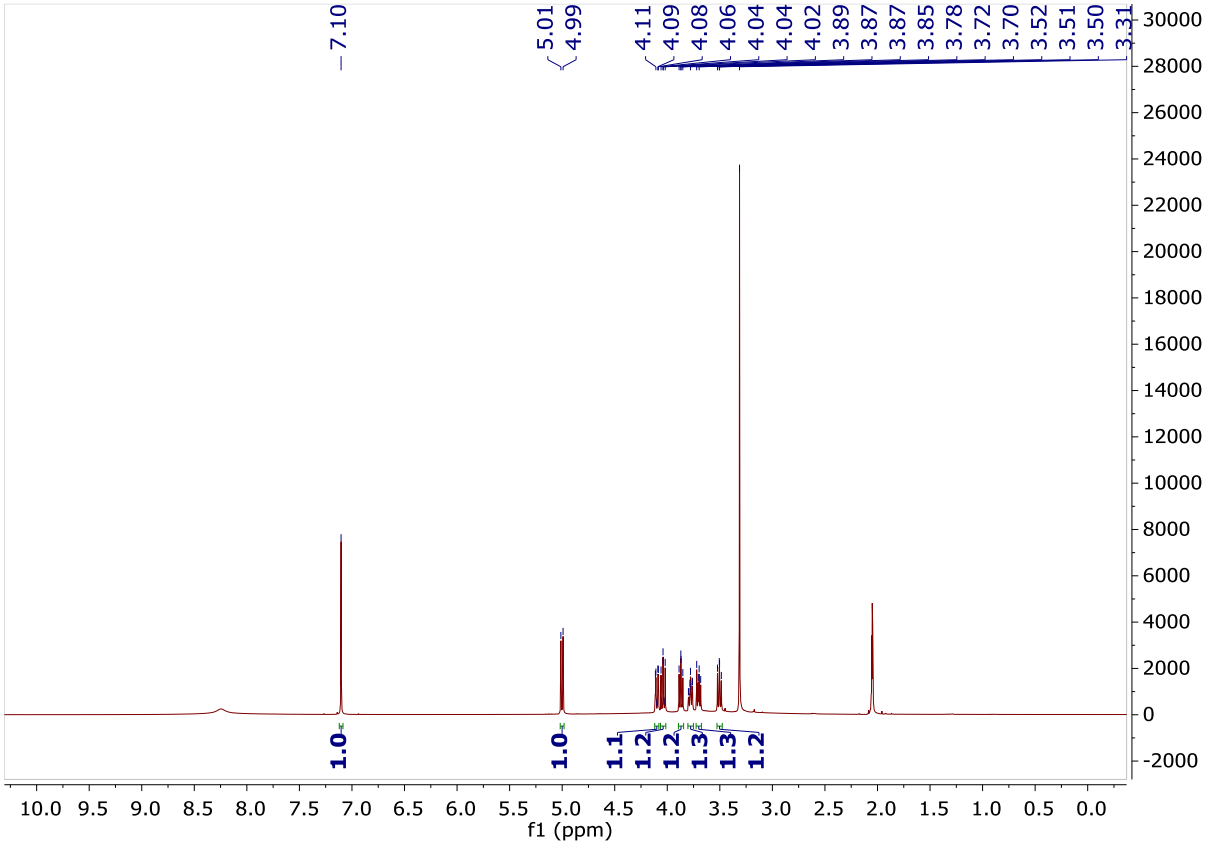

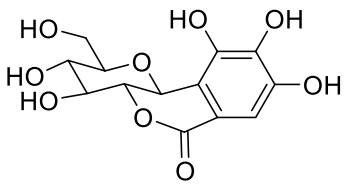

8.1

^{13}C NMR of Norbergenin (8.1) in Acetone-d6

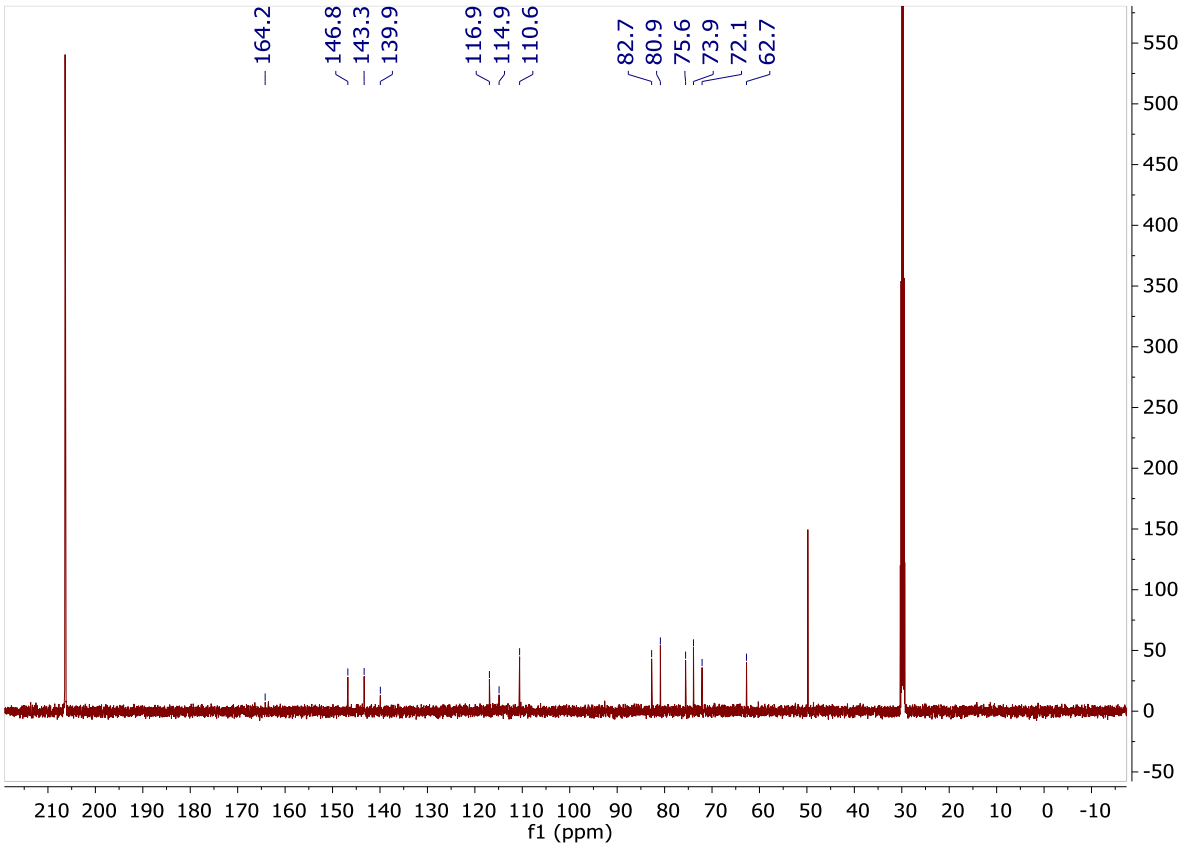

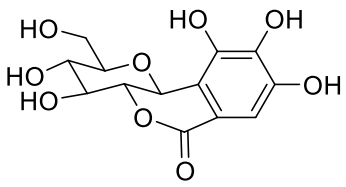

8.1

^{1}H NMR of Bergenin (8.2) in Acetone-d6

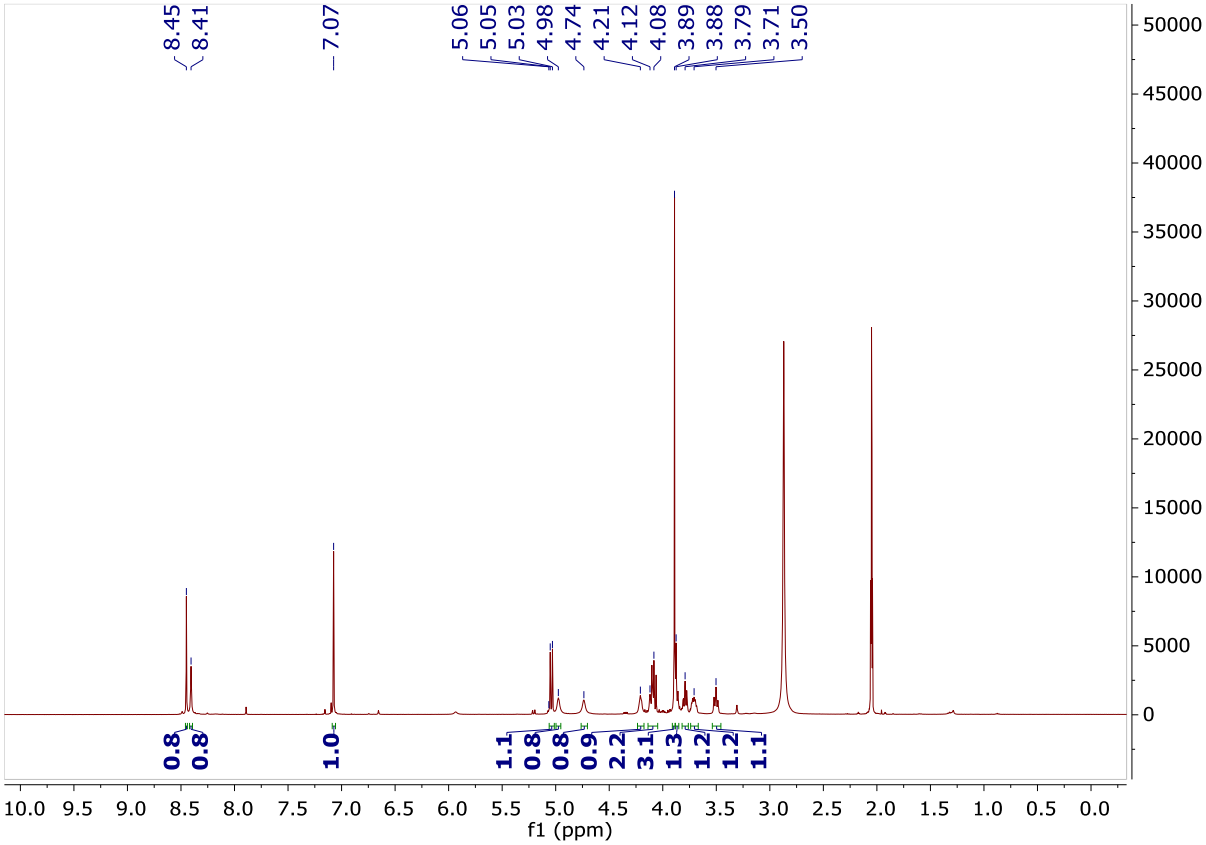

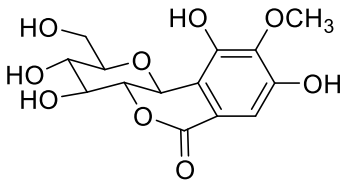

8.2

^{13}C NMR of Bergenin (8.2) in Acetone-d6

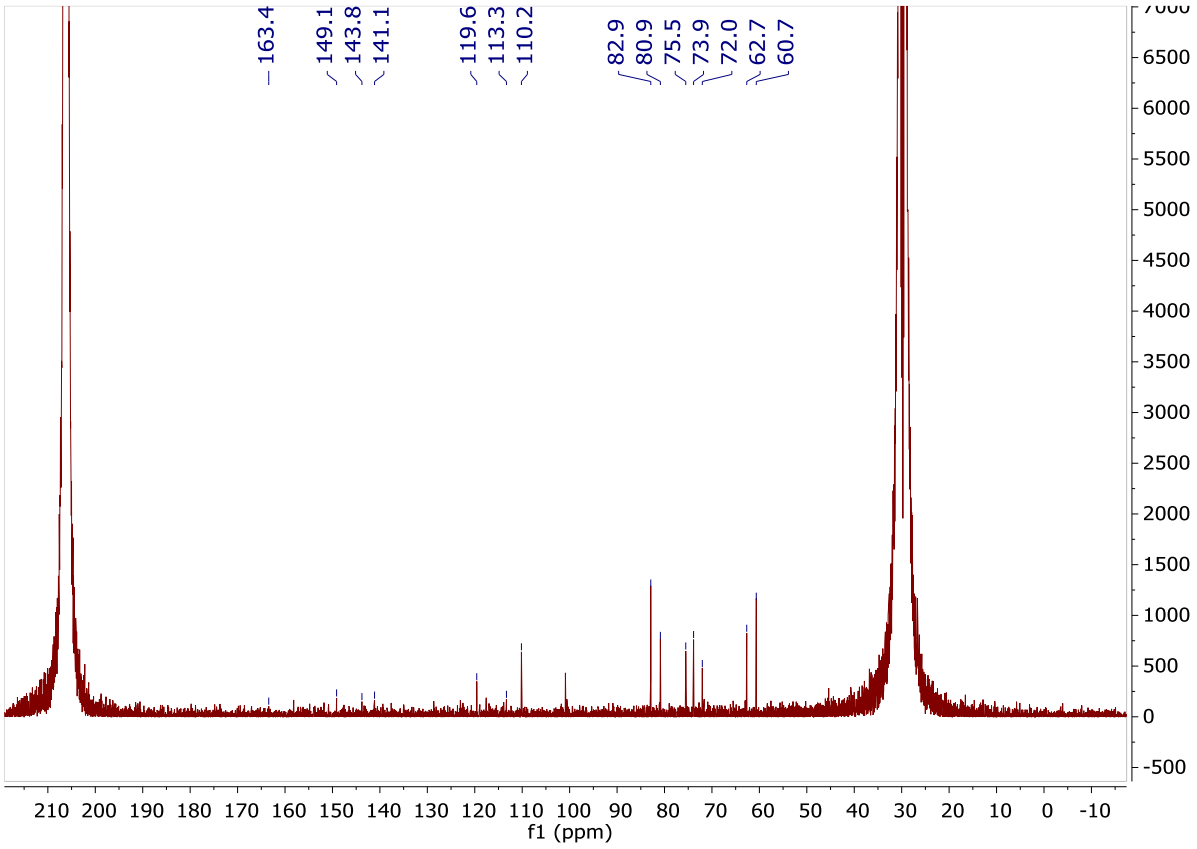

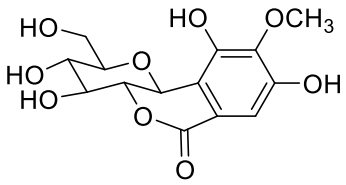

8.2

^{1}H NMR of Canthin-6-one (8.3) in $CDCl_3$

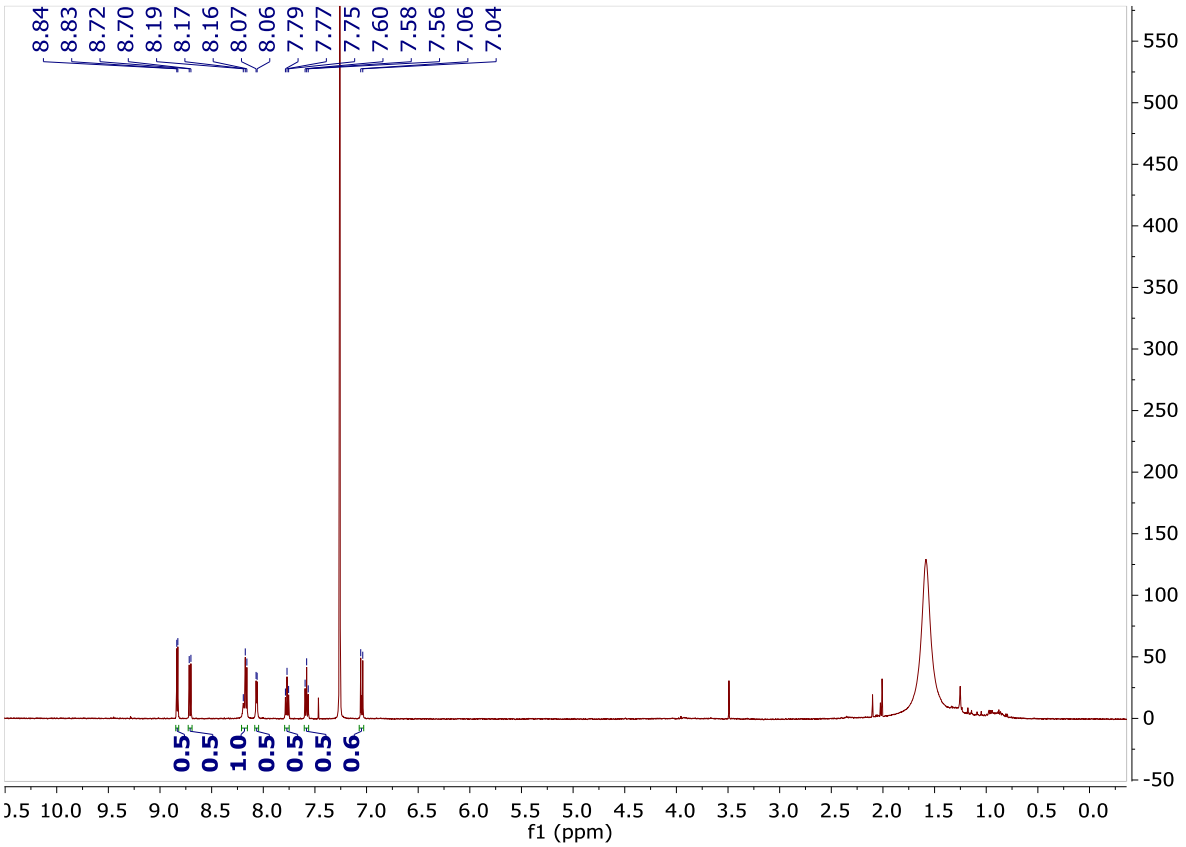

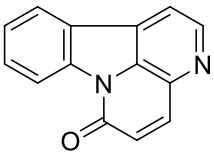

8.3

^{1}H NMR of 1-Methoxycanthin-6-one (8.4) in $CDCl_3$

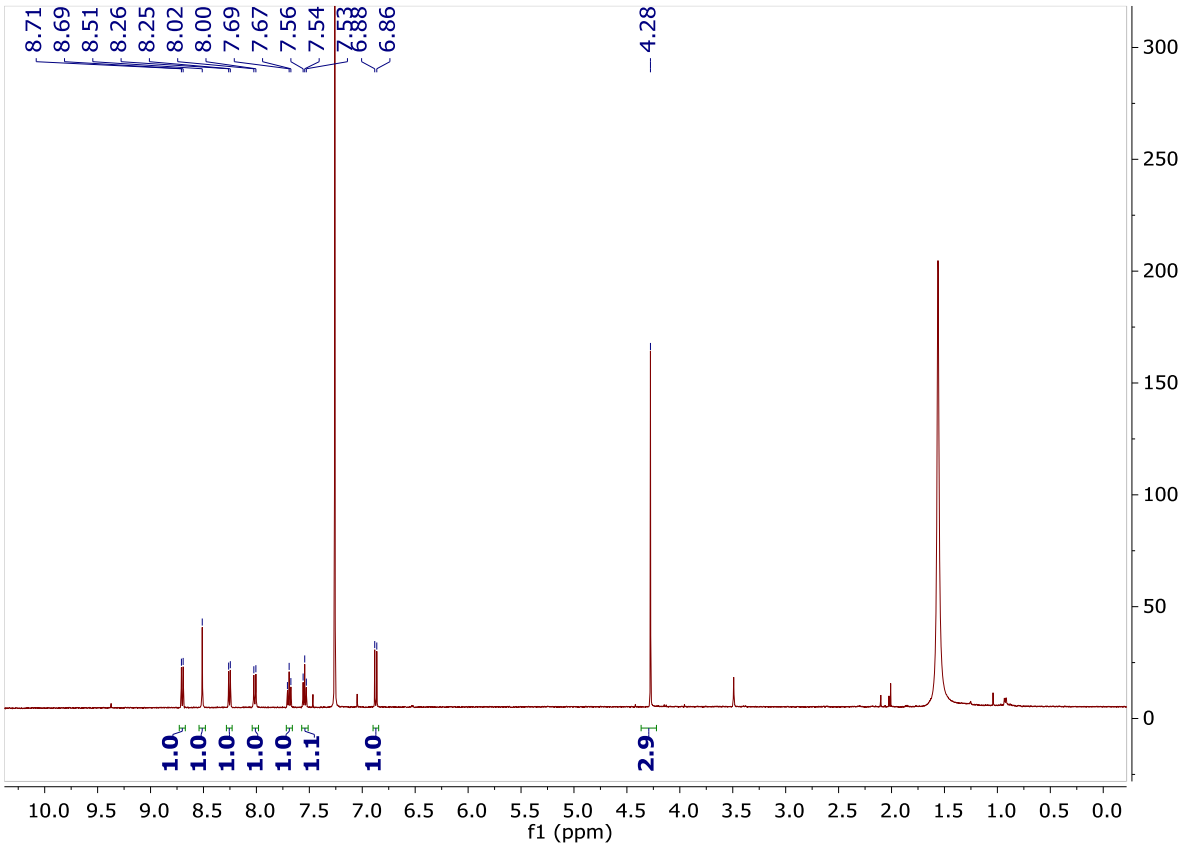

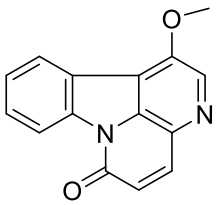

8.4

^{1}H NMR of 5-Methoxycanthin-6-one (8.5) in $CDCl_3$

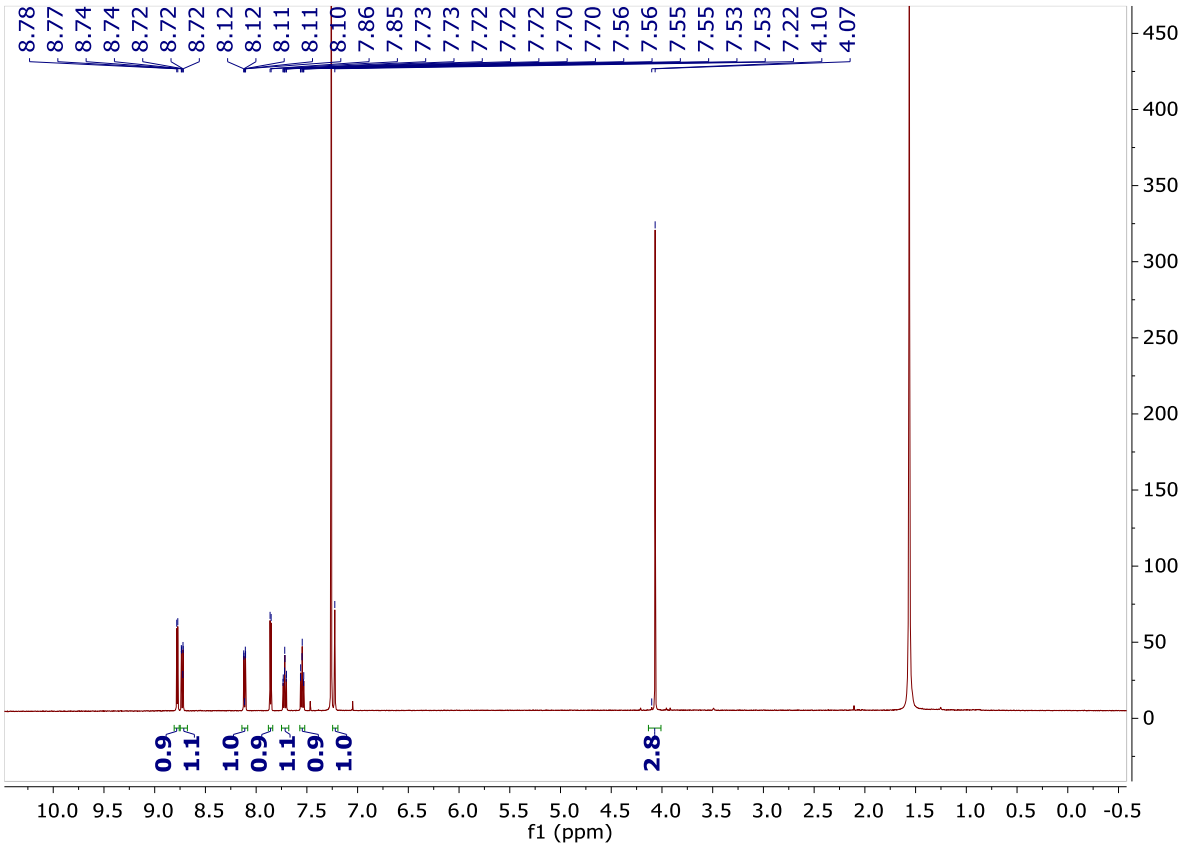

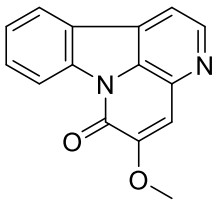

8.5

^{1}H NMR of (+)-Lariciresinol (8.6) in $CDCl_3$

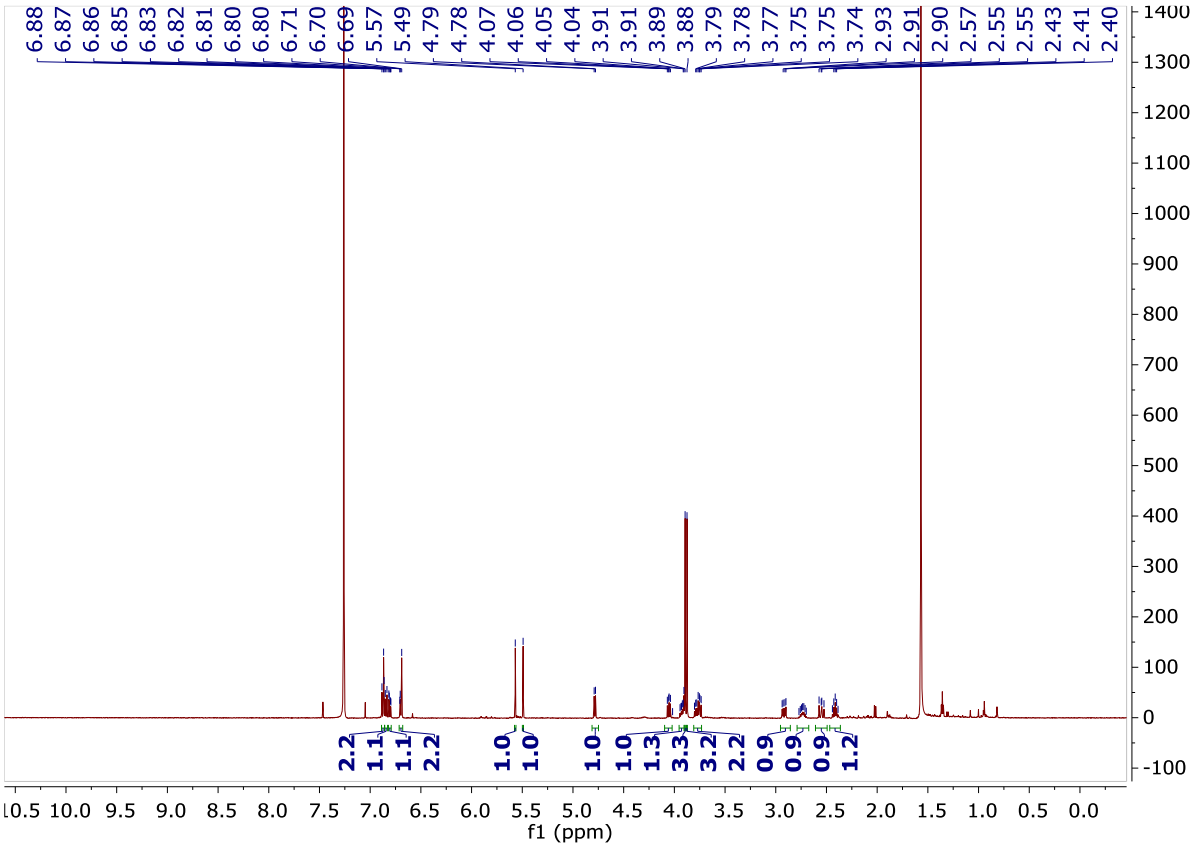

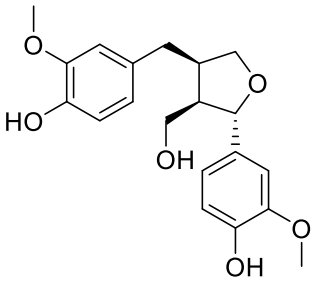

8.6

^{1}H NMR of 4-(Acetylthio)benzoic acid (9.5) in CD_3OD

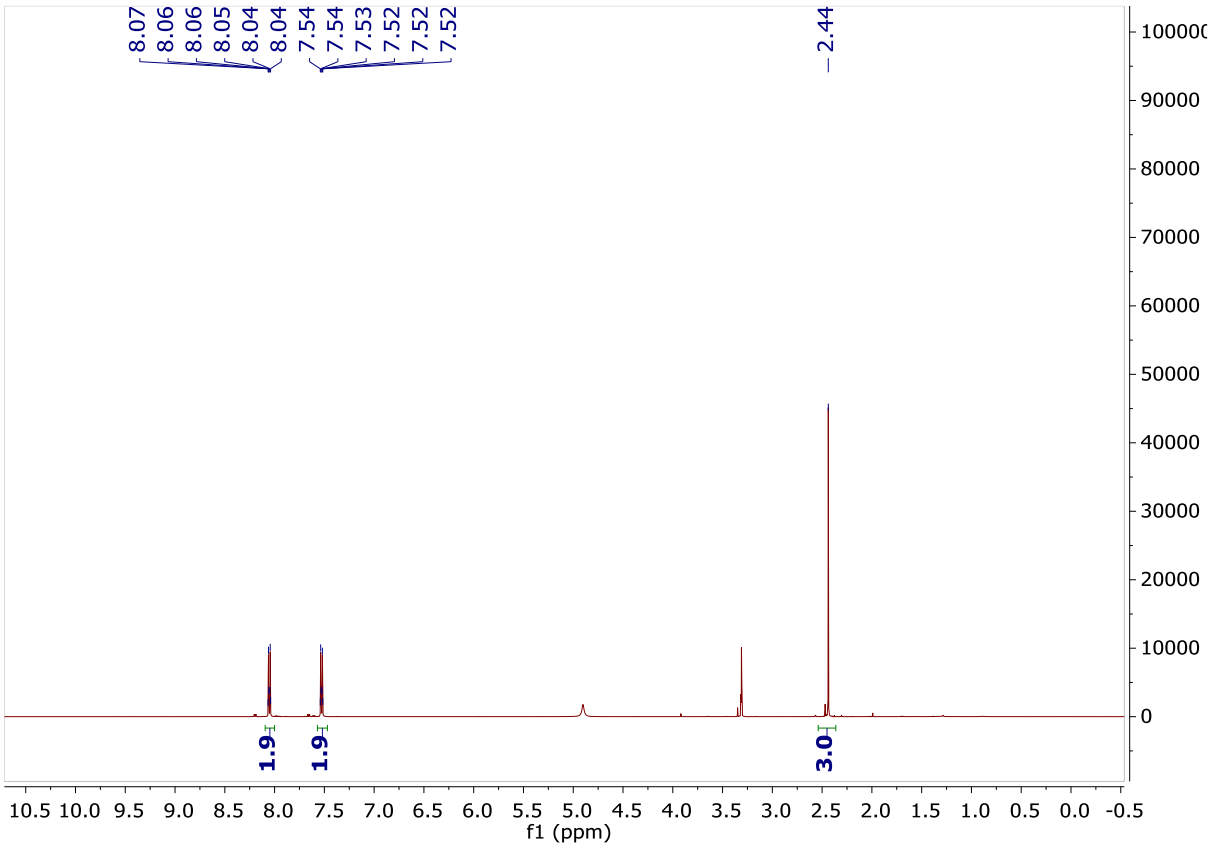

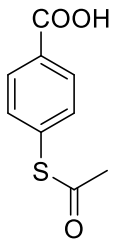

9.5

^{13}C NMR of 4-(Acetylthio)benzoic acid (9.5) in CD_3OD

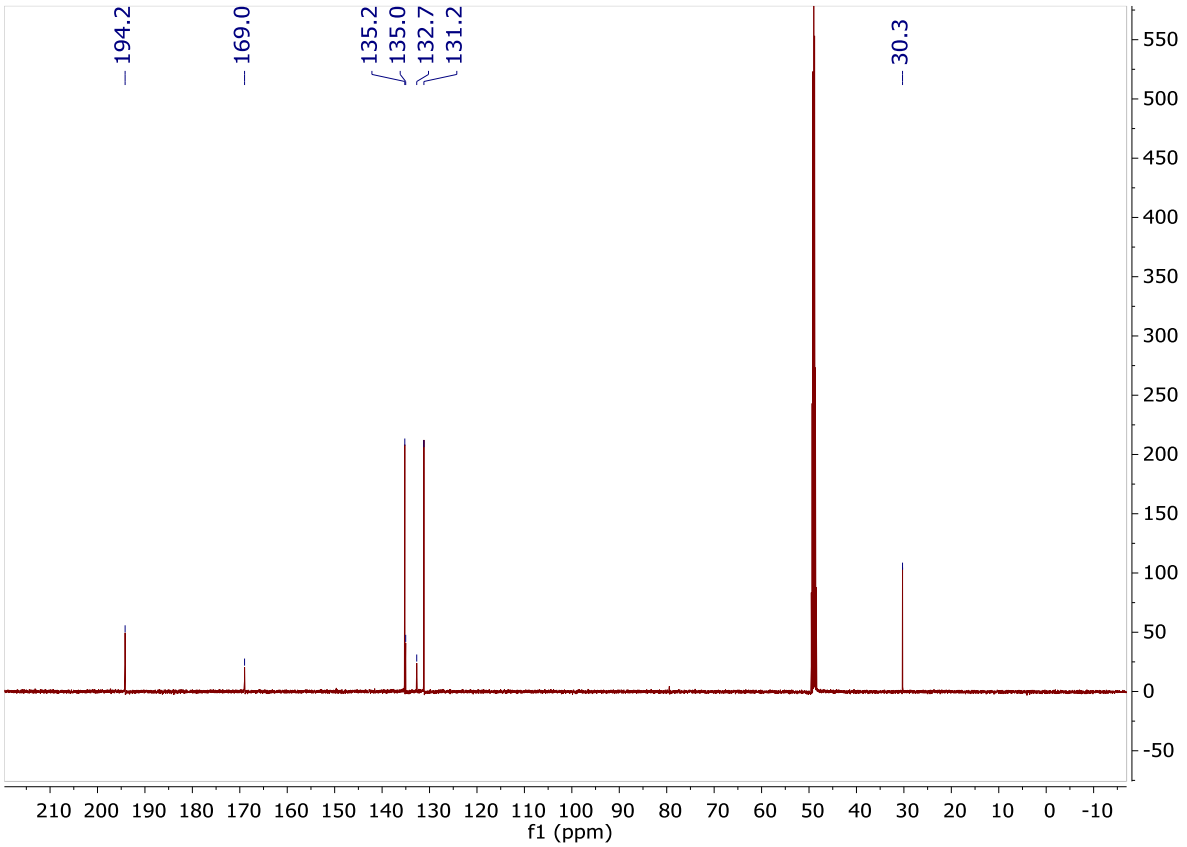

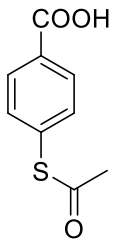

9.5

^{1}H NMR of S-(4-(hydroxymethyl)phenyl) ethanethioate (9.6) in CD_3OD

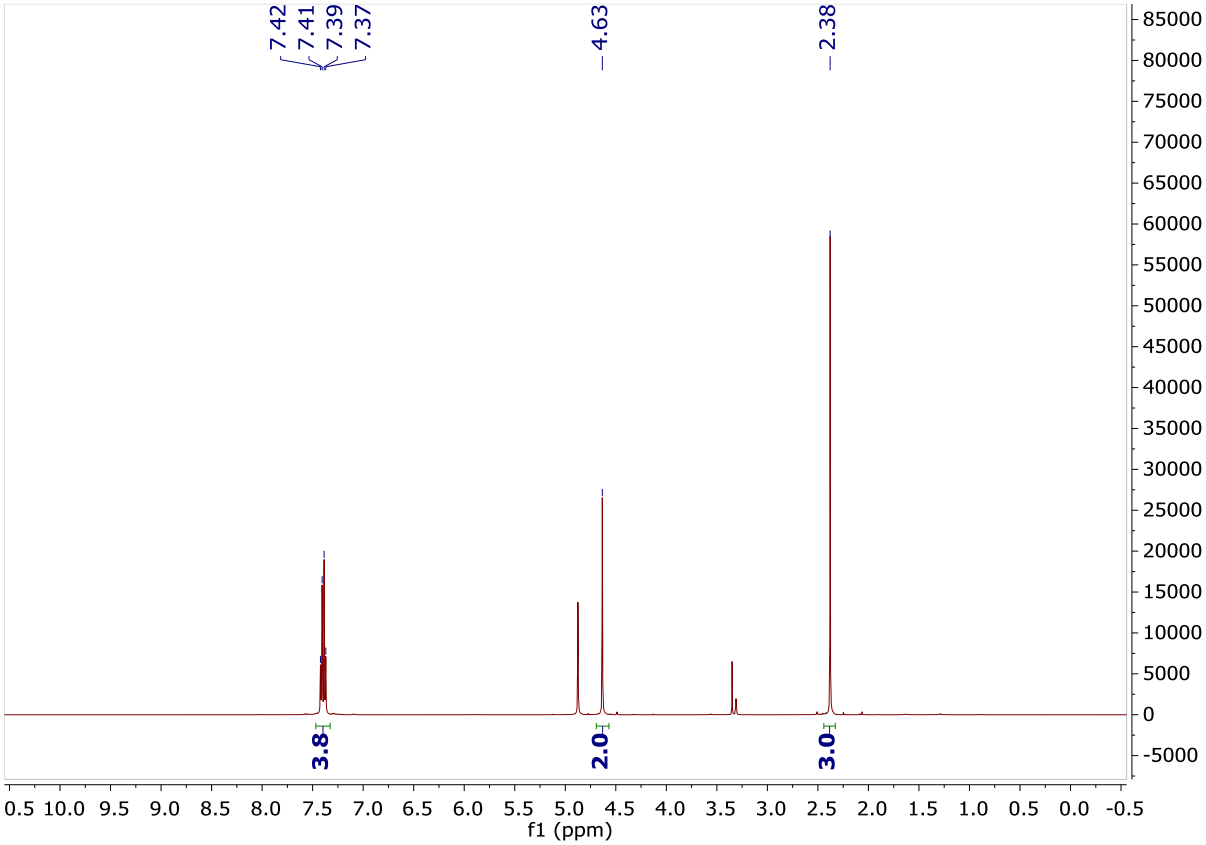

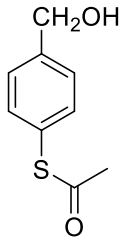

9.6

^{13}C NMR of S-(4-(hydroxymethyl)phenyl) ethanethioate (9.6) in CD_3OD

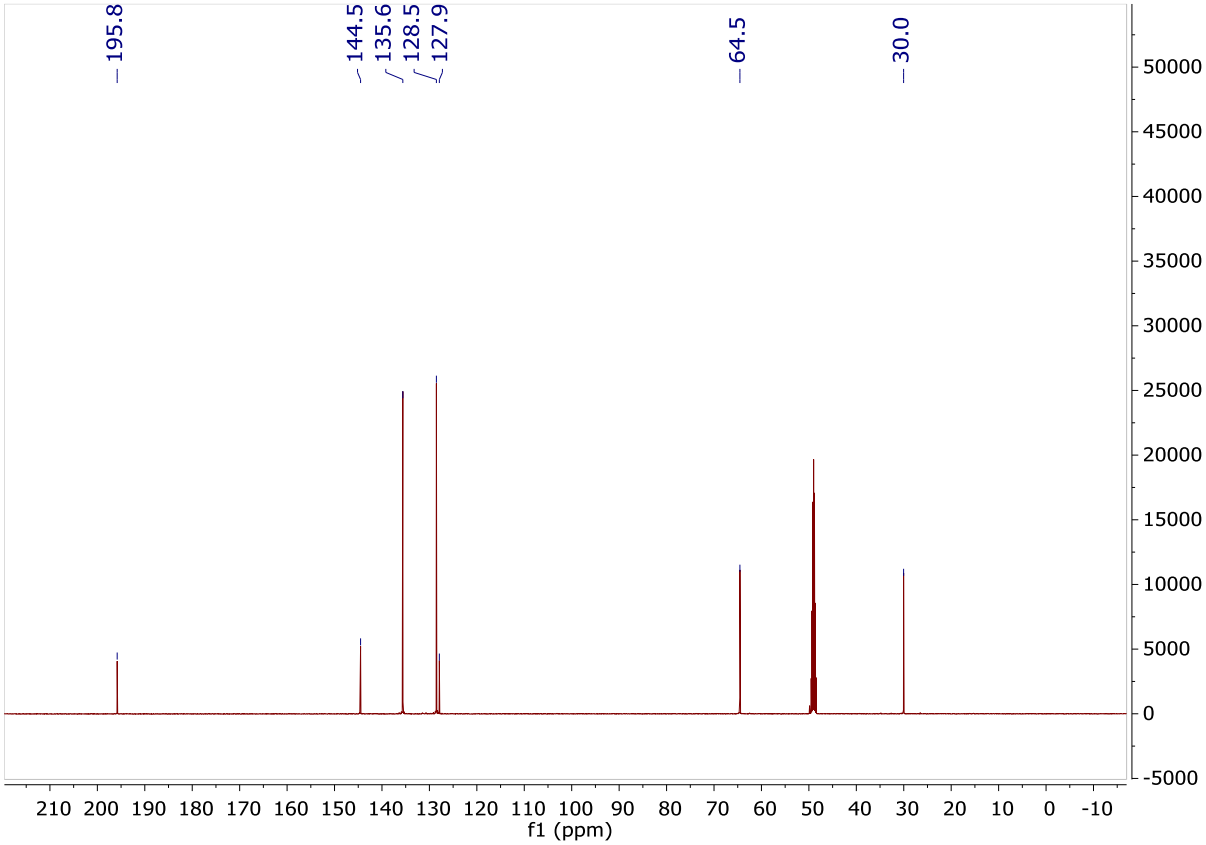

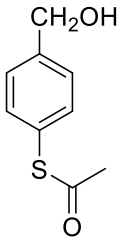

9.6

^{1}H NMR of S-4-((((4-nitrophenoxy)carbonyl)oxy)methyl)-phenyl ethanethioate (9.7) in $CDCl_3$

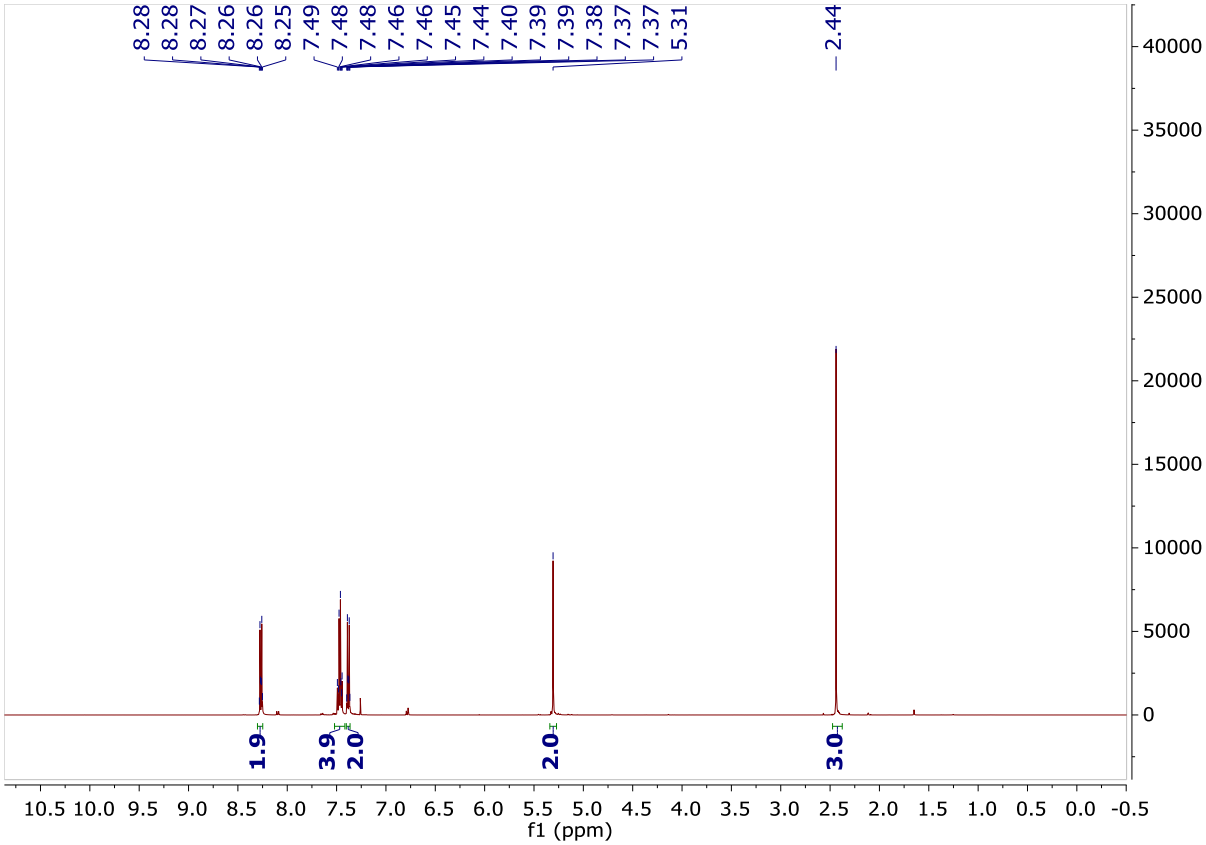

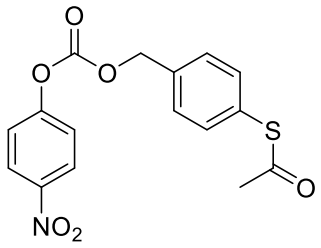

9.7

^{13}C NMR of S-4-((((4-nitrophenoxy)carbonyl)oxy)methyl)-phenyl ethanethioate (9.7) in $CDCl_3$

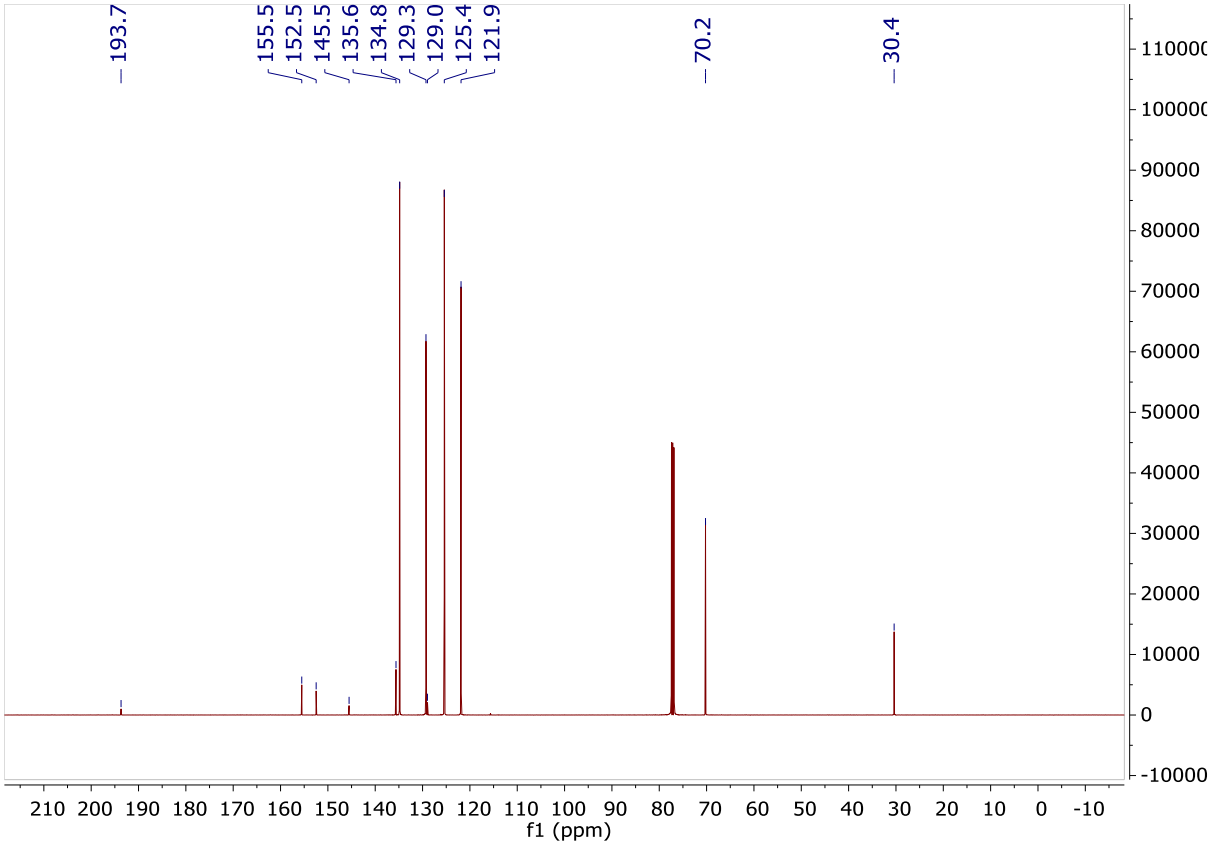

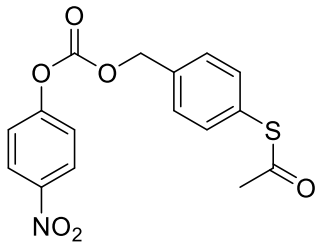

9.7

^{1}H NMR of *S*-(4-(((((2*S*,3*S*,4*S*,6*R*)-3-hydroxy-2-methyl-6-(((1*S*,3*S*)-3,5,12-trihydroxy-3-(2-hydroxyacetyl)-10-methoxy-6,11-dioxo-1,2,3,4,6,11-hexahydrotetracen-1-yl)oxy)tetrahydro-2H-pyran-4yl)carbamoyl)oxy) methyl)phenyl) ethanethioate (9.3) in $CDCl_3$

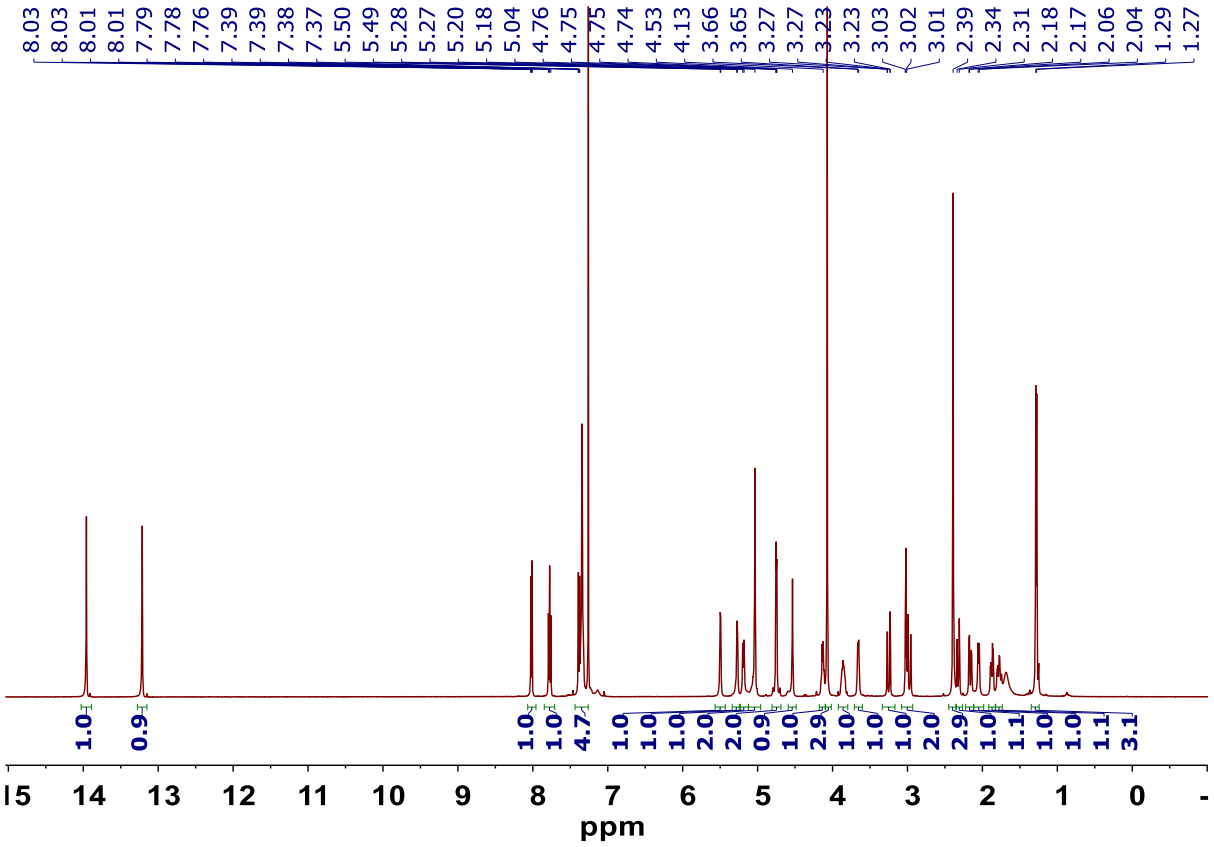

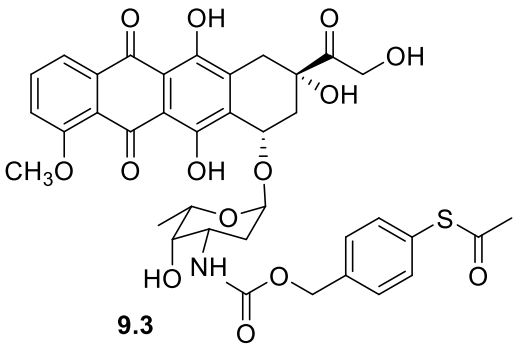

9.3

^{13}C NMR of *S*-(4-(((((2*S*,3*S*,4*S*,6*R*)-3-hydroxy-2-methyl-6-(((1*S*,3*S*)-3,5,12-trihydroxy-3-(2-hydroxyacetyl)-10-methoxy-6,11-dioxo-1,2,3,4,6,11-hexahydrotetracen-1-yl)oxy)tetrahydro-2H-pyran-4yl)carbamoyl)oxy) methyl)phenyl) ethanethioate (9.3) in $CDCl_3$

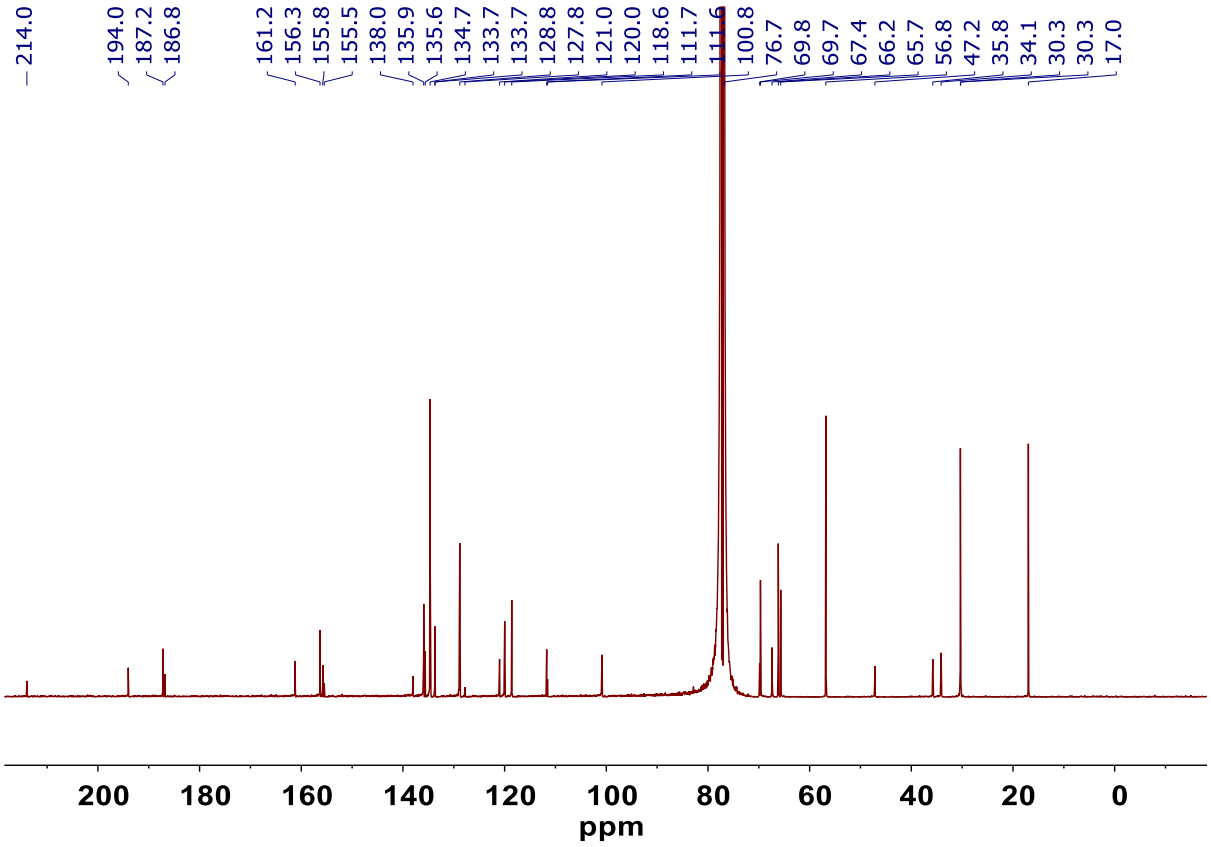

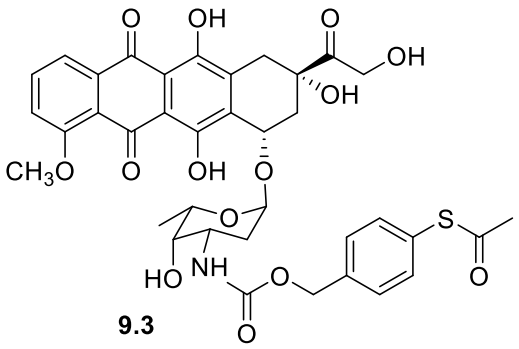

9.3